MANUEL ESTEBAN VILA MARTÍN

NEURAL CIRCUITS FOR SOCIAL RECOGNITION IN MICE:
A NEUROANATOMICAL, BEHAVIOURAL AND ELECTROPHYSIOLOGICAL STUDY

PhD Dissertation

VNIVERSITAT DE VALÈNCIA

SUPERVISORS
Dr. Enrique Lanuza Navarro
Dr. Vicent Teruel Martí

DEPARTAMENTO DE BIOLOGÍA CELULAR, FUNCIONAL Y ANTROPOLOGÍA FÍSICA

PROGRAMA DE DOCTORADO EN NEUROCIENCIAS

Manuel Esteban Vila Martín

Neural circuits for social recognition in mice:
a neuroanatomical, behavioural and electrophysiological study.

january, 2024
Universitat de València

The author of this Thesis dissertation was a predoctoral fellowship of the Atracció de Talent program of the University of Valencia.

NOTE OF THE EDITION

This document was written using LaTeX with the ArsClassica template, a modification of the ClassicThesis style designed by André Miede, inspired by *The Elements of Typographic Style* by Robert Bringhurst.

Vicent Teruel Martí, Profesor Titular del Departamento de Anatomía y Embriología Humana de la Facultad de Medicina de la Universidad de Valencia y Enrique Lanuza Navarro, Catedrático del Departamento de Biología Celular, Biología Funcional y Antropología Física de la Facultad de Biología de la Universidad de Valencia

CERTIFICAN QUE:

Manuel Esteban Vila Martín, graduado en Biología por la Universidad de Valencia, ha realizado bajo su dirección la Tesis Doctoral titulada «***Neural circuits for social recognition in*** *mice: a neuroanatomical, behavioral and electrophysiological study*», y consideramos que reúne las condiciones necesarias para optar al grado de Doctor.

Y para que conste, en cumplimiento de la legislación vigente, firmamos el presente certificado:

En Valencia a 19 de enero de 2024

VICENT MANUEL\| TERUEL\|MARTI 2024.01.26 18:20:51 +01'00'

Dr. Vicent Teruel Martí

ENRIQUE\| LANUZA\| NAVARRO Firmado digitalmente por ENRIQUE\|LANUZA\| NAVARRO Fecha: 2024.01.26 20:41:37 +01'00'

Dr. Enrique Lanuza Navarro

"Los halagos de la vanidad, las efusiones del instinto, las caricias de la fortuna, palidecen ante el soberano placer de sentir cómo brotan las alas del espíritu y cómo, al compás del esfuerzo, superamos la dificultad y rendimos a la esquiva naturaleza."

Santiago Ramón y Cajal. Los tónicos de la voluntad.

ACKNOWLEDGEMENTS

Escucho que este periodo de la vida científica es desagradable, que la etapa doctoral es una condena autoimpuesta que se debe llevar con penitencia y desasosiego. Supongo que la fortuna ha hecho que desde mis ojos se viera precisamente lo contrario. Los que me conocen saben, sin embargo, que no me gusta atribuir virtud a la suerte. Las virtudes son menester de los seres humanos, y tengo la certeza de que éstos han sido los responsables de mi desfigurada, pero agraciada, visión de la realidad. Por ello, quiero agradecer esta buena suerte de lentes que han sostenido delante de mis ojos.

A Enrique Lanuza. Conocí la ciencia cuando atravesé la puerta de su despacho hace casi siete años. Ha sido mi primer mentor, y a su lado he aprendido las ideas y la técnica que me han hecho el profesional que soy hoy. Ha hecho que cada hipótesis enrevesada, cada experimento fallido y cada resultado indiscutible parecieran simples, acertados y rebatibles. Sin embargo, esto no es ni de lejos lo que destacaría de su carácter. De él me llevo otra recompensa más importante, tener claro mi objetivo en la vida. Mi principal objetivo en la vida es que las personas hablen de mí cuando estoy ausente como hablan de él cuando lo está. Es una buena persona, y desde mi humilde opinión, con la que seguro él coincidirá, es el mejor elogio que se le puede decir a nadie.

A Vicent Teruel. Redescubrí lo que es ser científico de su mano. Conocí la ambición del que ha abierto su propio camino, llevando al resto con él. Es por abrir su propio camino por lo que despierta mi admiración. Es por llevar al resto consigo, que delante de una tormenta todo el mundo mira hacia él para no estrellar los barcos contra la costa. Y debe ser ardua la tarea del faro, incansable y solitaria. Me mataría si leyera que el símil que le pertoca hace referencia al mar, y no a la montaña. Siempre he encontrado un modelo en su persona y vida, y deseo que el tiempo me permita seguir por sendas científicas iguales, sino mejores, a las que hemos caminado juntos durante esta etapa.

A Mario. Mi primer compañero de laboratorio. Nos sobró tiempo para hacernos buenos amigos, y a él siempre le sobraba tiempo para ayudar en cualquier tarea, como hacen los buenos amigos. Con él crecí enormemente, tanto literal como figuradamente. Aún conservo aquel poema que escribió cuando conocí y me enamoré de Paula. Y conservo en la cabeza la voz que repetía insistentemente que podía una más, después de haber podido otra más. Como toda persona controvertida, héroe y villano a la vez, pero como todo buen amigo, una guarida donde crecer.

A Anna Teruel. Entró como una revolución en el laboratorio. Después del primer paso de una inmuno, un paso muy corto, ya conocía su vida como si llevase en ella años. Y después de llevar en ella años, y siempre con su beneplácito, nos podemos llamar amigos. La revolución que supuso su llegada apuntó alto, y puedo decir que es actriz protagonista del científico que soy ahora. Además de aquella mala manía del perfeccionismo, me contagió de un extraño gusto por subir montañas. Y aprendí que las montañas y las amigas no se mueven, siempre están ahí cuando las necesitas. Algo me dice que nuestros caminos científicos se volverán a juntar en algún momento, pero debo reconocer que no me preocupa, porque como me ha enseñado ella, las montañas y las amigas siempre están ahí cuando las necesitas.

A Camila. Fue la primera y la última compañera que llegar, ambas a la vez. Y con su llegada formamos un equipo de ensueño. Se requiere un singular don para escuchar los desvaríos del que habla poco. Me sorprende el poco tiempo que se necesita para crear una amistad tan sólida y real. Me temo que la lealtad es un pago demasiado generoso como para necesitar dedicarle más tiempo. Si bien la lealtad es la moneda más valiosa, se pagó con muchas otras. Asumo que la curiosidad nos

llevará a practicar más deportes anómalos o a hacer más viajes interminables sin sentido, o quizás la vida ponga distancia. Siguiendo la definición de amistad que me ha enseñado tengo claro que ambas posibilidades concluyen en el mismo punto.

A Esteban. Extraño ser. Al llegar a la primera clase de máster, tarde, le vi y me senté a su lado, así que asumo que yo tampoco debo ser demasiado normal. Pudimos haber compartido mucho más científicamente, pero las circunstancias no lo permitieron. Sí que pudimos hacerlo a nivel personal, y siempre ha tenido la habilidad de sacarme una sonrisa con algún chascarrillo. Y de justo lo contrario.

A María Sancho y Lorena. Desgraciadamente llegaron al final. Ojalá hubieran aparecido mucho antes. Incombustibles, siempre dispuestas a ayudar y escuchar mis delirios científicos y personales. Se puede causar mucho impacto positivo en la vida de una persona en poco tiempo, y espero haber causado yo en la suya un ápice de lo que ellas en la mía.

A Elena, María Abellán, Sergio, Ceci, Jose, Joana, Ana Cervera, Sylwia, Patrick, Gniewosz, Gaba, Anna y Tomasz Blasiak.

A mis amigos, Juan Fran, Héctor, Laura, Jenni, Samu, María, Fran, Riki. Los defensores de la alegría y la imperfección. Los niños de abajo, con los pantalones rotos por las rodillas. Los que no se rindieron, ni cedieron, en las malas ocasiones, ni dejaron de disfrutar de las buenas. Estuvieron antes o estarán después de esta etapa, pero todos han llevado la amistad a un nivel superior. Prácticamente han sido mi familia. Y nos quedan muchas ocasiones, de las buenas.

A mis padres. No alcanzo a distinguir si este es el ascensor del que nos habían hablado a los tres, pero tiene buen aspecto. Debo confesar que no tengo la menor idea de qué hago aquí, constantemente me ronda en la cabeza que yo pertenezco a otro lugar. Supongo que debe ser cuestión de cabezonería y de esfuerzo. Cabezonería, la mía; esfuerzo, el suyo; claro. Durante esta etapa ha habido que sortear muchos obstáculos, algunos más terrenales, otros más funestos, y durante todo momento no han dejado de protegerme a mí por encima de sí mismos. Eso es lo que imagino que me habrá traído a este inhóspito lugar, a hacer cosas que les son ajenas, para sonreír con ilusión mientras se las explican. Espero algún día poder compensar todo ese esfuerzo.

A Paula. Mi compañera de vida. Manantial de ilusión y esperanza, que hace comprender al resto que mientras quede algo de vida merece la pena seguir luchando. Que el ser humano puede ser bueno por naturaleza, y que cuidar es la forma más pura de amor que existe. Me ha enseñado que en las pequeñas cosas y los gestos diarios residen las pruebas más importantes que se deben enfrentar. Durante todos estos años no he pensado que el mundo pudiera ser un lugar cruel, gracias a que ella me sacaba de él. Me asusta pensar la distancia que hemos recorrido para llegar a este punto, el esfuerzo que hemos hecho para llegar hasta aquí. Hemos evolucionado como compañeros, dándonos igual el tiempo y la distancia, hemos sorteado cada dificultad. Si de algo puedo estar convencido, es de que estos caminos ya no se pueden separar.

Humildes seres humanos, que piensan que lo que obtengo de esta etapa es una tesis doctoral, y no se dan cuenta de que esa es la recompensa menos valiosa que me llevo.

ABSTRACT

Rodents are macrosmatic animals, primarily relying on their keen sense of olfaction to perceive dynamic changes in their environment. The olfactory sensory system in rodents divides into two anatomical divisions: the main olfactory system and the accessory, or vomeronasal, olfactory system. The main olfactory system is responsible for gathering general information about volatile chemicals in the animal's surroundings, while the vomeronasal olfactory system specializes in detecting and processing information about the status of other individuals.

The study of vomeronasal information in mice highlights the intricate relationship between olfactory cues and social behaviors. Mice utilize vomeronasal chemosignals to facilitate social interactions like territorial marking and individual recognition. These signals are rich in biological significance, influencing behaviors such as aggression, motherhood, and territoriality. Territorial behavior involves urine marking to establish territory boundaries, where scents play a vital role in deterring intruders. The individuality code of these urine marks is attributed to major urinary proteins, which vary in concentration and composition between individuals.

The individual recognition mechanism in mice, essential for adapting to social hierarchies and navigating territorial spaces, is encoded in these urine chemical patterns. Considering the role of major urinary proteins in spatial learning and individual identity encoding and the involvement of the amygdala and hippocampal formation in processing vomeronasal and spatial information, respectively, the existence of an anatomical amygdalar-hippocampal pathway becomes imperative for integrating these particular types of information.

The primary hypothesis of this doctoral dissertation posits that vomeronasal chemosignals act as a unique identity barcode that is discernible by other conspecifics. This chemical barcode is encoded in the chemosensory amygdala and integrated into a comprehensive multisensory hippocampal spatial map. To explore this hypothesis, we employed a multifaceted methodological approach, combining tract-tracing, behavioral, histological, and electrophysiological techniques, complemented by a diverse array of analytical methods.

We delineated a neuroanatomical pathway that putatively transmits vomeronasal information to the hippocampal formation. In the circuit we outlined, vomeronasal information captured by the VNO is conveyed to the AOB, which subsequently transmits this information through glutamatergic projections to the chemosensory amygdala. This information undergoes further processing in cortical-like structures of the chemosensory amygdala, including the PMCo, ACo, NLOT, and CxA. Notably, the PMCo demonstrates significant connectivity with the hippocampal formation, sending direct glutamatergic projections to the ventral hippocampal CA1 and indirectly connecting to the dorsal hippocampal CA1 via glutamatergic projections to a specific subset of reelin-positive neurons in the dLEnt's layer II. In addition, the dLEnt establishes reciprocal glutamatergic connections with these cortical-like amygdaloid structures.

The presence of a direct and an indirect pathway for vomeronasal information flow to the hippocampus, which share overlapping neuronal engagement in the PMCo, in conjunction with the positive excitatory feedback between PMCo and dLEnt, indicates that this amygdalar-entorhinal-hippocampal pathway operates under attractor dynamics and signal amplification mechanisms.

To functionally evaluate this neuroanatomical pathway, we conducted a series of behavioral tests followed by measurements of neuronal activation in the various nodes comprising the pathway. We designed an olfactory-vomeronasal behavioral

paradigm wherein female mice were exposed to male-derived urine or the neutral odorant citralva. This experiment uncovered a female preference for male urine and increased neuronal activation in most pathway nodes. The neural response of these nodes to such stimuli demonstrated remarkably similar activation patterns, indicating a coordinated reaction to stimuli exposure. Furthermore, females exposed to male-derived urine constituted the primary source of neuronal activation variance elicited in the behavioral paradigm. This functional assessment indicates that the amygdalar-entorhinal-hippocampal pathway serves as the neural substrate for the transmission and integration of vomeronasal information into the hippocampal formation.

As the animal's territorial environment is dynamic and ever-changing, we devised a behavioral paradigm that incorporated the spatial rearrangement of male landmarks. The spatial reorganization of male-derived stimuli, designed to mimic a reconfiguration of the female's territory, provokes a remapping behavioral response. This response specifically modifies neuronal activation in the MEnt-dorsal CA1 segment, indicating that the encoding of the "what" and "where" components of episodic memory is compartmentalized within this pathway.

This remapping behavioral response, triggered by spatial changes in male-derived stimuli, is not observed when similar spatial modifications are applied to inanimate objects. When comparing neuronal activation following the spatial rearrangement of both item types, it becomes evident that the nuclei along the direct and indirect pathways show heightened activation in response to spatial changes in conspecific stimuli. Conversely, spatial changes in objects predominantly activate the MEnt and dorsal CA3 regions of the hippocampus. These observations suggest that the pathway is specifically engaged in recognizing social information from conspecifics, thus encoding the "who" subcomponent of episodic memory, namely the individual's identity.

Drawing from our tract-tracing and functional histology experiments, we conclude that the amygdalar-entorhinal-hippocampal pathway is the neural substrate for transmitting and integrating vomeronasal information into the hippocampal formation. Within this pathway, the PMCo is neuroanatomically pivotal. Therefore, we hypothesize that this cortical amygdaloid structure might be functioning as a decoder of the chemical patterns found in urine into neural codes representing individual identity, acting as a barcode identity reader.

To evaluate this hypothesis, we conducted in vivo extracellular electrophysiological recordings in the PMCo using a head-fixed system. In this setup, the animal was systematically exposed to a series of diverse conspecific stimuli across 10 consecutive trials. We subjected the female mice to a range of stimuli, including urine from two different males, a synthetic mixture of these males' urines, urine from one male countermarked over the others, and the own urine of the female being studied. These final two scenarios are designed to shed light on how complex natural phenomena like countermarking and self-recognition are processed in the mouse brain.

Tensor decomposition analysis uncovered intricate activity patterns in PMCo neurons in response to urine from different individuals. These patterns include neurons that react to a wide array of stimuli and those that specifically activate in response to a particular stimulus. Such findings suggest that within the PMCo, a dual mechanism operates: one that generalizes and adapts to different stimuli, and another geared towards precise and unequivocal recognition. This double-sloped approach supports adaptive behavioral outcomes, allowing for broad pattern recognition and ensuring distinct individual identification.

On the other hand, examining the PMCo's global neural activity through CEBRA spatial embedding revealed that the PMCo displays unique global activity patterns corresponding to each stimulus from different conspecifics. This suggests its capacity for hierarchically distinguishing these stimuli based on their chemosensory properties. Changes in activity patterns arise following repeated exposures to

the same stimulus, suggesting adaptive processes such as habituation or sensitization. Moreover, biological phenomena like countermarking and self-recognition are found to induce distinct activity patterns in the PMCo.

These findings collectively indicate that the amygdalar-entorhinal-hippocampal pathway is functionally involved in vomeronasal-dependent individual recognition. Within this pathway, the PMCo acts as the individual identity decoder, transmitting this information to the hippocampus for integration into complex spatial memories.

CONTENTS

List of Abbreviations xvii
1 INTRODUCTION 1
1.1 The olfactory system. 1
1.1.1 The organs of olfaction. 1
1.1.2 The olfactory bulbs. 2
1.1.3 The chemosensory amygdala. 3
1.1.4 The posteromedial cortical amygdaloid nucleus. 5
1.2 Vomeronasal information. 6
1.2.1 Territorial behavior. 6
1.2.2 Individual recognition in mice. 6
1.3 The hippocampal formation. 7
1.3.1 Hippocampal circuitry. 8
1.3.2 Navigating in space. 11
1.3.3 Processing social memory. 12
2 GENERAL HYPOTHESIS AND OBJECTIVES 13
3 MATERIALS AND METHODS 15
3.1 Experimental subjects. 15
3.2 Tract-tracing methods. 15
3.2.1 General surgical procedure. 15
3.2.2 Tracer injections. 16
3.2.3 Histology. 18
3.2.4 Image acquisition and processing. 19
3.3 Behavioral tests and neuronal activation study techniques. 20
3.3.1 Urine vs. citralva exposure test. 20
3.3.2 Social stimuli spatial manipulation test. 21
3.3.3 Social vs. object spatial manipulation test. 22
3.3.4 Behavioral analysis. 22
3.3.5 Histological processing. 24
3.3.6 Image acquisition and cell quantification. 24
3.3.7 Principal component analysis. 25
3.4 In vivo electrophysiological procedures. 25
3.4.1 Headbar implantation surgery. 25
3.4.2 Head-fixed setup implementation. 25
3.4.3 Habituation and exposure protocols. 26
3.4.4 Signal acquisition. 27
3.4.5 Data analysis. 28
3.4.6 Histological verification of the recording sites. 34
3.5 Statistical analysis. 35
4 RESULTS 37
4.1 Tract-tracing. 37
4.2 Behavioral tests and neuronal activation study. 48
4.2.1 Urine vs. citralva exposure test. 48
4.2.2 Social stimuli spatial manipulation test. 56
4.2.3 Social vs. object spatial manipulation test. 61
4.3 Single unit recordings in the PMCo. 67
5 DISCUSSION 75
6 CONCLUSIONS 85
Appendix 87
Resumen 89
References 97

LIST OF FIGURES

Figure 1 Anatomical organization of sensory neurons axonal projections in the main olfactory and vomeronasal systems. 2
Figure 2 Diagram of mouse olfactory circuits in lateral perspective. 4
Figure 3 General circuitry and connections of the hippocampal formation. 9
Figure 4 Experimental protocol of the urine vs. citralva exposure test. 20
Figure 5 Experimental protocol of the social stimuli spatial manipulation test. 21
Figure 6 Experimental protocol of the social vs. object spatial manipulation test. 22
Figure 7 Labels used to train the DLC neural networks both for the mouse and the arena. 23
Figure 8 Experimental layout illustrating the physical arrangement of the surgical and head fixation methods. 26
Figure 9 Timeline detailing the automated time-stamped exposure protocol. 27
Figure 10 Illustrative drawing of the tensor decomposition. 30
Figure 11 Representative example of the tensor decomposition. 31
Figure 12 Illustrative schematic of the methodology employed for the extraction of neuronal activity patterns. 32
Figure 13 Anterograde labeling in the chemosensory amygdala following a TBDA injection in the AOB. 38
Figure 14 Glutamatergic projection from the AOB to the PMCo's layer I. 39
Figure 15 The PMCo emits a dense glutamatergic projection to the CA1 of the ventral hippocampus as well as to both divisions of the Ent, the lateral and the medial. 40
Figure 16 The PMCo is indirectly connected to the CA1 of the dorsal hippocampus via a restricted population of reelin-positive cells in dLEnt layer II. 43
Figure 17 FG retrograde tracing confirms direct neuroanatomical connection between the dlEnt and the PMCo. 44
Figure 18 A subset of PMCo neurons exhibits dual projections to both the dLEnt and the ventral CA1 region of the hippocampus. 45
Figure 19 Beyond the perforant path, the dLEnt emits corticofugal glutamatergic projections to the PMCo. 47
Figure 20 Behavioral outcome of the urine vs. citralva exposure test. 49
Figure 21 Neuronal activation results of the urine vs. citralva exposure test. 50
Figure 22 Significant correlations between neuronal activation and behavioral outcome in the urine vs. citralva exposure test. 53
Figure 23 PCA reveals common c-Fos expression pattern in the amygdalar-entorhinal-hippocampal pathway. 56
Figure 24 Behavioral outcome of the social stimuli spatial manipulation test. 58
Figure 25 Neuronal activation results of the social stimuli spatial manipulation test. 59
Figure 26 Significant correlations between neuronal activation and behavioral outcome in the social stimuli spatial manipulation test. 61

Figure 27 Behavioral outcome of the social vs. object spatial manipulation test. 63
Figure 28 Neuronal activation results of the social vs. object spatial manipulation test. 65
Figure 29 Significant correlations between neuronal activation and behavioral outcome in the social vs. object spatial manipulation test. 66
Figure 30 Raw rastergrams of the responses of selected neurons in presence different stimuli 67
Figure 31 Tensor decomposition of the firing rates for particular neurons. 68
Figure 32 Clustergram for the neuronal activity in response to urines. 69
Figure 33 CEBRA reveals that the PMCo can differentiate between various types of urine, indicating a time-related influence in the label trial. 71
Figure 34 Dynamic representation of CEBRA embeddings across multiple trials and their decoding accuracy over time. 73

LIST OF TABLES

Table 1 Total number of animals used throughout the experimentation. 15
Table 2 CEBRA labels. 33
Table 3 Average decoding accuracy among trials. 73

LIST OF ABBREVIATIONS

AAV Anterior amygdaloid area ventral division

ABC Avidin-biotin complex

ACo Anterior cortical amygdaloid nucleus

AhiAL Amygdalohippocampal area anterolateral division

AHiPM Amygdalohippocampal area posteromedial division

AOB Accessory olfactory bulb

AON Anterior olfactory nucleus

aot *Accessory olfactory tract*

AP Anteroposterior

APir Amygdalopiriform transition area

aPir Piriform cortex anterior division

BAOT Bed nucleus of the *accessory olfactory tract*

BDA Biotinylated dextran amines

BLA Basolateral amygdaloid nucleus anterior division

BLP Basolateral amygdaloid nucleus posterior division

BMA Basomedial amygdaloid nucleus anterior division

BST Bed nucleus of the *stria terminalis*

BSTmpm Bed nucleus of the *stria terminalis* medial posteromedial division

CA1 Field *cornu ammonis* 1 of the hippocampus

CA2 Field *cornu ammonis* 2 of the hippocampus

CA3 Field *cornu ammonis* 3 of the hippocampus

cAcb Nucleus accumbens core

CANDECOMP Canonical decomposition

CP Canonical polyadic

CPu Caudate putamen (striatum)

CxA Cortex-amygdala transition area

DAB Diaminobenzidine

DG Dentate gyrus

DGlb Dentate gyrus lower blade

DGub Dentate gyrus upper blade

dLEnt Dorsal aspect of the lateral entorhinal cortex

DV Dorsoventral

Ect Ectorhinal cortex

Ent Entorhinal cortex

FG FluoroGold

GAD 65/67 Glutamic acid decarboxylase 65/67

GlA Accessory olfactory bulb glomerular cell layer

Gnd Electrical ground

GrA Accessory olfactory bulb granule cell layer

IHC Immunohistochemistry

kNN K-Nearest Neighbors

LEnt Lateral entorhinal cortex

lot *Lateral olfactory tract*

LTP Long-term potentiation

Me Medial amygdaloid nucleus

MeAD Medial amygdaloid nucleus anterodorsal division

MEnt Medial entorhinal cortex

MePD Medial amygdaloid nucleus posterodorsal division

MePV Medial amygdaloid nucleus posteroventral division

MiA Accessory olfactory bulb mitral cell layer

ML Mediolateral

MOB Main olfactory bulb

MOE Main olfactory epithelium

MUP Major urinary protein

NDS Normal donkey serum

NGS Normal goat serum

NHS Normal horse serum

NLOT Nucleus of the *lateral olfactory tract*

opt *Optic tract*

OT Olfactory tubercle

PARAFAC Parallel factors

PB Phosphate buffer

PC Principal component

PCA Principal component analysis

Pir Piriform cortex

PLCo Posterolateral cortical amygdaloid nucleus

PMCo Posteromedial cortical amygdaloid nucleus

pPir Piriform cortex posterior division

PRh Perirhinal cortex

Py Pyramidal cell layer

Reel Reelin

Ref Electrical reference

ROI Region of interest

RRX Rhodamine Red-X

S Subiculum

sAcb Nucleus accumbens shell

SLM *Stratum lacunosum-moleculare*

SO *Stratum oriens*

SR *Stratum radiatum*

st *Stria terminalis*

SuM Supramammillary nucleus

TB Tris buffer

TBDA Tetramethylrhodamine and biotin-conjugated dextranamines

TBS Tris-buffered saline

V1R Vomeronasal receptor type I

V2R Vomeronasal receptor type II

VGLUT1 Vesicular glutamate transporter 1

VNO Vomeronasal organ

VTA Ventral tegmental area

WGA Wheat germ agglutinin

1 INTRODUCTION

1.1 THE OLFACTORY SYSTEM.

Environment perception in living organisms is a dynamic and active mechanism heavily reliant on each species' sensory capabilities. Sensory systems have evolved to actively seek, capture, and process the dynamic changes in the environment. This environmental input is crucial, as it provides insights into the external circumstances surrounding every organism. This continuous stream of environmental information is essential for the individual to develop appropriate behavioral strategies that are vital for survival and reproduction success.

Most terrestrial vertebrates possess two primary olfactory systems, a feature particularly significant for macrosmatic species, where olfaction is the dominant sense. Rodents, which fall under this category, are the most frequently used animal models in global research (Robinson *et al.*, 2019). Rodents' olfactory systems are finely adapted to identify a broad spectrum of chemicals in their environment, enabling them to perceive and dynamically respond to their surroundings (Trinh and Storm, 2004).

The olfactory sensory system in rodents divides into two anatomical divisions: the main olfactory system and the accessory, or vomeronasal, olfactory system. The main olfactory system provides general information about volatile chemicals surrounding the animal (Buck, 2000), whereas the accessory olfactory system takes on the detection and processing of volatile and non-volatile chemicals of high biological relevance (Leinders-Zufall *et al.*, 2000; Mucignat-Caretta, 2010). Broadly speaking, the main olfactory system identifies the environment and its resources, while the accessory olfactory system specializes in detecting information related to other individuals.

1.1.1 The organs of olfaction.

The olfactory system meets the dual requirement for general odor sensing and specific individual detection by initially segregating those functions in different sensory neurons and neural pathways (Halpern, 1987; Hildebrand and Shepherd, 1997).

The sensory cells of the main olfactory system are located in the main olfactory epithelium (MOE), a specialized pseudostratified epithelial tissue that lines the dorsal part of the nasal cavity, the nasal septum, and the superior turbinate bones (Figure 1). This cell layer is highly convoluted, forming turbinates to increase the surface area available for odor detection. This epithelium presents diverse cell types, such as basal cells, supporting cells, and the olfactory sensory neurons, responsible for transducing olfactory chemical information into neural signals. These bipolar neurons are characterized by the expression of odorant receptors on their apical pole non-motile cilia (Hussain, 2011). Odorant receptors are G-protein-coupled seven-transmembrane domain proteins (Buck and Axel, 1991). The mouse genome encompasses 1,141 intact genes for odorant receptors (Barnes *et al.*, 2020). Typically, a mature olfactory sensory neuron expresses just a single gene for these receptors (Malnic *et al.*, 1999), and specifically one allele of that gene (Chess *et al.*, 1994). The receptor gene expressed by an olfactory sensory neuron determines the types of odorants it can detect (Bozza *et al.*, 2002) and the specific glomerulus its axon will target (Mombaerts *et al.*, 1996). Therefore, the expressed receptor gene shapes the functional and anatomical identity of the olfactory sensory neuron, but not its location along the epithelium (Zapiec and Mombaerts, 2020). After passing through the

cribriform plate, the axons of the olfactory sensory neurons reach their destination in the olfactory bulb, where they synapse with the dendritic processes of mitral cells located within the glomeruli of the main olfactory bulb (MOB).

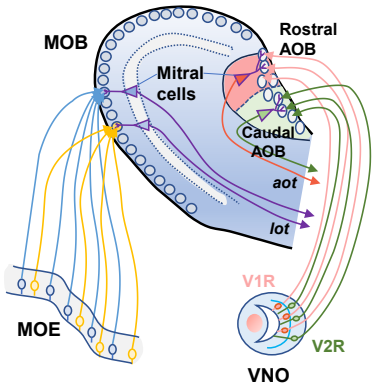

Figure 1: Anatomical organization of sensory neurons axonal projections in the main olfactory and vomeronasal systems. Schematic representation of olfactory and vomeronasal sensory neurons extending their axons to the MOB and AOB, respectively. Olfactory sensory neurons, which express the same olfactory receptor, are represented in two different populations (blue and yellow). These neurons project their axons to a single glomerulus in each half of the MOB. Within the MOB, each mitral cell extends a single apical dendrite that innervates one of these glomeruli. Vomeronasal sensory neurons located in the apical part of the VNO express V1R and project their axons to the rostral portion of the AOB (pink). Sensory neurons situated in the basal part of the VNO express V2R and extend their axons to the caudal division of the AOB (green). Upon reaching the AOB, individual sensory axons can divide to terminate in multiple glomeruli. Within the AOB, each mitral cell can extend its apical dendrite into several glomeruli.

In parallel, the accessory olfactory system senses non-volatile and volatile chemical signals of high biological relevance via sensory neurons housed in the Jacobson's or vomeronasal organ (VNO) (Figure 1). The VNO is a paired tubular diverticulum located at the vomer bone, in the ventral portion of the proximal nasal septum. This organ features an epithelium composed of two cell types. Situated in the VNO's apical layer, Type I vomeronasal sensory cells express Type I vomeronasal receptors (V1R) (Dulac and Axel, 1995) along with the G protein's $G_{\alpha i2}$ subunit (Berghard and Buck, 1996). On the other hand, located in the VNO's basal layer, Type II vomeronasal sensory cells exhibit Type II vomeronasal receptors (V2R) (Herrada and Dulac, 1997; Matsunami and Buck, 1997; Ryba and Tirindelli, 1997) and the $G_{\alpha o}$ subunit of the G protein (Berghard and Buck, 1996). These VNO sensory cells project to the accessory olfactory bulbs (AOB) topographically. Type I neurons in the apical VNO project to the anterior part of the AOB whereas the basal VNO's Type II neurons direct their axonal projections towards the posterior division of the AOB (Jia and Halpern, 1996; Jia *et al.*, 1997). Upon reaching the AOB, individual axons can divide to terminate in multiple glomeruli (Larriva-Sahd, 2008). Therefore, unlike the MOB, axons of sensory neurons expressing a given receptor form multiple glomeruli in the AOB (Belluscio *et al.*, 1999; Rodriguez *et al.*, 1999). Besides their morphological distinctions, vomeronasal sensory neurons utilize a transduction mechanism that differs from that of olfactory sensory neurons, a factor that underpins their functional segregation (Lucas *et al.*, 2003).

1.1.2 The olfactory bulbs.

The olfactory bulbs are part of the forebrain and sit on the underside of the frontal lobe. Axons originating from the sensory neurons in the MOE and the VNO traverse

horizontally along the outermost olfactory nerve layer of the olfactory bulbs before entering into the glomerular layer of the MOB or the AOB, respectively.

Within the MOB glomeruli, sensory neurons establish axodendritic synapses with projection neurons, including mitral and tufted cells, as well as engage in synaptic interactions with periglomerular interneurons. Additionally, olfactory bulb projection neurons form reciprocal dendrodendritic synapses with the periglomerular cells (White, 1972). Mitral and tufted cells are glutamatergic projection neurons that share similar morphological characteristics. They present a solitary primary dendrite that projects to a single glomerulus and secondary dendrites that extend within the external plexiform layer, located below the glomerular layer (Macrides and Schneider, 1982; Mori *et al.*, 1983). In the external plexiform layer, mitral and tufted cells' secondary dendrites engage in dendrodendritic synapses with granule cells, a distinct interneuron type (Rall *et al.*, 1966). The external plexiform layer houses most tufted cell somata, whereas the mitral cell somata reside in a different layer beneath the external plexiform layer, the mitral cell layer. Below the mitral cell layer lies the granule cell layer, the MOB's most voluminous layer, consisting of granule cells' somata (Schneider and Macrides, 1978). The internal plexiform layer, a narrow layer between mitral and granule cell layers, contains the axonal collaterals of tufted cells (Liu and Shipley, 1994). The MOB projection neurons send their axons via the lateral olfactory tract (*lot*) to the brain (Figure 2).

The AOB lies in the posterodorsal region of the MOB. The AOB mitral cells receive the synaptic inputs from vomeronasal neurons in the mitral cell layer, which, as in the MOB, is located on the region's surface (Barber *et al.*, 1978). As noted in the previous section, axons of vomeronasal sensory neurons expressing a given receptor form multiple glomeruli in the AOB (Belluscio *et al.*, 1999; Rodriguez *et al.*, 1999). AOB mitral cells are situated beneath the glomeruli, in the mitral cell layer. These projection neurons are characterized by their multiple primary dendrites, which branch out to innervate several glomeruli (Takami and Graziadei, 1991). Their secondary dendrites are stretched into the layer beneath the glomeruli, establishing dendrodendritic connections with granule cells that are located in the AOB deep granule cell layer (Yonekura and Yokoi, 2007). Mitral neuron axons leave the AOB as bundles and proceed through a layer interspersed between the somata of mitral and granule cells. They ultimately gather around the *lot*, forming the accessory olfactory tract (*aot*) (Figure 2). This axon bundle is responsible for transporting vomeronasal information to higher brain regions (von Campenhausen and Mori, 2000).

1.1.3 The chemosensory amygdala.

Despite their initial anatomical segregation, the main and accessory olfactory systems function synergistically, allowing animals to display appropriate behaviors (Pardo-Bellver *et al.*, 2017). This interaction is made evident through anatomical findings that show convergence of inputs from the main and accessory olfactory bulbs in specific amygdalar regions (Gutiérrez-Castellanos *et al.*, 2010). Considering also the ability of the MOE to detect pheromones (Lin *et al.*, 2004) and the detection of volatile odorants by both olfactory and vomeronasal epithelia (Trinh and Storm, 2004), we are drawn towards a unified hypothesis of olfactory information processing. The amygdaloid areas acting as convergence points for both types of information likely represent the anatomical basis of this interaction.

The amygdala has been traditionally divided into the central amygdala, the basolateral complex, and the chemosensory or corticomedial amygdala (Martínez-Marcos, 2009). The chemosensory amygdala encompasses all structures that directly receive olfactory inputs from the projection cells of the MOB and the AOB. This categorization yields three terms: "olfactory amygdala" for areas with inputs only from the MOB, "vomeronasal amygdala" for those receiving inputs just from

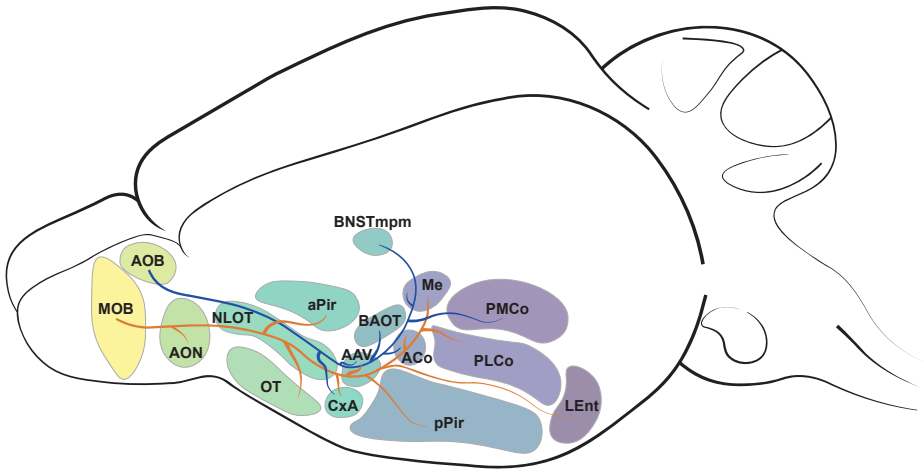

Figure 2: Diagram of mouse olfactory circuits in lateral perspective. Main olfactory pathway (*lot*) is shown in orange and vomeronasal pathway (*aot*) in blue.

the AOB, and "mixed chemosensory amygdala" for regions where inputs from both the MOB and AOB converge (Gutiérrez-Castellanos *et al.*, 2010) (Figure 2).

Following this nomenclature, the olfactory amygdala encompasses the posterolateral cortical nucleus (PLCo) and the amygdalo-piriform transition area (APir). These areas are located close to the lateral entorhinal cortex (LEnt) and are recognized for their extensive connectivity. The PLCo gives rise to connections to the ventral striatum (Ubeda-Bañón *et al.*, 2007), to the central extended amygdala (Canteras *et al.*, 1992), to the hippocampal formation, apart from intra-amygdaloid projections targeting the lateral nucleus (Majak and Pitkänen, 2003). On the other hand, the APir is the recipient of significant thalamic afferents from the midline nuclei and the parabrachial nucleus associated with taste and visceroception. As the PLCo, the APir projects to the central amygdala and the ventral striatum (Brog *et al.*, 1993; McDonald *et al.*, 1999; Jolkkonen *et al.*, 2001).

The vomeronasal amygdala comprises the posteromedial cortical nucleus (PMCo) and the posteromedial part of the medial bed nucleus of the *stria terminalis* (BSTmpm). A detailed PMCo description will be provided in the following section. Regarding the BSTmpm, vomeronasal inputs to this region originate from the anterior section of the AOB, transmitting information from neurons in the vomeronasal organ that express V1R (Mohedano-Moriano *et al.*, 2007). This structure establishes connections with the hypothalamus and brainstem and is believed to play a role in defensive and reproductive behaviors triggered by vomeronasal stimuli (Dong and Swanson, 2004).

It should be noted that the vast majority of chemosensory amygdala nuclei belong to the mixed chemosensory amygdala category, receiving inputs from both the MOB and the AOB. For ease of description, we will distinguish between nuclei predominantly influenced by olfactory input and those with a higher vomeronasal influence (Gutiérrez-Castellanos *et al.*, 2010).

The structures of the mixed chemosensory amygdala with olfactory predominance are the anterior cortical nucleus (ACo), the cortex-amygdala transition zone (CxA), and the nucleus of the lateral olfactory tract (NLOT). The ACo maintains connections with the olfactory system, basal forebrain, hypothalamus, and various amygdala regions, including the chemosensory, central, and basomedial amygdala. It has been suggested to be involved in emotional learning processes involving chemosensory stimuli (Cádiz-Moretti *et al.*, 2017). The CxA exhibits limited intratelencephalic connections but presents notable inputs from the amygdala and the

ventral tegmental area (VTA), suggesting a role in processing biologically rewarding olfactory information (Cádiz-Moretti *et al.*, 2016). Likewise, the NLOT displays notably robust bilateral efferences to the basolateral nucleus of the amygdala and the ventral striatum, indicating a potential involvement in the reward processing of chemosensory stimuli (Santiago and Shammah-Lagnado, 2004).

The mixed chemosensory amygdala with vomeronasal predominance encompasses the medial amygdala (Me), the bed nucleus of the accessory olfactory tract (BAOT), and the ventral part of the anterior amygdaloid area (AAV). The Me stands as the most thoroughly investigated region within the chemosensory amygdala, largely due to its association with numerous behavioral phenomena such as motherhood, aggression, sexual behavior, social recognition, and the establishment of social hierarchies (Unger *et al.*, 2015; McCarthy *et al.*, 2017; Abellán-Álvaro *et al.*, 2022). The Me exhibits strong interconnectivity with the chemosensory amygdala, moderate connections to the basolateral amygdaloid complex, and significant outputs to the bed nucleus of the *stria terminalis* (BNST) and hypothalamus (Pardo-Bellver *et al.*, 2012). This area is commonly divided into three subdivisions with their own functional features: anterior medial amygdala (MeA), posterodorsal medial amygdala (MePD), and posteroventral medial amygdala (MePV). Conversely, there is limited knowledge regarding the functionality and connectivity of the BAOT and AAV, as these structures have been the subject of few studies.

1.1.4 The posteromedial cortical amygdaloid nucleus.

In the present work, we will focus on the PMCo guided by the insights and findings garnered during the experimental process. This nucleus is located at the caudal end of the cortical amygdalar area, lying in the ventral part of the mice encephalon. The PMCo is characterized by a distinctive three-layer structure. Layer I, or molecular layer, is the entry point for vomeronasal input from the *aot* (Winans and Scalia, 1970), along with other extra and intra-amygdalar inputs (Canteras *et al.*, 1992; Kemppainen *et al.*, 2002). Layer II is marked by a high density of small somata cells, while layer III, less dense in comparison, contains larger neurons with polymorphic shapes.

The PMCo is a sexually dimorphic nucleus (Vinader-Caerols *et al.*, 1998) that regulates different aspects of male copulatory behavior, including direct chemosensory investigation and the onset of sexual satiety (Maras and Petrulis, 2008). It is the only pallial derivative structure among the vomeronasal centers that receive substantial direct input from the AOB since the Me and the BNST are mainly of subpallial origin (Bupesh *et al.*, 2011a; Bupesh *et al.*, 2011b). Moreover, the PMCo lamination depends on reelin (Boyle *et al.*, 2011), which leads us to consider this nucleus as the primary vomeronasal cortex.

The PMCo exhibits extensive connectivity within the vomeronasal system, forming reciprocal connections with the AOB and other amygdalar structures. Additionally, its integration with the olfactory system is evidenced through connections with the piriform cortex, olfactory-responsive amygdalar nuclei, and the entorhinal cortex. The PMCo also engages in moderate interactions with the basomedial associative amygdala and the ventral hippocampus. Furthermore, a distinguishing feature of the PMCo is its zinc-enriched projections to the ventrolateral septum and ventromedial striatum. The specific nature of its intracortical connections, primarily with the olfactory cortex and hippocampus, coupled with cortico-striatal excitatory projections to the olfactory tubercle and septum, reinforces its hypothesized function as the primary vomeronasal cortex (Gutiérrez-Castellanos *et al.*, 2014).

1.2 VOMERONASAL INFORMATION.

"Vomeronasal stimuli" is a term that describes the set of chemosignals with high biological relevance detected by the VNO. These signals elicit innate and stereotyped responses in the animals that sense them, and those sensed by V2R are characteristically non-volatile and of high molecular weight (Brennan, 2001). While this definition might be somewhat oversimplified and the terminology could benefit from greater nuance, this general categorization is instrumental for a proper understanding of the topic to be addressed in this work.

This set of chemosignals include sexual pheromones (Kimoto *et al.*, 2005; Roberts *et al.*, 2010), signals indicative of predators (Pérez-Gómez *et al.*, 2015), illness-derived cues (Boillat *et al.*, 2015), signals linked to stress (Nodari *et al.*, 2008), and chemicals that trigger behaviors related to aggression (Chamero *et al.*, 2007; Chamero *et al.*, 2011), motherhood (Martín-Sánchez *et al.*, 2015), and territoriality (Hurst and Beynon, 2004).

1.2.1 Territorial behavior.

Numerous mammalian species utilize vomeronasal cues to signal territorial ownership, a different method from the visual or acoustic signals commonly employed in animal communication. Vomeronasal signals, in contrast to transient visual or auditory cues, are capable of being deposited in the environment as enduring scent marks. These scent marks retain their presence and relevance long after the emitting animal has left the area, effectively conveying information to conspecifics in the scent owner's absence. This form of communication is extensively employed by terrestrial vertebrates to demarcate and defend their territories (Gosling, 1982). Vomeronasal marks are ideally suited as reliable indicators of competitive ability, with most territorial mammals using them to mark their defended areas, ensuring that their scent marks predominate as a sign of their successful dominance over that territory (Rich and Hurst, 1998).

Male mice are highly territorial and use urine landmarks to demarcate their territories (Desjardins *et al.*, 1973; Hurst, 1990). When encountering marks from familiar or unfamiliar competitors, territory owners increase their scent marking rate in the immediate area, placing their urine close to their competitors' marks (Humphries *et al.*, 1999). These scent markings play a significant role in interactions with intruders. Intruders, upon detecting these cues, are less likely to challenge a male whose scent matches those in the territory (Gosling and McKay, 1990). Remarkably, when a small drop of the territory owner's fresh urine is added to an already-existing landmark, it increases the chances that intruders or lower-ranking mice will run away when they meet the territory owner. Conversely, the introduction of urine from a neighboring territory owner can decrease evasion and intensify challenges against the resident male, regardless of any previous direct aggressive interactions (Hurst and Beynon, 2004). The idea of a fine individual recognition mechanism in mice becomes necessary to explain this complex behavioral display.

1.2.2 Individual recognition in mice.

In their ability to distinguish between individuals, mice rely on individual-specific patterns of proteins present in urine, known as major urinary proteins (MUPs) (Hurst *et al.*, 2001; Nevison *et al.*, 2003). MUPs are secreted by both male and female mice. However, the concentration in adult male urine is typically around 20-40 mg/ml, which is approximately three to four times higher than that found in female urine (Beynon and Hurst, 2003). MUPs bind and stabilize the release of volatile organic compounds from urinary scent marks (Kwak *et al.*, 2013). Upon being deposited as a scent mark, the interaction of signaling volatiles with MUPs

significantly reduces the rate of scent mark evaporation, lengthening the time that the landmark can be perceived (Hurst *et al.*, 1998; Robertson *et al.*, 2001).

Female mice are more attracted to the scent of dominant than subordinate males when they are in estrus. During estrus, females increase their sensitivity to male urine MUPs by upregulating the expression of VNO receptors (Dey *et al.*, 2015). This exposure to male pheromones not only influences female olfactory preferences towards these substances but also accelerates their progression into puberty (Jouhanneau and Keller, 2013). Studies have observed that male mice in competitive environments tend to have an increased concentration of MUPs in their urine (Luzynski *et al.*, 2021). Furthermore, dominant males present an upregulation in the excretion of certain MUPs, such as the pheromone MUP20 (darcin) (Thoi *et al.*, 2019). Darcin is a predominantly male-expressed urinary protein that elicits place preference and a 14-day spatial learning in female mice (Roberts *et al.*, 2012).

The mouse reference genome encodes 21 MUPs, all species-specific. However, an individual does not express all of the 21 MUPs (Logan *et al.*, 2008). Instead, individual males present stable discrete subsets of 4-12 MUPs throughout their lifespan (Robertson *et al.*, 1997). Within this pattern of MUP expression lies the "barcode" for individual recognition, unique to each animal within the territorial space (Kaur *et al.*, 2014).

Considering that MUPs elicit spatial learning and are crucial for encoding individual identities within a spatial context, and acknowledging that vomeronasal information is processed by the amygdala while the hippocampal formation handles spatial information, it is imperative to posit the existence of an anatomical amygdalar-hippocampal pathway for the integration of vomeronasal and spatial information.

1.3 THE HIPPOCAMPAL FORMATION.

Since the early days of brain research, hippocampal formation has consistently held a position of profound interest in the scientific community. Santiago Ramón y Cajal (1893) laid the groundwork for the contemporary understanding of the hippocampal formation, meticulously detailing the layered arrangement of inputs on the apical dendrites of CA1 principal cells, an idea inspired and intrigued by their densely packed and orderly monolayer structure. Since the pioneering insights of Ramón y Cajal, the hippocampal formation has stood at the forefront of neuroscience, yielding some of the field's most revolutionary discoveries.

Within the realm of the hippocampal formation Kandel, Spencer and Brinley elucidated the nature of excitatory and inhibitory synapses (Kandel *et al.*, 1961; Kandel and Spencer, 1961; Spencer and Kandel, 1961a; Spencer and Kandel 1961b), Tim Bliss and Terje Lomo characterized long-term potentiation (Bliss and Lomo, 1973), first in vitro electrophysiological recordings were conducted on tissue slices (Schwartzkroin and Wester, 1975), and John O'Keefe, along with Edvard and May-Britt Moser, uncovered the brain's spatial mapping system (O'Keefe and Dostrovsky, 1971; O'Keefe, 1976; Fyhn *et al.*, 2004; Hafting *et al.*, 2005; Sargolini *et al.*, 2006). Adding to its scientific significance, the hippocampal formation has also been a focal point in clinical research, particularly in understanding the neural basis of Alzheimer's disease (Oddo *et al.*, 2003) and epilepsy (Menéndez de la Prida *et al.*, 2015). Characterized by its vulnerability to ischemic events, chronic stress, and degenerative processes (Bartsch and Wulff, 2015), along with the eternal debate on adult neurogenesis (Spalding *et al.*, 2013; Sorrells *et al.*, 2018), the hippocampus has been instrumental in advancing knowledge in neuroscience.

Despite the significant amount of research focusing on hippocampal formation, there seems to be a surprisingly limited number of studies addressing the impact of vomeronasal information on hippocampal spatial memory processes. Although seminal works exist in this field (Roberts *et al.*, 2012), they predominantly address

the behavioral dimension and fall short of analytically exploring the neural pathways engaged in individual recognition and vomeronasal-dependent spatial learning. Before delving into the above-mentioned neuroanatomical pathways, it seems appropriate to provide a general overview of the hippocampal atlas.

1.3.1 Hippocampal circuitry.

The hippocampal formation is a group of brain areas situated in the medial temporal lobe. It comprises the dentate gyrus (DG), the hippocampus proper (CA3, CA2, and CA1), the subicular complex, and the entorhinal cortex (Ent) (Andersen *et al.*, 2009). The foundations of hippocampal terminology were established by Santiago Ramón y Cajal (1893) and his disciple Lorente de Nó (1934), who meticulously delineated the borders, regions, and directionality of projections within the hippocampus using Golgi staining techniques. This formation is associated with a wide array of functions, including the formation and storage of memories, spatial navigation and representation, associative learning, the regulation of stress, and a significant role in emotional processing (Lisman *et al.*, 2017).

The hippocampal formation in rodents exhibits an elongated shape, beginning medially near the septum, extending dorsally towards the caudal end, and then curving laterally to descend along the temporal lobe. Its long and curved form is present across all mammalian orders and runs along a dorsal (septal)-to-ventral (temporal) axis, corresponding to a posterior-to-anterior axis in humans. The distinction between the dorsal and ventral hippocampus is intricate, arises from the curvature of the septotemporal axis, and carries significant implications for connectivity, functionality, and gene expression (Strange *et al.*, 2014). Apart from the longitudinal or septotemporal axis, we can identify an orthogonal transverse or proximo-distal (Laurent *et al.*, 2015; Yu *et al.*, 2020) and a radial or deep-superficial axis with their own topographical organization (Valero and Menéndez de la Prida, 2018). The radial axis of the hippocampus presents a somewhat non-intuitive layout, attributed to its nature as an inwardly folded cortex. In this structure, areas like the CA1 or the subiculum have their superficial zones facing the interior of the brain, whereas the deeper zones are more outwardly positioned adjacent to the cortex. To delve into the complex organization of the hippocampal formation, we embark on a comprehensive examination of its individual components.

The Ent is considered the starting point of the hippocampal circuit as the principal input and output structure of the hippocampal formation. This region is divided into the medial entorhinal cortex (MEnt) and the lateral entorhinal cortex (LEnt), terms that not only describe their anatomical positions but also hold significant implications for their functionality and connectivity (Steward and Scoville, 1976; Insausti *et al.*, 1997; Witter *et al.*, 2017). The MEnt displays cortical connectivity with the presubiculum, parasubiculum, retrosplenial cortex, and postrhinal cortex, which are all commonly recognized as part of the cortex's spatial processing domain. Conversely, the LEnt maintains robust connections with olfactory regions, the insular, medial- and orbitofrontal areas, as well as the perirhinal cortex. These regions are related with the processing of olfaction, object information, attention, and motivation (Witter *et al.*, 2000; Eichenbaum *et al.*, 2012; Knierim *et al.*, 2013).

The Ent comprises four cellular layers (II, III, V, and VI) and two plexiform layers (I and IV). Superficial cell layers II-III of the Ent form the primary projection to the hippocampus via the perforant and temporoammonic pathways. Within MEnt layer II, we find two distinct types of excitatory cells: a predominant population of reelin-positive stellate cells (grid cells typically belong to this cell type) and a smaller group of calbindin-positive pyramidal cells (Alonso and Klink, 1993; Gatome *et al.*, 2010; Ray *et al.*, 2014; Tang *et al.*, 2014). Meanwhile, MEnt layer III predominantly comprises pyramidal cells that do not express any markers found in layer II (Kitamura *et al.*, 2015). These projection neurons form a dense bundle of axons that penetrate through the subicular complex and the hippocampal fissure,

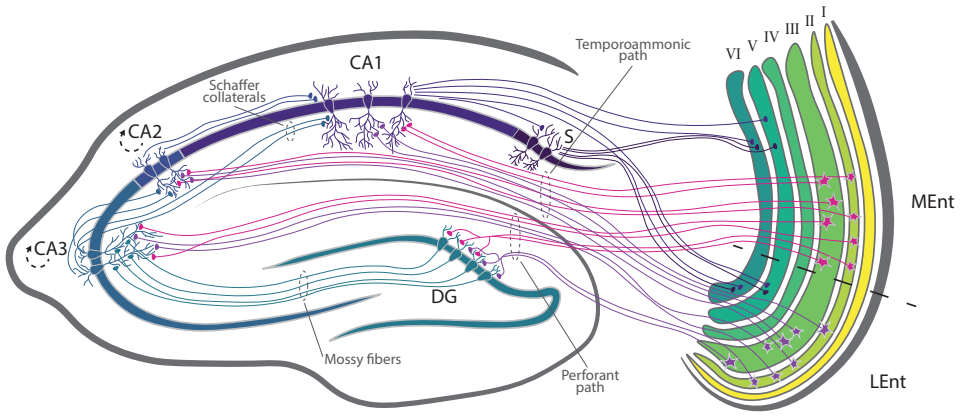

Figure 3: General circuitry and connections of the hippocampal formation.

subsequently dispersing into the DG and the hippocampus proper (Amaral y Witter, 1989). Layer II stellate cells of the MEnt project to the DG and CA3 region via the perforant pathway, while projection cells from layers II-III target the CA1 region and the subiculum through the temporoammonic pathway (Gloveli *et al.*, 1997; Varga *et al.*, 2010). Conversely, within the LEnt layer II, we find reelin-positive fan cells conveying information to the DG, CA3, and CA2 while calbindin-positive neurons project to the olfactory cortex and the olfactory bulb (Leitner *et al.*, 2016; Nilssen *et al.*, 2018; Traub and Whittington, 2022). The CA1 and the subiculum of the hippocampus project back to the Ent layer V, with a sparser projection to layers II and III (Witter *et al.*, 2017). In both MEnt and LEnt, neurons in layer V are the major output neurons projecting to diverse cortical and subcortical structures (Kosel *et al.*, 1982; Xu *et al.*, 2016). Despite the wealth of additional details known about the cytoarchitecture and connectivity of the Ent (Vandrey *et al.*, 2022; Osanai *et al.*, 2023), the provided description is sufficient to facilitate an appropriate interpretation of the current work.

The DG is a three-layered cortical structure that function as the entry point to the hippocampus, forming the initial stage in the trisynaptic loop that receives inputs from the Ent. Within the outermost molecular layer, the perforant pathway's excitatory axons form synapses with the apical dendritic spines of granule cells in the DG. Axons originating from the LEnt connect in the upper third of this layer, while those from the MEnt establish synapses in the middle third (Blackstad, 1956). The Ent-DG connection is strongly divergent (Amaral *et al.*, 1990), enabling the DG to enhance the distinctions in the contextual information encoded by the Ent. Essentially, this initial link in the trisynaptic pathway functions as a pattern separator, facilitating the detection of differences in similar contexts (Leutgeb *et al.*, 2007; Robert *et al.*, 2020). The DG granule cells originate the renowned mossy fibers, which transfer the DG excitatory output to the dendrites of the CA3 pyramidal cells and CA2 (Kohara *et al.*, 2014), continuing with the trisynaptic pathway. Recent studies have identified distinct patterns of activity between the upper and lower blades of the DG (Fredes *et al.*, 2023).

As we mentioned in the previous paragraph, the primary destination of the DG mossy fibers is the CA3 region, which serves as an entry point into the hippocampus proper. Axons from DG form synapses with the dendritic spines of CA3 pyramidal cells across multiple layers: the stratum oriens, stratum lucidum, and stratum radiatum. CA3 pyramidal cells also receive monosynaptic excitatory inputs from Ent layer II to the stratum lacunosum-moleculare (Andersen *et al.*, 2009). Unlike the divergent Ent-DG connection, the DG-CA3 connection is characterized by high convergence (Amaral *et al.*, 1990). Moreover, the most distinctive and renowned feature of the CA3 is the recurrent connections between its pyramidal cells, a characteristic

already evident in the early drawings of Ramón y Cajal (1899). The convergence of the DG-CA3 connection and the auto-connectivity, coupled with the high firing frequency of CA3 pyramidal cells (Guzman *et al.*, 2016), render this brain region a perfect generalizer (Neunuebel and Knierim, 2014; Grande *et al.*, 2019). This network has the ability to retrieve patterns from partial or noisy cues, a process referred to as auto-associative recall, attractor dynamics, or pattern completion (Eom, 2023). Concerning its efferences, CA3 is the main source of excitation of CA1 pyramidal cells through the bundle of unmyelinated fibers known as Shaffer collaterals (Schaffer, 1892).

As we journey through the hippocampal formation, it becomes anatomically imperative to investigate the intricacies of CA2 before we delve into the narrative of CA1. Hippocampal CA2 emerged a decade ago as a region primarily associated with social information processing (Hitti and Siegelbaum, 2014; Stevenson and Caldwell, 2014). Advances in understanding its anatomy, physiology, and the correlation between CA2 neural activity and behavior suggest a broader involvement in hippocampal-dependent memory processing (Bhasin and Nair, 2022; Whitebirch *et al.*, 2022; Oliva *et al.*, 2023). CA2 is tightly connected with all hippocampal regions and receives extensive neuromodulatory projections (Robert *et al.*, 2021). Pyramidal cells in CA2 receive direct excitatory input from CA3, the DG, and the Ent (Ishizuka *et al.*, 1990; Chevaleyre and Siegelbaum, 2010; Kohara *et al.*, 2014; Sun *et al.*, 2014; Llorens-Martín *et al.*, 2015). In turn, the axons of CA2 pyramidal cells extensively branch into the dorsal and ventral CA1 and CA3 regions (Hitti and Siegelbaum, 2014) while also forming recurrent connections with other CA2 pyramidal cells (Okamoto and Ikegaya, 2018). While projections from CA2 to CA1 are unidirectional, CA2-CA3 and CA2-Ent are bidirectionally connected (Tamamaki *et al.*, 1988; Ishizuka *et al.*, 1990; Rowland *et al.*, 2013).

CA1 is the principal destination for CA3 Schaffer collaterals, projections from CA2 pyramidal cells, and monosynaptic connections from the Ent arriving through the temporoammonic pathway. Concerning Schaffer collaterals, the proximal region of CA3 primarily targets the septal and distal levels of CA1 within the superficial layer of the stratum radiatum, while the distal region of CA3 directs its axons to the temporal and proximal areas of CA1, and to the deeper segment of the stratum radiatum. On the other hand, the axon terminals of CA2 pyramidal cells project to the stratum oriens in the proximal sector of CA1 (Ishizuka *et al.*, 1990). To conclude with the CA1 intrahippocampal inputs, the Ent to CA1 projection through the temporoammonic pathway exhibits a topographic organization, with the MEnt connecting to CA1 proximal portions and the LEnt linking to its distal regions, forming one-to-one cell connections in both scenarios (Witter *et al.*, 1988; Masurkar *et al.*, 2017).

As stated in the previous paragraphs, DG accomplish pattern separation through the detection of subtle differences in Ent inputs, whereas recurrent connections of CA3 are involved in the recall of previously stored information and pattern completion (Neunuebel and Knierim, 2014). Following this computational terminology of hippocampal memory processing, the CA1 region functions as a context decoder (Allen *et al.*, 2016; Nagelhus *et al.*, 2023). The CA1 integrates the monosynaptic input from the Ent with the information arriving from the Ent-DG-CA3-CA1 trisynaptic pathway, translating complex and sometimes partially reconstructed information into context-enriched neural representations that communicate to other brain regions (Barrientos and Tiznado, 2018).

The CA1 region emits two intrahippocampal projections: one towards the subicular complex and another to the deeper layers of the Ent, thus completing the hippocampal loop. Regarding the efferent connections to the subiculum, axons from the CA1 pyramidal cells descend into the alveus, located in the hippocampus's deep ventricular edge. These axons then extend distally, looping back in a topographically organized manner to the subiculum stratum pyramidale. The axons from proximal CA1 pyramidal cells emit long projections to the distal subiculum, while

those from the distal CA1 predominantly terminate along the proximal border of the subiculum (Amaral *et al.*, 1991). Concerning CA1-to-Ent projections, CA1 sends return topographic projections to Ent cell layers V and VI (Hamam *et al.*, 2002). The septal and distal region of CA1 mainly sends its efferents to the LEnt, whereas the temporal and proximal area preferentially projects to the MEnt (Strange *et al.*, 2014). Likewise, the CA1 region of the hippocampus extends extrahippocampal outputs to the prefrontal and perirhinal cortices, the septum, the mammillary bodies in the hypothalamus, and the amygdala (Andersen *et al.*, 2009).

To conclude the hippocampal formation, the subicular complex is usually divided into three subdivisions, namely, the subiculum proper, the presubiculum and the parasubiculum. The subiculum is the primary projection area of the hippocampal formation (Swanson and Cowan, 1975), extending its axons to the presubiculum, the deep layers of the entorhinal cortex, as well as to the prefrontal cortex, cingulate and retrosplenial cortex (Wyass and Groen, 1992), amygdaloid complex (Canteras and Swanson, 1992), hypothalamic mammillary nuclei, and the nucleus reuniens, among other midline thalamic nuclei (Meibach y Siegel, 1977).

1.3.2 Navigating in space.

The hippocampal formation has long been proposed to underlie both memory formation and spatial navigation. Following the discovery of dorsal CA1 place cells (O'Keefe and Dostrovsky, 1971), John O'Keefe himself laid the foundation of the theory of spatial mapping when proposing the hippocampal formation as a cognitive map (O'Keefe and Nadel, 1978). Place cells in the hippocampal CA1 region are neurons that show preferential activity when an animal is in a specific location within its environment, known as the receptive field or place field. The collective place cells firing fields encompass the entire environment, thus offering a complete map-like representation of the animal's surroundings (Jeffery *et al.*, 1997).

Since the discovery of place cells, our understanding of the brain's spatial navigation system has expanded to comprise other components (Moser *et al.*, 2017). These include head-direction cells, which convey information about the animal's head orientation (Taube *et al.*, 1990a; Taube *et al.*, 1990b), goal and goal-direction cells, signaling egocentric directions towards navigational targets (Hok *et al.*, 2005; Sarel *et al.*, 2017; Ormond and O'Keefe, 2022), speed cells, sensitive to running speed (Kropff *et al.*, 2015), and border or boundary vector cells, which respond to environmental borders (Savelli *et al.*, 2008; Solstad *et al.*, 2008; Lever *et al.*, 2009), in addition to the renowned MEnt grid cells (Hafting *et al.*, 2005). Unlike place cells, grid cells display multiple firing fields that are situated at the vertices of equilateral triangles, effectively tiling the entire environment. These regular, six-fold symmetric firing patterns aid in spatial navigation by offering a coordinate system for the environment even if neural activity is dissociated from external sensory cues (Waaga *et al.*, 2022).

The firing of place and grid cells conveys positional information to navigate Euclidean space. These cells engage in a process called global remapping (Bostock *et al.*, 1991; Leutgeb *et al.*, 2004), which enables the creation of numerous distinct and uncorrelated maps for various cognitive spaces. These maps can be dynamically reactivated using attractor dynamics (detailed in section 1.3.1.). Likewise, the sequential firing of place and grid cells, particularly during replay events (Wilson and McNaughton, 1994; Skaggs and McNaughton, 1996; Gardner *et al.*, 2019; Gardner *et al.*, 2022) and theta oscillations (Johnson and Redish, 2007), facilitates the simulation of paths through diverse points in cognitive spaces, a process critical for adaptive cognitive functioning and behavior (Fernández-León *et al.*, 2022). These two features of the spatial navigation system, global remapping and path simulation, are behaviorally vital for animals as they navigate through their territories. Consequently, in an ever-changing environment, there must be a continuous influx of vomeronasal information to the hippocampal spatial map. This ongoing flow is essential for en-

abling constant remapping, which is based on recognizing individuals who have left their vomeronasal signals within the territory and constantly integrating that social information into CA1 context-enriched neural representations (Chung *et al.*, 2020).

1.3.3 Processing social memory.

For animals living in social groups, the ability to recognize and retain memories of other individuals is fundamental to demonstrating appropriate interactions with conspecifics. The recently discovered link between two hippocampal regions, namely the dorsal CA2 and ventral CA1, has been identified as crucial for encoding, consolidating, storing, and retrieving social memories (Meira *et al.*, 2018).

Inactivating the dorsal CA2 region using AAVs leads to impairments in social memory while leaving other types of hippocampal-dependent episodic memory unaffected (Hitti and Siegelbaum, 2014). Furthermore, pharmacogenetic and optogenetic methods to inhibit dorsal CA2 neurons, offering precise temporal resolution, demonstrate that dorsal CA2 activity is essential for encoding, consolidating, and retrieving social memories (Meira *et al.*, 2018). Notably, the consolidation of social memory relies on the reactivation of CA2 neurons during sharp-wave ripples. This is evidenced by the fact that optogenetic disruption or enhancement of these ripples in CA2 neurons either suppresses or extends social memories (Oliva *et al.*, 2016; Oliva *et al.*, 2020). Furthermore, recent studies have demonstrated the role of dorsal CA2 in the normal encoding of social stimuli and its involvement in social behavioral dysfunctions associated with diseases (Donegan *et al.*, 2020; Shih *et al.*, 2023).

Besides this, neurons from the supramammillary nucleus (SuM) project to both the CA2 and the DG. The SuM-CA2 circuit is predominantly activated by novel social interactions, while the SuM-DG circuit responds to contextual novelty (Chen *et al.*, 2020). In vivo physiological experiments show that a significant number of CA2 pyramidal neurons exhibit increased firing rates during interactions with a novel mouse, as opposed to a familiar one (Donegan *et al.*, 2020). CA2 pyramidal neurons provide extensive excitatory input to ventral CA1. The inhibition of dorsal CA2 projections to the ventral CA1 leads to a notable impairment in social memory formation (Meira *et al.*, 2018).

Parallel to these discoveries, it was observed that while the dorsal CA2 encodes social memory, the function of the ventral CA1 is to storage all these social memories into social memory engrams (Okuyama *et al.*, 2016). Ventral CA1 social memory neurons are characterized by enhanced firing in response to memorized individuals. These neurons are primarily reactivated during sharp-wave ripples, and the spike sequences in these social replays mirror the temporal sequence of neuronal activities that occur within theta cycles during social interactions. Both these electrophysiological markers and the associated discriminatory social behavior are disrupted under pathophysiological conditions (Tao *et al.*, 2022). It has been hypothesized that ventral CA1 pyramidal neurons in rodents could serve as concept cells (Watarai *et al.*, 2021), performing a role similar to that of the Jennifer Aniston neurons in the human medial temporal lobe (Quiroga *et al.*, 2005; Quiroga, 2012).

It becomes evident that if the connection between dorsal CA2 and ventral CA1 is responsible for encoding and storing social memory in rodents, and these animals identify each other through vomeronasal patterns in their MUPs (Hurst *et al.*, 2001), then the integration of vomeronasal information into this hippocampal circuit is essential. This integration must be crucial at the initial stages of encoding and consolidating social memories, as well as during the retrieval of those memories in response to vomeronasal cues reexploration.

2 GENERAL HYPOTHESIS AND OBJECTIVES

The central hypothesis driving the present doctoral dissertation is that vomeronasal chemosignals convey individual recognition information in mice. The identity information would reside in patterns of protein concentrations present in the urine, acting as a unique identity barcode discernible by other conspecifics. This identity barcode detected by the VNO is encoded in the chemosensory amygdala. The information about identity needs to be incorporated and integrated with other sensory modalities into a detailed hippocampal spatial map, which is essential for animals to display adaptative behavioral outcomes as they navigate their territories. To approach this broad hypothesis from different methodological prisms, we will combine tract-tracing, behavioral, histological, and electrophysiological techniques to address the following objectives.

I. To delineate the neuroanatomical pathway conveying vomeronasal information to the hippocampal spatial map.

II. To functionally test the identified pathway under an olfactory-vomeronasal behavioral paradigm to determine the relevant nodes of vomeronasal information flow and integration.

III. To conduct functional tests using behavioral paradigms that involve spatial rearrangement of items, assessing if distinct episodic memory components engage with specific pathway segments, indicating compartmentalization.

IV. To deduce, based on histological and behavioral results, which structure within the pathway is pivotal in the processing of individual recognition.

V. To evaluate whether an individual urinary signature selectively triggers a specific neuronal motif in that structure, thus deciphering the identity code in mice.

VI. To understand the complexity of individual identity neuronal assemblies, focusing on how the mice brain encodes natural phenomena like countermarking and self-recognition.

3 MATERIALS AND METHODS

3.1 EXPERIMENTAL SUBJECTS.

All protocols and experimental procedures were carried out in accordance with current Spanish legislation (RD 1201/2005, L.32/2007, and L.6/2013), with the European Community Council Directive on the protection of animals used for scientific purposes (2010/63/UE) and were approved by the Research Ethics and Animal Welfare Committee of the University of Valencia (A20191115164620, A20211014182646, and A20221115214515).

Experiments were performed on adult CD1 (Janvier, France) naïve female mice (*Mus musculus*; n=90; see Table 1) aged 2-6 months, with weights ranging from 24-60 g. Animals were housed in cages with water and food available ad libitum, in a 12 h light/dark cycle with constant ambient temperature (22 ± 1 °C) and humidity. Neuroanatomy and behavior experiments were performed during the light phase of the cycle, whereas for the electrophysiology experiment, it was possible to reverse the cycle and carry out the experimentation during the animal's dark phase.

Set of experiments	**90**
Neuroanatomy (A20191115164620)	**42**
TBDA in AOB combined with VGLUT1 IHC	4
TBDA in PMCo combined with VGLUT1 or GAD IHC	8
BDA in PMCo, FG in dorsal CA1 and WGA in ventral CA1	8
FG in dorsal CA1 combined with reelin and calbindin IHC	4
FG in dLEnt	4
FG in dorsal CA1 and WGA in ventral CA1	6
FG in dLEnt and WGA in ventral CA1	4
TBDA in dLEnt combined with VGLUT1 IHC	4
Behavior and neuronal activation (A20211014182646)	**34**
Urine vs. citralva exposure test	12
Social stimuli spatial manipulation test	12
Social vs. object spatial manipulation test	12
Extracellular single units in PMCo (A20221115214515)	**14**

Table 1: Total number of animals used throughout the experimentation. The table details the total number of experimental subjects utilized across the research, along with a specification of the number of animals per experiment and their associated ethical procedures.

3.2 TRACT-TRACING METHODS.

3.2.1 General surgical procedure.

Animals were anesthetized with isoflurane (1.5-2%) in oxygen (0.8-1.5 L/min) (SomnoSuite, Kent Scientific, USA) delivered via a mouse anesthetic mask affixed to the stereotaxic apparatus (David Kopf, 963-A, USA). Analgesia was provided by a subcutaneous butorphanol injection (5 mg/kg in saline solution; Torbugesic vet, Zoetis S.L., Spain) prior to the start of the surgical procedure. This was followed by an

intraperitoneal injection of atropine (0.05 mg/kg in saline solution; Atropine sulfate, Sigma-Aldrich, USA) to reduce salivary and respiratory secretions, prevent bradycardia and balance autonomic nervous system responses.

Adequate induction of anesthesia was tested by the loss of pedal withdrawal and palpebral reflexes, decreased respiratory rate, and absence of whisker movement. Throughout the surgery, the animal's vital signs such as heart rate, respiratory rate, blood pressure, and oxygen saturation were closely monitored (SomnoSuite, Kent Scientific, USA) to ensure safety while under anesthesia. Mice rested on a warming pad to maintain constant body temperature, and eye drops (Siccafluid, Thea S.A. Laboratories, Spain) were dispensed to prevent eye ulceration. Regional lidocaine (B. Braun Medical, Germany) was applied to the inner ear to reduce the discomfort caused by the ear bars.

Once the mouse was securely placed in the stereotaxic frame and ear bars were carefully adjusted, the surgical area was shaved and cleaned using antiseptic solution to minimize the risk of infection. A midline scalp incision was made, and the underlying tissues were gently retracted to expose the skull while maintaining hemostasis. The exposed skull was cleaned and dried thoroughly to ensure a clear view of anatomical landmarks bregma and lambda. Skull was leveled in the anteroposterior axis by aligning bregma and lambda in the same horizontal plane, and in the mediolateral axis by matching the depth of both parietotemporal ridges. Small holes were drilled above the specified coordinates while irrigating with saline to prevent bone overheating. After completing the tracer injection, the incision was closed using the surgical adhesive Histoacryl (1050052; B. Braun, Germany). Postoperative care consisted of subcutaneous butorphanol injections (5 mg/kg in saline solution) every 12 hours for three days following surgery.

3.2.2 Tracer injections.

TBDA in AOB combined with VGLUT1 IHC.

To study the efferent connections of the AOB, and hence the feasible first areas of vomeronasal information relay, the anterograde tracer tetramethylrhodamine and biotin-conjugated dextran amine (TBDA, 10000 MW, lysine fixable, 5% in PB 0.01 M, pH 7.6, Invitrogen, USA) was injected into the right AOB (AP: 3.5 mm, ML: 1 mm, DV: -1.6 mm). To examine the neurochemical characteristics of AOB outputs, iontophoretic TBDA injection (Appendix) was combined with the immunofluorescence detection of the glutamatergic marker VGLUT1.

TBDA in PMCo combined with VGLUT1 or GAD 65/67 IHC.

Aiming to find a direct connection from the cortical amygdala to the hippocampal formation, the anterograde tracer TBDA was injected bilaterally into the PMCo (AP: -2.8 mm, ML: $\pm$2.95 mm, DV: -6 mm). To investigate the neurochemical properties of PMCo efferences, iontophoretic TBDA injection (Appendix) was combined with the immunofluorescence detection of the glutamatergic marker VGLUT1 or the GABAergic marker GAD 65/67.

BDA in PMCo, FG in dorsal CA1 and WGA in ventral CA1.

Since no direct connection between the cortical amygdala and the dorsal hippocampus was found, we searched for intermediate areas where information flow may be relaying. Three simultaneous injections were performed: the anterograde tracer biotinylated dextran amine (BDA, 10000 MW, lysine fixable, 5% in PB 0.01 M, pH 7.6, Invitrogen, USA) was injected bilaterally into the PMCo (AP: -2.8 mm, ML: $\pm$2.95 mm, DV: -5.8 mm), the retrograde tracer FluoroGold (FG, hydroxystilbamidine bis methanesulfonate, 4% in distilled water, Cat 39286, Sigma-Aldrich, USA) was injected bilaterally into the dorsal CA1 (AP: -2.3 mm, ML: $\pm$1.2 mm, DV: -1.4

mm), and the retrograde tracer wheat germ agglutinin, Alexa Fluor 594-conjugated (WGA-594, 2% in PBS 0.01 M, pH 7.6, Invitrogen, USA) was injected bilaterally into the ventral CA1 (AP: -3.28 mm, ML: ±2.8 mm, DV: -4 mm). BDA and FG injections were performed by iontophoretic method whereas WGA was injected by pressure (Appendix).

FG in dorsal CA1 combined with reelin and calbindin IHC.

Considering that the dorsal part of the lateral entorhinal cortex (dLEnt) was one of the essential relay areas found in the last tract-tracing experiment, the retrograde tracer FG was bilaterally injected into the dorsal CA1 (AP: -2.3 mm, ML: ±1.2 mm, DV: -1.4 mm). To determine the responsible neuronal subpopulation of information relay, we combined iontophoretic FG injection (Appendix) with immunofluorescence detection of reelin and calbindin, the two major excitatory neuronal subpopulations present in the layers II/III of the dLEnt (Leitner *et al.*, 2016).

FG in dLEnt.

To confirm the PMCo to dLEnt projection and assess the PMCo subregions originating these projections, the retrograde tracer FG was bilaterally injected by iontophoresis (Appendix) targeting the layers II/III of the dLEnt (AP: -2.92 mm, ML: ±5 mm, DV: -4.2 mm).

FG in dorsal CA1 and WGA in ventral CA1.

Since technical difficulties prevented the prior experiments from accurately examining the brain regions projecting to ventral CA1, the retrograde tracer FG was bilaterally injected into the dorsal CA1 (AP: -2.3 mm, ML: ±1.2 mm, DV: -1.4 mm), and the retrograde tracer WGA-594 was injected bilaterally into the ventral CA1 (AP: -3.28 mm, ML: ±3.15 mm, DV: -4.90 mm). The primary goal of this study was to investigate whether there are neurons in the dLEnt region that project simultaneously to both dorsal CA1 and ventral CA1. FG injection was performed by iontophoresis whereas WGA was injected by pressure (Appendix).

FG in dLEnt and WGA in ventral CA1.

As two of the principal PMCo projections are ventral CA1 and dLEnt, we tested whether the PMCo neuronal populations projecting to these two structures are segregated or, on the contrary, some PMCo neurons project to both areas simultaneously. To assess this, the retrograde tracer FG was injected bilaterally into the dLEnt (AP: -2.92 mm, ML: ±5 mm, DV: -4.2 mm), and the retrograde tracer WGA-594 was injected bilaterally into the ventral CA1 (AP: -3.28 mm, ML: ±3.15 mm, DV: -4.90 mm). FG injection was performed by iontophoresis whereas WGA was injected by pressure (Appendix).

TBDA in dLEnt combined with VGLUT1 IHC.

To study the region of the dorsal hippocampus that directly receives the vomeronasal information relayed from layers II/III of the dLEnt, and if the dLEnt projects back to the PMCo, the anterograde tracer TBDA was injected bilaterally targeting the layers II/III of the dLEnt (AP: -2.8 mm, ML: ±2.95 mm, DV: -6 mm). To examine the neurochemical characteristics of dLEnt outputs, we combined an iontophoretic TBDA injection (Appendix) with the immunofluorescence detection of the glutamatergic marker VGLUT1.

3.2.3 Histology.

After 7-10 days of survival to allow for proper tracer transport, animals were deeply anesthetized with sodium pentobarbital (100 mg/kg, Dolethal Vetoquinol, Spain) and transcardially perfused with 40 ml of heparinized saline (heparin sodium salt, Thermo Fisher Scientific, USA) followed by 80 ml of paraformaldehyde 4% diluted in PB (0.1 M, pH 7.6). Brains were carefully extracted from the skulls, postfixed overnight in the same fixative solution at 4°C, and cryoprotected in 30% sucrose (in PB 0.1M, pH 7.6) at 4°C until they sank. Using a freezing microtome, 40-µm-thick coronal slices were obtained and collected in five parallel series. In cases involving injections into the accessory olfactory bulb, the bulbs were cut apart along the sagittal plane to enhance visualization of the injection site.

To analyze the neurochemical properties of the efferences mentioned in section 2.2.2., anterograde tracer injections were combined with the immunofluorescence detection of the vesicular glutamate transporter VGLUT1 to identify glutamatergic outputs or the glutamic acid decarboxylase GAD 65/67 to detect GABAergic innervation. Selected series were blocked for 2 hours with 4% normal goat serum (NGS, G9023, Sigma-Aldrich, USA) and 0.3% Triton X-100 (Tx-100, PanReac AppliChem, Germany) in Tris-buffered saline (TBS, 0.05 M, pH 7.6). Subsequently, the sections were incubated overnight at 4°C in blocking solution (2% NGS and 0.3% Tx-100 in TBS) with rabbit anti-VGLUT1 (Cat #135 302, Synaptic Systems, Germany, AB_887877, 1:1000) or rabbit anti-GAD 65/67 (Cat #G5163, Sigma-Aldrich, USA, AB_477019, 1:1000). The next day, slices were incubated for 2 hours at room temperature in blocking solution with Alexa 488-conjugated goat anti-rabbit (Cat #111-545-003, Jackson ImmunoResearch, USA, AB_2338046, 1:200). Finally, sections were counterstained with DAPI (1 µg/ml, Molecular BioProducts, USA) in distilled water for 5 minutes.

Referring to the experiment where BDA was injected into PMCo, FG into dorsal CA1, and WGA into ventral CA1, we processed one of the free-floating series for simultaneous permanent detection of BDA and FG, another for simultaneous permanent detection of BDA and WGA, and a third for simultaneous fluorescence detection of the three tracers.

For the histochemical permanent detection of BDA, endogenous peroxidase was inactivated with 1% H_2O_2 in TBS for 15 minutes at room temperature. Sections were then incubated for 2 hours in ABC complex (Vectastain ABC kit, Vector Labs, PK-6100, USA) diluted 1:50 in TBS-Tx-100. Peroxidase activity was visualized using 0.025% 3,3'-diaminobenzidine (DAB, Sigmafast tablets, Sigma-Aldrich, USA) in TB (0.1M, pH 8.0) as chromogen, 0.01% H_2O_2 as substrate, and 0.2% nickel ammonium sulfate as enhancer, yielding a black precipitate as reaction product.

We conducted immunohistochemical detection of FG or WGA in the two series of sections where BDA had previously been revealed. Sections were incubated for 2 hours at room temperature in a blocking solution of TBS-Tx 0.3% containing 3% NGS for the slices aimed at detecting FG or 3% normal horse serum (NHS, H0146, Sigma-Aldrich, USA) for the series where WGA was to be detected. Subsequently, sections were incubated overnight at 4°C in their corresponding blocking solution containing rabbit anti-FluoroGold (Cat #AB153-I, Merck Millipore, USA, AB_2632408, 1:1000) or goat anti-Wheat Germ Agglutinin (Cat #AS-2024, Vector, USA, AB_2315608, 1:1000). The following day, slices were incubated for 2 hours at room temperature in blocking solution with biotinylated goat anti-rabbit (Cat #BA-1000, Vector, USA, AB_2313606, 1:200) or biotinylated horse anti-goat (Cat #BA-9500, Vector, USA, AB_2336123, 1:200), and for another 2 hours in ABC complex diluted 1:50 in TBS-Tx at room temperature. In both cases, the resulting peroxidase labeling was revealed with 0.025% 3,3'-DAB in TB (0.1M, pH 8.0) with 0.01% H2O2. The resulting precipitate exhibited a distinctive brown color, clearly distinguishable from the black coloration produced during the histochemical detection of BDA.

A third series underwent processing to detect all three tracers simultaneously using fluorescence techniques. Tissue autofluorescence was mitigated by treating it with a 1% sodium borohydride solution in TBS for 30 minutes. Sections were then incubated in a blocking solution of TBS-Tx 0.3% containing 3% NGS and 3% normal donkey serum (NDS, D9663, Sigma-Aldrich, USA) for 2 hours at room temperature. Afterward, sections were incubated overnight at 4°C in a blocking solution containing rabbit anti-FluoroGold (Cat #AB153-I, Merck Millipore, USA, AB_2632408, 1:1000) and goat anti-Wheat Germ Agglutinin (Cat #AS-2024, Vector, USA, AB_2315608, 1:1000). Following this incubation period, sections were immersed for 2 hours at room temperature in Alexa 488-conjugated goat anti-rabbit (Cat #111-545-003, Jackson ImmunoResearch, USA, AB_2338046, 1:200) and tetramethylrhodamine (TRITC)-conjugated donkey anti-goat (Cat #705-025-147, Jackson ImmunoResearch, USA, AB_2340389, 1:100) in blocking solution. Finally, sections were incubated in Rhodamine Red^{TM}-X (RRX) Streptavidin (Cat #016-290-084, Jackson ImmunoResearch, USA, AB_2337247, 1:100) in blocking solution for 2 hours at room temperature. This procedure yields retrogradely labeled somata in green for FG and in red for WGA, along with anterogradely red-labeled BDA fibers.

As described in the previous paragraph, despite the intrinsic fluorescence of FG and WGA-594, we conducted additional immunohistochemical counterstaining for both tracers. This was necessary because the confocal microscopes available were unable to detect the golden-blue fluorescence of FG and because the inherent labeling of the WGA was very faint. This strategy was carried out for the same purposes in other tract-tracing experiments, following the above-described immunostaining protocol.

Retrograde FG injections in the dorsal CA1 were combined with the detection of reelin and calbindin to identify the dLEnt neuronal subpopulation responsible for the vomeronasal information relay. To that end, sections were incubated for 2 hours in a blocking solution of TBS-Tx 0.3% containing 4% NGS, followed by overnight incubation in the same solution at with the respective primary antibody: mouse anti-reelin (Cat #MAB5364, EMD Millipore, USA, AB_2179313, 1:1000) or rabbit anti-calbindin (Cat #CB38, Swant, Switzerland, AB_10000340, 1:1000). To stain reelin and calbindin, the secondary antibodies Rhodamine Red-X goat anti-mouse (Cat #R6393, Thermo Fisher Scientific, USA, AB_2556550, 1:200) or Alexa 488-conjugated goat anti-rabbit (Cat #111-545-003, Jackson ImmunoResearch, USA, AB_2338046, 1:200) were incubated for 2 hours in blocking solution at room temperature.

Permanent sections were mounted onto gelatinized glass slides, dehydrated in graded alcohols, cleared in xylene, and cover-slipped with Entellan (Merck Millipore, USA). Fluorescent slices were mounted onto gelatinized glass slides and covered with FluorSave^{TM} (Merck Millipore, USA).

3.2.4 Image acquisition and processing.

Permanent sections were photographed using a digital Olympus XC50 camera attached to an Olympus CX41RF-5 microscope. Fluorescent slices were examined using a Leica DMRB or a Leica DMI3000 B epifluorescence microscope and photographed with a Leica DFC495 C digital camera. Confocal images were obtained in an Olympus FV1000 confocal microscope mounted on a motorized inverted Olympus IX81 fluorescence microscope or in a Leica TCS-SP8 confocal microscope with a Hy-Volution system for high-resolution images.

Acquired images were digitally processed and enhanced using Adobe Photoshop (v22.4.0, Adobe Systems) and FIJI software (v2.1.0/1.53c and v2.14.0/1.54f) (Schindelin *et al.*, 2012). Contrast and brightness adjustments were applied to improve the clarity of the images. Illustrations were designed with Adobe Illustrator (v25.2.1, Adobe Systems).

The injections placement and subsequent labeling analysis were conducted in accordance with the nomenclature of the Paxinos and Franklin mouse brain atlas (2004).

3.3 BEHAVIORAL TESTS AND NEURONAL ACTIVATION STUDY TECHNIQUES.

3.3.1 Urine vs. citralva exposure test.

To study the differences in neuronal activation resulting from exposure to male-derived urine, containing volatile and non-volatile molecules, versus exposure to a neutral odorant, containing only volatiles, 10 CD1 naïve female mice were isolated in individual cages. Two experimental groups were generated by counterbalancing subjects according to their original home cage, so that in both groups there would be an equal number of animals with similar previous experience. For the same purpose, the individual cages were stabled in the housing rack in a counterbalanced arrangement to prevent the animals in one group from having more social contact or exposure to odors than the others. All behavioral sessions were conducted under an illumination of 60 lux, with constant temperature and humidity. Environmental enrichment was removed before recording and returned upon completion.

Both groups of animals were habituated for three days prior to the test. Habituation consisted of a daily 10-minute session in which an open glass jar containing 5 g of clean bedding was introduced in the center of the subject's cage (Figure 4). The glass jar was stuck to the base of the cage with odorless double-stick tape to prevent animals from moving the jar. The sequence of habituation started with the group that would later be exposed to male urine on the test day, followed by the group set to encounter citralva as a neutral odorant. Recording was conducted in pairs, leaving the remaining odd animal in each group to be recorded individually. A barrier made of opaque methacrylate was placed in between the cages being simultaneously recorded and around both cages, to avoid any visual contact between the animals and with the external environment.

During the habituation sessions, stimuli of an identical nature to those presented on the day of the test were placed 20 cm away from the cages to avoid any novelty effect on the day of testing. In the external environment of the urine-exposed group, there was a jar containing 30 g of CD1 male-soiled bedding, while the citralva-exposed group had a jar with 30 g of clean bedding infused with 100 µL of citralva.

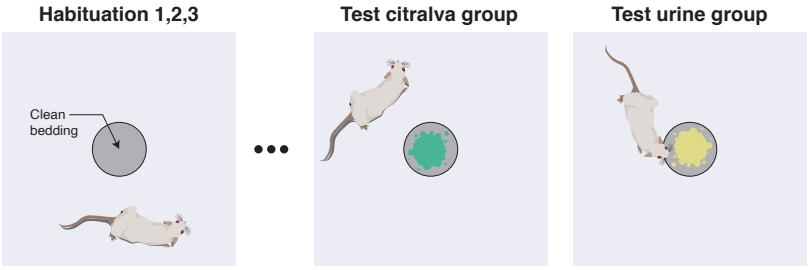

Figure 4: Experimental protocol of the urine vs. citralva exposure test. Following a three-day habituation period to clean bedding, animals were exposed to clean bedding infused with either male urine or citralva, used as a neutral odorant.

The preference test consisted of the exposure to a glass jar containing 5 g of clean bedding impregnated with 30 µL of CD1 male urine (n=5) or 0.5 µL of citralva (n=5) as a neutral odorant (Figure 4). The male urine sample used for the test was obtained by free micturition from the same male who provided the male-soiled

bedding used during the habituation sessions, and all the experimental guidelines described previously for those sessions were faithfully reproduced on the test day. The test lasted for 90 minutes from the introduction of the stimulus until the sacrifice of the animal.

3.3.2 Social stimuli spatial manipulation test.

To determine the effect of spatial rearrangement of social landmarks on neuronal activation, we conducted an experiment where social cues were relocated after three days of training to an invariant position. To address this, 12 CD1 naïve female mice were housed in individual cages. All the counterbalancing directives, and light, temperature, and humidity conditions described for the experiment in section 2.3.1 were followed. Nonetheless, in the context of this experiment, environmental enrichment was not removed, as it helps females maintain accurate orientation, which is integral to the nature of this study.

The social stimuli employed consisted of urine from three different CD1-unrelated males. To ensure the absence of kinship between these males, and thus facilitate the discrimination of their cues by the female, urine samples were extracted from three males sourced from different suppliers, animal facilities, and with varying ages. Urine samples from male subjects were collected after free micturition.

Female mice underwent a three-day training period before the test. Training consisted of a daily 10-minute session in which three glass jars containing 5 g of clean bedding soaked with 30 µL of urine from different males were placed in three corners of the female's cage, with each jar holding urine from a distinct male (Figure 5). During these training sessions, each individual male stimulus was placed in the same location and introduced in the same order. The glass jars were affixed to the bottom of the cage using odorless double-sided tape to immobilize them and prevent the animals from displacing them. The corners where the specific stimuli were placed were counterbalanced between the two upcoming groups. Recording was conducted in pairs and alternating between both groups, beginning with the experimental group. Every pair of animal cages recorded together was separated by an opaque methacrylate wall to prevent visual contact between both mice.

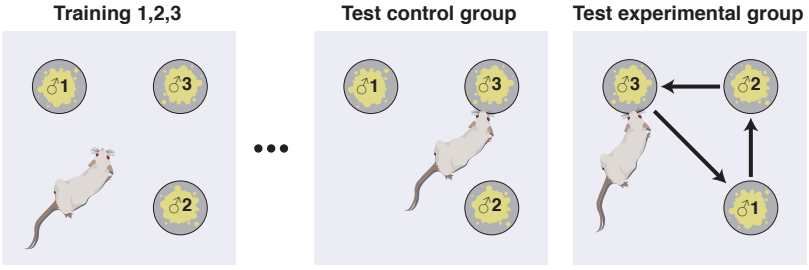

Figure 5: Experimental protocol of the social stimuli spatial manipulation test. Following three days of training, which involved exposure to three male urine samples set in fixed positions, the experimental group stimuli rotated one position counterclockwise from their original location.

On the test day, the experimental group of animals (n=6) had the stimuli rotated one position counterclockwise from their original location during the training sessions, whereas in the control group (n=6) the male stimuli remained in the same place (Figure 5). The test lasted for 90 minutes after introducing the stimuli, at the end of which the animal was euthanized.

3.3.3 Social vs. object spatial manipulation test.

To assess how spatial reorganization affects neuronal activation and whether the effects differ when such reorganization is provoked by shifts in social cues or inanimate objects, two different experimental groups were established to experience changes in the spatial conformation of their environment. As in the previous experiment, 12 CD1 naïve female mice were individually housed. All the counterbalancing guidelines, and light, temperature, and humidity conditions described for the experiment in section 2.3.1 were followed. As in the previous spatial manipulation test, we chose not to remove the environmental enrichment since it assists females in maintaining precise orientation, which is essential to the study's nature.

The social group of the present experiment was exposed to the same stimuli as the experimental group in section 2.3.2. For the group that was exposed to objects, three objects with varying colors, weights, and shapes were chosen to help the identification process. A white chess pawn, a black checkers piece, and a blue domino were used, all made of plastic to prevent being impregnated with the subject's odor.

A three-day training period was conducted for both groups before the test. The social-exposed group (n=6) underwent training through daily 10-minute sessions during which three glass jars, each containing 5 g of clean bedding soiled with 30 µL of CD1 male urine from distinct males, were positioned in three corners of the female's cage. Simultaneously, the group exposed to objects (n=6) underwent training using the same procedure but substituting the social stimuli with the three different objects (Figure 6). It should be noted that the objects were placed inside glass jars and upon the same amount of bedding to faithfully replicate the training conditions of the group exposed to social stimuli. In both groups, the allocation of specific stimuli to the corners was counterbalanced. The video was recorded in pairs, alternating between the two groups, starting with the social-exposed group. Each pair of animal cages that were recorded together was divided by an opaque methacrylate plate to ensure there was no visual contact between the animals.

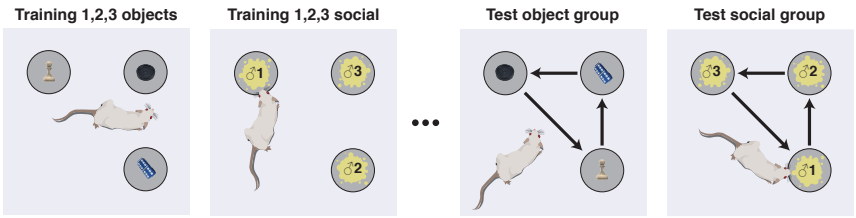

Figure 6: Experimental protocol of the social vs. object spatial manipulation test. Over a period of three days, the animals underwent training with either three male urine samples or three objects, each consistently placed in the same position. On the test day, for both groups, all items were rotated one position counterclockwise.

On the test day, the spatial arrangement of the stimuli was changed for both groups of animals by rotating them one position counterclockwise from their original location during training sessions (Figure 6). The animals were exposed for 90 minutes, after which they were sacrificed.

3.3.4 Behavioral analysis.

Exploratory behavior was quantified using DeepLabCut (DLC) (Mathis *et al.*, 2018), an open-source software for animal pose estimation. We trained three independent ResNet-50-based neural networks with default parameters to track points of interest (Figure 7) from recorded videos (30 fps). Twenty frames were extracted from selected videos using k-means clustering, attempting to represent a sufficient sample of the experimental condition's diversity. The networks were trained within the computer cluster of the Bioinformatics and Biostatistics Unit at Principe Felipe

Research Center (CIPF, Valencia, Spain). When networks exhibited a considerable error after training, we extracted 20 outlier frames from both the training videos with high error and new videos, and points with a likelihood < 0.9 were relabeled to refine the networks.

The urine vs. citralva exposure test network (v2.2.0) was trained from 240 frames for 400,000 iterations, achieving a final train error of 2.09 pixels and a test error of 2.91 pixels. The social stimuli spatial manipulation test network (v2.2.0.6) was trained from 580 frames for 509,400 iterations, reaching a train error of 4.15 pixels and a test error of 11.44 pixels. The social vs. object spatial manipulation test network (v2.3.3) was trained from 460 frames for 522,800 iterations, obtaining a train error of 3.26 pixels and a test error of 7.62 pixels. These networks were then used to analyze videos from similar experimental settings. Subsequent data generated by DeepLabCut was then processed using Python (v3.9) and MATLAB (v2022a) code developed in the lab.

In the urine vs. citralva exposure test, we selected the region of interest (ROI) for exploration analysis as the upper circular area of the glass jar. We deemed exploration to be positive when the mice's body points "nose", "right ear", "left ear", "head", and "spine1" were all concurrently within the ROI (Figure 7b).

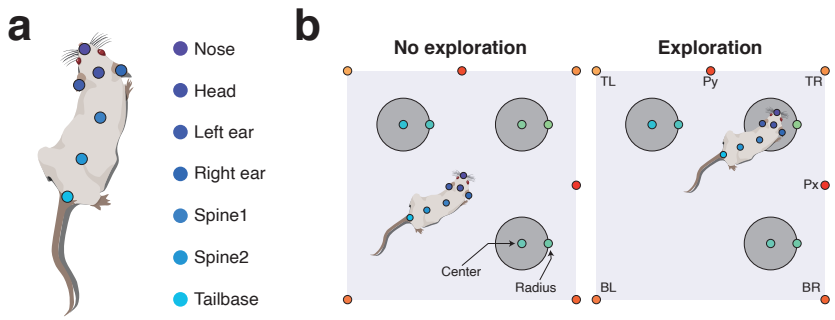

Figure 7: Labels used to train the DLC neural networks both for the mouse and the arena. **a.** Body parts used for mouse tracking. **b.** Landmarks used to outline the arena. Labels indicating the center and radius of the jar were utilized to define the circular ROI for exploratory quantification. Meanwhile, labels demarcating the outer edge of the cage were employed to assess the speed and total distance traveled by the animal.

In the cases of the behavioral paradigms with a spatial component, networks could not be ideally refined due to the high variability of conditions among the videos. Therefore, an interpolation was performed using the coordinates with likelihood values exceeding 0.95 for the cage and the glass jars points, 0.85 for the animal body points, and 0.9 for the plastic objects. All coordinates with likelihood values under the defined thresholds were interpolated using the adjacent coordinates with above-threshold likelihood values, improving the overall reliability of the data and giving a more accurate representation of the animal movements during the analysis.

In the social stimuli spatial manipulation test and the social-exposed group of the social vs. object spatial manipulation test the selected ROI was defined as the circular area of the glass jar top part. In the object-exposed group the ROI was demarcated as a circular area with the same dimensions as the glass jar's upper part, with its center coinciding with the center of the plastic object. Exploration was considered as positive when the mice's body parts "right ear", "left ear", "head", and "spine1" were all simultaneously contained within the defined ROI (Figure 7b), which allowed us to measure exploration time and jar entries. Furthermore, we measured the velocity and distance covered within and outside the ROI.

3.3.5 Histological processing.

At the end of the tests, animals were deeply anesthetized with sodium pentobarbital (100 mg/kg, Dolethal Vetoquinol, Spain) and transcardially perfused with 40 ml of heparinized saline (0.9%, heparin sodium salt, Thermo Fisher Scientific, USA) followed by 80 ml of paraformaldehyde 4% diluted in PB (0.1 M, pH 7.6). Brains were postfixed overnight in the same fixative and cryoprotected in 30% sucrose in 0.1 M PB until they sank. Using a freezing microtome, 40-µm-thick coronal slices were obtained and collected in five parallel series.

Slices were treated with 1% sodium borohydride in Tris-buffered saline (TBS, 0.05 M, pH 7.6), and blocked with 4% normal goat serum (NGS, G9023, Sigma-Aldrich, USA) and 0.3% Triton X-100 (Tx-100, PanReac AppliChem, Germany) in TBS. After the blocking step, sections underwent an overnight incubation at 4°C in primary antibodies in blocking buffer, consisting of 2% NGS and 0.3% Tx-100 in TBS. The primary antibodies used were rabbit anti-c-Fos (Cat #SC-52, Santa Cruz Biotech, USA, AB_2106783, 1:500) and mouse anti-reelin (Cat #MAB5364, EMD Millipore, USA, AB_2179313, 1:1000). Slices were then incubated in corresponding secondary antibodies for 2 hours in blocking buffer. The secondary antibodies were Alexa Fluor 488 goat anti-rabbit (Cat #111-545-003, Jackson ImmunoResearch, USA, AB_2338046, 1:200) and Rhodamine Red-X goat anti-mouse (Cat #R6393, Thermo Fisher Scientific, USA, AB_556550, 1:200). Finally, sections were counterstained with DAPI (1 µg/ml, Molecular BioProducts, USA) in distilled water for 5 minutes. Stained slices were mounted onto gelatinized glass slides and covered with FluorSave^{TM} (Merck Millipore, USA).

3.3.6 Image acquisition and cell quantification.

The fluorescent sections were imaged using an Olympus Fluoview FV1000 confocal microscope (Olympus). Three-channel (405, 488, and 559 nm laser wavelengths) image files were acquired while maintaining unique excitation and acquisition parameters for all samples. Z-series were obtained using sequential scanning mode and applying Kálmán filter. Each stack consisted of 6-10 1.94-µm-thick optical sections.

Quantitative c-Fos data were collected by automated image analysis using a custom FIJI macro (V2.1.0/1.53c) (Schindelin *et al.*, 2012). Macro ran the following steps: (i) enhance contrast in the c-Fos channel (488 nm) by increasing the brightness difference between objects and background by 0.2%; (ii) a threshold of 0.1% of the highest intensity value was applied to each image, resulting in a 16-bit image; (iii) median filter was applied using the Despeckle tool; (iv) pixels were added to the edges of objects using the Dilate tool; (v) noisy pixels were eliminated with the Remove outliers tool; (vi) thresholded particles over 10 pixels were measured and numbered using the 3D Object Counter tool (v2.0).

Automated digital image analysis using FIJI software was also employed to evaluate the reelin expression (channel 559) in the dLEnt layer II. The stacks were subjected to a maximum intensity Z projection. A 16-bit binarized image of channel 559 was obtained by applying a 3% threshold of the highest intensity value for each image. Thresholded particles above 150 pixels were measured and numbered by the outlines FIJI function, generating an image of reelin-positive cells.

Counting ROIs were selected using the DAPI channel (405 nm) as a reference and delineated as precise polygons according to Paxinos and Franklin's mouse brain atlas (2004). A blind experimenter performed nuclei delimitation by selecting representative coordinates for each nucleus. Detected objects and ROI areas were automatically saved and c-Fos results were expressed as the cell density of positively labeled cells normalized by the area. We assessed the percentage of reelin-positive activated cells in the dLEnt layer II by overlapping and comparing the results of

both counts. This comparison was expressed as a percentage of reelin-activated cells relative to the total reelin-IR neurons analyzed.

3.3.7 Principal component analysis.

We conducted Principal Component Analysis (PCA) as a method of exploratory data analysis to enhance the understanding of our comprehensive c-Fos results. This model simplifies the broad set of initial variables (density of immunoreactive cells in each nucleus) into fewer dimensions, known as principal components. These components capture the majority of the variance from the original dataset, thereby minimizing the model's noise. Our dataset displayed significant variance among variables, prompting us to perform PCA post-z-score normalization. We identified two principal components, which effectively grouped our experimental categories and accounted for 61.0% of the total variance (PC1 contributing 44.1% and PC2 contributing 16.9%). To increase the PCA's reliability, we employed the fast-minimum covariance determinant, orthogonalized Gnanadesikan-Kettenring, and Olive-Hawkins estimates. These methods rely on Mahalanobis distance to robustly identify outliers in multivariate data. Outliers were left in the analysis.

3.4 IN VIVO ELECTROPHYSIOLOGICAL PROCEDURES.

3.4.1 Headbar implantation surgery.

Animals were anesthetized with isoflurane (1.5-2%) in oxygen (1-1.5 L/min) (MSS Isoflurane Vaporizer, Medical Supplies and Services, UK) delivered through a mouse anesthetic mask attached to the stereotaxic apparatus (Stoelting, 51730U, USA). Specifications for pre- and intra-operative pharmacological protocols, animal anesthetic induction and health status control, skull alignment and general surgical guidelines are rigorously detailed in section 2.2.1.

We drilled two ellipse-shaped holes of 1.5 mm AP and 1 mm ML dimensions above the PMCo of both hemispheres (AP: -2.8 mm, ML: $\pm$2.95 mm), and ink marks were drawn stereotaxically at the four vertices of the ellipse to guide the silicon probe entry on the recording day. Two additional holes were drilled in the back of the skull above the cerebellum for future reference and grounding (Figure 8a). We made grooves with a scalpel on the exposed skull to increase the contact surface with the implant. An adhesive (OptiBond All-In-One, 33381E, Kerr Dental, Spain) was applied over the entire skull and cured with ultraviolet light to harden the bond between the skull and the implant cement.

A stainless steel headbar was placed in the anterior part of the skull using the stereotaxic arm to make it perfectly straight, and two male jumper connectors were introduced into the reference and ground holes (Figure 8a). All these metal parts were bonded to the skull using dental cement (DuraLay, Reliance Dental Manufacturing, USA), carefully avoiding the cement from entering into the holes intended for probe insertion. Finally, the craniotomies were covered using bi-component surgical silicone (Kwik-Sil, World Precision Instruments, USA). Mice were housed in individual cages and monitored until fully recovered. Postoperative care consisted of subcutaneous butorphanol injections (5 mg/kg in saline solution) every 12 hours for five days following surgery.

3.4.2 Head-fixed setup implementation.

The setup consisted of a cylindrical treadmill for head-fixed mice (Cibertec S.A., Spain) with an associated stereotaxic frame (SR-6N/SM-15R, Narishige, Japan). An engine was placed in front of the animal to gradually approach cotton swabs im-

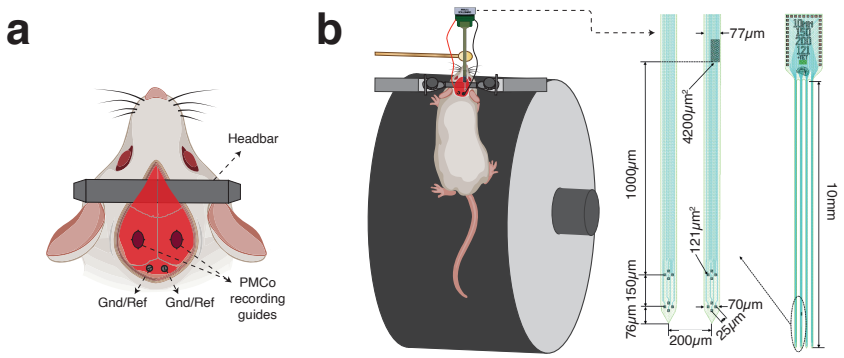

Figure 8: Experimental layout illustrating the physical arrangement of the surgical and head-fixation methods. **a.** Overhead view showing the outcome of an implantation surgery conducted for single-unit recording in the PMCo. Visible elements include a stainless steel bar positioned at the anterior part of the skull for head fixation, two guide holes intended for probe insertion, and two male jumpers located above the cerebellum at the posterior part of the skull, serving for grounding and referencing. **b.** Comprehensive drawing showing the spatial arrangement of components within the head-fixed system during an electrophysiological recording session. It includes the cylindrical treadmill, the head-fixed apparatus per se, a swab holding the stimulus, and the recording probe. A detailed schematic provides an in-depth view of the specific structure of the recording probe.

pregnated with different stimuli to the animal's snout (Figure 8b). This engine was connected to an Arduino board (Mega 2560 Rev3) programmed with self-developed code, which in turn was connected to the Open Ephys acquisition system, providing accurate synchronization of stimuli presentation and electrophysiological recording. A rotary encoder was attached to the engine to ensure the necessary physical contact with the stimulus while reducing any potential disturbance to the animal, allowing a precise sticking of the cotton swab to each animal's snout. The treadmill height was adjusted individually for each subject, ensuring proper head alignment and allowing the animal to run on the wheel comfortably, minimizing any torsion on the headbar.

3.4.3 Habituation and exposure protocols.

Upon recovering their pre-surgical weight, approximately one week after the intervention, the animals underwent habituation to the experimental conditions. The habituation process spanned a five-day protocol designed to gradually acclimate the animals to the experimental environment. On day one, two 10-minute handling sessions were conducted with 1 hour of rest in between, to familiarize the mice with the experimenter. Day two continued this progression with two sessions of 5-minute handling followed by 5 minutes of the animals being gently held by the headbar in 10-second intervals. By day three the animals had become used to the experimenter, so after a brief handling, we let the mice run freely for 7 minutes on the treadmill, to subsequently head-fixed them for 5 minutes. On day four, the animals were subjected to a 15-minute head-fixed treadmill running session, followed by another 15 minutes in the same conditions while receiving clean cotton swabs. On the fifth day the head-fixed animals experienced an exposure protocol identical to that of the forthcoming recording days, but with saline-soaked cotton swabs instead of the actual stimuli. All experimentation was carried out in dark conditions.

On the recording day, mice were exposed to a sequence of conspecific stimuli pipetted onto sterile cotton swabs to investigate the electrophysiological response of PMCo neurons. The animals were first exposed to 100 µL of the urine of a male (♂1), followed by 100 µL of the urine of a different male (♂2). Subjects were then

exposed to a 100 µL equal parts mixture of the previously mentioned urine samples (♂1+♂2), blended together in an Eppendorf tube. Consecutively, to simulate a natural countermarking scenario, the mice were exposed to a cotton swab impregnated with 100 µL dry urine from male 2, onto which 100 µL fresh urine from male 1 had been pipetted (♂1→♂2). To conclude, we exposed the female subjects to 100 µL of their own urine (♀0).

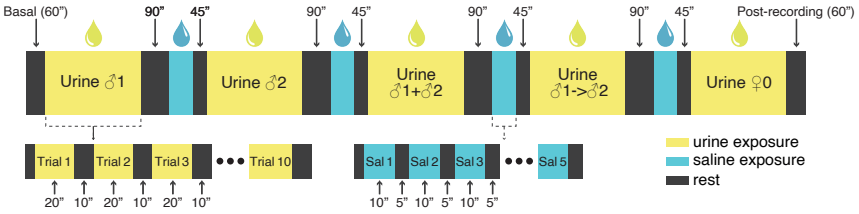

Figure 9: Timeline detailing the automated time-stamped exposure protocol. The diagram illustrates the sequential exposure to various conspecific stimuli and saline (serving as control) over the entire duration of the recording.

All samples were obtained by free micturition, and were presented in a sequence of 10 consecutive trials, each lasting 20 seconds with a 10-second inter-trial resting period. As a control, in between each stimuli presentation, we presented saline-soaked swabs in 5 trials of 10 seconds with a 5-second inter-trial period. After completing the exposure trials to conspecific stimuli, a resting period of 90 seconds was left, whereas a 45-second rest period followed exposure to saline (Figure 9). The male-derived stimuli employed consisted of urine from two different CD1-unrelated male mice. To ensure the absence of kinship between these males, thus maximizing the dissimilarity of their urine components, urine samples were extracted from two CD1 males sourced from different suppliers, animal facilities, and of different ages.

3.4.4 Signal acquisition.

For acute head-fixed mice recording, a 32-channel silicon probe (a4x2-tet-10mm-150-200-121, NeuroNexus Technologies, USA; Figure 8b) was inserted under the guidance of a portable digital microscope (Bysameyee, USA) up to the PMCo (AP: -2.8 mm, ML: ±2.95 mm, DV: -5.8 mm). The design of this probe was intended to simultaneously record layers II and III of the PMCo at four different anteroposterior levels to study whether there is a topographic distribution in these neurons' response. We chose for this purpose 50 µm-thick four-shank probes with two tetrodes per shank at two different dorsoventral heights.

We used probes with A32 and H32 format connectors. The A32 probes were connected to an A32-OM32 adapter (NeuroNexus Technologies, USA) that was attached directly to the stereotaxic arm, while for the H32 probes, a custom device was crafted to serve as an intermediary to affix the probe to the stereotaxic frame. The wiring setup combined an internal reference integrated into the neural probe and an external reference from the probe connector to the male jumper contralateral to the recorded hemisphere. Hybrid referencing allowed us to minimize common-mode noise and maximize signal quality. The ground wire was connected from the probe connector to the male jumper ipsilateral to the recorded hemisphere (Figure 8b). Both the ground and the external reference wires ended in female jumpers, which were irrigated with saline periodically throughout the recording to improve electrical conductivity and ensure continued performance and stability of the recording.

Data were acquired using an RHD2132 32-channel amplifier chip with unipolar inputs and common reference (Intan Technologies, USA) and the Open Ephys acquisition board (Siegle *et al.*, 2017) with a sampling frequency of 30 kHz.

The initial impedance of the recording sites was measured upon contact with the brain surface. The probe was inserted into the brain at a rate of 50 µm/min to avoid

tissue inflammation and a severe rise in electrode impedance until reaching the specified coordinates. To monitor the insertion of the probe, we employed various electrophysiological markers of the adjacent areas, such as the signal amplitude increase when passing through the ventral hippocampus or the characteristic signal of the fiber tract underneath PMCo. Once the PMCo was reached, we allowed a window of 90-120 minutes for probe stabilization, after which a new impedance measurement was conducted to ensure the correct condition of the recording sites.

At the end of the recording, the probe was withdrawn at a rate of 200 µm/min while monitoring the electrode signals to prevent any mechanical damage. After explanting the electrode from the brain, the probe shanks were soaked in distilled water for 10 minutes. The implantable region of the probe was then submerged in a protease solution of 1% Terg-a-zyme (Sigma-Aldrich, USA) in distilled water for 90 minutes. After removing from the protein-dissolving solution, the probe was soaked for 10 minutes in distilled water, let dry for 30 minutes in an upright position, and stored in its shipping anti-static box.

3.4.5 Data analysis.

Spike sorting and data preprocessing.

Automatic spike sorting was performed using Kilosort 2.5 with default parameters (Steinmetz *et al.*, 2021; Pachitariu *et al.*, 2023). The Kilosort algorithm consists of three principal steps: (i) a raw-data alignment that detects and corrects for spatial drift of the recording shanks relative to the surrounding tissue; (ii) an iterative template-matching process employing low-rank, variable-amplitude waveform templates to extract and categorize individual single-unit spikes; (iii) a curation procedure to detect appropriate template merging and splitting operations based on spike train auto- and cross-correlograms.

The Kilosort output was inspected using Phy2 (kwikteam/phy) for further manual curation. Some community-developed plugins (petersenpeter/ phy2-plugins; jiumao2/PhyWaveformPlugin) were incorporated to integrate additional functionalities to Phy2, thus improving the quality of curated data.

We followed the *Petersen Lab Book* pipeline for manual curation. Before starting the procedure, all clusters with a frequency <0.05 Hz or less than 500 spikes were marked as noise. We also categorized as noise the clusters that displayed triangular-shape auto-correlogram, those having a distinctly unusual non-spike-like waveform shape, those detected on either a single recording channel or across all recording channels with varying amplitude, and those whose auto-correlogram exhibited strong periodicity or no clear valley in the refractory period. Only those clusters with a physiologically appropriate waveform, evidence of a refractory valley in the auto-correlogram, plausible amplitude changes, and clearly separated principal components reached the manual cleaning process.

For each cluster manual cleaning, we removed outliers by applying the Mahalanobis distance with a threshold of 10 standard deviations 2-3 times in a row until it converged. If the cluster principal components plot still exhibited spikes widely dispersed from the centroid after this step, we manually removed the more distant dots. Once the cluster had dense non-dispersed centroid, we discarded it if the refractory period showed contamination higher than 20% level of the auto-correlogram shoulders. Waveforms and amplitude changes continued to be reviewed during this process as indicators of the manual cleaning validity. Spikes violating the refractory period were visualized, and we eliminated those on the periphery while those contained within the cluster were left. Finally, we manually removed the few remaining noisy waveforms if they were clearly distant from the waveform group.

Throughout the manual cleaning process, the principal component scatterplots may reveal more than one spherical cloud shape. This may indicate that multiple units had been accidentally merged during the automatic sorting. In these cases,

we manually split the clouds from their principal components space and applied the above-described manual cleaning process from the beginning. When splitting subcluster units, we checked that newly generated clusters displayed different amplitudes and waveforms. If not, we merged them back. Burst-firing neurons may exhibit different amplitudes and more than one centroid in the principal components. In these specific cases, we looked for periods of high firing rates followed by lower activity and for the display of a reliable valley in the auto-correlogram. If these conditions were met, the cluster was not separated.

For all good clean units and remaining suspected multiunits, we selected the most similar cluster in the similarity view. If the compared clusters exhibited identic waveforms and amplitudes, cross-correlograms with clean refractory periods, and overlapped each other in the principal component space, we merged them. This process was repeated until the cluster of interest could no longer be merged. When generating a new merged-originated unit, it underwent the manual cleaning process from the beginning.

Therefore, only those single units displaying an auto-correlogram refractory period contamination under 20% of the auto-correlogram shoulders, distinctive action potential-shaped waveforms, signal detected in multiple channels, a relatively high firing rate, unit activity in a dense spherical shape in the principal components space, and stable amplitude through the recording session were included for subsequent analysis.

Tensor decomposition of the neuronal activity.

Neural circuits exhibit a wide range of dynamic behaviors across various time scales. The dynamics of circuits involved in neural processing occur over a few hundred milliseconds. Recent advancements in experimental techniques have allowed for the detailed monitoring of these complex dynamics by recording large numbers of neurons with high temporal precision over extended periods.

Analyzing these large-scale datasets requires unraveling simple and low-dimensional features of circuit dynamics, which need to encompass both rapid and slower neural processing. Additionally, these analytical approaches should be developed using unsupervised methods, facilitating the identification of novel and unexpected dynamics that vary across diverse trials. This approach is crucial for understanding the complex behaviors and patterns that emerge in neural circuitry over different timescales.

In conventional methods of dimensionality reduction, the focus often lies on simplifying the complexity of fast, within-trial neural firing dynamics, while slower, across-trial patterns tend to be overlooked. A common strategy is to average neural activity across trials (Churchland *et al.*, 2012; Gao and Ganguli, 2015), which limits the ability to understand changes occurring on a trial-by-trial basis across different temporal scales.

We propose a straightforward enhancement to PCA that facilitates dimensionality reduction at multiple timescales, both within individual trials and across multiple trials. The central concept involves arranging the neural firing rates into a three-dimensional data structure refereed as a third-order tensor. This tensor, containing the firing rates of the neurons, is structured across three dimensions: neurons, time within each trial, and trial number.

Essentially, a tensor is a multidimensional array. A first-order tensor is a vector (a one-dimensional array), a second-order tensor is a matrix, and tensors of third order or higher are known as higher-order tensors. In summary, a tensor is a way of organizing information. The *i*th element in a vector a is represented as a_i. For a matrix A, the element located at the intersection of the *i*th row and *j*th column is indicated as a_{ij}. In the case of a third-order tensor X, the element at the coordinates (i, j, k) is denoted by x_{ijk}.

Consider our scenario where we record the activity of N neurons across K experimental trials for each urine stimulus. In each trial for a particular stimulus, neural activity is captured at t distinct time points. We can represent this data as an $N \times U \times K \times T$ array of firing rates, which, in mathematical terms, is a fourth-order tensor. Within this tensor, each element, denoted as x_{nukt}, represents the firing rate of the nth neuron at the tth time point during the kth trial for stimulus uth. Here, the indices n, u, k, and t each range from 1 to N, K, and K, respectively.

Hitchcock proposed expressing tensors as sums of rank-one tensors, termed the *polyadic* form (Hitchcock, 1927). The core concept of tensor decomposition is centered on dissecting a tensor into more manageable and simpler components. This process is analogous to how PCA decomposes data into vectors for matrices (two-dimensional arrays), but applied to more complex data structures that encompass three or more dimensions. The primary goal of tensor decomposition is to reveal underlying patterns, simplify the data structure, and enhance interpretability. Through decomposing a tensor into a sum of rank-one tensors (or lower-dimensional components), the process of decomposition sheds light on the intrinsic relationships among the diverse dimensions of the original tensor (Figure 10).

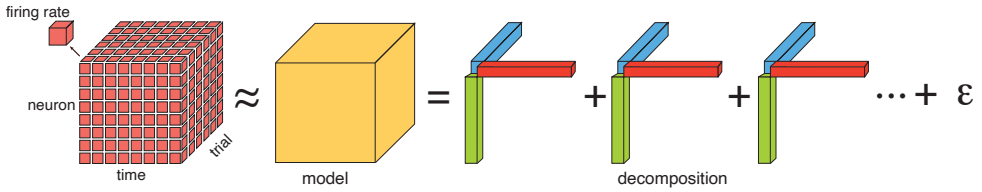

Figure 10: Decomposition of a rank-3 tensor using the PARAFAC method. The tensor F is expressed as the combination of three factorized matrices: U, K, and T, each corresponding to a mode of the tensor. This technique enables the representation of the original tensor through the sum of outer products of rank-one components, providing an effective decomposition and a detailed understanding of the underlying structure. Rank-three third-order tensor, $F = U \otimes K \otimes T$, is represented by the neuronal response U to urines, for different trials K during an epoch T of 20 s.

Canonical Decomposition (CANDECOMP) and Parallel Factors (PARAFAC) are closely related methods used for tensor decomposition, generically named as CP (Canonical Polyadic). The CP decomposition factorizes a tensor into a sum of component rank-one tensors. In our fourth-order tensor $F_4 \in \mathbb{R}^{N \times U \times K \times T}$ with firing rate as variable, the selection of a dimension results in a third-order tensor. For example, if we select the dimension *neuron*, the third-order tensor will be $F_3 \in \mathbb{R}^{U \times K \times T}$. This resulting tensor specifically represents the characteristics associated with a single neuron across the remaining dimensions (Figure 11).

If we applied the CP decomposition:

$$F_3 \approx \sum_{r=1}^{R} u_r \otimes k_r \otimes t_r + \xi$$

we obtain the factors related to the experimental paradigm, which represent the firing rate of neurons. In the context of tensor decomposition, the outer product is used to express each term in the CANDECOMP/PARAFAC decomposition as the combination of factors along each dimension of the tensor.

Thus, we construct the model with the outer product between the vectors that compose the original tensor of higher dimensionality. As example, given two vectors $\mathbf{u}$ and $\mathbf{k}$, the outer product is denoted as $\mathbf{u} \otimes \mathbf{k}$ and is defined as a matrix, where each element (i, j) is the product of the i-th element of $\mathbf{u}$ and the j-th element of $\mathbf{k}$.

$$\mathbf{u} \otimes \mathbf{k} = \begin{bmatrix} u_1 k_1 & u_1 k_2 & \cdots & u_1 k_n \\ u_2 k_1 & u_2 k_2 & \cdots & u_2 k_n \\ \vdots & \vdots & \ddots & \vdots \\ u_m k_1 & u_m k_2 & \cdots & u_m k_n \end{bmatrix}$$

Here, $\mathbf{u} = [u_1, u_2, \ldots, u_m]$ and $\mathbf{k} = [k_1, k_2, \ldots, k_n]$ are the original vectors of dimensions m and n, respectively.

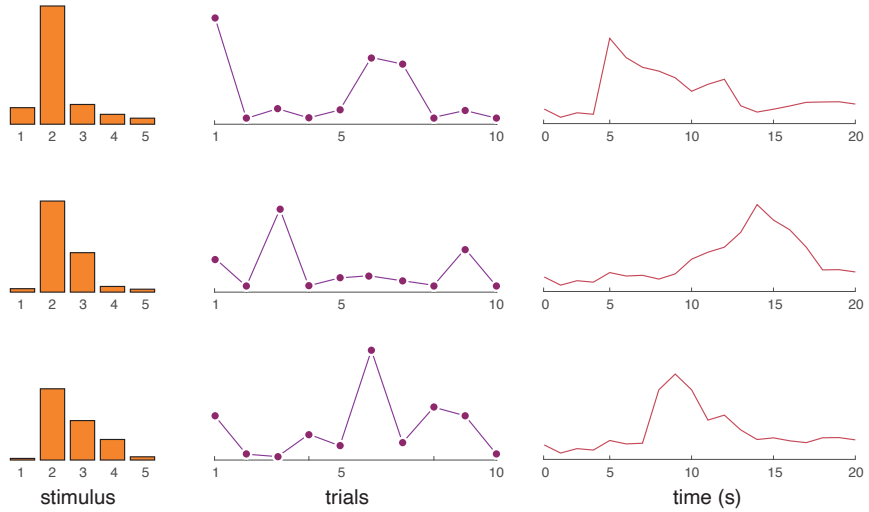

Figure 11: Tensor decomposition of a rank-4 tensor containing the firing rates of neurons in response to five urine stimuli (bars) distributed across ten trials (scatter points), each with a duration of 20 seconds (red line). The advantage of the described tensor decomposition lies in its ability to disentangle and represent complex, multi-dimensional data. This facilitates a compact representation of the underlying structure, aiding in the analysis and understanding of neural activity across different experimental conditions.

The experimental design we have proposed involves a level of complexity that is challenging to address, given the high number of neural responses structured in a tensor with dimensions of $173 \times 5 \times 10 \times 20$ (neurons $\times$ urines $\times$ trials $\times$ time). This complexity underscores the necessity of employing advanced analytical techniques like PCA and clustering to effectively distill and interpret the data (Figure 12).

In our study, tensor decomposition is employed to identify representative patterns of activity, specifically in the form of firing rates of recorded neurons, during periods when stimuli are in contact with the experimental animal. Our objective is to define a canonical representative of these response patterns to each of the urines in various exposures. To achieve this, we propose the utilization of PCA to extract the foremost component. This approach allows us to isolate the pattern that accounts for the greatest variability, thus representing the most significant aspect of neuronal activity. By focusing on this principal component, we aim to capture the essence of neuronal response patterns in a succinct and meaningful way.

This approach of clustering based on the first principal component offers significant insights into the neural encoding of sensory stimuli. By distilling complex neuronal patterns into a more manageable form, it enhances our ability to discern subtle differences in neural responses to varied stimuli. This methodology not only underscores the robustness of PCA in simplifying and interpreting high-dimensional data, but also paves the way for more detailed understandings of neuronal behavior. The findings from this analysis have the potential to contribute substantially to our knowledge of neural processing mechanisms, especially in the realm of sensory perception.

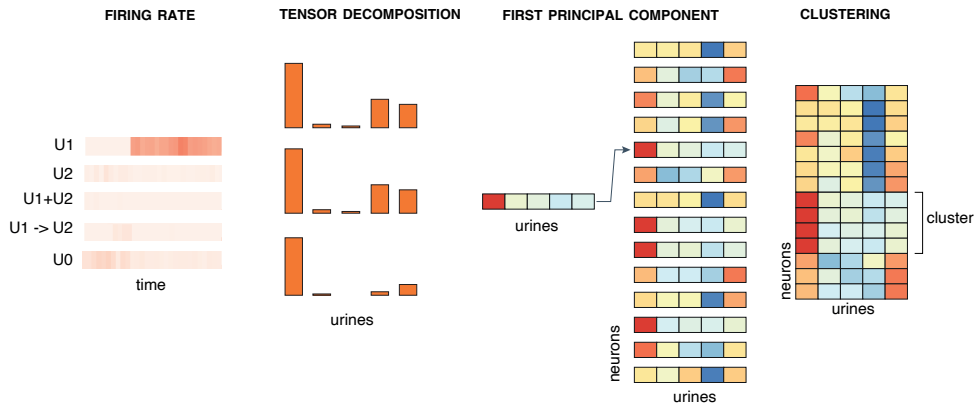

Figure 12: Schematic diagram explaining the method used to extract patterns of neuronal responses to different urine stimuli. The procedure begins with the decomposition of a tensor constructed from the firing rate of each neuron in response to the 5 urine stimuli. Each neuron, through a decomposition into four components, is represented by a specific response pattern or motif derived from the first component obtained through principal component analysis. Thus, each neuron has a canonical representation of its responses to the five urine stimuli. The collection of extracted patterns represents the response of the entire population of recorded neurons. Similarity-based rearrangement facilitates the identification of neuron clusters exhibiting closely related response patterns.

CEBRA.

We used the Consistent Embeddings of high-dimensional Recordings using Auxiliary variables (CEBRA) (Schneider *et al.*, 2023) for analyzing the PMCo single-unit recordings, particularly focusing on individual recognition tasks. CEBRA offers a significant advantage over traditional methods, like PCA, by combining nonlinear independent component analysis with contrastive learning, enabling the generation of more nuanced and interpretable neural embeddings. Unlike linear methods, CEBRA can consistently handle high-dimensional data across various subjects and sessions, making it especially suitable for complex neural decoding tasks where time information and auxiliary variables are crucial. This innovative approach ensures both the identifiability and generalizability of our findings, making it a superior choice for our analysis.

Specifically, we use CEBRA to obtain low-dimensional task embeddings by jointly fitting neural data and task-relevant behavioural variables as a function of time. In particular, we generated temporal labels expressing the structure of the task, including trials and presented stimuli (urines), both discrete labels. We then fitted them together with the neural data by minimising an InfoNCE contrastive loss target. Consequently, taking the data from all animals, we obtained latent informative embeddings.

For the implementation of the CEBRA model in our study, we carefully selected specific parameters following extensive hyperparameter tuning to ensure optimal performance. The finalized model configuration included an `'offset10-model'` architecture, a `batch_size` of `1024`, a `'cosine'` distance metric, `'time_delta'` as the conditional variable, a `'constant'` setting for temperature, set as `temperature = 1`, a `learning_rate` of `0.005`, a maximum of `5000` iterations, an output dimension of `3`, a `time_offset` of `1`, and `hybrid` set to `True`. This selection process was conducted by fitting various CEBRA models to the entire dataset and evaluating different parameter sets. The chosen parameters were those that consistently resulted in a reduced InfoNCE loss value, indicating enhanced model efficiency and accuracy in capturing the complexities of our neural data. This meticulous approach to parameter

optimization plays a crucial role in the robustness and reliability of our model's findings.

The learning rate, set at 0.005, was carefully calibrated to balance the speed and quality of learning: a too-high rate could lead to premature convergence on suboptimal solutions, while a too-low rate might slow the learning process excessively. We chose a cosine distance metric for its effectiveness in measuring the similarity between different data points as set to a constant value. This decision ensures a consistent level of sharpness in the probability distribution over classes. Maintaining a fixed temperature is crucial for the stability and interpretability of the embeddings, as it directly influences the variability in the model's predictions. This consistent setting aids in a more straightforward visualization and interpretation of the data, as it avoids the dynamic adjustments that can complicate the analysis.

The output dimension, fixed at 3, reflects a balance between capturing the complexity of our data and avoiding overfitting, a key consideration in the dimensionality of the output embedding space. Lastly, the *time_offset* parameter was set to 1, which in our contrastive learning framework, determines the temporal distance between positive pairs relative to anchor points, crucial for understanding the temporal dynamics in our data.

We carefully selected these parameters with a focus on reducing the InfoNCE loss value. This represents a key loss function in self-supervised learning that improves the model's ability to distinguish between similar and different data points. We ensured that our CEBRA model could accurately capture the intricacies of our neural data. This process of tailored parameter optimization underscores the importance of specifically tuning the model to enhance the accuracy and clarity of the neural representations it creates, thereby achieving reliable and robust results from high-dimensional data analysis.

In our study, we adopted a comprehensive approach to understand the impact of different labels (Table 2) on our CEBRA model's performance. Specifically, we trained three variations of the model using the same parameters but with different label types: one using only the *urine* label, another using only the *trial* label, and a third combining both *trial* and *urine* labels. This approach allowed us to assess the relative influence of each label type on the model's ability to capture and represent the underlying neural data. Furthermore, to evaluate the significance and effectiveness of these labels, we also trained equivalent models with shuffled labels. Shuffling the labels and observing the model's performance with these incorrect labels serves as a critical test. It helps us understand the extent to which the correct labeling of data contributes to the model's ability to form accurate and meaningful embeddings. If the model performs significantly worse with shuffled labels, it indicates that the correct labels are indeed crucial for the model to effectively represent the data.

Label Name	**Range**	**Type**
Trials	[0,1,2,3,4,5,6,7,8,9]	Discrete
Stimuli (urines)	[0,1,2,3,4]	Discrete

Table 2: CEBRA labels.

To assess the distinctiveness of activity patterns associated with different urines, we focus on calculating the average Euclidean distances between each unique pair of urine samples within the embedding space. Initially, we identify all unique urine sample types present in our dataset. For each pair, we compute the average distance between the embedding points corresponding to these samples. When considering pairs of the same urine type, we calculate the distances among all points within this group. For different urine types, we determine the distances between each point of one type to all points of the other, ensuring a comprehensive comparison.

This approach allows us to quantify the similarity between various urine samples: shorter average distances indicate greater similarity in their activity patterns. By averaging these distances, we obtain a nuanced understanding of the relationships among different urine types in the embedding space, facilitating a more detailed interpretation of our data.

For the decoding process, we utilized a K-Nearest Neighbors (kNN) classifier, leveraging its instance-based learning algorithm with a cosine-distance metric. This metric choice is pivotal as it emphasizes the orientation of vectors in the feature space rather than their magnitude, facilitating a more nuanced interpretation of similarities. Our kNN classifier was configured to identify the single nearest neighbor (k=1), offering a focused and precise prediction for each data point. To determine the k=1, we cross-validated the decoding performance exploring a range of k values, from 1 to 50. Remarkably, we found that k=1 yielded the best result, indicating that for our specific dataset the closest neighbor provides the most reliable prediction for each data point. This outcome suggests a strong local similarity among data points within the same label in our embedding space.

In our decoding task, we selected the decoding accuracy metric as our primary measure of performance due to its direct and intuitive interpretation. Accuracy, defined as the proportion of correct predictions out of all predictions made, provides a clear and straightforward way to evaluate the effectiveness of our model in classifying and decoding various stimuli. For each trial, our model generated predictions for each data point. These predictions were then compared to the true labels of the data points. The accuracy for each trial was calculated by dividing the number of correct predictions by the total number of predictions made, giving us a percentage accuracy for that trial. This process was repeated across all trials, and the results were then averaged to obtain an overall.

To establish a baseline for comparison, we also calculated a baseline accuracy. This was essential for understanding the effectiveness of our model in relation to a simpler, more fundamental level of prediction. For the baseline, we employed a random prediction strategy, where predictions for each data point were made randomly, according to the distribution of the classes in the dataset. Given that our classes were equally represented, this meant choosing randomly among the classes with equal probability. The accuracy of these random predictions was then calculated in the same way as the model's accuracy: by comparing these predictions to the true labels and calculating the proportion of correct predictions. By juxtaposing the model's accuracy with this random baseline accuracy, we could effectively gauge the added value and performance improvement brought by our model. This comparison is crucial, as it helps to determine whether our model is genuinely learning from the data and making meaningful predictions, or merely performing at a level equivalent to random guessing.

In our study we employed a refined method to calculate the decoding accuracy over time, using a sliding window approach with a bin size of 100 and step size of 1. This technique involved segmenting the data for each trial into overlapping bins, where each bin contained a subset of the data points (100 at a time) and their corresponding labels. We then calculated the decoding accuracy for each bin, which involved comparing the predicted labels with the actual labels within that bin. With this method, we obtained a detailed temporal profile of the decoding accuracy.

3.4.6 Histological verification of the recording sites.

At the end of the recording, animals were deeply anesthetized with sodium pentobarbital (100 mg/kg; Dolethal Vetoquinol, Spain) and transcardially perfused with 40 ml of heparinized saline (heparin sodium salt, Thermo Fisher Scientific, USA) followed by 80 ml of paraformaldehyde 4% diluted in PB (0.1 M, pH 7.6). Brains were postfixed overnight in the same fixative solution at 4°C, and cryoprotected in 30%

sucrose (in PB 0.1M, pH 7.6) at 4°C until they sank. Using a freezing microtome, 40-µm-thick coronal slices were obtained and collected in three parallel series.

Selected sections were counterstained with DAPI (1 µg/ml, Molecular BioProducts, USA) in distilled water for 10 minutes for overall tissue visualization and post hoc location of the recorded area. Fluorescence slices were mounted onto gelatinized glass slides, covered with FluorSave™ (Merck Millipore, USA), and photographed using a digital Leica DFC450 C camera attached to a Leica DMI3000 B inverted fluorescence microscope.

3.5 STATISTICAL ANALYSIS.

Statistical analysis was performed in RStudio (v4.0.5) and MATLAB (v2022b, The MathWorks Inc., USA).

In the behavioral analysis, within-group comparisons involving continuous variables were analyzed using a parametric Repeated Measures ANOVA, provided they met normality (assessed by the Shapiro-Wilk test) and sphericity (verified via the Mauchly test) criteria. Following significant results, post-hoc pairwise comparisons were conducted using t-tests with Bonferroni correction for multiple comparisons. If normality or sphericity assumptions were violated, a non-parametric Friedman test was employed, complemented by the Conover test for post-hoc pairwise analyses. If only sphericity was violated, we applied the Greenhouse-Geisser adjustment to the Repeated Measures ANOVA. For within-group comparisons involving discrete variables, we used the Friedman test followed by post-hoc Conover's test for pairwise comparisons.

For between-group session comparisons involving continuous variables, we utilized independent t-tests, provided the data adhered to normality (determined by the Shapiro-Wilk test) and homoscedasticity criteria (assessed with the Levene test). Otherwise, we applied the non-parametric Mann-Whitney U test. Between-group session comparisons involving discrete variables were assessed by means of a parametric Poisson regression model if the data met both the no zero-inflation and equidispersion criteria, as verified by the dispersion test. If these conditions were not fulfilled, we utilized a negative binomial regression approach.

To examine c-Fos levels, pairwise comparisons among groups were conducted through either a parametric t-test for independent samples or a non-parametric Mann-Whitney U test. The test choice was contingent upon the fulfillment of normality and homoscedasticity criteria, as determined by the Shapiro-Wilk and Levene's tests, respectively. In the cases where the sample sizes were unequal, we employed Welch's t-test. A beta regression model was utilized to compare individual c-fos/reelin proportions. For all pairwise comparisons between groups, outliers were evaluated using the Grubbs' test for univariate data. To assess statistical correlations between variables, we used the Pearson correlation test. When confronted with missing data during the correlation analyses, we employed the multiple imputation by chained equations (MICE) method to impute those missing values. Principal component analysis was performed after z-score normalization by the covariance method.

4 RESULTS

4.1 TRACT-TRACING.

In outlining the extent of the injections and the resulting labeling, we adhered to the nomenclature of the Paxinos and Franklin's atlas of the mouse brain (2004).

For clarity in our descriptions, we employed the terms "olfactory amygdala" (Kevetter and Winans, 1981a) and "vomeronasal amygdala" (Kevetter and Winans, 1981b). "Olfactory amygdala" denotes amygdaloid structures receiving inputs from the main olfactory bulb, while "vomeronasal amygdala" refers to those targeted by the accessory olfactory bulb. Hereafter, the term "chemosensory amygdala" will be used to collectively describe both the olfactory and vomeronasal amygdala, and the term mixed chemosensory amygdala to define those amygdalar regions receiving concurrent input from the main and the accessory olfactory bulb (Gutiérrez-Castellanos *et al.*, 2010).

When referring to the hippocampal formation, as defined by a broader perspective, we include a complex network of interrelated structures encompassed by the dentate gyrus, hippocampus proper, entorhinal cortex, subiculum, presubiculum, and parasubiculum (Andersen *et al.*, 2007). Likewise, we will use the terms dorsal, intermediate, and ventral hippocampus to describe the anteroposterior divisions of the hippocampus proper. In the adopted terminology, the dorsal hippocampus encompasses the region from bregma -1.34 mm to -2.30 mm, the intermediate hippocampus extends from approximately -2.30 mm to -2.80 mm, and the ventral hippocampus ranges from -2.80 mm to -4.04 mm. These terms serve not only to guide the reader but also carry significant anatomical, functional, and connectivity implications (Fanselow and Dong, 2010).

The accessory olfactory bulbs emit extensive ipsilateral glutamatergic projections to the posteromedial cortical amygdala and related chemosensory amygdalar regions.

Although the AOB's efferences have been established in the literature for decades (Winans and Scalia, 1970; Scalia and Winans, 1975), the specifics of their neurochemical nature remain a subject of ongoing exploration. In the knowledge of the presence of metabotropic glutamate receptors in target areas of the AOB projection fibers (Wada *et al.*, 1998) and the establishment of glutamate as the primary neurotransmitter utilized by the AOB's output neurons (Quaglino *et al.*, 1999), we performed an anterograde TBDA injection in the right AOB combined with immunofluorescence detection of the glutamate transporter VGLUT1.

Four injections targeted the AOB, of which only one displayed TBDA deposits restricted to this structure. The remaining three injections exhibited TBDA traces in the MOB, attributable to the tracer's diffusion. In this particular case, confirming the injection's extent was straightforward since injections reaching the MOB led to distinctly visible *lot* labeled axons. Our restricted injection reached the full extension of the AOB, affecting all the layers and, therefore, all cell types present in this nucleus (Figure 13a).

According to the literature, the anterograde AOB injection resulted in labeling along the *aot*. From the AOB, the *aot* extended caudally and medially along the ventral surface of the brain, medial to the *lot*. As the *aot* arose from the AOB, it descended ventrally and shifted slightly lateral, entering the amygdala. Within the amygdaloid complex, it coursed anteroposteriorly, innervating in its path multiple areas from the chemosensory subdivision of the amygdala. From rostral to caudal, the *aot* successively innervated the AA, NLOT, ACo, CxA, BAOT, and all the

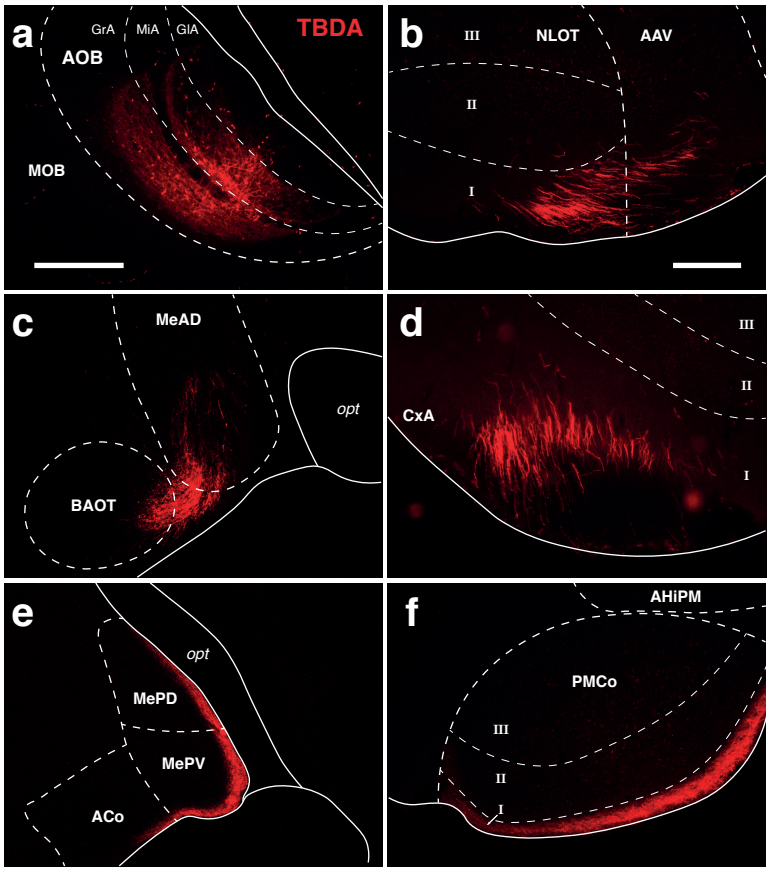

Figure 13: Anterograde labeling in the chemosensory amygdala following a TBDA injection in the AOB. The panels depict the trajectory of the *aot* originating in the AOB as it passes through the chemosensory amygdala, innervating multiple structures along its path. **a.** Restricted TBDA injection in the AOB affecting all its layers and thereby impacting every cell type within the AOB. **b-f.** *Aot* TBDA^{+} axons innervating the different structures of the chemosensory amygdala while traversing in an anteroposterior direction. **Scale bars.** In a, valid for e: 150 μm. In b, valid for c, d, f: 50 μm.

Me subdivisions to culminate in the PMCo at its posterior end (Figure 13b-f). Furthermore, some *aot* axons coursed at the superior surface of the posterior Me, where they turned dorsally and entered the amygdala-*stria terminalis* transition area. From this point, the axons routed dorsally and rostrally until they innervated the medial dense-cell column of the BSTmpm (not shown) (von Campenhausen *et al.*, 2000), considered as part of the medial extended amygdala (Winans, 1999).

Within the array of structures receiving vomeronasal input, our attention was particularly focused on the PMCo. This cortical-like nucleus is positioned caudally and laterally to the Me at its anterior aspect, and as it proceeds caudally, it lies medial to the PLCo and ventrolateral to the AHiPM. In this nucleus, the *aot* labeled axons appeared densely packed, confined to the mediolateral extension of the PMCo layer I. At the nucleus's lateral edge, the axons ascended dorsally into the plexiform layer, closely skirting the nucleus's lateral border. These labeled axons spanned the full anteroposterior length and mediolateral width of PMCo layer I, consistently remaining within its boundaries without invading adjacent PLCo or AHiPM areas. Confocal microscopy allowed us to observe the presence of numerous TBDA^{+}-VGLUT1^{+} double-labeled terminal boutons in the deep layer I of the PMCo (Figure 14). This observation corroborated the glutamatergic nature of the projection from the AOB to the PMCo.

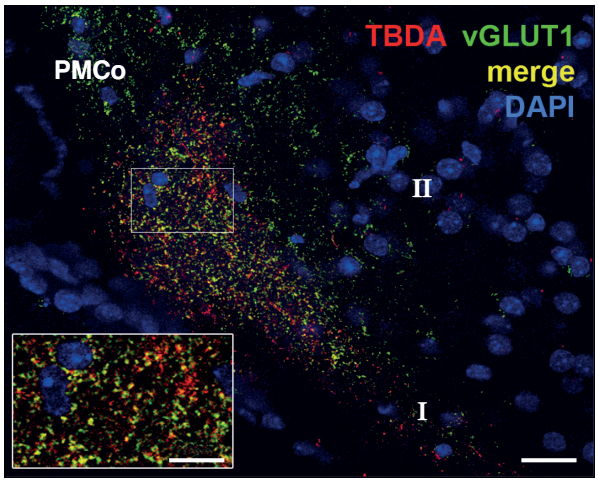

Figure 14: Glutamatergic projection from the AOB to the PMCo's layer I. Confocal microscopy image captured following a TBDA injection in the AOB (red), combined with immunofluorescence detection of VGLUT1 (green), reveals numerous double-labeled terminal boutons (yellow) in the PMCo layer I. An inset shows a detailed view of the highlighted square area. **Scale bars.** Main image: 20 µm. Inset: 10 µm.

The posteromedial cortical nucleus of the amygdala lacks direct pathways to the dorsal hippocampus but links to the hippocampal formation through direct glutamatergic projections to the ventral hippocampus and the entorhinal cortex.

The existence of reciprocal connections between the PMCo and the hippocampal formation has been documented in rats and mice studies dating back several decades (Ottersen, 1982; Canteras *et al.*, 1992; Gutiérrez-Castellanos *et al.*, 2014). However, as in the previous subsection, the specific nature of these connections has not been described in depth in neurochemical and neuroanatomical terms. Due to the limited literature on the PMCo neurochemical properties, TBDA anterograde injections were combined with fluorescence immunohistochemistry for both the glutamatergic marker VGLUT1 and the GABAergic marker GAD 65/67.

Out of eight bilateral injections aimed at the PMCo, three cases yielded successful results in at least one hemisphere, with proper tracer transport observed. However,

for the neurochemical study, we primarily used one animal. In this particular instance, the injection in one hemisphere was accurately restricted, while the opposite side's injection had been missed below the brain, ensuring no interference in the study (Figure 15a). The remaining landed injections served to corroborate the neuroanatomical findings observed in this animal.

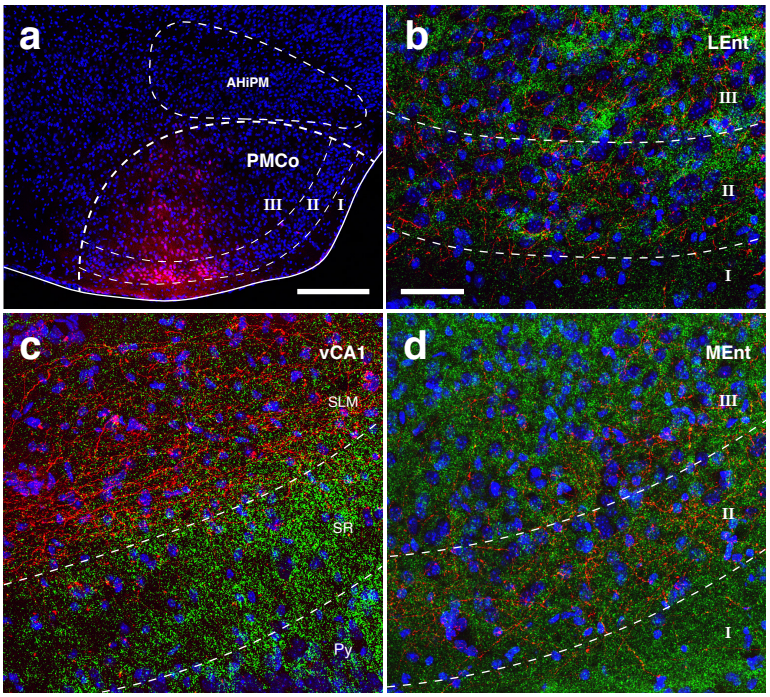

Figure 15: The PMCo emits a dense glutamatergic projection to the CA1 of the ventral hippocampus as well as to both divisions of the Ent, the lateral and the medial. **a.** Restricted anterograde TBDA injection in the PMCo. **b.** Moderate glutamatergic projection emanates from the PMCo to layers II-III of the LEnt. **c.** Very dense glutamatergic projection from the PMCo targets the distal apical dendrites of the pyramidal cells in the CA1 region of the ventral hippocampus. **d.** Sparse glutamatergic projection emanates from the PMCo to layers II-III of the MEnt. **Scale bars.** In a: 200 µm. In b, valid for c,d: 50 µm.

It is essential to note the PMCo's considerable anteroposterior extent since this factor precludes the possibility of an injection targeting the entirety of the nucleus. Nevertheless, the case used in the neurochemical study presents a remarkable extension that allowed us, together with the bibliography, to generalize our results.

Consistent with the literature, we found no direct connection between the PMCo and the dorsal hippocampus. However, we did observe fibers emerging from the PMCo that reach the overlying caudal hippocampal area. These fibers travel through the uppermost and ventral parts of the hippocampus. As a result, it rendered a dense network of forward-projecting fibers in the stratum lacunosum-moleculare and the stratum radiatum in the CA1 region of the ventral hippocampus (Figure 15c). These strata contain the apical dendrites of the CA1 pyramidal cells (Andersen *et al.*, 1971), with the PMCo densely innervating both the proximal and distal regions of these apical dendrites. In this region, we observed numerous $TBDA^{+}$-$VGLUT1^{+}$ double-labeled synaptic boutons (Figure 15c), confirming a glutamatergic projection from the PMCo to the CA1 region of the ventral hippocampus. This projection bears resemblance to the perforant path both neurochemically and neuroanatomically, as it similarly targets the apical dendrites of hippocampal pyramidal cells through glutamatergic innervation (Andersen *et al.*, 1966). This projection could be observed notably in those injections that substantially affected the PMCo outer layer III.

Concerning the entorhinal cortex, we observed a substantial group of axons traveling caudally and dorsally from the PMCo, entering the lateral portion of the entorhinal cortex and extending along its entire length. These axons circulated laterally and within the boundaries of the cortical areas that lie posterior to the PMCo. As the PMCo-labeled axons travel along the full anteroposterior extent of the LEnt, they distribute across all its layers, with a notably higher concentration observed in cell layers II/III and V/VI. The PMCo's glutamatergic innervation of the LEnt is widespread across this entire region, as evidenced by the numerous $TBDA^{+}$-$VGLUT1^{+}$ double-labeled synaptic boutons observed (Figure 15b).

Following the extensive innervation to the LEnt, some of the PMCo-derived axons progressed further posteriorly, beyond the LEnt into the ventral aspect of the MEnt. In contrast to their widespread distribution in the LEnt, the axons demonstrated a more targeted approach in the MEnt, predominantly localizing within the more external cell layers II/III. As with the LEnt, the presence of $TBDA^{+}$-$VGLUT1^{+}$ double-labeled synaptic boutons within these layers of the MEnt indicates that the PMCo's glutamatergic influence extends into this region as well, albeit with a less extensive synaptic deployment (Figure 15d). The projection from the PMCo to the entorhinal cortex was particularly evident in cases where the injections significantly targeted the layer II of the PMCo.

This posterior extension and termination of PMCo axons in the MEnt not only highlights the anatomical continuity between the lateral and medial aspects of the entorhinal cortex but also underscores the relevant role the PMCo plays across different parts of this critical cortical area of the hippocampal formation. Together with the PMCo-to-ventral CA1 projection described above, this connection pattern places the PMCo as a pivotal mediator in the interplay between cortical chemosensory processing and hippocampal function. Notably, this interplay seems to be mediated exclusively by excitatory connections, as indicated by the lack of colocalization between PMCo-labeled axons and the marker GAD65/67.

The posteromedial cortical amygdaloid nucleus and the dorsal hippocampus are indirectly connected through a restricted population of reelin-positive neurons in the dorsal aspect of the lateral entorhinal cortex.

In a series of experiments conducted by our group, which are not directly related to the present dissertation, we found that tetanic electrical stimulation of the fiber tract connecting the AOB and the PMCo led to LTP in the dorsal hippocampus. Concurrently, the introduction of male urine into the nostrils of female mice elicited physiological LTP in both the PMCo-AOB pathway and the dorsal hippocampus. A separate experiment revealed a bidirectional relationship between the population activity of the PMCo and the dorsal hippocampus CA1, exhibiting alternating causal directionality across distinct time periods. Additionally, both structures showed a common theta oscillation during exploratory behavior. This detail was evidenced by the measure of synchrony between both regions, accompanied by local gamma activity coupled with the theta rhythm within both areas (Villafranca-Faus *et al.*, 2021).

Building on these findings, we formulated a hypothesis suggesting an indirect link between the PMCo and the dorsal hippocampus. To investigate this possibility, we employed a dual-tracing approach by administering the anterograde tracer TBDA into the PMCo and the retrograde tracer FG into the CA1 region of the dorsal hippocampus. The objective of this tract-tracing experiment was to identify potential relay regions where vomeronasal information could be processed before reaching the CA1 area of the dorsal hippocampus.

As outlined in the methods section, we initially conceptualized this experiment to incorporate a triple injection strategy aimed at elucidating the role of the ventral hippocampus in this circuitry as well. However, our previous results preemptively addressed this aspect by revealing the direct glutamatergic projection from the PMCo

to the CA1 region of the ventral hippocampus. Consequently, this section will focus exclusively on the outcomes of the dual injections in PMCo and dorsal CA1.

Out of eight animals that underwent double injections, only two successfully received simultaneous injections in both PMCo and dorsal CA1. The injections in dorsal CA1 exhibited a broader spread compared to those in the PMCo, which were more confined to the nucleus. Nevertheless, the hippocampal injections were largely contained within that specific hippocampal proper subdivision, possibly extending slightly into the anteroposterior area corresponding to the intermediate hippocampus yet remaining within the limits of the CA1 region (not shown).

During the labeling analysis, we identified a restricted subset of neurons retrogradely labeled in layer II/III of the dorsal aspect of the lateral entorhinal cortex (dLEnt) and the neighboring perirhinal cortex (Figure 16a). In these layers, we also noticed anterogradely labeled fibers, complete with synaptic boutons (Figure 16b). Remarkably, these were the only areas where simultaneous retrograde and anterograde labeling co-occurred, as no similar dual labeling was detected in any other region.

The LEnt has been suggested to mediate the flow of olfactory information into the hippocampus (Strauch and Manahan-Vaughan, 2020). Moreover, the dLEnt region, where the retrogradely labeled neurons projecting to CA1 are located, receives a direct olfactory input from the main olfactory bulb (Schwerdtfeger *et al.*, 1990), as well as an indirect olfactory input from the piriform cortex (Haberly and Price, 1978; Kerr *et al.*, 2007). In light of this information, our attention was drawn to focus our study on the dLEnt.

The two major excitatory neuronal subpopulations in layers II/III of the dLEnt are reelin-positive and calbindin-positive cells (Leitner *et al.*, 2016), so we decided to combine retrograde FG injection in the dorsal CA1 of the hippocampus with immunofluorescence detection for both markers. The extent of the dorsal hippocampus injections was similar to those described above (not shown). This experiment enabled us to demonstrate that the reelin-positive neuron population in layer II of the dLEnt is the neural substrate that potentially relays vomeronasal information from the PMCo to the CA1 area of the dorsal hippocampus, as evidenced by the observed colocalization of FG and reelin (Figure 16c).

The entire extension of the posteromedial cortical amygdaloid nucleus emits projections to layer II/III of the dorsolateral entorhinal cortex.

To determine the significance of the PMCo's output to the dLEnt, we injected the retrograde tracer FG into layers II/III of the dLEnt. This specific target was informed by our previous finding of retrogradely labeled somata in these dLEnt layers following FG injection in the dorsal CA1. Additionally, this tract-tracing study aimed to discover whether other regions within the vomeronasal or mixed chemosensory amygdala serve as potential processing hubs for vomeronasal information on its way to the dLEnt before it reaches the dorsal CA1.

Of the four retrograde injections attempted in the dLEnt, precise placement was achieved in just one hemisphere of a single animal. This injection was notably confined to the dorsal portion of the nucleus, with the core of the injection located exclusively within layers II/III, causing minimal effect on adjacent layers (Figure 17a).

Following FG injection in the dLEnt layers II/III, we detected retrograde labeling throughout the entire anteroposterior length of the PMCo, encompassing both cell layers II and III (Figure 17b-d). The labeling in PMCo's layer II appeared relatively denser than in layer III, which might be attributed to its inherently dense composition. During our labeling analysis, we also identified other cortical-like structures within the chemosensory amygdala, the ACo, NLOT, and CxA, that project to the dLEnt (not shown). These structures, although also projecting to layers II/III of the dLEnt, exhibited retrograde labeling that was considerably much less extensive

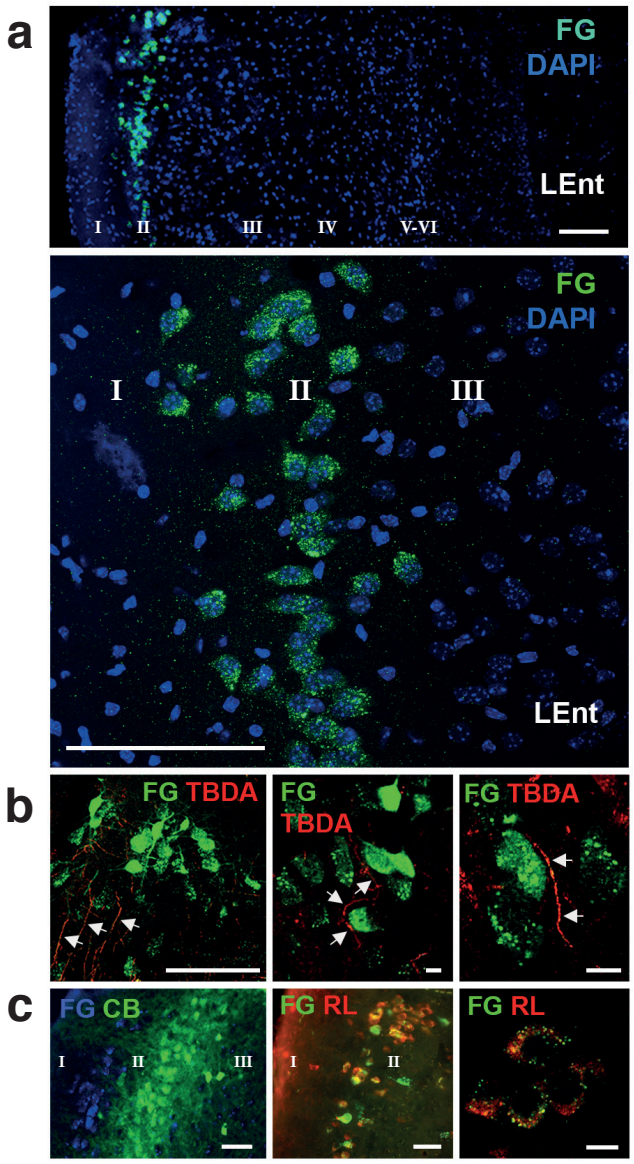

Figure 16: The PMCo is indirectly connected to the CA1 of the dorsal hippocampus via a restricted population of reelin-positive cells in dLEnt layer II. **a.** Retrogradely labeled cells (green) in the layer II of the dLEnt following FG injection in the dorsal CA1. **b.** Anterograde tracer injection into the PMCo resulted in the presence of labeled fibers (red) surrounding retrogradely labeled cells (green) in the dLEnt, evidencing an indirect anatomical pathway from the PMCo to the dorsal hippocampus. **c.** Double-labeling of FG with calbindin (left) and reelin (middle and right panels) shows that only reelin-positive dLEnt neurons project to the dorsal CA1. **Scale bars.** In a: 100 µm. In b. Left: 100 µm. Center and right: 10 µm. In c. Left: 100 µm. Center and right: 10 µm.

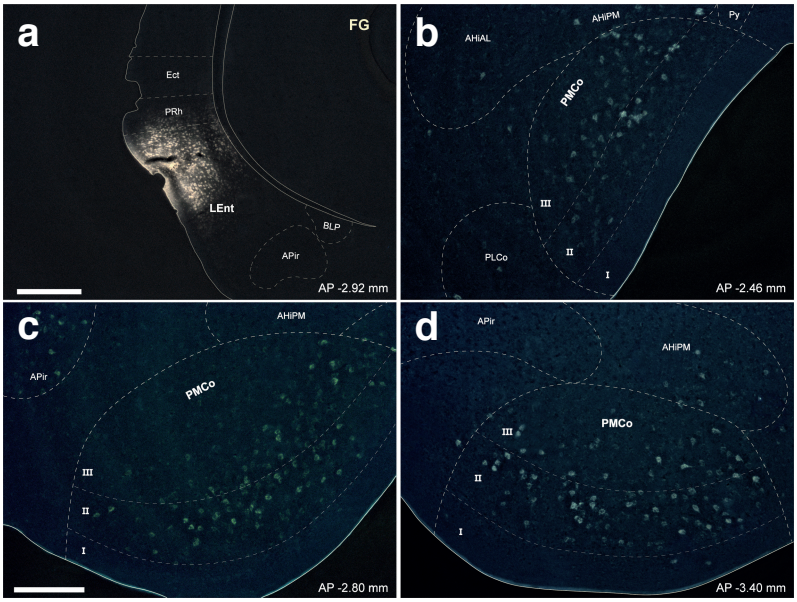

Figure 17: FG retrograde tracing confirms direct neuroanatomical connection between the dlEnt and the PMCo. **a.** FG restricted injection into the dlEnt layers II/III, at an anteroposterior level where anterograde labeled fibers were present after TBDA injection in the PMCo. **b-d.** Photomicrographs showing retrograde labeled somata through different PMCo rostrocaudal coordinates, confirming direct output from all the PMCo extent to the dlEnt. **Scale bars.** In a: 500 μm. In c, valid for b,d: 100 μm.

compared to that observed in the PMCo, underscoring a more prominent role of the PMCo in this amygdalar-entorhinal neural pathway. Conversely, the subcortical structures within the chemosensory amygdala, such as the Me and the BSTmpm, lack direct connections with either the dLEnt or the dorsal hippocampus.

These findings ultimately confirm the existence of an indirect neural pathway from the chemosensory cortical amygdala to the dLEnt, which in turn relays vomeronasal information to the dorsal CA1. Within this pathway, the PMCo emerges as a critical element, acting as a primary area for processing and transfer of chemosensory information before its integration into the hippocampal function.

The pathways from the posteromedial cortical amygdaloid nucleus to the dorsal and the ventral hippocampus are independent, yet exhibit a partially shared neuronal engagement.

Having identified the neuroanatomical pathways that transmit vomeronasal information from the PMCo to the dorsal and ventral hippocampus, it prompts the inquiry of whether the information sent via the direct pathway to the ventral hippocampus and the indirect pathway through the dLEnt to the dorsal hippocampus segregates or overlaps between these two routes. To explore these possibilities, we performed a simultaneous dual retrograde injection, administering FG in the dorsal CA1 and WGA in the ventral CA1. This approach aimed to determine if, alongside the direct pathway from the PMCo to the ventral CA1, there is an alternate indirect route for information to reach the ventral hippocampus, potentially involving a relay through the LEnt.

Of the six animals that underwent dual injections targeting the CA1 region of both hippocampi, only one successfully received both injections as intended. Although the injections had a widespread reach, they were specifically localized to the CA1 region of the nucleus without extending into adjacent areas (not shown).

For the labeling analysis, we looked for colocalization of both retrograde labelings in areas influenced by vomeronasal inputs, directing our examination toward

these specific regions. We particularly focused on the entorhinal cortex, as previous experiments had already demonstrated the lack of a direct connection between the chemosensory amygdala and the dorsal hippocampus. However, in none of these areas did we observe any colocalization of the FG and WGA labelings, suggesting that the vomeronasal processing pathways for the dorsal and ventral hippocampi operate independently.

While this experiment indicates that the vomeronasal information processing pathways to the dorsal and ventral hippocampus are independent, it leaves open the possibility that the same neurons within the PMCo could be responsible for transmitting information along these distinct routes. To address this question, we employed a dual retrograde tracing approach, injecting FG into the dLEnt and WGA into the ventral CA1 to explore the potential existence of PMCo neurons projecting concurrently to both areas.

Of the four animals subjected to this dual retrograde tracing technique, successful targeting of both retrograde injections was achieved in only one hemisphere of a single animal. In this case, the FG injection in the dLEnt accurately targeted layers II/III of the nucleus while marginally affecting the rest of the structure, although to a much lesser extent. On the other hand, the WGA injection into the ventral CA1 remained tightly confined to that specific area (Figure 18a,b).

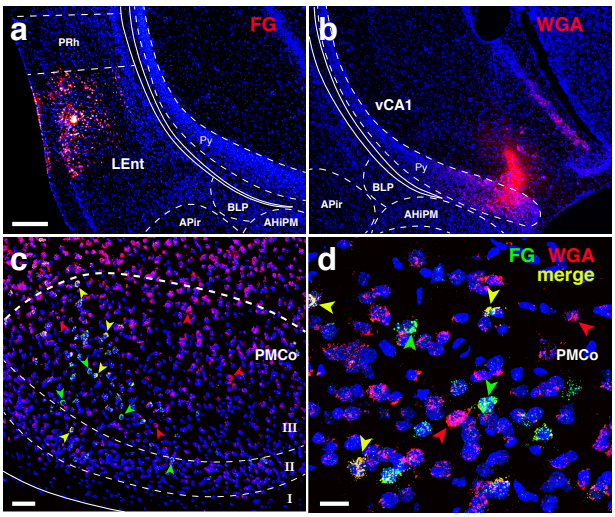

Figure 18: A subset of PMCo neurons exhibits dual projections to both the dLEnt and the ventral CA1 region of the hippocampus. **a,b.** Restricted FG injection into the dLEnt layers II-III and WGA injection into the pyramidal cell layer of the ventral hippocampus. **c,d.** Labeling study conducted in the PMCo revealed distinct populations of projecting neurons. Four distinct groups can be identified: neurons projecting to the dLEnt (green), neurons projecting to the ventral CA1 region of the hippocampus (red), neurons that simultaneously projected to both structures (yellow), and neurons that did not project to either of these areas. **Scale bars.** In a, valid for b: 150 µm. In c: 50 µm. In d: 20 µm.

The results of the labeling study revealed the presence of FG^+, WGA^+, and FG^+-WGA^+ retrogradely labeled somata within the PMCo. This labeling pattern indicates the existence of distinct projection neuron populations in the PMCo, some projecting exclusively to the dLEnt, others solely to the ventral CA1, and a third group targeting both nuclei simultaneously (Figure 18c,d). Despite visual observations suggesting a higher proportion of FG^+ neurons in layer II of the PMCo and a higher prevalence of WGA^+ neurons in layer III, limitations inherent to the tract-tracing methods prevent the assertion of topographic segregation in the PMCo's outputs. Although the tract-tracing techniques employed are constrained by the scope of the injections, it can be stated that the transmission of vomeronasal in-

formation from the PMCo to the two hippocampal subdivisions shares a common, albeit partial, neuronal origin.

Beyond the well-documented perforant path, the dorsal aspect of the lateral entorhinal cortex emits a corticofugal glutamatergic projection to the posteromedial cortical nucleus of the amygdala.

To complete the neuroanatomical description of the amygdalo-entorhinal-hippocampal pathway, the remaining aspect to assess is the nature of the anterograde connections originating from the layers II/III of the dLEnt. Previous observations showed that multiple structures within the cortical chemosensory amygdala send projections to this region, with the most significant projection originating from the PMCo. Nonetheless, an important aspect that remains to be explored is the potential for reciprocal connectivity. Unraveling whether the dLEnt not only receives input from but also sends projections back to the cortical chemosensory amygdala could provide a more comprehensive understanding of this complex neural network. To test this hypothesis, we injected the anterograde tracer TBDA into layers II/III of the dLEnt. As these layers give rise to the perforant path, known by its glutamatergic nature (Dudar, 1974; Storm-Mathisen, 1977), we complemented this injection with the immunofluorescence detection of the glutamatergic marker VGLUT1.

Out of four anterograde injection attempts in the dLEnt, accurate targeting was achieved bilaterally in two separate animals. For the labeling analysis, we utilized a particularly successful injection where the scope was notably confined to the dorsal portion of the nucleus. The core of this injection was precisely located within layers II/III, causing no effect on adjacent layers (Figure 19a).

The most prominent axon tract observed following this injection is the well-established perforant pathway. This axon bundle proceeded posteriorly and medially, entering the hippocampus through the subiculum, which serves as an essential gateway for directing entorhinal inputs into the hippocampal circuitry. Upon reaching the dorsal hippocampus, the perforant path fibers predominantly terminated in the dentate gyrus. However, some of these perforant path fibers extended beyond the dentate gyrus, projecting into the CA3 region and, to a lesser extent, to the CA2 and CA1 regions of the hippocampus. In these scattered fibers arriving at the CA1 and CA2 regions of the dorsal hippocampus, we were able to observe $TBDA^{+}$-$VGLUT1^{+}$ double-labeled terminal boutons (Figure 19b,c). While this part of the experimentation does not contribute new insights to the field, it has been instrumental in confirming that the anterodorsal region of the LEnt on which we have based our subsequent studies shares characteristics with the traditionally studied LEnt caudal regions.

Beyond this pathway, a smaller contingent of axons from layers II/III of the dLEnt travel ventrally and rostrally, entering the amygdaloid complex. Within the amygdaloid complex, they proceed laterally and anteriorly, innervating different areas of the chemosensory amygdala during their course. Since the purpose of this experiment was to determine whether the connections between the chemosensory cortical amygdala and the dLEnt are reciprocal, our attention was directed toward analyzing the labeling in these areas. We found anterogradely labeled fibers in all of the chemosensory cortical amygdalar nuclei that we identified that projected to the dLEnt, including the ACo, NLOT, CxA, and PMCo. In the PMCo, we observed $TBDA^{+}$-$VGLUT1^{+}$ double-labeled synaptic boutons (Figure 19d), confirming a glutamatergic corticofugal projection from the dLEnt to the cortical amygdala.

This reciprocal connectivity between the dLEnt layers II/III and the cortical chemosensory amygdala likely plays a crucial role in modulating the flow and integration of information within these regions. This bidirectional communication may facilitate a dynamic feedback loop, where inputs from the amygdala can influence entorhinal-hippocampal processing, and in turn, entorhinal outputs can modulate

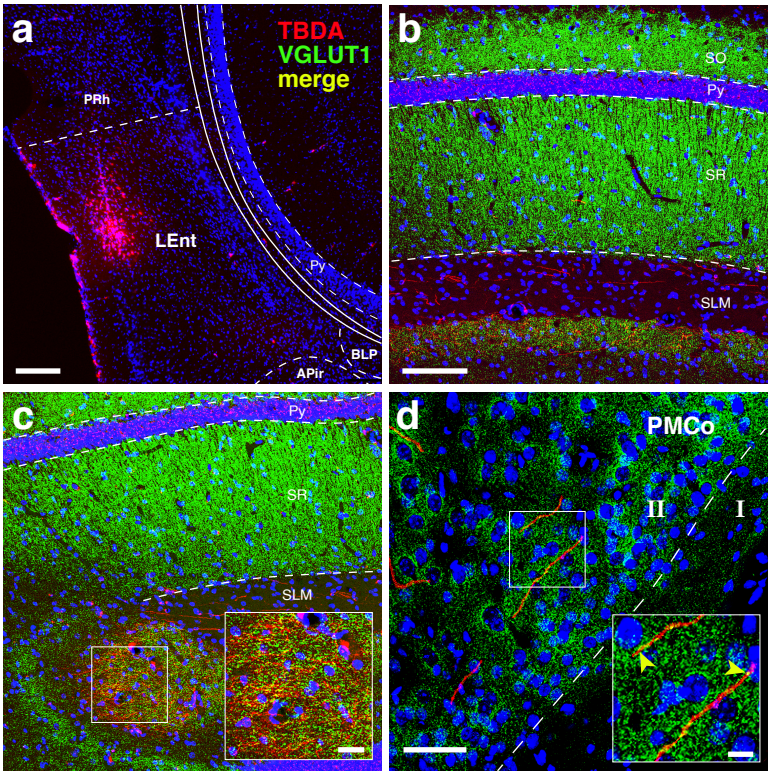

Figure 19: Beyond the perforant path, the dLEnt emits corticofugal glutamatergic projections to the PMCo. **a.** TBDA restricted injection into the dlEnt layers II/III, at an anteroposterior level where anterograde labeled fibers were present after TBDA injection in the PMCo. **b,c.** Labeled axons of the perforant path as they travel in a proximo-distal direction through the stratum lacunosum-moleculare of the dorsal hippocampal CA1. Approaching the region adjacent to the dorsal CA2, the inset highlights a remarkable concentration of $TBDA^{+}$-$VGLUT1^{+}$ double-labeled terminal boutons. **d.** Corticofugal axons projecting from the dLEnt to the layer II of the PMCo. While the projection is not as dense as the perforant path, numerous double-labeled synaptic boutons are observable. **Scale bars.** In a: 150 µm. In b, valid for c main: 100 µm. In c inset: 20 µm. In d: 50 µm. In d inset: 20 µm.

amygdalar responses, thereby contributing to more sophisticated and adaptive behavioral outcomes.

The amygdalar-entorhinal-hippocampal pathway emerges as the neural substrate for the transmission and integration of vomeronasal information into the hippocampal cognitive map.

The experiments detailed in this section primarily elucidate the neuroanatomical pathway conveying vomeronasal information to the hippocampal formation. In the neuroanatomical circuit we have outlined, vomeronasal information captured by the VNO reaches the AOB, which, in turn, projects this information via glutamatergic projections along the chemosensory amygdala. Further processing occurs in cortical-like structures of the chemosensory amygdala, such as the PMCo, ACo, NLOT, or CxA. Among these structures, the PMCo shows the most relevant connectivity with the hippocampal formation, emitting direct glutamatergic projections to the ventral hippocampal CA1 and connecting indirectly to the dorsal hippocampal CA1 via a glutamatergic projection to a specific subset of reelin-positive neurons in the dLEnt's layer II/III. Likewise, the dLEnt emits glutamatergic reciprocal connections back to these cortical-like amygdaloid structures, originating a feedback loop that might allow for the integration and modulation of chemosensory information.

Although the tract-tracing methods employed have revealed a circuit potentially involved in processing vomeronasal information, they do not definitively establish the functional relevance of the pathway. To fully understand the significance of this identified circuit, additional experiments are required, particularly those analyzing the circuit's activity following different behavioral paradigms. Such in-depth exploration will be crucial to understanding the role of this circuit in the context of actual behavioral responses and its real impact on chemosensory integration.

4.2 BEHAVIORAL TESTS AND NEURONAL ACTIVATION STUDY.

4.2.1 Urine vs. citralva exposure test.

The presence of male conspecific urine induces a preference in female individuals, in contrast to a neutral odorant.

To examine how non-volatiles contained in the male urine influence the neuroanatomical pathway elucidated in the previous section, we designed an experiment where two groups of female mice were exposed to either male urine or the neutral scent citralva. Considering urine comprises both volatile and non-volatile molecules, whereas citralva contains only volatiles, we hypothesize that any observed differences in behavior and neuronal activation between groups can be primarily attributed to the urine's non-volatile components.

The analysis of the chemoinvestigatory behavior of the animals on the test day showed that male urine induced a significantly higher exploration time when compared to the neutral odorant (independent samples t-test; $t_8 = 3.59; p = 0.007$; Figure 20a). To confirm that the heightened exploration of urine by the females in the experimental group was a result of increased interest and not due to a complete lack of general exploration by the control group, we plotted heatmaps and ethograms to track and visually compare the movement trajectories and exploration patterns of the animals during the test. Upon visually analyzing the heatmaps and the ethograms, we observed that the spatial trajectory and exploration patterns in both groups appeared normal (Figure 20b,c). This observation indicates that the differences in exploration are likely due to a preference for male urine rather than any abnormalities in general motility or exploration.

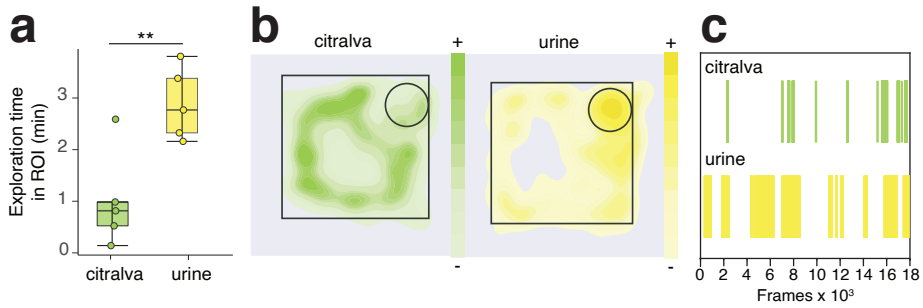

Figure 20: Behavioral outcome of the urine vs. citralva exposure test. **a.** Exploration time (min) in the stimulus area in the test during the first 10 min. Two-sided independent t-test: $^{**}p < 0.01$. **b.** Heatmaps representative of the animals in the citralva and urine groups, demonstrating a preference for exploring male urine and a normal motor activity in both groups. **c.** Representative ethograms depicting exploratory behavior of the animals in the citralva and urine groups. The ethograms highlight a marked increase in the exploration of the male conspecific urine compared to citralva.

Male conspecific urine triggers increased neuronal activity along the amygdalar-entorhinal-hippocampal pathway over neutral odorants.

To assess how male urine differentially impact nuclei involved in chemosensory signal processing, we conducted immunohistochemistry using the neuronal activation marker c-Fos. Examining the expression of this immediate early gene enabled us to map the whole neural circuitry and pinpoint neurons responsive to this specific stimulus. This approach allows a comprehensive exploration of all brain regions potentially involved in the behavioral preference for male conspecific urine over the neutral scent citralva. The foremost objective of this strategy is to analyze neuronal activation within the successive nuclei of the amygdalar-entorhinal-hippocampal pathway, enabling us to identify the most relevant regions in vomeronasal information transmission for further in-depth study.

Considering that the MOB processes volatile odorants while the AOB handles both volatile and non-volatile chemical signals (Leinders-Zufall *et al.*, 2000; Brennan and Zufall, 2006), our initial focus was to compare neuronal activation between the groups in these two olfactory bulb subdivisions. In line with our expectations, since both animal groups encountered volatiles, the MOB showed no significant neuronal activation differences ($t_8 = 1.03; p = 0.353$). Conversely, as anticipated, the AOB exhibited a higher density of c-Fos in the group exposed to male conspecific urine ($t_8 = 3.44; p = 0.021$). The absence of changes in the MOB coupled with the observed differences in the AOB supports our hypothesis that the vomeronasal stimuli in the male urine are responsible for the previously noted behavioral preference.

Subsequently, we analyzed the c-Fos distribution in the vomeronasal amygdala and associated areas. Initially, we noted increased activity in the PMCo when females were exposed to male urine ($t_8 = 4.51; p = 0.005$). This method of evaluating neuronal activation was instrumental in enabling us to discern differences within the functional subdivisions of the Me: MeA, MePD, and MePV. Notably, within the Me, we observed significant activity differences in the MePD ($t_8 = 2.51; p = 0.040$) and MePV ($t_8 = 2.82; p = 0.039$) sections, while the MeA showed no notable changes (Mann-Whitney U test; $U = 6; p = 0.222$). In the rest of the vomeronasal system, analysis of c-Fos-IR cell density indicated increased activation in the BSTmpm ($t_8 = 2.51; p = 0.038$) and the AAV ($t_8 = 2.35; p = 0.049$) in the group exposed to conspecific cues. Conversely, the BAOT did not exhibit a significant rise in c-Fos expression ($t_8 = 1.34; p = 0.217$).

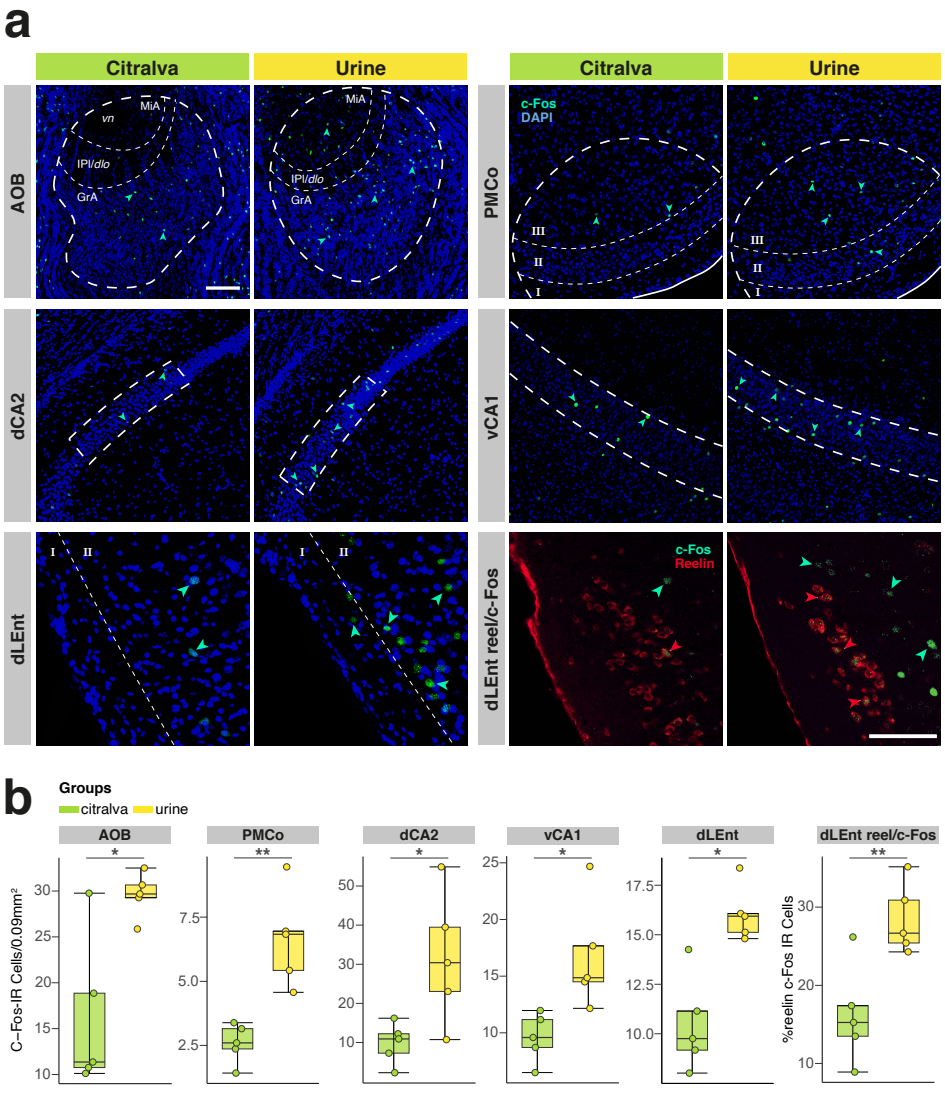

Figure 21: Neuronal activation results of the urine vs. citralva exposure test. **a.** Confocal microscopy images illustrating differential c-Fos expression between citralva and urine groups, exemplified by the most relevant structures of the amygdalar-entorhinal-hippocampal network that yielded significant results. Thick dashed lines indicate the selected ROI for quantification. Red arrows indicate active reelin-positive neurons coexpressing reelin and c-Fos markers. **b.** Boxplots depict the data distribution for the structures illustrated in panel a, providing a detailed visual representation of the variability and central tendencies within the groups. Beta regression, two-sided independent t or Mann-Whitney U test: *$p < 0.05$; **$p < 0.01$.

To investigate the impact of urine volatiles and the potential indirect influence of non-volatile compounds on the main olfactory system, we evaluated neuronal activation in the Pir and related structures of the olfactory amygdala, specifically in the NLOT, the ACo, and the CxA. When comparing to the c-Fos expression in the group exposed to citralva, we found that exposure to male urine did not significantly alter neuronal activation in the Pir ($t_8 = 0.77; p = 0.478$), the ACo ($t_8 = 1.22; p = 0.261$), or the NLOT ($t_8 = 0.48; p = 0.647$). However, unexpectedly, the CxA demonstrated a pronounced response to conspecific male urine exposure ($U = 0; p = 0.008$).

Moving forward, we conducted an in-depth analysis of c-Fos-IR neuronal density across the hippocampal formation. Given the wide-ranging counting capacity of the employed methodology, our analysis encompassed the entire hippocampal formation, not just the nodes constituting the neuroanatomical pathway outlined in the previous section. This comprehensive approach ensured that no potentially significant nodes were overlooked during our earlier anatomical delineation. We found a significantly higher c-Fos expression in the dLEnt ($t_8 = 4.34; p = 0.002$), the region where the axonal projections from the PMCo overlap with neurons projecting to the hippocampal CA1. In this nucleus, we investigated the proportion of double-labeled cells for c-Fos and reelin in each group, and our findings revealed a notably higher proportion of double-labeled neurons in the group exposed to male-derived urine (beta-regression; $Z = 3.51; p = 0.0001$). Similarly, we found a higher density of c-Fos-IR neurons in the CA1 of the ventral hippocampus ($t_8 = 3.04; p = 0.025$) and in the CA2 of the dorsal hippocampus ($t_8 = 2.94; p = 0.041$), two areas deeply related to social memory processing (Meira *et al.*, 2018). In contrast, no notable differences in neuronal activation were observed in the dorsal CA1 ($t_8 = 0.22; p = 0.828$), dorsal CA3 ($t_8 = 1.26; p = 0.250$), as well as in the DG overall ($t_8 = 0.30; p = 0.772$), or individually within its upper blade ($t_8 = 0.48; p = 0.660$) and lower blade ($t_8 = 0.06; p = 0.957$) subdivisions.

In our extensive c-Fos analysis, significant neuronal activity differences induced by male conspecific urine were observed all along the amygdalar-entorhino-hippocampal pathway. The observed differences between groups in the AOB, PMCo, ventral CA1, dorsal CA2, and dLEnt are particularly significant (Figure 21). Even more remarkable are the differences detected in the reelin-positive neuron subpopulation of dLEnt layer II/III, a region emerging as critically relevant, where vomeronasal information potentially relays before reaching the dorsal hippocampus. These findings suggest that the neuroanatomical pathway we have traced has a functional output, thereby highlighting its importance in the processing of chemosensory signals of high biological relevance.

Nonetheless, the lack of differences in the CA1 region of the dorsal hippocampus between the two groups is somewhat surprising. Given this region's primary role in encoding the cognitive spatial map, it might be expected to exhibit greater activation in response to a social cue compared to a neutral odorant. This finding suggests the need for further experimentation to gain a more comprehensive understanding.

Female mice preference for male conspecific urine is independent of the reward system activation.

Alongside our investigation of the amygdalar-entorhino-hippocampal pathway, we expanded our research to include an analysis of the reward system due to the notable preference exhibited by female mice for the urine of conspecific males. In this extended study, we focused on examining potential variations in c-Fos expression within the components of the reward system, specifically targeting the tegmental-striatal and amygdalar-striatal circuits. However, we did not detect any significant differences in the mesolimbic pathway's neuronal activation, including the VTA ($t_8 = 0.40; p = 0.701$), as well as both the core ($t_8 = 1.39; p = 0.202$) and medial shell ($t_8 = 0.49; p = 0.646$) of the nucleus accumbens. In our examination of the

basolateral complex of the amygdala, we also found no variance in the density of activated neurons between groups. This lack of difference was consistent across the basolateral ($t_8 = 0.28; p = 0.786$) and basomedial ($t_8 = 0.50; p = 0.632$) parts of the complex.

These findings indicate that exposure to male-derived chemosignals does not alter the neural response in the reward system, leading to the conclusion that the observed preference for these chemosignals does not depend on the activation of the reward system.

To exclude possible inaccuracies during the histological processing or other non-controlled factors in the previous individual comparisons, we evaluated the c-Fos expression in the caudate-putamen, an area non-related to chemosensory processing. The results showed that exposure to male urine did not influence the activity in the caudate-putamen ($t_8 = 0.02; p = 0.982$) compared to citralva exposure, thus serving as a reliable control for our previous measurements.

Consistent activation patterns across the vomeronasal system are shared with neuroanatomically related regions of the hippocampal formation.

To determine whether there is a relationship between the activation patterns in the hippocampal formation and the vomeronasal, olfactory, and reward systems, we conducted statistical correlation analyses of c-Fos densities, comparing each analyzed nucleus with all others (Figure 22). These correlations were evaluated by combining data from all subjects, regardless of their experimental group assignment. This approach allowed for a comprehensive assessment of potential interconnections among these brain regions and their response to stimuli.

Numerous positive correlations were found within the vomeronasal system, showing that vomeronasal nuclei had consistent neuronal activation in response to the stimuli. The PMCo's c-Fos cell density showed significant positive correlations with all the medial amygdala functional divisions: MePD (Spearman's rank correlation coefficient; $r = 0.85; p = 0.002$), MePV ($r = 0.89; p = 0.0004$), and MeA ($r = 0.71; p = 0.023$), in addition to other positive correlations with the BAOT ($r = 0.70; p = 0.025$), AAV ($r = 0.73; p = 0.016$), and a trend with the AOB ($r = 0.62; p = 0.055$). Notably, in the medial amygdala, strong positive correlations were evident between the MePV and MePD ($r = 0.88; p = 0.001$), MePV and MeA ($r = 0.87; p = 0.001$), and MePD and MeA ($r = 0.66; p = 0.038$), suggesting a unified response of these three Me subdivisions. Additionally, neuronal activation in the BAOT showed a direct positive correlation with both the MePV ($r = 0.64; p = 0.046$) and the MeA ($r = 0.69; p = 0.028$), whereas the AAV exhibited a notably high positive correlation with the MePD ($r = 0.93; p = 0.0001$) and the MePV ($r = 0.76; p = 0.011$), suggesting a related response pattern between these regions.

Within the hippocampal formation, several positive correlations were noted. As expected, a strong correlation emerged between overall dLEnt activation and the activity of reelin-positive neurons in layer II/III of this nucleus ($r = 0.78; p = 0.008$). In the dorsal hippocampus, the CA1 region displayed positive correlations with all other proper hippocampal areas except for the CA2. There was consistent neuronal activation observed between the dorsal CA1 and CA3 ($r = 0.64; p = 0.048$), the entire DG ($r = 0.79; p = 0.007$), and its two main subdivisions, DGub ($r = 0.68; p = 0.032$) and DGlb ($r = 0.86; p = 0.001$). Furthermore, a positive correlation in c-Fos expression was evidenced between dorsal CA2 and dorsal CA3 ($r = 0.75; p = 0.013$), while both DG blades showed a natural strong correlation in their activities ($r = 0.73; p = 0.017$).

Multiple significant positive correlations were found between the neuronal activities of nuclei in the vomeronasal system and the hippocampal formation, hinting at a potential synergistic activation between these two systems. Encouragingly, the ventral CA1 area, renowned for its role in social memory storage (Okuyama

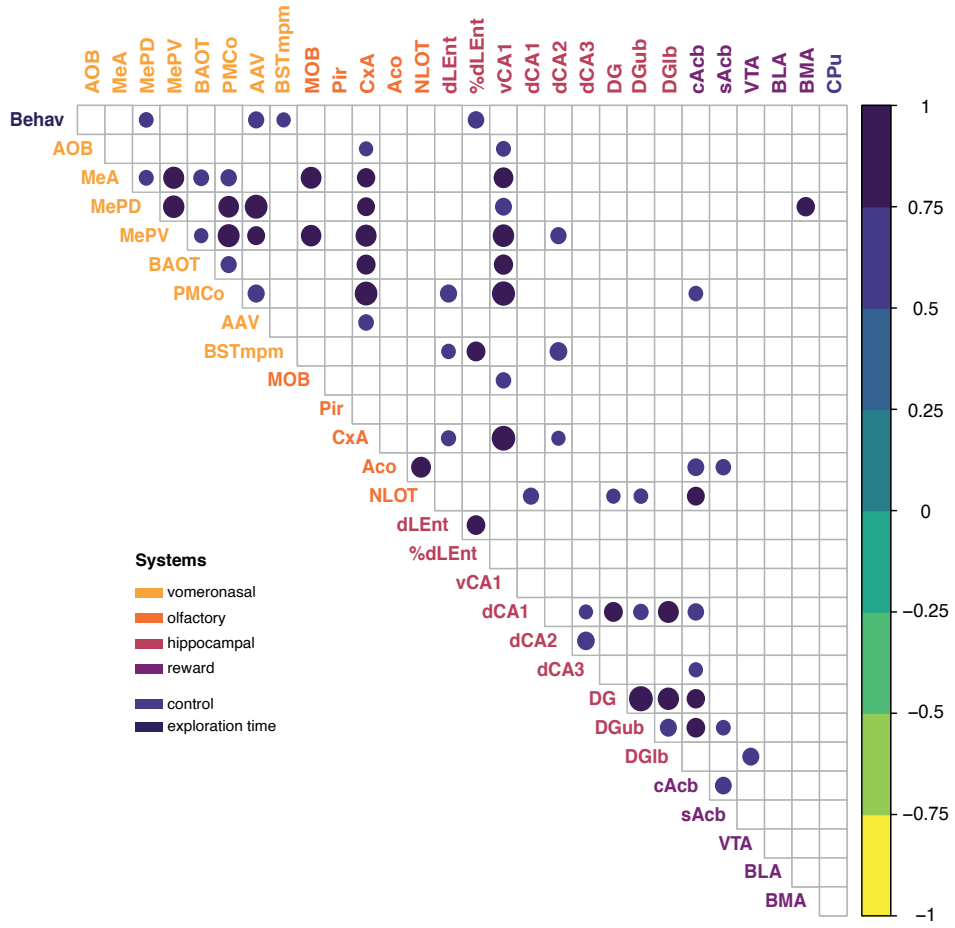

Figure 22: Significant correlations between neuronal activation and behavioral outcome in the urine vs. citralva exposure test. Correlogram displays significant statistical correlations between pairs of variables, comparing altogether c-Fos cell density in all nuclei and exploratory behavior. The size and color of each circle represent the Pearson's correlation coefficient (r-value), and circles are only shown when $p < 0.05$. Circle radius has been rescaled according to the minimum significant Pearson's r-value to enhance the visual comparability of the data. The nuclei analyzed have been organized according to their functional systems, facilitating easier comparison across different systems.

et al., 2016) and influenced by PMCo inputs, showed pronounced positive correlations with several structures of the vomeronasal system, such as the PMCo ($r = 0.94; p = 0.00005$), the AOB ($r = 0.66; p = 0.038$), the MeA ($r = 0.82; p = 0.004$), the MePD ($r = 0.72; p = 0.018$), the MePV ($r = 0.88; p = 0.0008$), and the BAOT ($r = 0.80; p = 0.005$), indicating strong interconnectedness between the ventral CA1 and the vomeronasal amygdala. Besides its strong correlation with the ventral CA1, PMCo's activity showed a robust correlation with the dLEnt ($r = 0.73; p = 0.016$), the other PMCo axon destination within the hippocampal formation. On the other hand, BSTmpm neuronal activation correlated with the overall neuronal activation in dLEnt ($r = 0.65; p = 0.016$) and also specifically with the activity of reelin-positive neurons in the dLEnt's layer II/III ($r = 0.79; p = 0.016$). Additionally, the dorsal CA2, known for its role in social information processing (Oliva *et al.*, 2020), exhibited correlated activities with the vomeronasal nuclei MePV ($r = 0.70; p = 0.024$) and BSTmpm ($r = 0.75; p = 0.012$), further underlining the intricate relationships within these two systems.

Surprisingly, the c-Fos cell density in the CxA displayed significant correlations with the activity of almost all vomeronasal nuclei, emphasizing its crucial role in processing conspecific signals, as highlighted during the group comparisons. The CxA showed substantial positive correlations with several vomeronasal structures such as the AOB ($r = 0.64; p = 0.047$), the MeA ($r = 0.77; p = 0.009$), the MePD ($r = 0.75; p = 0.012$), the MePV ($r = 0.86; p = 0.001$), the BAOT ($r = 0.79; p = 0.006$), the PMCo ($r = 0.93; p = 0.0001$), and the AAV ($r = 0.68; p = 0.030$). While the CxA has been typically considered a part of the mixed chemosensory amygdala with a predominance of olfactory functions (Gutiérrez-Castellanos *et al.*, 2010), our data suggest a more nuanced role. The significant correlations we observed between the CxA and nearly all the vomeronasal nuclei, together with the group's comparison result, suggest that the CxA collaborates closely with the vomeronasal system in the processing of socially relevant signals.

Finally, some correlations were observed between the MOB and other accessory olfactory system structures: MeA ($r = 0.86; p = 0.002$), MePV ($r = 0.85; p = 0.002$), and a suggestive trend with the PMCo ($r = 0.60; p = 0.067$). Interestingly, there was no significant correlation between the MOB and the Pir ($r = 0.03; p = 0.945$). Likewise, the activity in the chemosensory systems showed very scarce correlations with the structures in the reward system. Significant correlations were found between the activity in the accumbens core and the PMCo ($r = 0.65; p = 0.042$), ACo ($r = 0.72; p = 0.019$), and NLOT ($r = 0.75; p = 0.012$). Furthermore, c-Fos cell density in the ACo also showed a significant correlation with the accumbens shell ($r = 0.68; p = 0.031$), and the MePD correlated with the BMA ($r = 0.77; p = 0.009$).

Beyond the vomeronasal system, the hippocampal formation neuronal activity also correlates with several structures of the olfactory and reward systems.

In this subsection, we delve into the relationships extending beyond the vomeronasal system, exploring whether the neuronal activity in the hippocampal formation correlate with the olfactory and reward systems (Figure 22). The hippocampal formation has intriguing connections with the main olfactory and reward systems (Swanson and Kohler, 1986; Cenquizca and Swanson, 2007; Britt *et al.*, 2012). This connectivity highlights the hippocampal formation's role in interpreting sensory inputs and associating them with motivational states, which is essential for adaptive behavior. Consequently, it was reasonable to expect positive correlations among these systems.

In examining the c-Fos density across the hippocampal formation and the main olfactory system, a prominent finding was an observable correlation between the CxA and several pivotal structures of the pathway under study, including the dLEnt ($r = 0.67; p = 0.035$), the ventral CA1 ($r = 0.96; p = 0.00001$), and the dorsal CA2 ($r = 0.64; p = 0.048$). These findings further emphasize the potential involvement

of the CxA in processing chemosensory signals. Additionally, we found positive correlations between the neuronal activation in the NLOT and the dorsal CA1 ($r = 0.70; p = 0.024$), the overall DG ($r = 0.64; p = 0.045$), and the DGub ($r = 0.65; p = 0.041$), and between the MOB and the ventral CA1 ($r = 0.68; p = 0.032$).

Upon comparing the neuronal activities of the hippocampal formation with the reward system, we also noted several positive correlations. The accumbens core showed significant correlations with different regions of the dorsal hippocampus proper, such as the CA1 ($r = 0.71; p = 0.022$), the CA3 ($r = 0.64; p = 0.046$), the entire DG ($r = 0.77; p = 0.009$), and the DGub ($r = 0.78; p = 0.008$). Similarly, the c-Fos expression in the DGub correlated with the accumbens shell ($r = 0.65; p = 0.040$), whereas the neuronal activation in the DGlb was linked to the VTA ($r = 0.72; p = 0.018$).

Furthermore, our analysis extended to examining the correlation between c-Fos expression in all nuclei and behavioral outcomes. This examination revealed a direct correlation between the duration of stimulus exploration and the activation in certain vomeronasal structures. Notably, the MePD showed a positive correlation ($r = 0.66; p = 0.040$), as did the AAV ($r = 0.70; p = 0.025$) and the BSTmpm ($r = 0.64; p = 0.046$). Interestingly, the proportion of double-labeled reelin-positive cells in layers II/III of the dLEnt also correlated with stimuli exploration time ($r = 0.71; p = 0.021$), suggesting their involvement in sensory processing related to behavioral chemosensory exploration. As expected, no correlation was found between the caudate-putamen and any other structure, thus confirming its validity as a control.

Common c-Fos expression pattern in the vomeronasal information transmission nodes of the amygdalar-entorhinal-hippocampal pathway.

To identify global activation patterns and thus interconnected neural response networks, we performed a PCA by pooling all the c-Fos data. This method has helped us to identify the structures that make the most significant contributions to the PCA model among the multitude of analyzed nuclei. We chose the first two principal components from the nine we obtained, as they distinctly separated both experimental groups and explained 61.0% of the total variance (with PC1 accounting for 44.1% and PC2 for 16.9%, (Figure 23a). It is worth mentioning that we compared the outcomes derived from selecting just two principal components with those from choosing three. As the conclusions were equivalent in both scenarios, we present the PCA results with two components for their interpretative simplicity and the straightforward nature of the resulting plots.

The biplot illustrates that subjects exposed to male urine grouped near the vectors representing the vomeronasal signal-conveying nuclei (bottom-right), while those exposed to citralva were dispersed in the opposite direction to the vectors (Figure 23b). This suggests that male conspecific urine elicited a neural response pattern that aligned with the activation of brain regions we theorized to be engaged in vomeronasal signal transmission, whereas citralva induced a less specific neural response pattern. The presence of the citralva-exposed group in the opposite direction of all vectors might indicate that the response to citralva involves variance in the dataset that is orthogonal to the variance explained by the response to male urine.

The PC1 loading factors were exclusively positive (X-axis; Figure 23b), representing a weighted average of the entire network's activity. Consequently, it did not enabled differentiation between functional systems. On the other hand, the PC2 exhibited both positive and negative loading factors (Y-axis; Figure 23b). This PC revealed that the vectors for nuclei unrelated to vomeronasal information flow are in the positive range. Included here, we found the entire reward system, hippocampal areas not initially associated with vomeronasal information processing and transmission, and certain parts of the olfactory chemosensory amygdala, such as the NLOT and ACo. In the negative range, we found clustered all the vectors representing regions

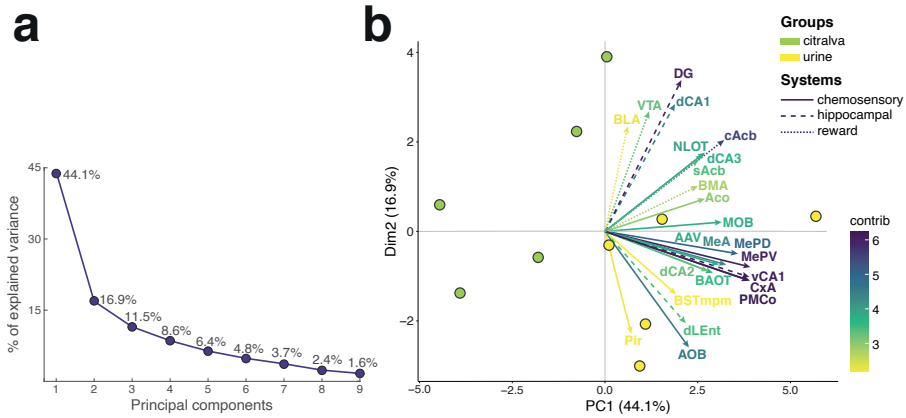

Figure 23: PCA reveals common c-Fos expression pattern in the amygdalar-entorhinal-hippocampal pathway. **a.** Percentage of explained variance by each PC. **b.** PCA biplot showing females exposed to male urine (yellow dots) or citralva (green dots). Dots represent the loading of each animal to the PCs. Solid vector lines represent chemosensory structures, dashed vector lines hippocampal formation nuclei, and dotted vector lines reward system areas. The vector orientation indicates its contribution to a PC: greater parallelism with a PC axis means higher contribution to that specific PC. The vector length shows how effectively the two principal components explain the variability in c-Fos expression density for that nucleus. Angles between vectors of different nuclei represent their correlation: small angles imply high positive correlation, right angles indicate no correlation, and vectors in opposite directions suggest high negative correlation. The biplot visually clusters vectors that correspond to the amygdalar-entorhinal-hippocampal pathway nodes. Dots representing urine-exposed animals appear clustered in proximity to these vectors.

hypothesized to be the neuroanatomical basis for the flow of vomeronasal information to the dorsal hippocampus. This includes the AOB, the complete vomeronasal chemosensory amygdala, hippocampal regions anatomically linked to the PMCo (dLEnt, ventral CA1, and dorsal CA2), as well as the CxA, which previous individual comparisons and correlation analyses have demonstrated to be collaborating in vomeronasal signal processing. This separation suggests that the nuclei examined belong to two distinct functional systems, each reacting differently to the stimuli.

Furthermore, we assessed the contribution of each variable to both PCs, quantifying it in terms of coefficients and percentage of variance explained for each PC. As mentioned earlier, the PC1 only exhibited positive values, representing a weighted average of the network's total activity. Notably, the nuclei making the most significant contributions to PC1 are MePV (principal components analysis; $coef : 0.286$; $var : 8.17\%$), PMCo ($coef : 0.285$; $var : 8.13\%$), and vCA1 ($coef : 0.284$; $var : 8.05\%$). Therefore, these nuclei emerge as the primary influencers in the network's overall activity pattern. In the PC2, which exhibited both positive and negative loading values, the AOB stands out as the nucleus with the highest influence in the negative range ($coef : -0.306$; $var : 9.38\%$), whereas the DG holds the highest weight within the positive value spectrum ($coef : 0.399$; $var : 15.91\%$).

4.2.2 Social stimuli spatial manipulation test.

Female mice exhibit an increased reexploration of their territories when male landmarks are shifted in space.

To evaluate how the spatial relocation of social male landmarks influences female behavior, we conducted an experiment where urine samples from three different

male mice were moved to a new location following three days of training. We aimed to ascertain whether a female can detect subtle changes in the spatial distribution of social cues present in her environment and if such changes are significant enough to elicit alterations in her behavior and neural responses.

To evaluate territory reexploration, we focused on two behavioral variables: total entries into glass jars (contacts), as a means of space identity confirmation and entries into different jars from the previously visited (transitions), reflecting a pursuit of exploring new landmarks. Furthermore, to comprehensively analyze this complex behavior, we assessed the average speed, total distance covered, and exploration time.

Regarding contacts, within-group comparisons indicated significant differences in the experimental group (Friedman test; $F\chi^2 = 9.75; p = 0.021$) but not in the control group ($F\chi^2 = 4.2; p = 0.241$). Post-hoc analysis using Conover's method showed that in the experimental group, the notable differences were present between training days 1-3 (Conover's test of multiple comparisons, $p = 0.029$), training days 2-3 ($p = 0.0002$), and between training day 3 and the test day ($p = 0.019$). This suggests that the animals' interest in reexploring landmarks decreased during the days with unchanging positions, but this interest was recovered to initial levels when the social cues were altered in space, as evidenced by the lack of significant differences between the test day and training days 1 ($p = 0.999$) and 2 ($p = 0.609$). Conversely, the assessment of contacts between groups did not yield statistically significant differences (Figure 24a). This outcome is likely attributed to the application of a restrictive negative binomial regression, a necessary approach given the lack of equidispersion in the dataset.

In line with the previous analysis, within-group comparisons for transitions indicated significant differences in the experimental group ($F\chi^2 = 8.1; p = 0.044$) but not in the control group ($F\chi^2 = 2.65; p = 0.449$). Post-hoc analysis revealed significant differences between training days 1-3 ($p = 0.041$), days 2-3 ($p = 0.041$), as well as between training day 3 and the test day ($p = 0.002$). As expected, no significant differences were found between the test day and training days 1 ($p = 0.815$) or 2 ($p = 0.815$). Diverging from the contacts variable analysis, the negative binomial regression on transitions highlighted an increased number of transitions on the test day in the experimental group (negative binomial regression; Intercept $\beta_0 = 3.13, p < 0.001$; Group effect $\beta_1 = 0.52, p = 0.016$) (Figure 24a).

Further analysis revealed no significant differences in average speed between groups or across days within the same group (Figure 24a). However, the repeated measures ANOVA for the total distance traveled showed notable differences within the control group (repeated measures ANOVA; $F_{3,15} = 12.68; p = 0.00002$) but not the experimental group ($F_{3,15} = 1.18; p = 0.350$). Post-hoc pairwise comparisons using t-tests with Bonferroni correction showed a distance traveled reduction in the control group from training day 1 to 3 ($p = 0.042$) and from training day 1 to the test ($p = 0.005$), reflecting a decreased inclination for reexploration as the environment remained static. In line with this finding, when comparing each day between groups, we observed an increase in distance traveled in the experimental group compared to the control group on the test day ($t_{10} = 2.87; p = 0.017$) (Figure 24a).

Concerning total exploration time, the analysis identified significant variations within the control group ($F_{3,15} = 0.82; p = 0.505$) but not in the experimental group ($F_{3,15} = 13.18; p = 0.00002$). Post-hoc comparisons within the control group showed a pronounced increase in exploration time from training days 1-3 ($p = 0.011$) and between training days 1 and 2 compared to the test day ($p = 0.001; p = 0.002$). Moreover, during the test day, the exploration time of the control group significantly exceeded that of the experimental group ($t_{10} = -3.73; p = 0.007$) (Figure 24a). As indicated by the previous results, the control group exhibited a lesser tendency to switch between different landmarks. This behavior suggests that female mice controls spent more time exploring preferent individual landmarks, leading to an overall increase in total exploration time. In contrast, the experimental group,

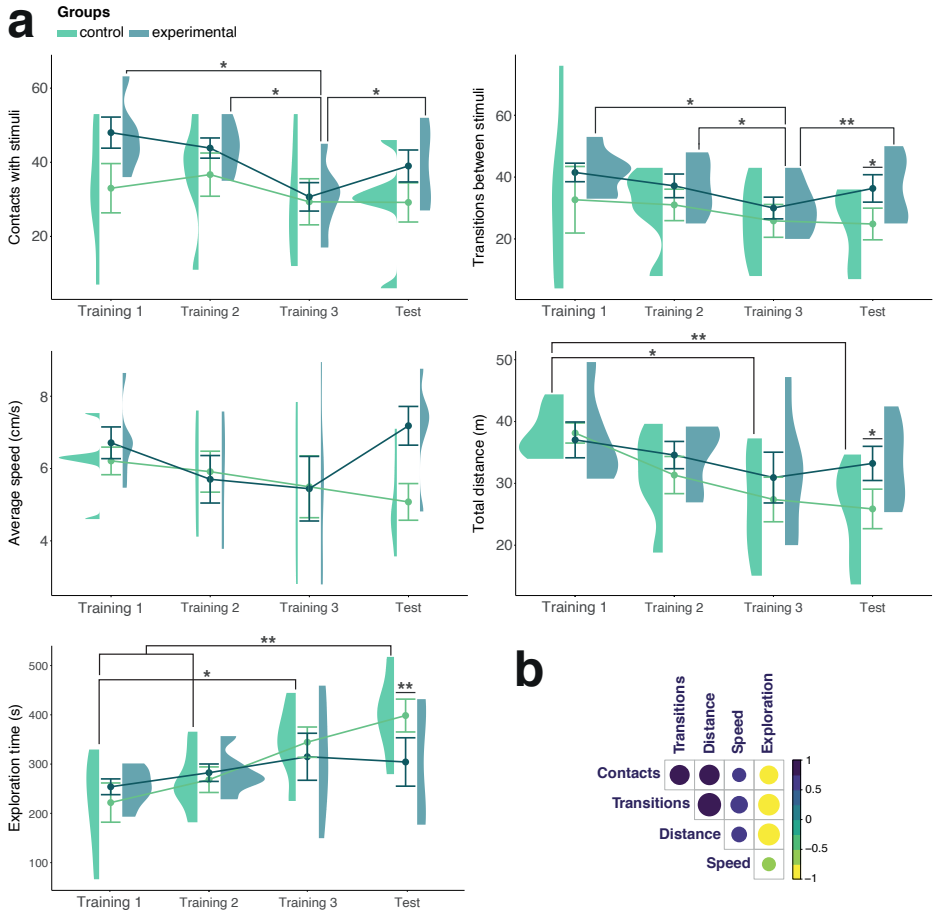

Figure 24: Behavioral outcome of the social stimuli spatial manipulation test. **a.** Line graphs display the behavioral results throughout the experimental protocol for the control and experimental groups across five behavioral variables: contacts, transitions, speed (cm/s), distance (m), and exploration time (s). Each day's mean for each group is represented by dots, with bars indicating the SEM. Adjacent to the bars, half violin plots provide a visual representation of data distribution: on the left for the control group and on the right for the experimental group. Differences between groups are denoted above the top error bar of the group with the higher mean. For the discrete variables, contacts and transitions, negative binomial regression was used. For the continuous variables, speed, distance, and exploration time, two-sided independent t-tests or Mann-Whitney U tests were employed. Within-group differences are highlighted by lines connecting days with significant differences, intersecting the half violin plot of the group exhibiting these differences. For discrete variables, the Friedman test followed by Conover post-hoc was applied. For continuous variables, repeated measures ANOVA followed by t-tests with Bonferroni correction for multiple comparisons was utilized. *$p < 0.05$; **$p < 0.01$. **b.** Correlogram displays significant statistical correlations between pairs of behavioral variables. The size and color of each circle represent the Pearson's correlation coefficient (r-value), and circles are only shown when $p < 0.05$. Circle radius has been rescaled according to the minimum significant Pearson's r-value to enhance the visual comparability of the data.

showing more frequent transitions, would spend comparatively less time on each landmark, thus accounting for their shorter exploration times. This explanation is corroborated by the strong inverse correlations observed between exploration time and all the other behavioral variables obtained: contacts ($r = -0.78; p = 0.003$), transitions ($r = -0.89; p = 0.00009$), average speed ($r = -0.91; p = 0.00003$), and covered distance ($r = -0.59; p = 0.044$) (Figure 24b).

This data collectively suggest that female mice are acutely aware of minor alterations in the spatial arrangements of social cues within their environment. These changes prompt them to thoroughly renavigate their surroundings, indicating that they actively monitor the ownership of territories and update their spatial cognitive map accordingly. This dynamic process ensures that their navigational knowledge remains current and aligned with the social reality of their environment.

The rearrangement of social landmarks leads to increased c-Fos expression in the dorsal CA1 and MEnt without affecting other parts of the pathway.

To assess the impact of spatially repositioning social landmarks on neuronal activation, we carried out an experiment in which urine from three different male mice shifted to a new location after three days of training in a stable placement. The primary aim of this experiment was to discern which nuclei within the pathway under study are more active in response to changes in the spatial orientation of territorial landmarks. Building on our previous experiments, where we identified the most relevant nodes of the amygdalar-entorhinal-hippocampal pathway, this study focuses on evaluating the activation levels of those specific nuclei that showed significant involvement in the processing and transmission of vomeronasal information to the hippocampus.

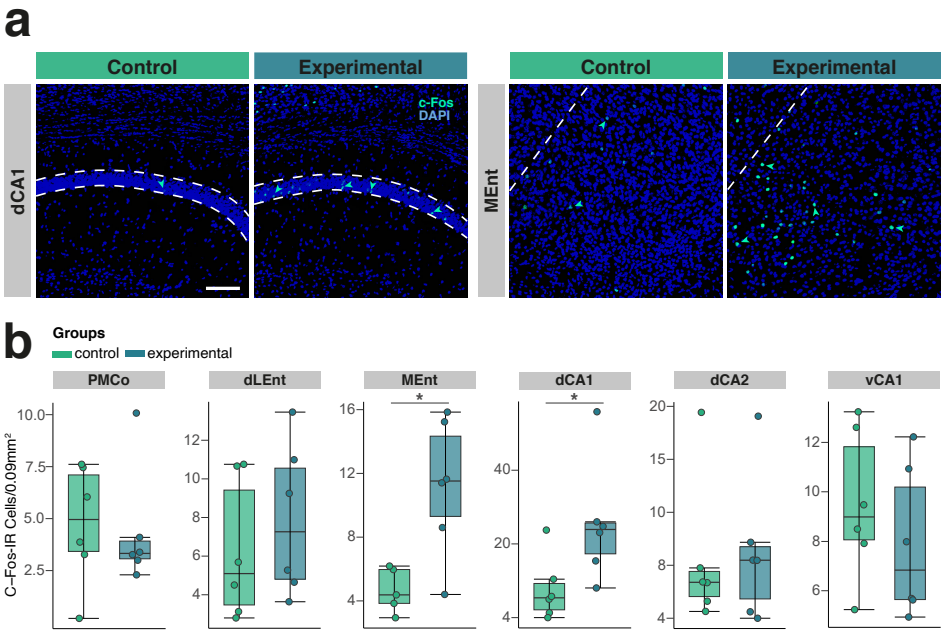

Figure 25: Neuronal activation results of the social stimuli spatial manipulation test. **a.** Confocal microscopy images illustrating differential c-Fos expression between control and experimental groups, exemplified by the most relevant structures of the amygdalar-entorhinal-hippocampal network that yielded significant results. Thick dashed lines indicate the selected ROI for quantification. **b.** Boxplots depict the data distribution for the structures illustrated in panel a and other relevant nodes of the pathway, providing a detailed visual representation of the variability and central tendencies within the groups. Two-sided independent t or Mann-Whitney U test: *$p < 0.05$.

In line with the literature, in the group subjected to a spatial shift, we observed a marked increase in c-Fos cell density in the dorsal CA1 region ($t_{10} = 2.36; p = 0.047$) and the MEnt ($t_9 = 3.53; p = 0.012$) (Figure 25). This finding aligns with established knowledge, as these areas are known to house place (O'Keefe and Dostrovsky, 1971) and grid (Hafting *et al.*, 2005) cells, respectively, which are integral to spatial navigation and memory. However, contrary to what we had anticipated, our analysis revealed a surprising uniformity across the rest of the analyzed regions. We observed no notable variations in the ventral CA1 ($t_{10} = 0.91; p = 0.384$), the dorsal CA2 ($t_9 = 1.11; p = 0.294$), the dorsal CA3 ($t_9 = 0.65; p = 0.541$), the overall DG ($t_{10} = 0.11; p = 0.912$), or the DGub ($t_{10} = 0.45; p = 0.665$) and DGlb ($U = 8; p = 0.122$) of the hippocampus proper. Similarly, the dLEnt as a whole exhibited no alteration in neuronal activity ($t_{10} = 0.74; p = 0.475$), a pattern that persisted when focusing on the reelin-positive neurons within layers II/III of the same nucleus ($Z = 0.38; p = 0.702$). To conclude, our examination extended to the PMCo, where we found no significant changes in c-Fos expression either ($t_{10} = 0.24; p = 0.819$).

These findings imply that the processing of social cues spatial changes may not rely on the activation of the pathway via the dLEnt, or at least the spatial changes may not be sufficiently engaging to induce a distinguishable activation level on this pathway. Nevertheless, the pronounced increase in activity within the dorsal CA1 and MEnt regions suggests that while the the rest of the pathway may not be broadly responsive to spatial reorientations of social cues, certain key areas within this pathway are selectively sensitive to such changes. This specificity indicates a potential compartmentalization of functions, where only certain nuclei are directly involved in processing these types of spatial information. Subsequent experiments could further explore these region's roles to unveil the neural basis of spatial navigation and memory in the context of territorial behavior and environmental adaptation.

Common activation pattern in the segments of the pathway that remained unaffected by the spatial relocation of social cues.

Despite the absence of significant differences in most of the nuclei examined in the previous section, we decided to perform a correlation analysis of the c-Fos dataset (Figure 26). This approach aimed to explore possible hidden relationships in the data that may not have been evident in the between-group comparisons.

Interestingly, a significant correlation emerged between the c-Fos expression in the dLEnt and the ventral CA1 ($r = 0.76; p = 0.004$), the primary areas of the hippocampal formation innervated by the PMCo axons. As expected, a robust correlation was observed between the overall activation in the dLEnt and the activity of reelin-positive neurons in layers II/III of the same nucleus ($r = 0.76; p = 0.005$). The activation of this neuron population also showed a correlation with the activity across all subdivisions of the dorsal hippocampus's Cornu Ammonis regions, namely CA1 ($r = 0.68; p = 0.014$), CA2 ($r = 0.77; p = 0.003$), and CA3 ($r = 0.73; p = 0.007$). Furthermore, the c-Fos expression within these three divisions showed interrelated patterns, with the CA1 correlating with the CA2 ($r = 0.77; p = 0.003$), the CA1 with the CA3 ($r = 0.69; p = 0.013$), and the CA2 with the CA3 ($r = 0.88; p = 0.0001$). Contrary to our expectations, we observed no statistical correlation between the activity of the dorsal CA1 and MEnt ($r = 0.48; p = 0.118$) despite being the two structures differentially activated by spatial changes in landmarks.

With regard of behavioral variables (Figure 26), a statistically significant correlation between average speed and c-Fos expression in the dLEnt was observed ($r = 0.59; p = 0.043$). Furthermore, it is noteworthy that MEnt neuronal activation exhibited a positive correlation with transitions ($r = 0.62; p = 0.032$) and distance

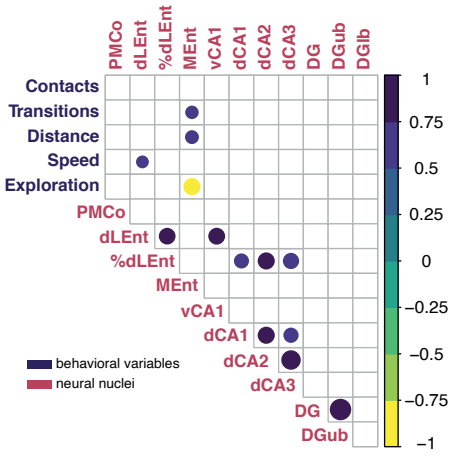

Figure 26: Significant correlations between neuronal activation and behavioral outcome in the social stimuli spatial manipulation test. Correlogram displays significant statistical correlations between pairs of variables, comparing altogether c-Fos cell density in all nuclei and exploratory behavior. The size and color of each circle represent the Pearson's correlation coefficient (r-value), and circles are only shown when $p < 0.05$. Circle radius has been rescaled according to the minimum significant Pearson's r-value to enhance the visual comparability of the data.

traveled ($r = 0.63; p = 0.027$), while exhibiting a strong negative correlation with total exploration time ($r = -0.77; p = 0.003$).

This brief analysis comparing all regions once more underscores the interconnected activity among various parts of the amygdalar-entorhinal-hippocampal pathway. Despite the absence of a significant correlation between the activity in the dorsal CA1 and MEnt, it is noteworthy that the activity in the dorsal CA1 parallels that in the dLEnt reelin-positive neurons, which are among its primary inputs. Overall, these results reveal a complex, perhaps compartmentalized, neural processing of the different components of social memories.

4.2.3 Social vs. object spatial manipulation test.

Rearranging male landmarks in space elicits changes in female exploratory behavior, while analogous spatial alterations of objects have no effect.

To evaluate the impact on female behavior of spatial reorganization of male-derived cues versus inanimate objects, we established two distinct experimental groups. In these groups, after three days of training with either different male urines or inanimate objects in a stable position, female mice encountered a change in the spatial arrangement of these items in their environment.

As in the social manipulation test behavioral analysis, we focused on five behavioral variables to evaluate reexploration: "contacts" as total entries into the ROIs, "transitions" as entries into different ROIs from the previously visited, average speed, total distance covered, and exploration time.

Regarding contacts, within-group comparisons indicated significant differences in the social-exposed group ($F\chi^2 = 9, p = 0.029$) but not in the object-exposed group ($F\chi^2 = 1.75, p = 0.626$). No differences were observed in the group exposed to male urine during the three training days. However, when male-derived urine samples were spatially shifted on the test day, there was a marked increase in the number of contacts, significantly exceeding the recorded number on each of the training days: day 1 ($p = 0.008$), day 2 ($p = 0.046$), and day 3 ($p = 0.003$). Nevertheless, the assessment of contacts between groups revealed a higher number of contacts in the object-exposed group for training 2 (Intercept $\beta_0 = 4.05, p < 0.001$; Group

effect $\beta_1 = -0.54, p = 6.7e-09$), training 3 (Intercept $\beta_0 = 4.25, p < 0.001$; Group effect $\beta_1 = -0.86, p = 1.3e-07$), and test day (Intercept $\beta_0 = 4.03, p < 0.001$; Group effect $\beta_1 = -0.24, p = 0.017$), along with a trend on training day 1 (Intercept $\beta_0 = 3.92, p < 0.001$; Group effect $\beta_1 = -0.52, p = 0.092$) (Figure 27). The contact results indicate that while animals generally approach objects more often during all days, likely due to their interactive nature, the spatial rearrangement of these objects does not affect female behavior, in contrast to the changes in behavior observed with the spatial alteration of landmarks.

For transitions, within-group analysis showed notable differences in the group exposed to social stimuli ($F\chi^2 = 8.35, p = 0.039$), while in the group exposed to objects no significant differences were present ($F\chi^2 = 4.05, p = 0.256$). Closely replicating the results from the experimental group of the social manipulation test, post-hoc analysis indicated a higher number of transitions on training day 2 compared to day 3 ($p = 0.036$), as well as on the test day relative to training day 3 ($p = 0.016$). In line with expectations, no significant differences were found between the test day and training days 1 ($p = 0.076$) or 2 ($p = 0.992$). In any case, it might be noted that the test day approached significance in exceeding the number of transitions compared to training day 1. In contrast to the contact analysis, the assessment of transitions between groups yielded no significant differences (Figure 27).

The repeated measures ANOVA for assessing average speed showed significant differences for the social-exposed group ($F_{3,15} = 6.53, p = 0.005$), but not in the object-exposed group ($F_{3,15} = 2.62 p = 0.089$). However, pairwise comparisons in the group exposed to male urine did not reveal any significant differences across the four days, likely due to the application of a stringent statistical correction (Figure 27).

Non-parametric tests were employed to analyze the distance traveled within both groups, given the data's non-normal distribution and the violation of sphericity. The analysis revealed within-group significant differences in both groups (urine-exposed group: $F\chi^2 = 11, p = 0.012$; object-exposed group: $F\chi^2 = 10.8, p = 0.013$). Post-hoc comparisons within the social group revealed an increased distance traveled on training day 1 compared to day 3 ($p = 0.017$), and on the test day against training days 2 ($p = 0.002$) and 3 ($p = 0.0001$). This result indicates a progressive decrease in the distance traveled during the days when the landmarks remained in fixed positions, followed by a resurgence in distance traveled to levels comparable to those of the initial exposure day, prompted by the spatial rearrangement of the urines. On the other hand, post-hoc comparisons for the object-exposed group indicated a reduction in the total distance traveled from training day 1 to subsequent days: training day 2 ($p = 0.0006$), training day 3 ($p = 0.0006$), and the test day ($p = 0.0006$) (Figure 27). This finding suggests that there was a high level of distance traveled on the first day the animals were exposed to the objects, likely due to novelty, followed by a sudden decrease in interest that did not recover the following days.

Concerning total exploration time, the repeated measures ANOVA identified significant variations within the social group ($F_{3,15} = 6.61, p = 0.018$) and the objects group ($F_{3,15} = 42.59, p = 1.4e-07$). Although the repeated measures ANOVA for the urine-exposed group indicated significance, post-hoc analysis revealed no significant differences across the days. Conversely, the post-hoc analysis for the object-exposed group showed a significant increase in total exploration time. This was evident when comparing training day 3 with days 1 ($p = 1.4e-07$) and 2 ($p = 2.2e-06$), as well as the test day with training days 1 ($p = 1.4e-07$) and 2 ($p = 2.2e-06$). This result indicates that animals engaged in extended exploration periods as they became familiar with the objects. Considering these results in conjunction with the overall data, it can be inferred that once animals become accustomed to the objects, they tend to focus their play on a favorite object rather than actively exploring the rest. However, between-group comparisons revealed

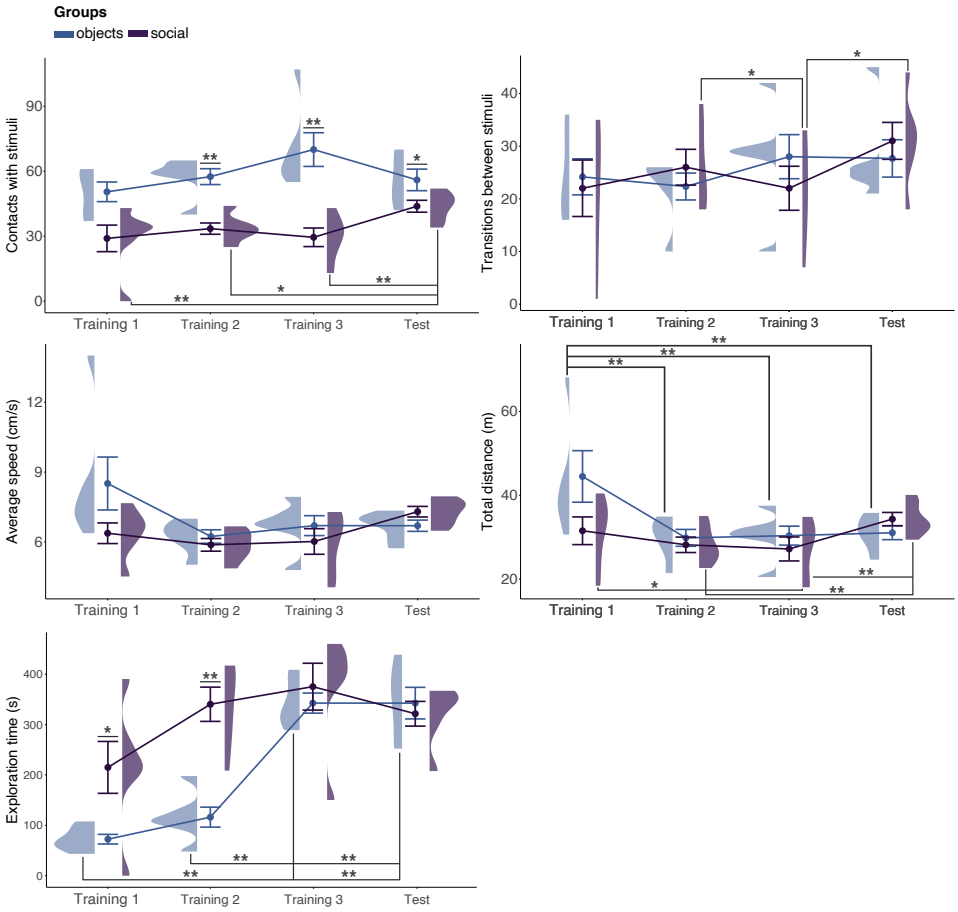

Figure 27: Behavioral outcome of the social vs. object spatial manipulation test. Line graphs display the behavioral results throughout the experimental protocol for the object-exposed and social-exposed groups across five behavioral variables: contacts, transitions, speed (cm/s), distance (m), and exploration time (s). Each day's mean for each group is represented by dots, with bars indicating the SEM. Adjacent to the bars, half violin plots provide a visual representation of data distribution: on the left for the object-exposed group and on the right for the social-exposed group. Differences between groups are denoted above the top error bar of the group with the higher mean. For the discrete variables, contacts and transitions, negative binomial regression was used. For the continuous variables, speed, distance, and exploration time, two-sided independent t-tests or Mann-Whitney U tests were employed. Within-group differences are highlighted by lines connecting days with significant differences, intersecting the half violin plot of the group exhibiting these differences. For discrete variables, the Friedman test followed by Conover post-hoc was applied. For continuous variables, repeated measures ANOVA followed by t-tests with Bonferroni correction for multiple comparisons was utilized. *$p < 0.05$; **$p < 0.01$.

an increased exploration time in the urine-exposed group during training day 1 ($t_{10} = 2.72; p = 0.039$) and 2 ($t_{10} = 5.69; p = 0.0004$) (Figure 27).

Despite the extensive behavioral data presented in this section, the lack of behavioral alterations following the spatial reorientation of the objects stands out as particularly significant. In contrast, the spatial manipulation of the urines did induce a rise in reexploration during the test day, as measured by the frequency of contacts, transitions, and total distance traveled.

The spatial manipulation of social cues triggers activation in different brain regions compared to the spatial relocation of objects, suggesting a functional compartmentalization in the processing of social and spatial information.

To determine the impact of spatial reorganization on neuronal activation and to understand if this impact varies when triggered by shifts in social cues as opposed to inanimate objects, we created two distinct experimental groups. Both groups underwent changes in the spatial layout of their environment following three days of training in a consistent location of either social landmarks or objects, tailored to each group's specific experimental conditions. The primary objective of this experiment is to examine the distinct impacts of these two elements' spatial changes and their related behavioral outcomes in the amygdalar-entorhinal-hippocampal pathway. This investigation is grounded in the hypothesis that spatial modifications in territorial conformation may lead to functional compartmentalization within this neural pathway.

Consistent with our predictions, the PMCo, a component of the vomeronasal chemosensory amygdala, exhibited heightened c-Fos expression in the group exposed to male-derived signals ($t_{10} = 3.21; p = 0.010$). Likewise, the primary targets of PMCo axons in the hippocampal formation, the ventral CA1 ($U = 5; p = 0.041$) and the dLEnt ($t_{10} = 2.31; p = 0.045$), demonstrated an increase in neuronal activity in the group with spatial repositioning of social cues compared to the group with spatial repositioning of objects. Within the dLEnt, the layer II/III reelin-positive neuron subpopulation also exhibited an enhanced activity response ($Z = 3.028; p = 0.002$) in the social-exposed group. Within the dorsal hippocampus proper, only the dorsal CA2 showed significant changes in neuronal activity following the reorientation of social landmarks ($t_{10} = 3.33; p = 0.011$) (Figure 28).

Unexpectedly, there was an increased activation in the MEnt region of the group exposed to objects ($t_{10} = -3.06; p = 0.016$), suggesting that objects might hold a higher valence for grid cells compared to urine samples. This group also exhibited a notable difference in neuronal activation within the dorsal CA3 region ($t_{10} = -2.34; p = 0.042$) (Figure 28). Conversely, we observed no notable between-groups variations in the dorsal CA1 ($U = 11; p = 0.310$), as well as in the DG overall ($t_{10} = 0.79; p = 0.456$), or individually within its upper blade ($t_{10} = 1.23; p = 0.256$) and lower blade ($U = 24; p = 0.377$) subdivisions.

When compared with previous findings, these observations suggest functional compartmentalization in the processing of episodic memory elements within the amygdalar-entorhino-hippocampal pathway. The information encoded in urines, representing the "what" and "who" aspects of episodic memory, stimulate distinct areas of the pathway compared to those activated by the "where" component. Additionally, it can be inferred that the spatial encoding of objects is distinct from that of conspecifics' territories, prompting specific neural responses in different regions of the pathway under study.

Consistent activation pattern across all nuclei involved in the transmission of social information.

Due to the intricate interactions suggested by the pairwise comparisons between groups, a correlation analysis was conducted to identify common activation patterns (Figure 29). This approach aimed at revealing specific compartments of infor-

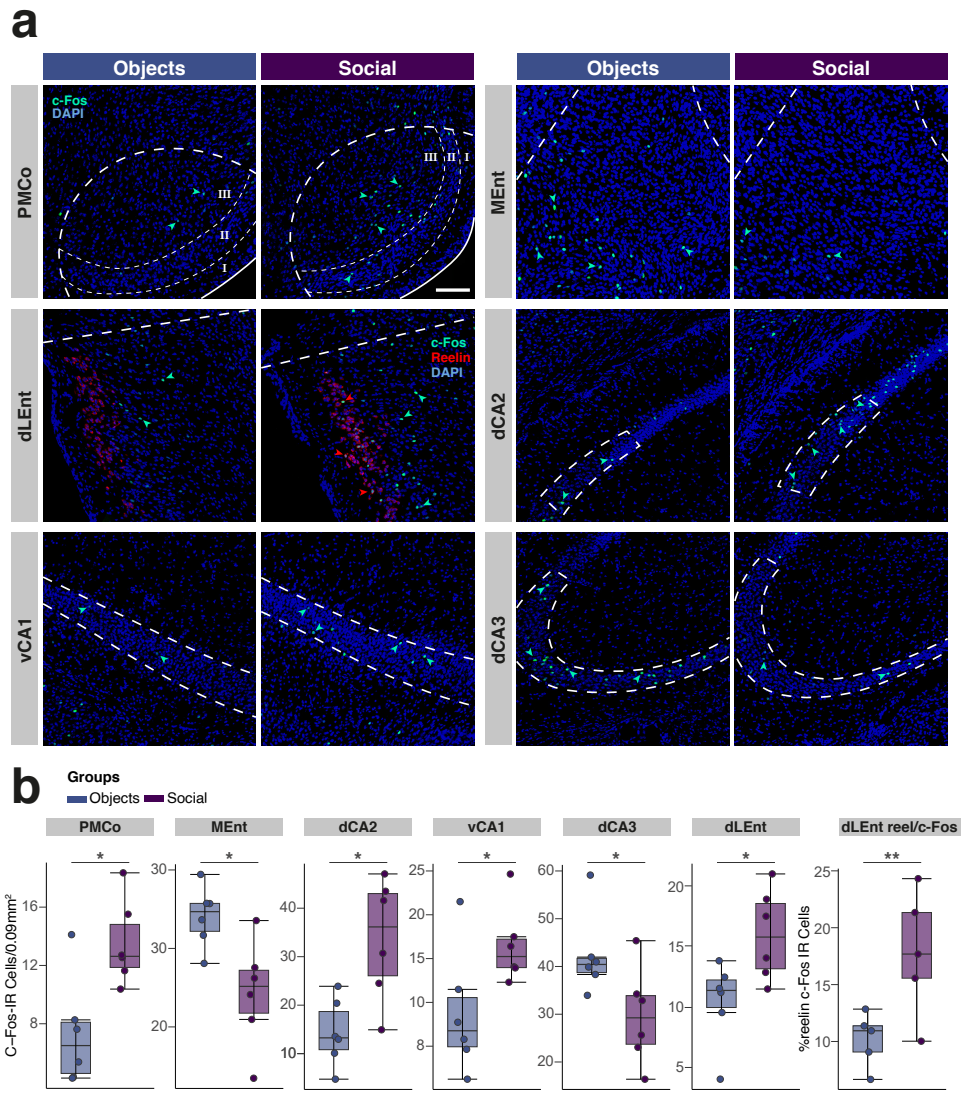

Figure 28: Neuronal activation results of the social vs. object spatial manipulation test. **a.** Confocal microscopy images illustrating differential c-Fos expression between object-exposed and social-exposed groups, exemplified by the most relevant structures of the amygdalar-entorhinal-hippocampal network that yielded significant results. Thick dashed lines indicate the selected ROI for quantification. Red arrows indicate active reelin-positive neurons coexpressing reelin and c-Fos markers. **b.** Boxplots depict the data distribution for the structures illustrated in panel a, providing a detailed visual representation of the variability and central tendencies within the groups. Beta regression, two-sided independent t or Mann-Whitney U test: *p < 0.05; **p < 0.01.

mation flow within the neuroanatomical pathway, was focused on identifying the nuclei that operate in synergy. By doing so, we sought to elucidate how these nuclei collaborate as a network to encode the diverse elements that ultimately contribute to forming complex social memories.

The c-Fos expression in the PMCo, the cornerstone of vomeronasal information transfer to the hippocampal formation, showed a positive correlation with the expression in the dLEnt ($r = 0.63; p = 0.027$) and with its layer II/III reelin-positive population ($r = 0.67; p = 0.018$). Additionally, there was an indicative trend in PMCo's c-Fos expression correlating with that in the ventral CA1 ($r = 0.52; p = 0.081$), and the dorsal CA2 ($r = 0.52; p = 0.079$). In line with expectations, we found a strong correlation between the general activation of the dLEnt and the activity of the reelin-positive neurons in its layers II/III ($r = 0.75; p = 0.005$). The activity of this specific neuronal subgroup also showed a correlation with the activities in dorsal CA1 ($r = 0.65; p = 0.023$) and CA2 ($r = 0.70; p = 0.012$) and hinted at a trend with ventral CA1 ($r = 0.66; p = 0.057$). Finally, neuronal activity in dorsal CA1 robustly correlated with dorsal CA2 activity ($r = 0.78; p = 0.003$).

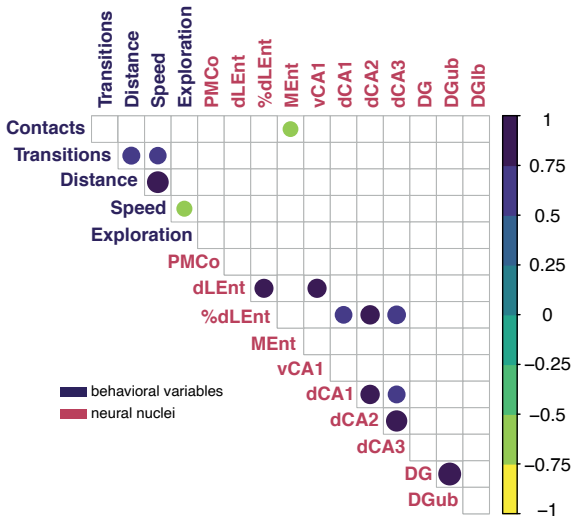

Figure 29: Significant correlations between neuronal activation and behavioral outcome in the social vs. object spatial manipulation test. Correlogram displays significant statistical correlations between pairs of variables, comparing altogether c-Fos cell density in all nuclei and exploratory behavior. The size and color of each circle represent the Pearson's correlation coefficient (r-value), and circles are only shown when $p < 0.05$. Circle radius has been rescaled according to the minimum significant Pearson's r-value to enhance the visual comparability of the data.

Interestingly, the neuronal activation in the MEnt displayed a tendency towards a negative correlation with both PMCo ($r = -0.55; p = 0.063$) and ventral CA1 ($r = -0.56; p = 0.057$), and a significant inverse correlation with the behavioral variable contacts ($r = -0.59; p = 0.045$) (Figure 29). The trends suggests that as the activity in the MEnt increases, there tends to be a corresponding decrease in activity in the PMCo and ventral CA1, or vice versa, hinting at a potentially inverse relationship in their functional connectivity and response patterns.

This analysis revealed a pattern of interconnected activity among the nuclei engaged in the processing, transmission, and storage of social information, implying certain level of functional compartmentalization within the various elements that form complex episodic memories. Taken together, these results highlight the sophisticated neural orchestration underlying the processing and encoding of complex social memories, and together with the literature identify the PMCo as a key node for individual recognition within the delineated pathway.

4.3 SINGLE UNIT RECORDINGS IN THE PMCO.

Unraveling neuronal response patterns to urine stimuli.

We delved into the intricate dynamics of neuronal responses by analyzing firing rates across 10 sequential trials, each lasting 20 seconds. By investigating the neuronal activity in response to urine, we aimed to unravel the underlying patterns that governed their behavior. This exploration shed light on variations in firing rates, providing valuable insights into the neuronal coding with which PMCo neurons process information from olfactory input.

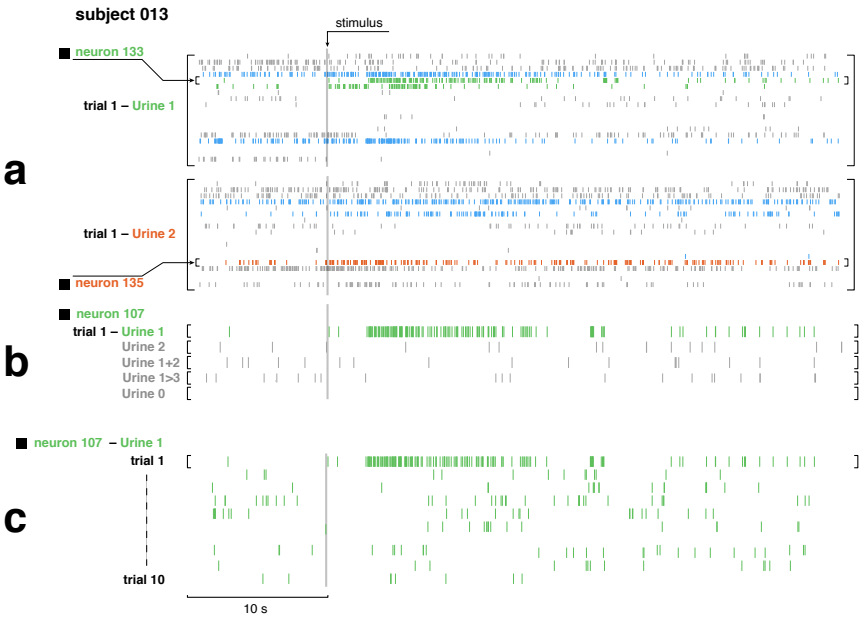

Figure 30: Rastergrams featuring representative examples of neuron firing times recorded in the PMCo are presented. **a.** The responses of the neuronal ensemble from subject 013 to urine 1 (top) and 2 (bottom) are depicted in the first trial of the experiment. Blue and green spikes indicate the timestamps of neurons that exhibit an increased firing rate when in the urine contacts with the nose. Specifically, neuron 107 exhibits a selective response to the presence of urine 1, with no discernible activity in response to urine 2. The rastergram also depicts neuron 135 exhibiting an increased firing rate in response to stimulation with urine 2. **b.** Displays the rastergram of neuron 107 when exposed to the entire urine set, providing a comprehensive view of its firing pattern across different stimuli. **c.** The rastergram of neuron 107 is presented exclusively in the presence of urine 1 for all trials. Notably, it is evident that the heightened activity observed in trial 1 is not sustained in subsequent trials.

Tensor decomposition of the neuronal activity in the presence of particular urines.

In the present study, we conducted a tensor decomposition analysis on the firing rates of neurons in response to various urine stimuli, across multiple trials and time intervals (Figure 31). This analysis yielded insightful observations about the neural processing of vomeronasal information.

The diversity in neuronal responses to different urine stimuli was prominently observed. Each graph in the figure represents the response of a specific neuron to five distinct urine stimuli. The variability in the height of the bars across different stimuli suggests differentiated neuronal responses to each stimulus. This finding is crucial for understanding how neurons uniquely process specific pheromonal information.

The analysis revealed consistency and variability in neuronal responses across repeated trials. The presence of multiple bars for each stimulus, likely representing different trials, indicates either a reliability or an adaptation in the neuronal response to repeated stimuli exposure. This aspect of the study is pivotal for understanding the robustness of neuronal responses and their adaptability to repeated exposition to urines. Temporal dynamics of the neuronal responses were also explored. If the bars represent different time intervals within each trial, as the 200 ms interval suggests, it illustrates how neuronal responses vary over time following stimulus exposure. This insight is significant for understanding the kinetics of neuronal response to olfactory stimuli.

In summary, this study contributes to our understanding of pheromone's encoding in the brain, highlighting individual differences among neurons in terms of sensitivity and response to social stimuli, as well as the temporal dynamics of neuronal activity.

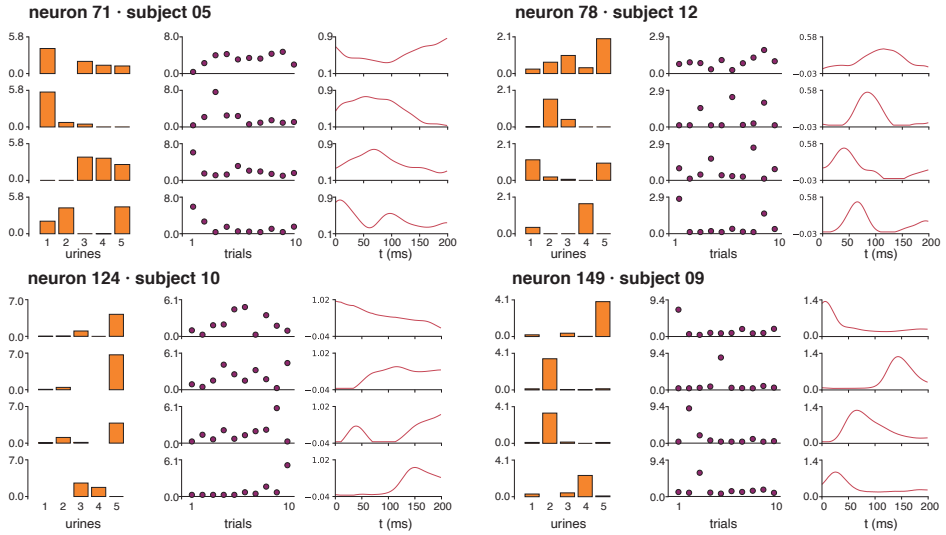

Figure 31: Representative cases of the tensor decomposition for specific neurons are presented. The decomposition of the firing rates in response to urine stimuli is illustrated through bar charts, representing different trials (scatter points) and the duration of each trial (20s, red line). Notably, certain neurons exhibit diverse response motifs to different urine stimuli (neurons 271 and 78). Some neurons predominantly respond to a specific urine type, such as neuron 124, which consistently shows a response to the subject's own urine, labeled as 5. Elevated firing rates are observed in response to various urine stimuli, albeit occurring in different trials (neuron 149). Notably, in the first trial, the neuron responds to the subject's own urine (5), in the second and fifth trials to urine 2, and in the third trial to urine 1, contrasting with urine 2.

We extracted the motifs of neuronal responses to urine samples using PCA methods, as described in Chapter 3. Thus, we could identify the possibility that neurons recognize and differentiate stimuli. This methodology allows us to dissect complex firing patterns, revealing the neural signatures associated with each pheromonal cues.

In the context of this neural response analysis, the heatmap represented in Figure 32 illustrates the firing rates of neurons in response the five distinct urine stimuli. Each row on the heatmap corresponds to the response, in the form of the first component of a single neuron to these stimuli, with the colors indicating the intensity of the neuron's firing rate.

The hierarchical clustering method employed has elucidated the differential response patterns of the diversity of neurons to stimuli present in urine samples. It can be generally observed that the response motifs (rows) exhibit considerable vari-

ability, reflecting the intricacy inherent in the neuronal processing of such stimuli within the PMCo. The overall variability of the neuronal responses, quantified by a standard deviation of approximately 0.4355, provides insight into the heterogeneity of the neuronal population's response to the different urine stimuli. This value is indicative of a neuronal population that is not homogeneous in its response characteristics. Such variability is expected in a complex system, where different neurons may be specialized to respond to certain chemical cues more than others. This specialization could be an adaptive feature of the detection of urines, enabling the discrimination of a wide range of chemicals.

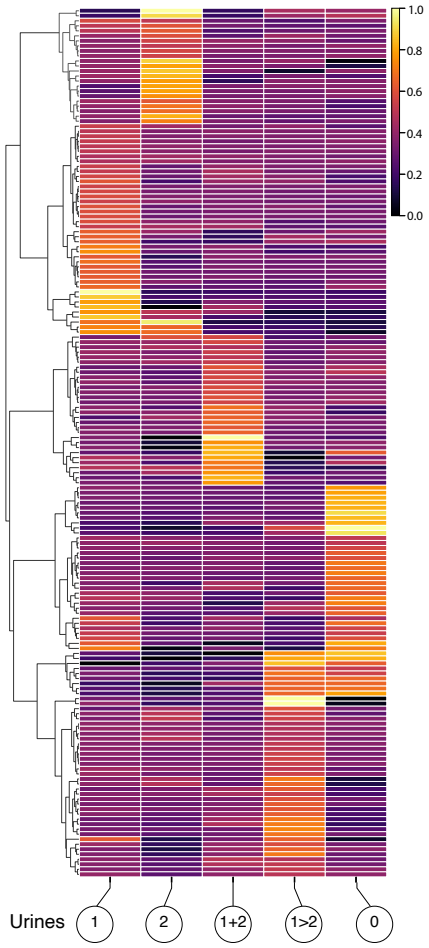

Figure 32: Clustergram illustrating differences in the activity of the entire set of recorded neurons in response to various urine stimuli. Colors represent the values of the first principal component of the tensor decomposition (4 components) of the neuron's firing rate in response to urine. Consequently, the four-element pattern becomes the one explaining the most variance in the total elements of the decomposition. On the left, a dendrogram indicates the clusters found in the complete set of patterns from the 173 neurons. Distinct groups of neurons exhibit differential responses to various stimuli.

Despite this variability, it is apparent that numerous neurons predominantly respond to one particular urine sample, or at least, it is possible to identify neurons whose response to one sample is significantly more pronounced compared to others, without undermining their involvement in responding to other urine samples.

In order to assess the clustering of response patterns to different urine samples, our goal was to obtain a numerical value that could explain the strength of the clustering. The Calinski-Harabasz score, recorded at 65.29, indicated a strong structure in the hierarchical clustering. This relatively high score suggests that the clusters

are well-defined, with a substantial degree of separation between them. It implies that the variance within each cluster is low compared to the variance between clusters, signifying that neurons within a cluster have similar response patterns to the stimuli, and are distinctly different from neurons in other clusters.

Similarly, with the intention of validating the effectiveness of our clustering methods on our samples, the Davies-Bouldin score of 0.9 complemented this interpretation, as it is considerably close to the ideal score of 0. This value indicated that each cluster is compact and well separated from other clusters. A score below 1, as observed, demonstrates that the clusters are distinct with minimal overlap with the others. The combination of these scores underlines the robustness of the clustering results, highlighting the presence of clear, meaningful groupings within the neuronal data. This level of clustering quality is indicative of a meaningful categorization of neurons, potentially reflecting different functional specializations in the processing of urine samples by PMCo neurons.

CEBRA analysis reveals distinct urine clustering, intra-trial variability, and hierarchical encoding in the PMCo's neural representations.

CEBRA embeddings of neural responses to different urine stimuli show discrete clusters corresponding to each urine type, indicative of distinct neural representations in the embedding space.

The top-left embedding was trained specifically to represent different urine samples (Figure 33a). The distinct clustering of points suggests that the CEBRA model has learned to differentiate effectively between the urine types based on their signatures. Each cluster likely corresponds to a different urine sample, and the tightness of these clusters indicates a strong within-sample similarity, implying that the neural responses to each urine type are highly consistent. The separation between clusters suggests that the model can capture the unique characteristics of each urine type, leading to distinct neural representations in the embedding space.

The top-middle embedding is trained to represent individual trials, which may include variability in the neural responses to the same urine stimulus (Figure 33a). The spread of points within each colored trajectory shows the variability in the neural responses to each urine sample during different trials. The trajectories are distinct but not as tightly clustered as in the urine embedding, reflecting a possible trial-to-trial variability. Despite this variability, the general pattern suggests that the model can still maintain a degree of separation based on the stimulus, although the distinction is less pronounced compared to the embedding trained only with urine labels.

By training a model together with urine and trial labels (top-right), we aimed to capture the combined variance (Figure 33a). The resulting trajectories show a more complex pattern, where the separation between different urine types is still observable but exhibits more overlap and intermingling of trials. This could reflect the combined effects of stimulus-specific information and trial variability. The colored trajectories seem to follow a general direction or flow, which might indicate a progression or a relationship between the stimuli and the responses across trials.

The bottom row, depicting shuffled stimuli and trials, serves as a control (Figure 33a). It demonstrates that the separation seen in the original data is not due to chance, affirming the specificity of the neural encoding. Together with these control embeddings, our tridimensional representations demonstrate the ability of CEBRA models to create neural representations that reflect both the specificity of the stimuli (urine) and the dynamics of the neural responses across time (trials).

Based on the InfoNCE loss trajectories depicted in Figure 33b, we observe that the three models converge to similar final loss values. However, the model incorporating both urine labels and trial data demonstrates a superior ability to separate patterns of neural activity. This is indicated by its loss trajectory, which descends more sharply before stabilizing at a lower plateau compared to the individual urine

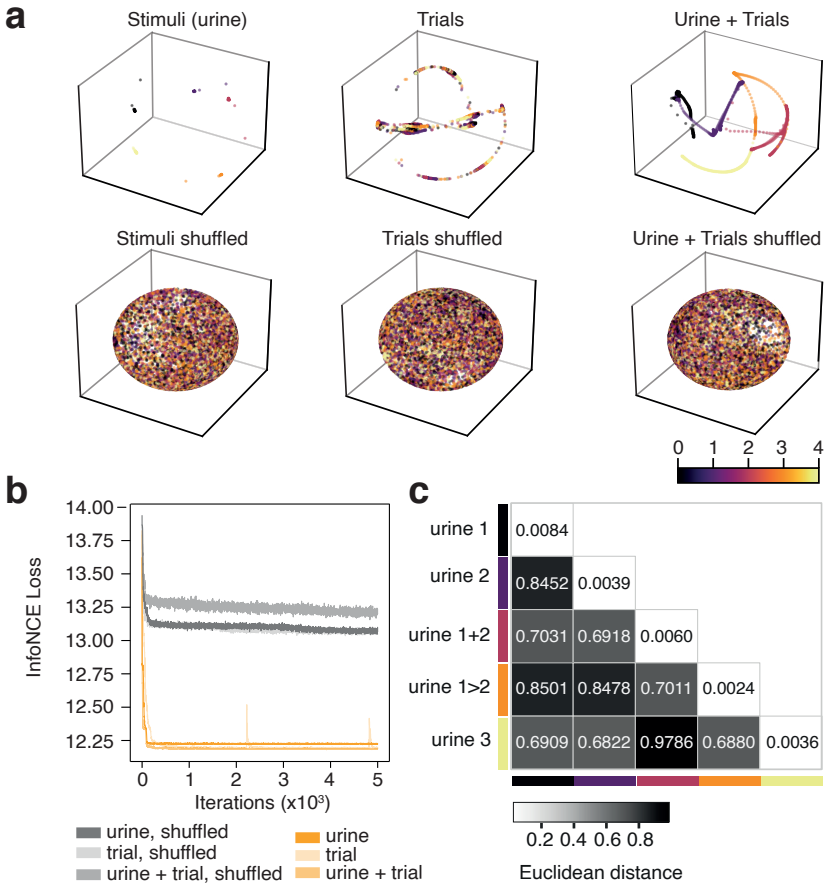

Figure 33: CEBRA reveals that the PMCo can differentiate between various types of urine, indicating a time-related influence in the label trial. **a.** Embedding plots for individual urine, trials, and combined urine and trial data demonstrate distinct clustering patterns, which are abolished upon shuffling, indicating a non-random structure in the data. The color bar represents urine 1 (0), urine 2 (1), urine 1+2 (2), urine 1→2 (3) and urine 0 (self, 4). **b.** Convergence of infoNCE loss over iterations highlights the improved modeling efficiency when urine and trial data are combined. **c.** Average Euclidean distance in the embedding space within and across urine samples.

and trial models. Notably, the shuffled models consistently exhibit higher loss values, and their loss decreases are less pronounced over iterations. This suggests that while all models learn to encode some structure present in the data, the combined model capitalizes on a richer set of features, leading to more effective differentiation and representation of the stimuli. The elevated and relatively stable loss in the shuffled models underscores the importance of the correct pairing between stimuli and trials. Without it, the model struggles to extract meaningful patterns, resulting in less effective learning as reflected by the higher InfoNCE loss.

The heatmap in Figure 33c offers a visual summary of the relationships between different urine samples in the embedding space. The diagonal elements, which are near-zero, affirm that points within the same label are closely packed, indicating high intra-label similarity or consistency in the neural representation of each urine type.

The off-diagonal elements represent the inter-label relationships. This suggests which urine samples lead to more distinct neural activity patterns from one another by looking for larger average distance values. For example, if the value in the cell for urine 1 and 3 is high, it indicates that these two urine types are well-separated in the embedding space, suggesting that their neural signatures are markedly different. Conversely, smaller off-diagonal values suggest that corresponding urine samples are not as well-separated, indicating closer similarity in their neural representations. This could be due to shared characteristics between the urine samples that lead to similar neural responses, or it might reflect limitations in the model's ability to distinguish between these particular samples.

Notably, urine samples 1 and 2 are well-separated in the embedding space, as indicated by the large average Euclidean distances between them. This separation suggests that the PMCo is effectively distinguishing between these two male-derived urine types, potentially identifying distinct vomeronasal signatures that the neural representation encodes.

Moreover, the mixture of urine 1 and 2, denoted as urine 1+2, occupies a position in the space that is relatively closer to both urine 1 and urine 2, as well as to urine 1→2. This proximity implies that while the combined urine sample maintains a unique identity in the embedding space, indicative of the newly generated mixture of MUPs, it shares some features with the urine samples that compose it. The fact that urine 1+2 is still discernibly separated from urine 1 and urine 2 underscores the model's nuanced capacity to represent combinatory effects while retaining information about the individual constituents.

The fact that urine 1+2 is also closer to urine 1→2 suggests that the PMCo is capturing a hierarchical or relational structure within the samples. This proximity may reflect shared characteristics or overlapping neural responses elicited by these samples, hinting at a commonality in how these distinct-nature mixtures are processed by the vomeronasal system.

To evaluate the variability of activity patterns in the PMCo across trials, we employed a hybrid CEBRA model, initially trained on the dataset from the first trial with urine samples as the predictive labels. We then examined the decoding accuracy across the series of 10 trials to determine the consistency of activity patterns corresponding to each urine sample.

Within the CEBRA embeddings for each trial, distinct clusters became apparent, showcasing the model's acute capability to distinguish among the various urine samples (Figure 34a). However, when attempting to decode a specific urine sample from the latent embeddings, a decline in decoding accuracy across the trials was noted (Figure 34b). Notably, the decoding performance began to wane from the fifth session onward. The decoding accuracy for each dataset is documented in Table 3. On average, the decoding accuracy across all trials was 83%. When we calculated the baseline accuracy, we arrived at a significantly lower figure of 19.9%. These findings affirm that our model substantially surpasses a random baseline for all datasets, which is a strong testament to the model's efficacy. It implies that

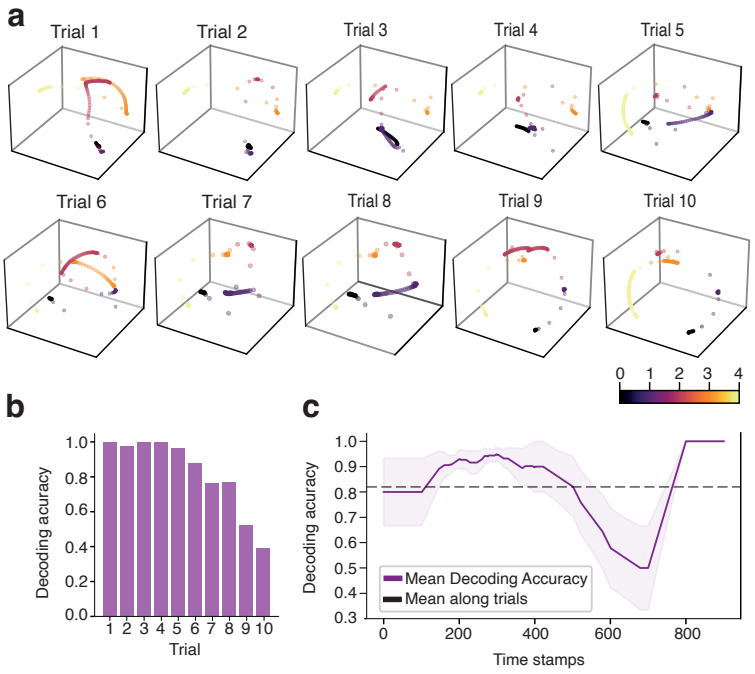

Figure 34: Dynamic representation of CEBRA embeddings across multiple trials and their decoding accuracy over time. **a.** CEBRA embeddings for the 10 trials, with color gradient representing distinct stimuli: urine 1 (0), urine 2 (1), urine 1+2 (2), urine 1→2 (3) and urine 0 (self, 4). **b.** Bar chart showing average decoding accuracy for each trial, indicating variability in the model performance. **c.** Decoding accuracy over time, with shaded area representing standard deviation across trials, highlighting temporal dynamics in the model accuracy.

the model is discerning meaningful patterns within the data rather than making arbitrary classifications.

Datasets	Accuracy	Baseline accuracy
Trial 1	1.0	0.198
Trial 2	0.98	0.193
Trial 3	1.0	0.192
Trial 4	1.0	0.193
Trial 5	0.97	0.204
Trial 6	0.878	0.201
Trial 7	0.763	0.199
Trial 8	0.773	0.189
Trial 9	0.523	0.226
Trial 10	0.391	0.199

Table 3: Average decoding accuracy among trials.

In the mean decoding accuracy over a sequence of time stamps, depicted in Figure 34c, we see a fluctuating yet gradually ascending trend in accuracy, culminating in a pronounced increase towards the end of the timeline. This upward trajectory in accuracy suggests that the model may be refining its decoding capabilities as it assimilates and learns from more data over time.

Together, these visual components weave a narrative that not only quantifies the decoding accuracy of CEBRA embeddings across multiple trials but also captures the dynamic nature of the data as it evolves over time. The visual data suggests a journey of experimental inquiry, one that starts with individual trials and culminates in an overarching temporal analysis, providing insights into the stability and precision of decoding over extended periods.

5 DISCUSSION

The amygdalar-entorhinal-hippocampal pathway putatively transmits vomeronasal information to the dorsal and ventral hippocampi.

In this study, we have outlined and functionally tested the neuroanatomical pathway that most likely serves as the neural substrate for the transmission of vomeronasal information to both septotemporal poles of the hippocampus. In this anatomical pathway, vomeronasal information captured by the VNO is relayed to the AOB, which in turn projects glutamatergic connections to the PMCo. The PMCo is believed to function as the primary vomeronasal cortex (Gutiérrez-Castellanos *et al.*, 2014), analogous to how the Pir operates for the main olfactory information. This primary vomeronasal cortex sends direct glutamatergic projections to the apical dendrites of ventral CA1 pyramidal cells, to the MEnt, and to a discrete set of reelin-positive neurons located in the dorsal aspect of layer II of the LEnt. These reelin-positive neurons, which we have identified as the relay of vomeronasal information from the PMCo to the dorsal CA1, are recognized as "fan cells" based on their morphology (Germroth *et al.*, 1989). To complete the circuitry, the dLEnt sends glutamatergic projections back to the PMCo, creating a positive feedback loop of excitatory connections.

The reelin-positive fan cells in LEnt layer II have recently garnered significant attention in the scientific community due to their role in episodic-like memory (Tsao *et al.*, 2018; Vandrey *et al.*, 2020) and their impact on MEnt grid cells (Vandrey *et al.*, 2022). These neurons contribute to the processing (Leitner *et al.*, 2016) and memory encoding of olfactory information (Lee *et al.*, 2021), learning of object locations (Fernández-Ruiz *et al.*, 2021), and processing of object-place-context associations (Vandrey *et al.*, 2020). While these neurons are recognized to process odors (Bitzenhofer *et al.*, 2022), our observations suggest that they are more responsive to male urine than to a neutral odorant. This could indicate that these neurons encode both main olfactory and vomeronasal information. Consequently, urine, which carries both types of information, activates these neurons more than citralva, a neutral odorant. On the other hand, despite high-impact studies focusing on the relationship between this cell type and object location learning (Wilson *et al.*, 2013; Fernández-Ruiz *et al.*, 2021), our findings indicate a higher activation of reelin-positive cells following a spatial change of male-derived urines when compared to objects.

Incorporating a negative control in the behavioral experiments, such as a group exposed to saline, would have provided a valuable baseline for comparison. This negative control would have allowed us to more effectively determine whether citralva or object rearrangement elicited greater activation of these reelin-positive cells above a baseline, thereby enabling a more direct comparison with recent bibliography. However, we can state that the simultaneous processing of olfactory and vomeronasal information by fan cells triggers more cellular activity than olfactory information alone. Additionally, the spatial manipulation of landmarks in the environment activates this cell type more than the manipulation of inanimate objects.

Returning the focus to the neuronal responses within the pathway, we observed that the PMCo and ventral CA1 pyramidal neurons displayed increased activity in experiments featuring the presence of urine, compared to a group that was not exposed to urine. This enhanced activity in response to vomeronasal stimuli suggests a heightened activation of the pathway's direct route to the ventral hippocampus. Additionally, the previously noted activation of the dLEnt, particularly its fan cells, indicates that the pathway's indirect route is similarly more responsive to vomeronasal stimuli. Collectively, these findings imply that vomeronasal

stimuli significantly influence the specified neuroanatomical pathway, which likely aids in the conveyance of vomeronasal information to both the dorsal and ventral hippocampi.

The existence of direct and indirect routes to the hippocampus reflects the possibility that vomeronasal information flow generates neuronal representation states governed by an attractor dynamics mechanism.

"Attractor dynamics" in the context of hippocampal memory processing is a concept from computational neuroscience that describes how neural networks in the hippocampus process and store memories based on the idea of an attractor in a dynamic system (Wu *et al.*, 2008). An attractor in a dynamic system, like a neural network, is a set of states towards which the system tends to evolve over time, regardless of the starting point. In the context of memory, these states represent specific memories or patterns of information (Khona and Fiete, 2022). When a new memory is formed, the associated sensory and cognitive information is encoded into a unique pattern of neuronal activity. This pattern becomes stabilized through synaptic changes and forms an attractor state (Niedringhaus *et al.*, 2013). When a partial or related cue is later encountered, it can push the network toward this attractor state, leading to quick retrieval of the corresponding memory (Steemers *et al.*, 2016). This mechanism can store multiple attractor states and move between these states in response to external inputs, allowing for both stable memory retention and dynamic memory retrieval.

Classic computational theories of the mnemonic functions of the hippocampus link the concept of attractor dynamics to the mechanisms of pattern separation and pattern completion. Within the hippocampus, the diverging Ent-DG connection is recognized as the pattern separator, while the converging DG-CA3 connection, coupled with the autorecursivity of CA3 pyramidal cells, functions as the pattern completer (Knierim and Neunuebel, 2016).

We hypothesize that the existence of an indirect and direct pathway from the PMCo to the dorsal and ventral hippocampus may rely on these same dynamics. On one side, the flow of vomeronasal information follows an indirect path via the LEnt, subsequently projecting to the dorsal CA1 through the trisynaptic Ent-DG-CA3-CA1 pathway, as well as directly via the temporoammonic pathway (Witter *et al.*, 1988). This route accesses the context-enhanced neural representations in the dorsal CA1 and extends to the dorsal CA2, a crucial area for encoding and processing social information (Hitti and Siegelbaum, 2014). On the other side, vomeronasal information from the PMCo directly reaches the ventral CA1, the primary site for storing social memory (Okuyama *et al.*, 2016), enabling quick retrieval of pre-existing social memories.

It is significant to note that despite the independence of these two anatomical pathways, they both originate, at least partially, from the same neurons in the PMCo. While it seems that neurons from layer II of the PMCo preferentially project to the Ent and those from layer III are more likely to project to the ventral CA1, the neuroanatomical technique used does not permit a definitive conclusion on this matter. However, we can state that there is a degree of shared neuronal involvement in both the direct and indirect pathways to the hippocampus. The overlap in neurons participating in both pathways could facilitate dynamic switching between direct and indirect processing modes, depending on the context or relevance of the sensory input. This could be crucial in situations where quick memory recall is essential or in contexts where more elaborate processing is needed.

As rodents navigate their environment, they encounter numerous vomeronasal signals, many of which are often incomplete due to time passage or other animal countermarking. A continuous influx of vomeronasal information into the spatial map becomes essential for avoiding predators or dominant competitors. Consequently, the flow of vomeronasal information must rely on pattern separation, com-

pletion, and attractor dynamic mechanisms to support the continuous and rapid remapping necessary for adaptive environmental navigation and survival. This framework allows a structurally constrained and robust neural representation of the territory while also displaying high capacity and flexibility to adapt to the ever-changing conditions of a natural habitat.

To complete the circuitry, we have identified a bidirectional glutamatergic connection between the PMCo and the LEnt. Similarly, there exists a reciprocal excitatory connection of the same nature between the Pir and the LEnt (Johnson *et al.*, 2000). In the realm of main olfactory information, this Pir-LEnt connection acts as a top-down modulator of olfactory cortical function and odor perception, facilitating accurate odor discrimination (Chapuis *et al.*, 2013). Consequently, it seems plausible that the bidirectional PMCo-LEnt connection might perform a similar role for vomeronasal information, acting as positive feedback to amplify relevant vomeronasal signals, thereby aiding in the rapid discrimination between individuals. In conjunction with the hypothesized attractor network, signal amplification appears to be another computational element essential for effective processing of vomeronasal information within the entorhinal-amygdalar-hippocampal pathway.

The olfactory-vomeronasal behavioral paradigm highlights the most relevant nuclei for the processing of vomeronasal information.

The primary concept behind the urine versus citralva exposure test is to discern which nuclei in the delineated pathway exert the most significant influence on the transmission and processing of vomeronasal information. This paradigm is based on the premise that urine encompasses volatile and non-volatile chemosignals, whereas citralva, a neutral odorant, only contains volatile olfactory signals. By conducting a comparative histological analysis, we aimed to isolate and understand the impact of vomeronasal information separate from the volatile components in urine.

However, this underlying premise regarding volatiles in urine is not entirely accurate, as the volatiles present in urine possess biological significance (Humphries *et al.*, 1999), unlike those in citralva, which a priori lack inherent biological relevance. In laboratory mice, some volatiles found in adult male urine, such as 2-secbutyl-4,5-dihydrothiazole (thiazole), 3,4-dehydro-exo-brevicomin (brevicomin), and both α and β farnesenes, have been linked to social dominance (Apps *et al.*, 1988; Harvey *et al.*, 1989; Novotny *et al.* 1990). These compounds are known to be attractive to females (Osada *et al.*, 2008), encouraging early reproductive maturation and estrus (Jemiolo *et al.*, 1986) while also inciting aggressive competition among males (Novotny *et al.* 1985). A method to isolate volatile from non-volatile information could have involved creating a group of anosmic animals through the intranasal administration of 50 µL of saline containing 10% zinc sulfate (McBride *et al.*, 2003; Villafranca-Faus *et al.*, 2021). However, since many of these volatiles are detected by the V1R of the VNO (Brennan and Keverne, 2004), creating a group that exclusively perceives non-volatiles is exceedingly complex.

Despite these limitations, we can assume that in comparison to exposure to citralva, exposure to urine revealed the nuclei of the pathway that exhibit a greater response to chemosensory signals of high biological relevance. Within the suggested anatomical pathway, notable differences between groups were observed in the AOB, PMCo, ventral CA1, dorsal CA2, dLEnt, and within the reelin-positive population of dLEnt LII fan cells. Furthermore, significant variations were also detected in other vomeronasal-related nuclei, such as the MePD, MePV, BSTmpm, AAV, and CxA. Alongside these findings, correlation analysis revealed numerous associations between the vomeronasal amygdala structures and both the ventral CA1 and CxA, suggesting that these two structures have a significant role in the processing of high biological significance chemosignals.

The observed shift in activity within the ventral CA1, along with its correlated activation pattern with the vomeronasal amygdala, is in line with expectations. As emphasized repeatedly during this dissertation, the ventral CA1 functions as a repository for social information (Okuyama *et al.*, 2016). Nonetheless, the results concerning the CxA were more unexpected. Despite being predominantly an olfactory structure, the CxA also receives limited direct innervation from the AOB (Cádiz-Moretti *et al.*, 2013). The neurochemical composition and connections of this area imply its potential role in processing olfactory information of significant biological relevance, such as male-derived volatiles (Cádiz-Moretti *et al.*, 2016). Our findings align with this perspective and suggest that the CxA serves as an important interface between the olfactory and vomeronasal amygdaloid structures.

To gain a deeper insight into the overall pattern of neural activity and pinpoint specific functional networks with varying responses to the stimuli, we conducted a PCA. Given the extensive set of variables in our analysis, this approach was instrumental in minimizing noise within the model to visualize the nuclei whose activation pattern were similar. Certainly, all the vectors derived from the activity of the pathway nodes are located within the same quadrant in the biplot, indicating similar loading factors for these areas across both components. These vectors appeared distributed around the dots representing the individuals exposed to male-derived signals. Furthermore, the PMCo and ventral CA1 are among the top three variables contributing most significantly to the percentage of variance explained in the model, underscoring their importance in vomeronasal signal encoding. Collectively, these findings cohesively depict the neuroanatomically described pathway as the neural substrate for vomeronasal information flow and processing.

The amygdalar-entorhinal-hippocampal pathway seems to compartmentalize the different components of multisensory episodic memory.

Episodic memory is defined as the ability to recall events in a spatiotemporal context (Sugar and Moser, 2019). The encoding of episodic memory encompasses information about the subject's position ("where"), the sequence of events ("when"), and the content of the experience itself ("what"). The ability to integrate these features of an event is considered fundamental to the subjective experience of episodic memory (DeVito and Eichenbaum, 2010) and is critically dependent on the hippocampal formation (Tulving and Markowitsch, 1998). Our experiments involving spatial manipulation of male urine samples or objects are based on the premise that different components of episodic memory arising from a multisensory exploratory event may engage different segments of the pathway under study, similar to the case with cognitive events of other natures (Dickerson and Eichenbaum, 2010). While the c-Fos counting technique, with its limited temporal resolution, is not suitable for addressing the "when" aspect, it ideally fits for examining the "where" and "what" components of memory.

The social stimuli spatial manipulation test aimed to isolate the episodic memory "where" component. By creating two animal groups and exposing them to identical urine samples from three easily distinguishable males, we ensured a consistent "what" component for both groups. Then, by altering the spatial location of the urine samples for the experimental group on the test day, we effectively introduced a change solely in the "where" aspect.

Implementing this spatial modification altered the exploratory behavior of the experimental group. After three days of training, which initially led to a diminished interest in the stimuli, the spatial change on the test day resulted in an increased number of contacts with the male-derived stimuli and more transitions between stimuli. Additionally, we found a difference in both the distance traveled and the number of transitions on the test day for the experimental group compared to the control group. While there are high-impact studies assessing the relation between context and social stimuli, these involve exposing the experimental subjects to either

novel or familiar whole animals (Alexander *et al.*, 2016; Oliva *et al.*, 2020). However, to the best of our knowledge, studies demonstrating this type of spatial manipulation have not previously been conducted with territorial landmarks.

As anticipated, the spatial rearrangement of urine samples led to heightened neuronal activity in the MEnt and dorsal hippocampal CA1, areas known to house the famous grid and place cells of the hippocampal spatial map (O'Keefe and Dostrovsky, 1971; Hafting *et al.*, 2005). Nevertheless, no significant differences were observed in any other region analyzed. It might be expected that if the PMCo plays a role in grid cells tuning via its direct glutamatergic connection to the MEnt, it would show increased activation in response to a spatial change for the same group of urines to be recognized. However, our results suggest two possible scenarios: either the spatial alteration does not induce noticeable changes in PMCo activity, or the spatial context is conveyed to the MEnt grid cells from another source (Raudies *et al.*, 2016) and integration with vomeronasal information occurs directly in the MEnt or in higher nodes of the pathway. On the other hand, the LEnt is known to be involved in the generation of long-term odor-context associative memories. Yet, we observed no significant differences in this area resulting from the spatial relocation of the urines. This could be attributed to the brief duration of our test, considering that the function of the LEnt in odor-context associations has been demonstrated after conducting dozens of tests over several days (Persson *et al.*, 2021).

Therefore, the "where" component appears to have greater significance in the MEnt-dorsal CA1 segment of the pathway. This compartmentalization prompted us to consider the functioning of the "what" component and whether there is a specialization within this component for identifying individuals, naturally termed the "who". To address this issue, we designed the social versus object spatial manipulation test. In this scenario, after recognizing the "where" component within the pathway, we established two experimental groups: one exposed to male urine and the other to objects. Both groups experienced the same spatial alteration in their respective items within their environment (same "where").

We observed in the group where social stimuli were spatially relocated a notable shift in the exploratory behavior of females. This social-exposed group showed a sharp increase in the number of contacts with the stimuli, transitions between stimuli, and overall distance traveled. This behavioral alteration following spatial rearrangement was not present in the group exposed to objects. However, likely because the objects were more interactive than the urine samples, a consistently higher number of contacts was observed in the group exposed to objects compared to the group exposed to urine throughout the entire experimental process.

Derived from this behavioral outcome, in the group subjected to a spatial change of male urines, we noted heightened c-Fos expression in the PMCo, ventral CA1, dorsal CA2, dLEnt, and within the reelin-positive neuron group of the dLEnt. Conversely, in the group that experienced a spatial rearrangement of objects, increased neuronal activation was observed in the dorsal CA3 and MEnt. These findings imply that the "who" component of episodic memory carries more significance in all the pathway segments not identified as responsible for the "where" aspect. This suggests that these parts of the pathway are primarily involved in processing identity information.

On the other hand, CA3 activation seems to be associated with the coding of object spatial changes. Although object detection and discrimination have traditionally been regarded as functions of the perirhinal cortex (Burke *et al.*, 2012; Olarte-Sánchez *et al.*, 2015; Kinnavane *et al.*, 2016), some literature suggests a link between object discrimination and the dorsal CA3. Increased c-Fos activity in the dorsal CA3 following an object discrimination task has been observed (Albasser *et al.*, 2010), as well as elevated theta band power during the exploration of displaced objects (Neves *et al.*, 2022). A really surprising finding was the heightened neuronal activation in the MEnt of the group that experienced the spatial rearrangement of objects. Objects may provide a richer experience in terms of spatial interaction, such as so-

matosensory and visual exploration, which could have resulted in higher MEnt and dorsal CA3 activation in comparison to male-derived stimuli (Høydal *et al.*, 2019; Dannenberg *et al.*, 2021).

Based on the c-Fos results, it can be suggested that there is a compartmentalization within the amygdalar-entorhinal-hippocampal pathway for episodic memory components. The "where" aspect appears to be more represented in the dorsal MEnt-CA1 region, whereas the "who" which is an advanced form of the "what" seems to be more represented in the rest of the pathway, engaging both the direct and indirect connections from the PMCo to the ventral and dorsal hippocampus.

The PMCo as a decoder of the mice chemical identity code.

We selected the PMCo as the focal node among all the components of the pathway guided by the findings of our experimental results. From a neuroanatomical perspective, this nucleus is positioned in a central position in the pathway, projecting glutamatergic connections to the dLEnt, MEnt, and ventral CA1. Additionally, this area demonstrated distinct differences in activation within the group exposed to urine in the urine versus citralva test and the group subjected to spatial rearrangement of urine in the social versus object spatial manipulation test. Furthermore, it was among the structures that accounted for the largest percentage of explained variance in the PCA following the urine versus citralva experiment.

The direct excitatory projection to ventral CA1, the area where social memory is stored (Okuyama *et al.*, 2016), is particularly illustrative. In this ventral hippocampal region, it is theorized that pyramidal cells embody the concept of an individual (Watarai *et al.*, 2021). In other words, sensory inputs from a familiar animal, whether scents, visual, or audible vocalizations, could trigger the retrieval of stored social memories about that individual in another animal. Therefore, if individual identity in mice is defined by a specific chemical pattern of MUPs (Hurst *et al.*, 2001), it is essential for the primary vomeronasal cortex to relay this information to the ventral hippocampus.

This concept finds a parallel in human recognition processes. Humans identify each other largely through facial recognition, occurring in the fusiform gyrus of the brain (Kanwisher *et al.*, 1997; Nestor *et al.*, 2011; Ghuman *et al.*, 2014). This area then transmits information about the individual face to the concept cells in the medial temporal lobe, better known as Jennifer Aniston neurons (Quiroga *et al.*, 2005; Quiroga, 2012). We propose that the PMCo, acting as a primary vomeronasal cortex, recognizes patterns encoded in the urine of other animals and conveys this information to the ventral CA1, where it is consolidated into a comprehensive concept of individual identity.

The complexity of neural coding in the PMCo revealed by tensor decomposition indicates adaptability and specificity in the neuronal responses to vomeronasal stimuli.

The tensor decomposition technique revealed that the patterns of neuronal activity in response to specific urine samples are neither invariant nor characteristic of a particular sample. It was observed that single neuronal activation is not exclusively linked to a determined urine sample. Instead, these neurons demonstrate active participation in detecting multiple samples. A plausible explanation suggests that the same neuron can participate in different neuronal assemblies, thus being involved in recognizing distinct individuals. This concept mirrors the pattern of codification found in the Jennifer Aniston neurons, in which a single neuron can codify multiple individual concepts (Quiroga *et al.*, 2005).

However, in some cases, there is a clear tendency where certain neurons show predominant activity in response to a specific urine sample, in contrast with others.

This finding suggests a highly dynamic and flexible neuronal system capable of adapting and responding to a wide range of vomeronasal stimuli. Such adaptability could be a key mechanism for efficient and precise recognition in an environment

where olfactory stimuli are numerous and varied. Moreover, the ability of some neurons to respond more intensely to a certain urine sample might indicate the existence of a specialized encoding mechanism optimized for the precise identification of critical vomeronasal stimuli in the biological context of the organism.

As exposed in previous sections, a limited number of chemicals contained in the urine act as individual signatures. The recognition of an individual by another involves encoding this relatively simple code of 8-12 specific MUPs (Hurst *et al.*, 2001; Nevison *et al.*, 2003; Kaur *et al.*, 2014). Our observations indicate that the response of neurons in the PMCo to urine from specific individuals involves the activation of distinct neuronal assemblies. Interestingly, these neurons exhibit varying patterns of activity when exposed multiple times to the same urine sample, suggesting a complex and dynamic process of neural response and encoding.

Interpreting these findings within the framework of Shannon's Information Theory offers a fascinating perspective on how information is processed in the brain, particularly in the context of pheromone-dependent individual recognition. Shannon's theory posits that entropy is a measure of uncertainty or unpredictability in information content (Shannon, 1948). The diverse neuronal responses to a limited set of pheromones, as observed in the PMCo, indicate high entropy. This suggests that each exposure to the same urine sample carries a significant level of unpredictability in terms of neuronal activation patterns.

In terms of information processing, the variability in neuronal responses might imply a highly sophisticated encoding system. Despite the seemingly simple input (a limited set of pheromones), the brain appears to generate a rich and complex array of outputs (neuronal patterns). This could mean that the brain interprets and encodes the pheromone signals in a nuanced manner, possibly taking into account contextual factors or subtle differences in the concentration and composition of the urine chemicals.

The variability and overlap in neuronal responses could be seen as a form of redundancy, ensuring that the essential signal (individual identification through MUPs) is reliably transmitted and understood, even in the presence of noise or other interfering signals. From an information theory standpoint, the PMCo seems to be striking a balance between efficiency and accuracy. While a more uniform response to the same stimulus might be more efficient, the observed variability could provide a richer, more detailed representation, enhancing the accuracy and reliability of individual recognition.

However, certain neurons responding exclusively to a specific urine sample add another layer of complexity and provide a complementary perspective to the previous findings in the context of Shannon's Information Theory. The presence of neurons that are exclusively activated by a particular urine sample indicates a level of specialization and specificity in the neural coding system. This specificity acts as a counterbalance to the high entropy observed with the broader, variable neuronal responses. It suggests that alongside a generalized and adaptable encoding system, there exists a parallel mechanism geared towards precise and unambiguous recognition.

These specialized neurons could be seen as dedicated information channels. They provide a clear and distinct signal amidst the more complex and variable background responses, ensuring that certain key pieces of information, like the identification of a specific individual, are reliably transmitted without ambiguity. The existence of neurons with exclusive responses to specific pheromones can be interpreted as a strategy to reduce errors in critical recognition tasks. In Shannon's terms, this could be seen as a method to decrease the overall system's entropy for certain crucial signals, thereby increasing the reliability of the information transmission.

The coexistence of neurons with variable responses and those with highly specific responses illustrates a sophisticated neural processing system. It suggests an integrative approach where the brain employs both generalized and specialized strategies for interpreting pheromone signals. This dual approach could enable

more nuanced and adaptive behavior, allowing for both broad pattern recognition and specific individual identification.

Nonetheless, it is relevant to acknowledge the primary limitation of this study. The analysis of the controls using saline exposure was relatively confusing, as some neurons ceased activity while others continued responding to the last stimulus received. Notably, the PMCo receives strong olfactory input from the olfactory amygdala and the Pir (Gutiérrez-Castellanos *et al.*, 2014). A plausible explanation is that the urine's volatile components persisted in the experimental environment even after the stimulus removal from the head-fixed system. In fact, the urine volatile component has the capability to induce social odor discrimination in CA2 pyramidal neurons (Hassan *et al.*, 2023). To mitigate this confounding factor, the proposed experiment replicates the current study's methodology with MOE-impaired animals. By isolating vomeronasal information and eliminating volatile influence, we anticipate a network noise reduction, leading to a system with decreased disorder.

Another limitation of our study is the challenge we faced in recording a large number of neurons simultaneously within the same animal and session. The literature on the morphological arrangement of PMCo neurons is sparse. However, the organization of PMCo neurons does not mirror the highly structured arrangement found in the hippocampus or neocortex, characterized by an almost perfect dipole and an open electric field flow (Feenstra and Holsheimer, 1979). The inability to record a large number of neurons from the same animal in a single session hinders the study of extensive neuronal assemblies, making it difficult to study individual recognition engrams.

PMCo activity patterns encode individual conspecific stimuli.

Our CEBRA models have demonstrated that the overall neural activity in the PMCo serves as an indicator of the conspecific stimulus encountered by the animal. In other words, the PMCo adjusts its activity in response to the urines, exhibiting a distinct global activity pattern unique to each type of urine. The model's effectiveness is evident in the distinct clustering of neural responses in the embedding space, with low intra-label distances suggesting consistent neural representation for each urine type in PMCo. Furthermore, inter-label distances in the embedding space were high between urine from different male individuals ♂1 and ♂2, suggesting that the female PMCo somehow can codify the differences of chemosignals contained in the different male urines into different activity patterns.

Our goal with the synthetic urine mixture (♂1+♂2) was to test whether by artificially blending two urines of varying concentrations, thereby creating a mixture of new MUPs concentration, we could produce a third urine distinct from the original two, representing a new individual. It could be supposed that this new, artificially generated urine, with its unique MUP pattern, might be uninterpretable due to its absence in the natural environment. However, this synthetic urine ♂1+♂2 has been shown to activate specific neurons in the tensor decomposition analysis. Furthermore, its relative Euclidean closeness to urines ♂1 and ♂2, as opposed to the ♂1→♂2 countermark scenario, indicates that the PMCo may follow a hierarchical pattern in recognizing these chemical concentrations. In essence, this suggests that the chemical gradient present in urine plays a role in influencing the PMCo's ability to recognize individual signatures.

In the context of our countermarking study, it is important to highlight that this particular urine sample (♂1→♂2) exhibited the greatest distance in Euclidean space compared to urines ♂1, ♂2, and ♂1+♂2. This implies that countermarking, perhaps due to its significant biological relevance, tends to elicit a distinct pattern of activity, markedly different from the urines involved in the countermarking process. Methodologically, our approach to countermarking involved applying the urine of ♂1 onto the urine of ♂2, which had been left to dry for several hours. However, it is worth noting that this laboratory method may not accurately replicate natural

behaviors observed in the wild, where male rodents sometimes mark near, rather than directly on, the scent marks of their competitors (Wilcox and Johnston, 1995; Hurst and Beynon, 2004). Own urine (♀0), on the other hand, seems to be somewhat closer in space to the three male-derived urines previously mentioned.

While we have discussed the spatial distances among the five stimuli presented to the female subjects, it is crucial to remember that each stimulus elicits a unique global activity pattern in the PMCo.

On the other hand, we observed a notable decrease in decoding accuracy from the fifth session onwards. Based on patterns of activity for each urine on Trial 1, the model cannot accuratelly predict which urine the animal is exploring in the last few trials. To explain this reduction in decoding accuracy, two theoretical scenarios are proposed. Repeated exposure to the same stimulus may be altering the activity pattern of the recorded neurons. In females, exposure to male urine induces LTP in the PMCo (Villafranca-Faus *et al.*, 2021). This synaptic potentiation might lead to a process of sensitization or habituation due to continuous exposure to the same stimulus. Alternatively, this phenomenon could be attributed to model overfitting. An overfitted model tends to predict very similar datasets specifically. Therefore, calculating the validation loss along with the InfoNCE loss of our model would be beneficial. Adjusting the number of iterations and the learning rate could further refine the model's predictions.

Further analysis is required to understand the changes in PMCo activity across different stimulus trials. Our analysis, aimed at assessing the decoding accuracy across individual trials, has yielded intriguing results. Initially, there's a tendency for accuracy to increase. However, this is followed by a noticeable decline in decoding accuracy, which then significantly improves again. Despite the overall high decoding accuracy, additional analysis is necessary to determine PMCo behavior. After prolonged stimulation with each stimulus, the activity might change, possibly due to habituation. However, the subsequent increase in decoding performance suggests a need to reevaluate the data. This could involve testing decoding by dividing our complete dataset into training and testing subsets, as well as examining decoding performance using models trained on different trial datasets.

6 CONCLUSIONS

Taking into account the results obtained, along with the analyses detailed in Section 3, and considering the interpretations and limitations discussed in Section 4, we conclude that:

I. Vomeronasal information captured by the VNO is relayed to the AOB, which transfers it to the PMCo via a unilateral glutamatergic projection. The PMCo, in turn, sends glutamatergic connections to both the ventral hippocampus and the LEnt and MEnt. This information is further relayed to the dorsal hippocampus by a subset of reelin-positive neurons in the dLEnt layer II. This connectivity establishes two vomeronasal outflow pathways to the hippocampus: a direct route to the ventral hippocampus and an indirect route to the dorsal hippocampus.

II. At their origin in the PMCo, the direct and indirect pathways exhibit partial overlap in neuronal engagement. This phenomenon underscores the potential of vomeronasal signals, carrying chemical molecules crucial for rodent individual recognition, to generate neuronal representation states in the hippocampus governed under an attractor dynamics mechanism.

III. Reciprocal excitatory connectivity between the dLEnt and the PMCo indicates a positive feedback mechanism within the indirect route of vomeronasal information flow to the hippocampus. In conjunction with the hypothesized attractor network, signal amplification appears to be another computational element essential for vomeronasal information effective processing within the delineated pathway.

IV. Exposing females to male urine, as opposed to a neutral odorant, results in heightened neuronal activation in most nodes of the described pathway. The neural response of all these nodes to such stimuli exhibits remarkably similar activation patterns, indicating a coordinated reaction to stimuli exposure.

V. PCA of the overall activity indicated that females exposed to male-derived urine account for the majority of the variance observed in the olfactory-vomeronasal behavioral paradigm. This functional test suggests that the described amygdalar-entorhinal-hippocampal pathway is the neural substrate for transmitting and integrating vomeronasal information into the hippocampal formation.

VI. Spatial rearrangement of male-derived stimuli, aimed at simulating a reorganization of the female territory, elicits a remapping behavioral outcome in the females. This outcome alters neuronal activation exclusively in the MEnt-dorsal CA1 segment of the pathway, suggesting that the encoding of the "what" and "where" components of episodic memory is compartmentalized.

VII. The remapping behavior observed in response to spatial changes in male-derived stimuli is not evident when the same spatial alterations are applied to inanimate objects. Upon comparing neuronal activation after spatial reorganization of both item types, it is apparent that the nuclei within the direct and indirect routes exhibit increased activation in response to conspecific stimuli spatial change. In contrast, spatial alterations in objects preferentially activate the MEnt and dorsal CA3 regions of the hippocampus. This indicates that the pathway is activated towards the recognition of social information derived

from conspecifics, encoding the "who" subcomponent of episodic memory, i.e. the identity of the individual.

VIII. Based on the findings from tract-tracing and functional histology studies, the PMCo emerges as a cornerstone in the flow of vomeronasal information within the amygdalar-entorhinal-hippocampal pathway.

IX. The PMCo neuronal activity patterns in response to urine from different individuals are sophisticated, comprising neurons that respond to a broad range of stimuli and neurons that specifically activate in response to a particular stimulus. This indicates the coexistence in the PMCo of a generalizing and adaptive mechanism alongside another mechanism dedicated to precise and unambiguous recognition. This dual approach facilitates adaptive behavioral outcomes by enabling broad pattern recognition while ensuring specific individual identification.

X. The PMCo exhibits distinct global activity patterns specific to each stimulus from different conspecifics, indicating its ability to hierarchically identify these stimuli based on their chemosensory characteristics. Behavioral changes in activity patterns emerge from repeated exposures to the same stimulus, hinting at adaptive processes like habituation or sensitization. Additionally, biological phenomena such as countermarking and self-recognition appear to elicit unique activity patterns in the PMCo.

APPENDIX

Iontophoretic tracer injections.

Iontophoretic injections were performed using glass micropipettes (1B150-4, World Precision Instruments Inc., USA) with an internal diameter tip of 20-40 μm, depending on the target area. The tracer was loaded in the micropipette by capillary action, and silver wires were placed in direct contact with the tracer solution (positive terminal) and with the animal's skin (negative terminal). When lowering the pipette, a continuous negative retaining current of -5 μA was applied using a current generator (Stoelting Co., USA) to prevent tracer leakage. After reaching the intended structure, the retaining current was stopped and a reasonable time was allowed before starting the injection. To carry out the iontophoretic injections, 5 μA positive pulses of current were given in a 7s on/off pattern for a total of 10 minutes. After injection, the micropipette was left in place for 5 minutes to avoid diffusion of the tracer during the withdrawal, and a continuous negative retaining current of -5 μA was applied.

Pressure tracer injections.

Pressure injections were performed using glass micropipettes (1B120F-4, World Precision Instruments Inc., USA) with an internal diameter tip of 30-40 μm, depending on the target area, and an internal glass filament to prevent blocking. The micropipette was filled with mineral oil (Sigma-Aldrich, USA), taking care to avoid air bubbles, and mounted gently in a microinjector (Nanoliter 2000, World Precision Instruments Inc., USA). After applying a small positive pressure to expel any possible air bubbles in the tip, a sufficient amount of tracer was loaded. To avoid any tracer leakage during the descent, a small volume of mineral oil was absorbed to coat the tip end. After reaching the specified coordinates, we waited until the pressure changes caused by passing through the tissue were reduced. To carry out the pressure injection, 10-12 pulses of 23 nl/pulse were administered in intervals of 30 seconds at a rate of 2.3 nl/s, to ensure accuracy in the injection spread and avoid any tissue damage. After injection, the micropipette was shifted a few microns dorsally to allow the remaining positive pressure to be realized and was left in place for 15 minutes before the withdrawal.

RESUMEN

Introducción y objetivos.

El sistema olfativo de los organismos terrestres es un mecanismo activo y dinámico esencial para la supervivencia y reproducción de los individuos. Los vertebrados terrestres poseen dos sistemas olfativos primarios: el principal y el accesorio. Los roedores, en particular, tienen sistemas olfativos altamente adaptados para identificar una amplia gama de químicos presentes en su entorno.

El sistema olfativo principal proporciona información general sobre los químicos volátiles en el ambiente, mientras que el sistema olfativo accesorio se especializa en detectar químicos volátiles y no volátiles de alta relevancia biológica que aportan información relacionada con otros individuos. Las células sensoriales del sistema olfativo principal se encuentran en el epitelio olfativo principal, y las del sistema accesorio en el órgano vomeronasal. Estos sistemas tienen divisiones anatómicas y mecanismos de transducción distintos, lo que subraya su segregación funcional.

Los bulbos olfativos son parte del cerebro anterior y están situados debajo del lóbulo frontal. En el bulbo olfativo principal, las neuronas sensoriales establecen sinapsis axodendríticas con neuronas de proyección y participan en interacciones sinápticas con interneuronas periglomerulares. En contraste, el bulbo olfativo accesorio se encuentra en la región posterodorsal del bulbo olfativo principal. Las neuronas mitrales del bulbo olfativo accesorio reciben entradas sinápticas de neuronas vomeronasales y se caracterizan por sus múltiples dendritas primarias que se ramifican para inervar varios glomérulos.

La amígdala quimiosensorial es una de las principales regiones anatómicas inervadas por los bulbos olfatorios. Desempeña un papel crucial en la interacción de los sistemas olfativos principal y accesorio, permitiendo a los animales mostrar comportamientos adecuados fruto de la interacción entre ambos sistemas. Esta interacción se evidencia a través de hallazgos anatómicos que muestran la convergencia de entradas de ambos bulbos olfativos en regiones específicas de la amígdala. Las estructuras de la amígdala quimiosensorial mixta reciben entradas tanto del bulbo olfativo principal como del accesorio, y se clasifican en aquellas con predominancia olfativa o vomeronasal.

El núcleo amigdalino cortical posteromedial (PMCo) es un núcleo sexualmente dimórfico que regula diferentes aspectos del comportamiento copulatorio masculino y es considerado la corteza vomeronasal primaria. Este núcleo muestra una extensa conectividad dentro del sistema vomeronasal, así como integración con el sistema olfativo a través de conexiones con la corteza olfativa, núcleos amigdalinos sensibles al olfato y la corteza entorrinal.

Los estímulos vomeronasales son señales químicas de alta relevancia biológica detectadas por el órgano vomeronasal. Estos incluyen feromonas sexuales, señales de depredadores, señales derivadas de enfermedades, señales relacionadas con el estrés y químicos que desencadenan comportamientos relacionados con la agresión, maternidad y territorialidad. Los mamíferos utilizan señales vomeronasales para indicar la propiedad territorial, dejando marcas duraderas en el entorno. Los ratones machos son altamente territoriales y usan marcas de orina para demarcar sus territorios, aumentando su tasa de marcado al encontrar marcas de competidores.

Los ratones dependen de patrones individuales de proteínas en la orina, conocidas como proteínas urinarias mayores (MUPs), para distinguir entre individuos. Estas MUPs son secretadas por ambos sexos, pero en los machos adultos, su concentración es significativamente más alta. Las MUPs se unen y estabilizan la liberación de compuestos orgánicos volátiles de las marcas de olor, prolongando el tiempo en que la marca puede ser percibida. Las hembras muestran una preferencia por

la orina de machos dominantes y su exposición a feromonas masculinas no solo influye en sus preferencias olfativas, sino que también acelera su entrada a la pubertad.

El genoma de referencia del ratón codifica 21 MUPs, pero un individuo no expresa todas estas MUPs. Los machos presentan subconjuntos discretos estables de 4-12 MUPs a lo largo de su vida. Dentro de este patrón de expresión de MUP se encuentra el "código de barras" para el reconocimiento individual, único para cada animal dentro del espacio territorial. Para ligar la función perceptiva de la información vomeronasal que lleva a cabo la amígdala quimiosensorial con la función espacial del hipocampo, es imperativa la existencia de una circuitería funcional amígdalo-hipocampal.

La formación hipocampal ha sido objeto de interés constante en la comunidad científica. Comprende el giro dentado, el hipocampo propiamente dicho (CA3, CA2 y CA1), el complejo subicular y la corteza entorrinal. Esta formación está asociada con una amplia gama de funciones, incluyendo la formación y almacenamiento de memorias, navegación y representación espacial, aprendizaje asociativo, regulación del estrés y un papel significativo en el procesamiento emocional.

La corteza entorrinal se considera el punto de inicio del circuito hipocampal, siendo la estructura de entrada y salida principal de la formación hipocampal. Esta región se divide en la corteza entorrinal medial y lateral, con diferencias significativas en funcionalidad y conectividad. El giro dentado es una estructura cortical de tres capas que funciona como punto de entrada al hipocampo, formando la etapa inicial en el circuito trisináptico que recibe entrada de información desde la corteza entorrinal. La región CA3 del hipocampo propiamente dicho sirve como punto de entrada al hipocampo propiamente dicho, recibiendo entradas excitatorias de la corteza entorrinal y del giro dentado. CA3 se caracteriza por conexiones recurrentes entre sus células piramidales. CA2 ha surgido recientemente como una región asociada principalmente con el procesamiento de información social, mientras que CA1 es el principal destino de los colaterales de Schaffer de CA3 y de las conexiones monosinápticas de la corteza entorrinal.

El complejo subicular se divide generalmente en el subículo propiamente dicho, el presubículo y el parasubículo, siendo el subículo la principal área de proyección de la formación hipocampal. El hipocampo ha sido propuesto como sustrato tanto en la formación de memoria como en la navegación espacial. Las células de lugar en la región CA1 dorsal del hipocampo son neuronas que muestran actividad preferencial cuando un animal se encuentra en una ubicación específica dentro de su entorno. Estas células de lugar, junto con las células de cuadrícula, las células de dirección de la cabeza, las células de objetivo y las células de borde, forman parte del sistema de navegación espacial del cerebro.

Para los animales que viven en grupos sociales, la capacidad de reconocer y retener recuerdos de otros individuos es fundamental para mostrar interacciones apropiadas con sus conespecíficos. Se ha descubierto que la conexión entre dos regiones hipocampales, CA2 dorsal y CA1 ventral, es crucial para codificar, consolidar, almacenar y recuperar memorias sociales. Inactivar la región CA2 dorsal conduce a alteraciones en la memoria social, mientras que el bloqueo de las proyecciones de CA2 dorsal a CA1 ventral conduce a una notable alteración en la formación de memoria social. Estos hallazgos sugieren que la integración de la información vomeronasal en este circuito hipocampal es esencial en las etapas iniciales de codificación y consolidación de las memorias sociales, así como durante la recuperación de esas memorias en respuesta a la reexploración de señales vomeronasales.

La hipótesis central de esta tesis doctoral propone que las señales químicas vomeronasales transmiten la información de reconocimiento individual en ratones. Esta información de identidad residiría en patrones de concentraciones de proteínas presentes en la orina, actuando como un código de barras único identificable por otros conespecíficos. Este código de barras de identidad detectado por el órgano vomeronasal se codificaría en la amígdala quimiosensorial. Es esencial que la infor-

mación sobre la identidad se incorpore e integre con otras modalidades sensoriales en un mapa espacial detallado en el hipocampo, lo que es crucial para que los animales muestren conductas adaptativas mientras navegan por sus territorios. Para abordar esta amplia hipótesis desde diferentes prismas metodológicos, se combinarán técnicas de trazado neuroanatómico, conducta, histología y electrofisiología.

Material y métodos.

El estudio realizado se adhirió a las normativas españolas y europeas sobre el uso de animales en investigación científica. Se emplearon ratones hembra CD1, en un rango de edad y peso específico, para realizar una serie de experimentos neuroanatómicos, conductuales y electrofisiológicos. Estos experimentos se orientaron a investigar la conectividad neuronal, así como las respuestas conductuales y neuronales a estímulos de conespecíficos.

En el aspecto neuroanatómico, se realizaron cirugías bajo anestesia con isoflurano, utilizando técnicas estereotáxicas para inyectar trazadores neuronales en diversas regiones cerebrales, como el AOB, PMCo, dLEnt o el hipocampo. La inyección de estos trazadores anterógrados y retrógrados (TBDA, BDA, FG y WGA), se combinó con técnicas de inmunohistoquímica para detectar marcadores específicos como VGLUT1, GAD 65/67, reelina o calbindina. El propósito de estos experimentos fue mapear las conexiones neuronales entre estas áreas para delinear posibles rutas neuroanatómicas para el procesamiento e integración de la información vomeronasal.

Posteriormente, se procesaron las muestras cerebrales para el análisis histológico. Se emplearon diversas técnicas inmunohistoquímicas y de microscopía para identificar la presencia de trazadores y marcadores en diferentes regiones del cerebro. Este análisis permitió una evaluación detallada de las conexiones neuronales y la identificación de áreas específicas del cerebro implicadas en el procesamiento de estímulos vomeronasales.

Para los experimentos conductuales, se diseñaron tres paradigmas conductuales distintos a los que se sometió a ratones hembra CD1. El primero, "test de exposición a orina vs. citralva", se enfocó en comparar la activación neuronal entre la exposición a orina de macho y un odorante neutro. El segundo, "test de manipulación espacial de estímulos sociales", investigó cómo la reubicación espacial de estímulos sociales (orinas de diferentes machos) afectaba la activación neuronal. El tercer experimento, "test de manipulación espacial social vs. objetos", comparó los efectos de reorganización espacial en la activación neuronal entre estímulos sociales y objetos inanimados.

El análisis de estos experimentos se realizó con técnicas avanzadas de videoanálisis para cuantificar el comportamiento exploratorio. La herramienta elegida fue DeepLabCut, un “software” para la detección y seguimiento de puntos específicos en los vídeos. Para ello, se entrenaron tres redes neuronales diferentes para optimizar el seguimiento de los animales en los distintos paradigmas conductuales. Los cerebros se procesaron para detectar c-Fos, un marcador de activación neuronal. Se utilizaron técnicas de microscopía confocal para la visualización de c-Fos, lo que permitió una evaluación precisa de la activación neuronal en respuesta a los diferentes estímulos para cada núcleo de interés.

Para el registro de la actividad neuronal unitaria extracelular en PMCo, se implementó un sistema de fijación de la cabeza del ratón para registrar neuronas en animales despiertos. Se habituaron los animales a las condiciones experimentales y se les expuso a estímulos de conespecíficos tales como la orina de diferentes ratones machos, la orina de la propia hembra siendo registrada, o combinaciones artificiales de las orinas de los machos para simular entornos naturales dinámicos.

La adquisición de la señal eléctrica neuronal se realizó mediante sondas de silicio de 32 canales, correctamente dispuestas en el PMCo. Esta señal cruda fue posteriormente procesada mediante “softwares” libres para realizar la clasificación de las espigas en neuronas unitarias. Se empleó la descomposición tensorial de la activi-

dad neuronal para identificar patrones representativos de respuesta a los estímulos de conespecíficos.

Además, se utilizaron modelos de CEBRA para generar incrustaciones informativas de baja dimensión de los datos neuronales. Este enfoque combinó análisis de componentes independientes no lineales y aprendizaje contrastivo, permitiendo obtener representaciones detalladas y distinguibles de los patrones de respuesta de todo en núcleo en su conjunto.

En cuanto al análisis estadístico, se emplearon métodos tanto paramétricos como no paramétricos para analizar los datos conductuales y de c-Fos, incluyendo ANOVA de medidas repetidas, t-tests independientes, regresión beta y análisis de correlación de Pearson.

Resultados trazado de conexiones.

El estudio se centra en las conexiones neuronales y la transmisión de información quimiosensorial en ratones, específicamente en cómo esta información se procesa y transmite al hipocampo. Utilizando diversas técnicas de trazado neuronal, se exploraron estas vías en detalle.

El AOB emite proyecciones glutamatérgicas hacia PMCo y áreas relacionadas de la amígdala quimiosensorial. A través de inyecciones de TBDA y la detección de VGLUT1, se confirmó la naturaleza glutamatérgica de estas proyecciones. Estas vías se extienden a lo largo de la superficie ventral del cerebro e inervan múltiples áreas dentro de la subdivisión quimiosensorial de la amígdala.

El PMCo, por su parte, no tiene conexiones directas con el hipocampo dorsal, pero se conecta con la formación hipocampal a través de proyecciones glutamatérgicas directas al hipocampo ventral y la corteza entorrinal. Estas conexiones fueron demostradas mediante inyecciones de TBDA y estudios de inmunohistoquímica. El PMCo, al enviar fibras al hipocampo ventral, afecta a la región que contiene las dendritas apicales de las células piramidales del CA1. Además, se observó que el PMCo proyecta a la corteza entorrinal lateral y medial, con una presencia notable en las capas II/III de estas regiones.

Se encontró que el PMCo y el hipocampo dorsal están indirectamente conectados a través de una población restringida de neuronas reelina positivas en la corteza entorrinal lateral dorsal (dLEnt). Estudios adicionales revelaron que estas neuronas reelina positivas en dLEnt son el sustrato neural que potencialmente transmite información vomeronasal desde el PMCo al área CA1 del hipocampo dorsal.

Además, se descubrió que toda la extensión del PMCo proyecta a las capas II/III de la dLEnt. Estas proyecciones fueron confirmadas mediante trazado retrogrado, destacando la importancia del PMCo en la ruta neuronal entre la amígdala quimiosensorial cortical y dLEnt.

Una investigación adicional sobre las vías desde el PMCo al hipocampo dorsal y ventral reveló que, aunque ambas rutas son independientes, comparten parcialmente el mismo origen neuronal. Se realizaron inyecciones retrogradas duales para explorar si las mismas neuronas dentro del PMCo podrían estar transmitiendo información a lo largo de estas rutas distintas. Se identificaron neuronas que proyectaban exclusivamente a dLEnt, otras solo al CA1 ventral y un grupo que inervaba simultáneamente a ambas estructuras.

Finalmente, se investigó la naturaleza de las conexiones anterógradas originadas en las capas II/III de la dLEnt. Se encontró que dLEnt, además de recibir entradas, también envía proyecciones corticofugales glutamatérgicas al PMCo. Este descubrimiento sugiere un circuito de retroalimentación bidireccional entre dLEnt y la amígdala quimiosensorial cortical, lo que podría facilitar una integración y modulación más sofisticadas de la información quimiosensorial.

En conjunto, estos experimentos detallan un circuito neuroanatómico que transmite información vomeronasal a la formación hipocampal, destacando el papel del PMCo en el procesamiento y la transferencia de esta información.

Resultados conducta y activación neuronal.

Esta fase de la experimentación se centró en la respuesta conductual de ratones hembra a diferentes estímulos, enfatizando la importancia del sistema vomeronasal y la vía amígdalo-entorrino-hipocampal en el procesamiento de la información social.

En una primera fase del experimento, se comparó la conducta y activación neuronal de ratones hembra frente a orina de macho o un olor neutro, citralva. Se observó una marcada preferencia por la orina. A nivel neuronal, la exposición a la orina resultó en una activación significativa del AOB, PMCo, CA1 ventral, CA2 dorsal y dLEnt, además de otras áreas de la amígdala vomeronasal. Curiosamente, no se detectó activación en regiones asociadas al sistema de recompensa, lo que sugiere que la preferencia por la orina no está vinculada a estos mecanismos de recompensa. El análisis de correlaciones y el PCA mostraron que la vía amígdalo-entorrino-hipocampal mostró en este paradigma conductual patrones de activación similares, manifestando un trabajo coordinado en el procesamiento de este tipo de estímulos.

En un segundo paradigma conductual, se alteró espacialmente la ubicación de diferentes orinas de macho para evaluar la capacidad de las hembras de detectar cambios en su entorno. Las hembras mostraron un aumento en la conducta reexploratoria tras estos cambios espaciales, además de un incremento de la actividad neuronal en la región CA1 dorsal del hipocampo y en MEnt. Esto indica que estas áreas cerebrales están implicadas en el procesamiento de cambios espaciales en estímulos sociales importantes, y ponen de manifiesto que las distintas componentes de la memoria episódica están compartimentalizadas dentro de la vía anatómica estudiada.

El tercer paradigma conductual comparó la respuesta de las hembras a la reubicación espacial de las orinas de macho y de objetos inanimados. Los resultados mostraron respuestas diferentes a estos dos tipos de estímulos. La reubicación de las orinas provocó un aumento en la conducta reexploratoria y la activación de áreas cerebrales específicas de la vía, como PMCo, dLEnt, CA1 ventral o CA2 dorsal. Por otra parte, la manipulación de objetos inanimados no generó cambios significativos en el comportamiento, sin embargo, sí que se pudo observar un aumento significativo en la expresión de c-Fos en el CA3 del hipocampo dorsal y el mEnt. Esto sugiere una especialización en el cerebro para el procesamiento de información social en comparación con estímulos no sociales.

Los resultados de estos experimentos destacan la especial sensibilidad del sistema vomeronasal y la vía amígdalo-entorrino-hipocampal al procesamiento de señales sociales en ratones. Se evidencia una respuesta diferenciada y especializada a la orina masculina frente a olores neutros y objetos inanimados, subrayando el papel crucial de ciertas áreas cerebrales en el reconocimiento y procesamiento de cambios espaciales en estímulos sociales relevantes.

Resultados registro unitario en PMCo.

En este estudio se analizó la respuesta neuronal en el PMCo de ratones hembra a distintos estímulos de orina de conespecíficos, utilizando una serie de técnicas avanzadas de análisis para desentrañar los patrones de activación neuronal.

Los resultados mostraron variaciones en las tasas de disparo, indicando cómo las neuronas del PMCo procesan la información social. Se pudieron observar respuestas neuronales selectivas a diferentes tipos de orina. Por ejemplo, una neurona respondía específicamente a la orina de un macho y no a la de otro, lo que sugiere un procesamiento diferenciado de los estímulos vomeronasales.

Para comprender mejor cómo las neuronas codifican información sobre la orina, se realizó un análisis de descomposición tensorial sobre las tasas de disparo neuronal. Este análisis reveló patrones distintos de respuesta a diferentes muestras de orina, mostrando consistencia y variabilidad en las respuestas neuronales a través de múltiples exposiciones e intervalos de tiempo. Se observó que algunas neuronas

respondían predominantemente a un tipo específico de orina, mientras que otras respondían generalmente a varios estímulos diferentes.

Además, se empleó un análisis de agrupamiento jerárquico, utilizando PCA, para explorar los patrones de respuesta neuronal. Esto reveló que las neuronas respondían de manera diferente a los cinco tipos de orina, con algunas neuronas especializadas en responder a un tipo particular. Los resultados del análisis de agrupamiento indicaron una fuerte estructura en los datos, con puntuajes de Calinski-Harabasz y Davies-Bouldin altos, lo que sugiere una categorización significativa de las neuronas en función de sus patrones de respuesta.

Para examinar la variabilidad de los patrones de actividad en el PMCo para los diferentes estímulos y a lo largo de las continuadas exposiciones, se utilizaron modelos de CEBRA. El análisis de CEBRA mostró distintos subespacios para cada tipo de orina, lo que indica que el modelo pudo diferenciar eficazmente entre los tipos de orina en función de sus firmas neuronales. Los “embeddings” de CEBRA para los distintos ensayos mostraron variabilidad en las respuestas neuronales a cada muestra de orina durante dichos ensayos. Asimismo, se pudo observar una pérdida en la precisión de la decodificación conforme el animal iba siendo expuesto continuadamente al mismo estímulo, sugiriendo algún tipo de adaptación neuronal que provocara algún cambio en los patrones de respuesta. No obstante, la precisión media de la decodificación fue generalmente alta, muy superior a la observada al aleatorizar los datos.

Este estudio proporciona una visión detallada de cómo las neuronas en el PMCo procesan y codifican los patrones químicos contenidos en las distintas orinas de conespecíficos. Las técnicas de análisis utilizadas permitieron identificar patrones específicos de actividad neuronal en respuesta a cada orina y destacaron la capacidad del PMCo para discriminar entre diferentes estímulos sociales.

Discusión.

Se describió la vía neuroanatómica que transmite información vomeronasal a los polos septotemporales del hipocampo. Esta vía comienza en el VNO, que envía la información vomeronasal al AOB, que a su vez la releva mediante conexiones glutamatérgicas al PMCo, considerado la corteza vomeronasal primaria. El PMCo proyecta conexiones glutamatérgicas a las dendritas apicales de las células piramidales de CA1 ventral, al MEnt y a un conjunto de neuronas reelina positivas en la capa II del aspecto dorsal del LEnt. Estas neuronas reelina positivas, conocidas como células "fan", se han vinculado recientemente con la memoria episódica. Además, se observó una mayor activación de estas células en respuesta a la orina de macho en comparación con un odorante neutral, lo que sugiere que codifican información tanto olfativa como vomeronasal.

En términos de la transmisión de información vomeronasal, se encontró que la activación del PMCo, CA1 ventral y CA2 dorsal aumentó en experimentos con presencia de orina. También se destacó la activación de dLEnt, especialmente en su población celular reelina positiva, indicando que los estímulos vomeronasales influyen significativamente en la vía propuesta. La existencia de rutas directas e indirectas hacia el hipocampo sugiere un mecanismo de dinámica de atracción en el procesamiento de la memoria social, con una separación de patrones y una compleción de patrones.

El paradigma de comportamiento olfativo-vomeronasal reveló los núcleos más relevantes para el procesamiento de información vomeronasal. La exposición a la orina, que contiene señales volátiles y no volátiles, se comparó con la exposición a citralva, un odorante neutral solo volátil. Se observaron diferencias notables en el AOB, PMCo, CA1 ventral, CA2 dorsal, dLEnt y en las neuronas reelina positivas de dLEnt. Esto implica que los estímulos vomeronasales afectan significativamente la vía neuroanatómica propuesta.

Se propone que el PMCo, como corteza vomeronasal primaria, juega un papel crucial en reconocer patrones químicos específicos en la orina de otros animales y transmitir esta información al CA1 ventral, donde se consolidan conceptos de identidad individual. Además, el análisis de descomposición tensorial sugiere un sistema neuronal dinámico y flexible en el PMCo, capaz de adaptarse y responder a una amplia gama de estímulos vomeronasales. Algunas neuronas mostraron respuestas predominantes a un tipo específico de orina, lo que indica una codificación especializada.

Los modelos de CEBRA demostraron que la actividad general en el PMCo sirve como indicador del estímulo del conespecífico. La capacidad del modelo para distinguir entre tipos de orina basándose en sus firmas neuronales sugiere que el PMCo puede codificar las diferencias en las señales químicas contenidas en distintas orinas masculinas en patrones de actividad distintos. Sin embargo, se observó una disminución en la precisión de decodificación a partir de la quinta sesión, lo que podría atribuirse a la sensibilización o habituación debido a la exposición continua al mismo estímulo o a un posible sobreajuste del modelo.

Este estudio proporciona una comprensión detallada de cómo las neuronas en el PMCo procesan y codifican información olfativa, particularmente en respuesta a diferentes tipos de orina. Las técnicas utilizadas permitieron identificar patrones específicos de actividad neuronal y destacaron la capacidad del PMCo para discriminar entre diferentes estímulos olfativos, sugiriendo una sofisticada y dinámica codificación neuronal en el procesamiento de información vomeronasal. Asimismo, la experimentación muestra cómo se integra esta información vomeronasal en memorias espaciales dependientes de hipocampo. La vía neuroanatómica propuesta, en la que el PMCo parece actuar como el reconocedor de la identidad, podría ser el sustrato neuronal de la navegación territorial y el reconocimiento individual en roedores.

Conclusiones.

Del estudio se concluye que la información vomeronasal capturada por el VNO se transmite al AOB y luego al PMCo, estableciendo dos vías de flujo de información hacia el hipocampo: una directa al hipocampo ventral y otra indirecta al dorsal. En el PMCo, estas vías presentan una superposición parcial en el origen neuronal, destacando la capacidad de las señales vomeronasales para generar estados de representación neuronal en el hipocampo bajo un mecanismo de dinámicas de atracción. La conectividad recíproca excitatoria entre el dLEnt y el PMCo indica un mecanismo de retroalimentación positiva en la ruta indirecta, lo que sugiere que la amplificación de señales es un elemento computacional esencial en el procesamiento efectivo de la información vomeronasal.

La exposición a orina de macho en contraposición a un odorante neutral lleva a una activación neuronal aumentada en la mayoría de los nodos de la vía descrita, con patrones de activación notablemente similares. El PCA de los datos de la actividad neuronal en el paradigma conductual olfativo-vomeronasal indica que son las hembras expuestas a orina de macho las que explican un mayor porcentaje de la varianza generada en el propio paradigma. Este resultado sugiere que la vía amigdalar-entorrinal-hipocampal delineada es el sustrato neural para la transmisión e integración de la información vomeronasal en la formación hipocampal.

El cambio espacial de estímulos derivados de macho, que simula una reorganización del territorio de la hembra, provoca un resultado conductual de remapeo en las hembras y altera la activación neuronal únicamente en el segmento MEnt-CA1 dorsal de la vía, sugiriendo que la codificación de los componentes "qué" y "dónde" de la memoria episódica está compartimentalizada. Además, la reorganización espacial de estímulos conespecíficos activa las rutas directa e indirecta en respuesta a un cambio espacial, mientras que las alteraciones espaciales en objetos activan preferentemente regiones MEnt y CA3 dorsal. Esto indica que la vía se activa hacia

el reconocimiento de información social derivada de conespecíficos, codificando el subcomponente "quién" de la memoria episódica, es decir, la identidad del individuo.

Por lo tanto, el PMCo surge como un elemento crucial en el flujo de información vomeronasal dentro de la vía amigdalar-entorrinal-hipocampal. Los patrones de actividad neuronal en el PMCo en respuesta a orina de diferentes individuos son sofisticados, incluyendo neuronas que responden a una amplia gama de estímulos y otras que se activan específicamente en respuesta a un estímulo particular. Esto indica la coexistencia en el PMCo de un mecanismo generalizador y adaptativo junto con otro mecanismo dedicado al reconocimiento preciso e inequívoco. El PMCo muestra patrones de actividad global distintos específicos para cada estímulo de conespecíficos diferentes, indicando su capacidad para identificar jerárquicamente estos estímulos basándose en sus características quimiosensoriales. Los cambios conductuales en los patrones de actividad surgen de exposiciones repetidas al mismo estímulo, insinuando procesos adaptativos como la habituación o la sensibilización. Además, fenómenos biológicos como el contramarcado y el auto-reconocimiento parecen provocar patrones de actividad únicos en el PMCo.

REFERENCES

Abellán-Álvaro, María, Fernando Martínez-García, Enrique Lanuza, and Carmen Agustín-Pavín

2022 "Inhibition of the medial amygdala disrupts escalated aggression in lactating female mice after repeated exposure to male intruders," *Communications Biology*, 5, 1, p. 980, DOI: 10.1038/s42003-022-03928-2.

Albasser, Mathieu M., Guillaume L. Poirier, and John P. Aggleton

2010 "Qualitatively different modes of perirhinal-hippocampal engagement when rats explore novel vs. familiar objects as revealed by c-Fos imaging," *European Journal of Neuroscience*, 31, 1, pp. 134-147, ISSN: 0953-816X, DOI: 10.1111/j.1460-9568.2009.07042.x.

Alexander, Georgia M., Shannon Farris, Jason R. Pirone, Chenguang Zheng, Laura L. Colgin, and Serena M. Dudek

2016 "Social and novel contexts modify hippocampal CA2 representations of space," *Nature Communications*, 7, 1, p. 10300, DOI: 10.1038/ncomms10300.

Allen, Timothy A., Daniel M. Salz, Sam McKenzie, and Norbert J. Fortin

2016 "Nonspatial Sequence Coding in CA1 Neurons," *The Journal of Neuroscience*, 36, 5, pp. 1547-1563, ISSN: 0270-6474, DOI: 10.1523/jneurosci.2874-15.2016.

Amaral, D.G. and M.P. Witter

1989 "The three-dimensional organization of the hippocampal formation: A review of anatomical data," *Neuroscience*, 31, 3, pp. 571-591, ISSN: 0306-4522, DOI: 10.1016/0306-4522(89)90424-7.

Amaral, David G., Cynthia Dolorfo, and Pablo Alvarez-Royo

1991 "Organization of CA1 projections to the subiculum: A PHA-L analysis in the rat," *Hippocampus*, 1, 4, pp. 415-435, ISSN: 1050-9631, DOI: 10.1002/hipo.450010410.

Amaral, David G., Norio Ishizuka, and Brenda Claiborne

1990 "Chapter 1 Chapter Neurons, numbers and the hippocampal network," *Progress in Brain Research*, 83, pp. 1-11, ISSN: 0079-6123, DOI: 10.1016/s0079-6123(08)61237-6.

Andersen, P., T. V. P. Bliss, and K. K. Skrede

1971 "Lamellar organization of hippocampal excitatory pathways," *Experimental Brain Research*, 13, 2, pp. 222-238, ISSN: 0014-4819, DOI: 10.1007/bf00234087.

Andersen, P., B. Holmqvist, and P. E. Voorhoeve

1966 "Excitatory Synapses on Hippocampal Apical Dendrites Activated by Entorhinal Stimulation," *Acta Physiologica Scandinavica*, 66, 4, pp. 461-472, ISSN: 0001-6772, DOI: 10.1111/j.1748-1716.1966.tb03224.x.

Andersen, Per, Richard Morris, David Amaral, Tim Bliss, and John O'Keefe

2006 "The Hippocampus Book," pp. 9-36, DOI: 10.1093/acprof:oso/9780195100273.003.0002.

Apps, P. J., A. Rasa, and H. W. Viljoen

1988 "Quantitative chromatographic profiling of odours associated with dominance in male laboratory mice," *Aggressive Behavior*, 14, 6, pp. 451-461, ISSN: 0096-140X, DOI: 10.1002/1098-2337(1988)14:6<451::aid-ab2480140606>3.0.co;2-2.

Barber, P.C., D.M. Parry, P.M. Field, and G. Raisman

1978 "Electron microscope autoradiographic evidence for specific transneuronal transport in the mouse accessory olfactory bulb," *Brain Research*, 152, 2, pp. 283-302, ISSN: 0006-8993, DOI: 10.1016/0006-8993(78)90256-1.

Barnes, If H. A., Ximena Ibarra-Soria, Stephen Fitzgerald, Jose M. Gonzalez, Claire Davidson, Matthew P. Hardy, Deepa Manthravadi, Laura Van Gerven, Mark Jorissen, Zhen Zeng, Mona Khan, Peter Mombaerts, Jennifer Harrow, Darren W. Logan, and Adam Frankish

2020 "Expert curation of the human and mouse olfactory receptor gene repertoires identifies conserved coding regions split across two exons," *BMC Genomics*, 21, 1, p. 196, DOI: 10.1186/s12864-020-6583-3.

Barrientos, Sebastian A. and Vicente Tiznado

2016 "Hippocampal CA1 Subregion as a Context Decoder," *The Journal of Neuroscience*, 36, 25, pp. 6602-6604, ISSN: 0270-6474, DOI: 10.1523/jneurosci.1107-16.2016.

Bartsch, T. and P. Wulff

2015 "The hippocampus in aging and disease: From plasticity to vulnerability," *Neuroscience*, 309, pp. 1-16, ISSN: 0306-4522, DOI: 10.1016/j.neuroscience.2015.07.084.

Belluscio, Leonardo, Georgy Koentges, Richard Axel, and Catherine Dulac

1999 "A Map of Pheromone Receptor Activation in the Mammalian Brain," *Cell*, 97, 2, pp. 209-220, ISSN: 0092-8674, DOI: 10.1016/s0092-8674(00)80731-x.

Berghard, A and LB Buck

1996 "Sensory transduction in vomeronasal neurons: evidence for G alpha o, G alpha i2, and adenylyl cyclase II as major components of a pheromone signaling cascade," *The Journal of Neuroscience*, 16, 3, pp. 909-918, ISSN: 0270-6474, DOI: 10.1523/jneurosci.16-03-00909.1996.

Beynon, R J and J L Hurst

2003 "Multiple roles of major urinary proteins in the house mouse, Mus domesticus," *Biochemical Society Transactions*, 31, 1, pp. 142-146, ISSN: 0300-5127, DOI: 10.1042/bst0310142.

Bhasin, Guncha and Indrajith R. Nair

2022 "Dynamic Hippocampal CA2 Responses to Contextual Spatial Novelty," *Frontiers in Systems Neuroscience*, 16, p. 923911, ISSN: 1662-5137, DOI: 10.3389/fnsys.2022.923911.

Bitzenhofer, Sebastian H, Elena A Westeinde, Han-Xiong Bear Zhang, and Jeffry S Isaacson

2022 "Rapid odor processing by layer 2 subcircuits in lateral entorhinal cortex," *eLife*, 11, e75065, DOI: 10.7554/elife.75065.

Blackstad, Theodor W.

1956 "Commissural connections of the hippocampal region in the rat, with special reference to their mode of termination," *Journal of Comparative Neurology*, 105, 3, pp. 417-537, ISSN: 0021-9967, DOI: 10.1002/cne.901050305.

Bliss, T. V. P. and T. Lí¸mo

1973 "Long-lasting potentiation of synaptic transmission in the dentate area of the anaesthetized rabbit following stimulation of the perforant path," *The Journal of Physiology*, 232, 2, pp. 331-356, ISSN: 0022-3751, DOI: 10.1113/jphysiol.1973.sp010273.

Boillat, Madlaina, Ludivine Challet, Daniel Rossier, Chenda Kan, Alan Carleton, and Ivan Rodriguez

2015 "The Vomeronasal System Mediates Sick Conspecific Avoidance," *Current Biology*, 25, 2, pp. 251-255, ISSN: 0960-9822, DOI: 10.1016/j.cub.2014.11.061.

Bostock, Elizabeth, Robert U. Muller, and John L. Kubie

1991 "Experience-dependent modifications of hippocampal place cell firing," *Hippocampus*, 1, 2, pp. 193-205, ISSN: 1050-9631, DOI: 10.1002/hipo.450010207.

Boyle, Maureen P., Amy Bernard, Carol L. Thompson, Lydia Ng, Andrew Boe, Marty Mortrud, Michael J. Hawrylycz, Allan R. Jones, Robert F. Hevner, and Ed S. Lein

2011 "Cell-type-specific consequences of reelin deficiency in the mouse neocortex, hippocampus, and amygdala," *Journal of Comparative Neurology*, 519, 11, Spc1-Spc1, ISSN: 0021-9967, DOI: 10.1002/cne.22708.

Bozza, Thomas, Anne Vassalli, Stefan Fuss, Jing-Ji Zhang, Brian Weiland, Rodrigo Pacifico, Paul Feinstein, and Peter Mombaerts

2009 "Mapping of Class I and Class II Odorant Receptors to Glomerular Domains by Two Distinct Types of Olfactory Sensory Neurons in the Mouse," *Neuron*, 61, 2, pp. 220-233, ISSN: 0896-6273, DOI: 10.1016/j.neuron.2008.11.010.

Brennan, P.A.

2001 "The vomeronasal system," *Cellular and Molecular Life Sciences CMLS*, 58, 4, pp. 546-555, ISSN: 1420-682X, DOI: 10.1007/pl00000880.

Brennan, Peter A. and Eric B. Keverne

2004 "Something in the Air? New Insights into Mammalian Pheromones," *Current Biology*, 14, 2, R81-R89, ISSN: 0960-9822, DOI: 10.1016/j.cub.2003.12.052.

Brennan, Peter A. and Frank Zufall

2006 "Pheromonal communication in vertebrates," *Nature*, 444, 7117, pp. 308-315, ISSN: 0028-0836, DOI: 10.1038/nature05404.

Britt, Jonathan" P., Faiza Benaliouad, Ross" A. McDevitt, Garret" D. Stuber, Roy" A. Wise, and Antonello Bonci

2012 "Synaptic and Behavioral Profile of Multiple Glutamatergic Inputs to the Nucleus Accumbens," *Neuron*, 76, 4, pp. 790-803, ISSN: 0896-6273, DOI: 10.1016/j.neuron.2012.09.040.

Brog, Judith S., Aimee Salyapongse, Ariel Y. Deutch, and Daniel S. Zahm

1993 "The patterns of afferent innervation of the core and shell in the Accumbens part of the rat ventral striatum: Immunohistochemical detection of retrogradely transported fluoro-gold," *Journal of Comparative Neurology*, 338, 2, pp. 255-278, ISSN: 0021-9967, DOI: 10.1002/cne.903380209.

Buck, Linda and Richard Axel

1991 "A novel multigene family may encode odorant receptors: A molecular basis for odor recognition," *Cell*, 65, 1, pp. 175-187, ISSN: 0092-8674, DOI: 10.1016/0092-8674(91)90418-x.

Buck, Linda B
2000 "The Molecular Architecture of Odor and Pheromone Sensing in Mammals," *Cell*, 100, 6, pp. 611-618, ISSN: 0092-8674, DOI: 10.1016/s0092-8674(00)80698-4.

Bupesh, Munisamy, Isabel Legaz, Antonio Abellán, and Loreta Medina
2011 "Multiple telencephalic and extratelencephalic embryonic domains contribute neurons to the medial extended amygdala," *Journal of Comparative Neurology*, 519, 8, pp. 1505-1525, ISSN: 0021-9967, DOI: 10.1002/cne.22581.

Burke, S.N., A.P. Maurer, A.L. Hartzell, S. Nematollahi, A. Uprety, J.L. Wallace, and C.A. Barnes
2012 "Representation of three-dimensional objects by the rat perirhinal cortex," *Hippocampus*, 22, 10, pp. 2032-2044, ISSN: 1050-9631, DOI: 10.1002/hipo.22060.

Cadiz-Moretti, B, F Martinez-Garcia, and E Lanuza
2013 "Neural Substrate to Associate Odorants and Pheromones: Convergence of Projections from the Main and Accessory Olfactory Bulbs in Mice," ed. by [East, Marion L Dehnhard, and Martin], pp. 3-16, DOI: 10.1007/978-1-4614-5927-9_1, https://doi.org/10.1007/978-1-4614-5927-9%5C_1.

Cádiz-Moretti, Bernardita, María Abellán-Álvaro, Cecília Pardo-Bellver, Fernando Martínez-García, and Enrique Lanuza
2017 "Afferent and efferent projections of the anterior cortical amygdaloid nucleus in the mouse," *Journal of Comparative Neurology*, 525, 13, pp. 2929-2954, ISSN: 0021-9967, DOI: 10.1002/cne.24248.

Cádiz-Moretti, Bernardita, María Abellán-Álvaro, Cecília Pardo-Bellver, Fernando Martínez-García, and Enrique Lanuza
2016 "Afferent and Efferent Connections of the Cortex-Amygdala Transition Zone in Mice," *Frontiers in Neuroanatomy*, 10, p. 125, ISSN: 1662-5129, DOI: 10.3389/fnana.2016.00125.

Campenhausen, Harald Von and Kensaku Mori
2000 "Convergence of segregated pheromonal pathways from the accessory olfactory bulb to the cortex in the mouse," *European Journal of Neuroscience*, 12, 1, pp. 33-46, ISSN: 0953-816X, DOI: 10.1046/j.1460-9568.2000.00879.x.

Canteras, N. S. and L. W. Swanson
1992 "Projections of the ventral subiculum to the amygdala, septum, and hypothalamus: A PHAL anterograde tract-tracing study in the rat," *Journal of Comparative Neurology*, 324, 2, pp. 180-194, ISSN: 0021-9967, DOI: 10.1002/cne.903240204.

Cenquizca, Lee A. and Larry W. Swanson
2007 "Spatial organization of direct hippocampal field CA1 axonal projections to the rest of the cerebral cortex," *Brain Research Reviews*, 56, 1, pp. 1-26, ISSN: 0165-0173, DOI: 10.1016/j.brainresrev.2007.05.002.

Chamero, Pablo, Vicky Katsoulidou, Philipp Hendrix, Bernd Bufe, Richard Roberts, Hiroaki Matsunami, Joel Abramowitz, Lutz Birnbaumer, Frank Zufall, and Trese Leinders-Zufall
2011 "G protein GÎ±o is essential for vomeronasal function and aggressive behavior in mice," *Proceedings of the National Academy of Sciences*, 108, 31, pp. 12898-12903, ISSN: 0027-8424, DOI: 10.1073/pnas.1107770108.

Chamero, Pablo, Tobias F. Marton, Darren W. Logan, Kelly Flanagan, Jason R. Cruz, Alan Saghatelian, Benjamin F. Cravatt, and Lisa Stowers
2007 "Identification of protein pheromones that promote aggressive behaviour," *Nature*, 450, 7171, pp. 899-902, ISSN: 0028-0836, DOI: 10.1038/nature05997.

Chapuis, Julie, Yaniv Cohen, Xiaobin He, Zhijan Zhang, Sen Jin, Fuqiang Xu, and Donald A. Wilson

2013 "Lateral Entorhinal Modulation of Piriform Cortical Activity and Fine Odor Discrimination," *The Journal of Neuroscience*, 33, 33, pp. 13449-13459, ISSN: 0270-6474, DOI: 10.1523/jneurosci.1387-13.2013.

Chen, Shuo, Linmeng He, Arthur J. Y. Huang, Roman Boehringer, Vincent Robert, Marie E. Wintzer, Denis Polygalov, Adam Z. Weitemier, Yanqiu Tao, Mingxiao Gu, Steven J. Middleton, Kana Namiki, Hiroshi Hama, Ludivine Therreau, Vivien Chevaleyre, Hiroyuki Hioki, Atsushi Miyawaki, Rebecca A. Piskorowski, and Thomas J. McHugh

2020 "A hypothalamic novelty signal modulates hippocampal memory," *Nature*, 586, 7828, pp. 270-274, ISSN: 0028-0836, DOI: 10.1038/s41586-020-2771-1.

Chess, Andrew, Itamar Simon, Howard Cedar, and Richard Axel

1994 "Allelic inactivation regulates olfactory receptor gene expression," *Cell*, 78, 5, pp. 823-834, ISSN: 0092-8674, DOI: 10.1016/s0092-8674(94)90562-2.

Chevaleyre, Vivien and Steven A. Siegelbaum

2010 "Strong CA2 Pyramidal Neuron Synapses Define a Powerful Disynaptic Cortico-Hippocampal Loop," *Neuron*, 66, 4, pp. 560-572, ISSN: 0896-6273, DOI: 10.1016/j.neuron.2010.04.013.

Chung, Myung, Mu-Yun Wang, Ziyan Huang, and Teruhiro Okuyama

2020 "Diverse sensory cues for individual recognition," *Development, Growth & Differentiation*, 62, 9, pp. 507-515, ISSN: 0012-1592, DOI: 10.1111/dgd.12697.

Churchland, Mark M., John P. Cunningham, Matthew T. Kaufman, Justin D. Foster, Paul Nuyujukian, Stephen I. Ryu, and Krishna V. Shenoy

2012 "Neural population dynamics during reaching," *Nature*, 487, 7405, pp. 51-56, ISSN: 0028-0836, DOI: 10.1038/nature11129.

Dannenberg, Holger, Hallie Lazaro, Pranav Nambiar, Alec Hoyland, and Michael E Hasselmo

2020 "Effects of visual inputs on neural dynamics for coding of location and running speed in medial entorhinal cortex," *eLife*, 9, e62500, DOI: 10.7554/elife.62500.

Desjardins, Claude, J. A. Maruniak, and F. H. Bronson

1973 "Social Rank in House Mice: Differentiation Revealed by Ultraviolet Visualization of Urinary Marking Patterns," *Science*, 182, 4115, pp. 939-941, ISSN: 0036-8075, DOI: 10.1126/science.182.4115.939.

DeVito, Loren M. and Howard Eichenbaum

2010 "Distinct contributions of the hippocampus and medial prefrontal cortex to the "what-where-when" components of episodic-like memory in mice," *Behavioural Brain Research*, 215, 2, pp. 318-325, ISSN: 0166-4328, DOI: 10.1016/j.bbr.2009.09.014.

Dey, Sandeepa, Pablo Chamero, James K. Pru, Ming-Shan Chien, Ximena Ibarra-Soria, Kathryn R. Spencer, Darren W. Logan, Hiroaki Matsunami, John J. Peluso, and Lisa Stowers

2015 "Cyclic Regulation of Sensory Perception by a Female Hormone Alters Behavior," *Cell*, 161, 6, pp. 1334-1344, ISSN: 0092-8674, DOI: 10.1016/j.cell.2015.04.052.

Dickerson, Bradford C and Howard Eichenbaum

2010 "The Episodic Memory System: Neurocircuitry and Disorders," *Neuropsychopharmacology*, 35, 1, pp. 86-104, ISSN: 0893-133X, DOI: 10.1038/npp.2009.126.

Donegan, Macayla L., Fabio Stefanini, Torcato Meira, Joshua A. Gordon, Stefano Fusi, and Steven A. Siegelbaum

2020 "Coding of social novelty in the hippocampal CA2 region and its disruption and rescue in a 22q11.2 microdeletion mouse model," *Nature Neuroscience*, 23, 11, pp. 1365-1375, ISSN: 1097-6256, DOI: 10.1038/s41593-020-00720-5.

Dong, Hong-Wei and Larry W. Swanson

2004 "Projections from bed nuclei of the stria terminalis, posterior division: Implications for cerebral hemisphere regulation of defensive and reproductive behaviors," *Journal of Comparative Neurology*, 471, 4, pp. 396-433, ISSN: 0021-9967, DOI: 10.1002/cne.20002.

Dudar, J.D.

1974 "In vitro excitation of hippocampal pyramidal cell dendrites by glutamic acid," *Neuropharmacology*, 13, 10-11, pp. 1083-1089, ISSN: 0028-3908, DOI: 10.1016/0028-3908(74)90099-9.

Dulac, Catherine and Richard Axel

1995 "A novel family of genes encoding putative pheromone receptors in mammals," *Cell*, 83, 2, pp. 195-206, ISSN: 0092-8674, DOI: 10.1016/0092-8674(95)90161-2.

Eichenbaum, Howard, Magdalena Sauvage, Norbert Fortin, Robert Komorowski, and Paul Lipton

2012 "Towards a functional organization of episodic memory in the medial temporal lobe," *Neuroscience & Biobehavioral Reviews*, 36, 7, pp. 1597-1608, ISSN: 0149-7634, DOI: 10.1016/j.neubiorev.2011.07.006.

Eom, Kisang

2023 "Partial EC outputs by degraded cues are amplified in hippocampal CA3 circuits for retrieving stored patterns," *PLOS ONE*, 18, 4, e0281458, DOI: 10.1371/journal.pone.0281458.

Fanselow, Michael S. and Hong-Wei Dong

2010 "Are the Dorsal and Ventral Hippocampus Functionally Distinct Structures?" *Neuron*, 65, 1, pp. 7-19, ISSN: 0896-6273, DOI: 10.1016/j.neuron.2009.11.031.

Feenstra, B.W.A and J Holsheimer

1979 "Dipole-like neuronal sources of theta rhythm in dorsal hippocampus, dendate gyrus and cingulate cortex of the urethane-anesthetized rat," *Electroencephalography and Clinical Neurophysiology*, 47, 5, pp. 532-538, ISSN: 0013-4694, DOI: 10.1016/0013-4694(79)90254-2.

Fernandez-Leon, Jose A., Ahmet Kerim Uysal, and Daoyun Ji

2022 "Place cells dynamically refine grid cell activities to reduce error accumulation during path integration in a continuous attractor model," *Scientific Reports*, 12, 1, p. 21443, DOI: 10.1038/s41598-022-25863-2.

Fernández-Ruiz, Antonio, Azahara Oliva, Marisol Soula, Florbela Rocha-Almeida, Gergo A. Nagy, Gonzalo Martin-Vazquez, and György Buzsáki

2021 "Gamma rhythm communication between entorhinal cortex and dentate gyrus neuronal assemblies," *Science*, 372, 6537, ISSN: 0036-8075, DOI: 10.1126/science.abf3119.

Fredes, Felipe, Laura Masaracchia, Marco Capogna, and Diego Vidaurre

2023 "Differential activity patterns in the upper and lower blade of the dentate gyrus," *bioRxiv*, p. 2023.06.07.544044, DOI: 10.1101/2023.06.07.544044.

Fyhn, Marianne, Sturla Molden, Menno P. Witter, Edvard I. Moser, and May-Britt Moser

2004 "Spatial Representation in the Entorhinal Cortex," *Science*, 305, 5688, pp. 1258-1264, ISSN: 0036-8075, DOI: 10.1126/science.1099901.

Gao, Peiran and Surya Ganguli

2015 "On simplicity and complexity in the brave new world of large-scale neuroscience," *Current Opinion in Neurobiology*, 32, pp. 148-155, ISSN: 0959-4388, DOI: 10.1016/j.conb.2015.04.003.

Gardner, Richard J., Erik Hermansen, Marius Pachitariu, Yoram Burak, Nils A. Baas, Benjamin A. Dunn, May-Britt Moser, and Edvard I. Moser

2022 "Toroidal topology of population activity in grid cells," *Nature*, 602, 7895, pp. 123-128, ISSN: 0028-0836, DOI: 10.1038/s41586-021-04268-7.

Gardner, Richard J., Li Lu, Tanja Wernle, May-Britt Moser, and Edvard I. Moser

2019 "Correlation structure of grid cells is preserved during sleep," *Nature Neuroscience*, 22, 4, pp. 598-608, ISSN: 1097-6256, DOI: 10.1038/s41593-019-0360-0.

Gatome, C.W., L. Slomianka, H.P. Lipp, and I. Amrein

2010 "Number estimates of neuronal phenotypes in layer II of the medial entorhinal cortex of rat and mouse," *Neuroscience*, 170, 1, pp. 156-165, ISSN: 0306-4522, DOI: 10.1016/j.neuroscience.2010.06.048.

Germroth, P., W.K. Schwerdtfeger, and E.H. Buhl

1989 "Morphology of identified entorhinal neurons projecting to the hippocampus. A light microscopical study combining retrograde tracing and intracellular injection," *Neuroscience*, 30, 3, pp. 683-691, ISSN: 0306-4522, DOI: 10.1016/0306-4522(89)90161-9.

Ghuman, Avniel Singh, Nicolas M. Brunet, Yuanning Li, Roma O. Konecky, John A. Pyles, Shawn A. Walls, Vincent Destefino, Wei Wang, and R. Mark Richardson

2014 "Dynamic encoding of face information in the human fusiform gyrus," *Nature Communications*, 5, 1, p. 5672, DOI: 10.1038/ncomms6672.

Gloveli, T, D Schmitz, R.M Empson, T Dugladze, and U Heinemann

1997 "Morphological and electrophysiological characterization of layer III cells of the medial entorhinal cortex of the rat," *Neuroscience*, 77, 3, pp. 629-648, ISSN: 0306-4522, DOI: 10.1016/s0306-4522(96)00494-0.

Gosling, L. M.

1982 "A Reassessment of the Function of Scent Marking in Territories," *Zeitschrift für Tierpsychologie*, 60, 2, pp. 89-118, ISSN: 0044-3573, DOI: 10.1111/j.1439-0310.1982.tb00492.x.

Gosling, L. M. and H. V. McKay

1990 "Competitor assessment by scent matching: an experimental test," *Behavioral Ecology and Sociobiology*, 26, 6, pp. 415-420, ISSN: 0340-5443, DOI: 10.1007/bf00170899.

Grande, Xenia, David Berron, Aidan J. Horner, James A. Bisby, Emrah Düzel, and Neil Burgess

2019 "Holistic Recollection via Pattern Completion Involves Hippocampal Subfield CA3," *The Journal of Neuroscience*, 39, 41, pp. 8100-8111, ISSN: 0270-6474, DOI: 10.1523/jneurosci.0722-19.2019.

Gutiérrez-Castellanos, Nicolás, Alino Martínez-Marcos, Fernando Martínez-García, and Enrique Lanuza

2010 "Chapter Seven Chemosensory Function of the Amygdala," *Vitamins & Hormones*, 83, pp. 165-196, ISSN: 0083-6729, DOI: 10.1016/s0083-6729(10)83007-9.

Gutiérrez-Castellanos, Nicolás, Cecília Pardo-Bellver, Fernando Martínez-García, and Enrique Lanuza

2014 "The vomeronasal cortex - afferent and efferent projections of the posteromedial cortical nucleus of the amygdala in mice," *European Journal of Neuroscience*, 39, 1, pp. 141-158, ISSN: 0953-816X, DOI: 10.1111/ejn.12393.

Guzman, Segundo Jose, Alois Schlögl, Michael Frotscher, and Peter Jonas

2016 "Synaptic mechanisms of pattern completion in the hippocampal CA3 network," *Science*, 353, 6304, pp. 1117-1123, ISSN: 0036-8075, DOI: 10.1126/science.aaf1836.

Haberly, Lewis B. and Joseph L. Price

1978 "Association and commissural fiber systems of the olfactory cortex of the rat. I. Systems originating in the piriform cortex and adjacent areas," *Journal of Comparative Neurology*, 178, 4, pp. 711-740, ISSN: 0021-9967, DOI: 10.1002/cne.901780408.

Hafting, Torkel, Marianne Fyhn, Sturla Molden, May-Britt Moser, and Edvard I. Moser

2005 "Microstructure of a spatial map in the entorhinal cortex," *Nature*, 436, 7052, pp. 801-806, ISSN: 0028-0836, DOI: 10.1038/nature03721.

Halpern, M

1987 "The Organization and Function of the Vomeronasal System," *Annual Review of Neuroscience*, 10, 1, pp. 325-362, ISSN: 0147-006x, DOI: 10.1146/annurev.ne.10.030187.001545.

Hamam, Bassam N., David G. Amaral, and Angel A. Alonso

2002 "Morphological and electrophysiological characteristics of layer V neurons of the rat lateral entorhinal cortex," *Journal of Comparative Neurology*, 451, 1, pp. 45-61, ISSN: 0021-9967, DOI: 10.1002/cne.10335.

Harvey, Scott, Bozena Jemiolo, and Milos Novotny

1989 "Pattern of volatile compounds in dominant and subordinate male mouse urine," *Journal of Chemical Ecology*, 15, 7, pp. 2061-2072, ISSN: 0098-0331, DOI: 10.1007/bf01207438.

Hassan, Sami I., Shivani Bigler, and Steven A. Siegelbaum

2023 "Social odor discrimination and its enhancement by associative learning in the hippocampal CA2 region," *Neuron*, 111, 14, 2232-2246.e5, ISSN: 0896-6273, DOI: 10.1016/j.neuron.2023.04.026.

Herrada, Gilles and Catherine Dulac

1997 "A Novel Family of Putative Pheromone Receptors in Mammals with a Topographically Organized and Sexually Dimorphic Distribution," *Cell*, 90, 4, pp. 763-773, ISSN: 0092-8674, DOI: 10.1016/s0092-8674(00)80536-x.

Hildebrand, John G. and Gordon M. Shepherd

1997 "Mechanisms of olfactory discrimination: Converging Evidence for Common Principles Across Phyla," *Annual Review of Neuroscience*, 20, 1, pp. 595-631, ISSN: 0147-006x, DOI: 10.1146/annurev.neuro.20.1.595.

Hitchcock, Frank L.

1927 "The Expression of a Tensor or a Polyadic as a Sum of Products," *Journal of Mathematics and Physics*, 6, 1-4, pp. 164-189, ISSN: 0097-1421, DOI: 10.1002/sapm192761164.

Hitti, Frederick L. and Steven A. Siegelbaum

2014 "The hippocampal CA2 region is essential for social memory," *Nature*, 508, 7494, pp. 88-92, ISSN: 0028-0836, DOI: 10.1038/nature13028.

Hok, V., E. Save, P. P. Lenck-Santini, and B. Poucet

2005 "Coding for spatial goals in the prelimbic/infralimbic area of the rat frontal cortex," *Proceedings of the National Academy of Sciences*, 102, 12, pp. 4602-4607, ISSN: 0027-8424, DOI: 10.1073/pnas.0407332102.

Hoydal, Oyvind Arne, Emilie Ranheim Skytoen¸en, Sebastian Ola Andersson, May-Britt Moser, and Edvard I. Moser

2019 "Object-vector coding in the medial entorhinal cortex," *Nature*, 568, 7752, pp. 400-404, ISSN: 0028-0836, DOI: 10.1038/s41586-019-1077-7.

Humphries, R.E., D.H.L. Robertson, R.J. Beynon, and J.L. Hurst

1999 "Unravelling the chemical basis of competitive scent marking in house mice," *Animal Behaviour*, 58, 6, pp. 1177-1190, ISSN: 0003-3472, DOI: 10.1006/anbe.1999.1252.

Hurst, Jane L.

1990 "Urine marking in populations of wild house mice Mus domesticus Rutty. III. Communication between the sexes," *Animal Behaviour*, 40, 2, pp. 233-243, ISSN: 0003-3472, DOI: 10.1016/s0003-3472(05)80918-2.

Hurst, Jane L. and Robert J. Beynon

2004 "Scent wars: the chemobiology of competitive signalling in mice," *BioEssays*, 26, 12, pp. 1288-1298, ISSN: 0265-9247, DOI: 10.1002/bies.20147.

Hurst, Jane L., Caroline E. Payne, Charlotte M. Nevison, Amr D. Marie, Richard E. Humphries, Duncan H. L. Robertson, Andrea Cavaggioni, and Robert J. Beynon

2001 "Individual recognition in mice mediated by major urinary proteins," *Nature*, 414, 6864, pp. 631-634, ISSN: 0028-0836, DOI: 10.1038/414631a.

Hurst, Jane L., Duncan H.L. Robertson, Ursula Tolladay, and Robert J. Beynon

1998 "Proteins in urine scent marks of male house mice extend the longevity of olfactory signals," *Animal Behaviour*, 55, 5, pp. 1289-1297, ISSN: 0003-3472, DOI: 10.1006/anbe.1997.0650.

Hussain, Ashiq

2011 "The Olfactory Nervous System Of Terrestrial And Aquatic Vertebrates," *Nature Precedings*, pp. 1-1, DOI: 10.1038/npre.2011.6642.1.

Imamura, Fumiaki, Ayako Ito, and Brandon J. LaFever

2020 "Subpopulations of Projection Neurons in the Olfactory Bulb," *Frontiers in Neural Circuits*, 14, p. 561822, DOI: 10.3389/fncir.2020.561822.

Insausti, Ricardo, M. Trinidad Herrero, and Menno P. Witter

1997 "Entorhinal cortex of the rat: Cytoarchitectonic subdivisions and the origin and distribution of cortical efferents," *Hippocampus*, 7, 2, pp. 146-183, ISSN: 1050-9631, DOI: 10.1002/(sici)1098-1063(1997)7:2<146::aid-hipo4>3.0.co;2-l.

Ishizuka, Norio, Janet Weber, and David G. Amaral

1990 "Organization of intrahippocampal projections originating from CA3 pyramidal cells in the rat," *Journal of Comparative Neurology*, 295, 4, pp. 580-623, ISSN: 0021-9967, DOI: 10.1002/cne.902950407.

Jeffery, K.J., James G. Donnett, Neil Burgess, and John M. O'Keefe

1997 "Directional control of hippocampal place fields," *Experimental Brain Research*, 117, 1, pp. 131-142, ISSN: 0014-4819, DOI: 10.1007/s002210050206.

Jemiolo, B, S Harvey, and M Novotny

1986 "Promotion of the Whitten effect in female mice by synthetic analogs of male urinary constituents." *Proceedings of the National Academy of Sciences*, 83, 12, pp. 4576-4579, ISSN: 0027-8424, DOI: 10.1073/pnas.83.12.4576.

Jia, Changping, Georgi Goldman, and Mimi Halpern

1997 "Development of vomeronasal receptor neuron subclasses and establishment of topographic projections to the accessory olfactory bulb," *Developmental Brain Research*, 102, 2, pp. 209-216, ISSN: 0165-3806, DOI: 10.1016/s0165-3806(97)00097-7.

Jia, Changping and Mimi Halpern

1996 "Subclasses of vomeronasal receptor neurons: differential expression of G proteins (Gi-alpha2 and G(o alpha)) and segregated projections to the accessory olfactory bulb," *Brain Research*, 719, 1-2, pp. 117-128, ISSN: 0006-8993, DOI: 10.1016/0006-8993(96)00110-2.

Johnson, Adam and A David Redish

2007 "Neural Ensembles in CA3 Transiently Encode Paths Forward of the Animal at a Decision Point," *The Journal of Neuroscience*, 27, 45, pp. 12176-12189, ISSN: 0270-6474, DOI: 10.1523/jneurosci.3761-07.2007.

Johnson, Dawn M. G., Kurt R. Illig, Mary Behan, and Lewis B. Haberly

2000 "New features of connectivity in piriform cortex visualized by intracellular injection of pyramidal cells suggest that "primary" olfactory cortex functions like "association" cortex in other sensory systems," *The Journal of Neuroscience*, 20, 18, pp. 6974-6982, ISSN: 0270-6474, DOI: 10.1523/jneurosci.20-18-06974.2000.

Jolkkonen, Esa, Riita Miettinen, and Asla Pitkanen

2001 "Projections from the amygdalo-piriform transition area to the amygdaloid complex: A PHA-l study in rat," *Journal of Comparative Neurology*, 432, 4, pp. 440-465, ISSN: 0021-9967, DOI: 10.1002/cne.1113.

Jouhanneau, Mélanie, Fabien Cornilleau, and Matthieu Keller

2014 "Peripubertal exposure to male odors influences female puberty and adult expression of male-directed odor preference in mice," *Hormones and Behavior*, 65, 2, pp. 128-133, ISSN: 0018-506X, DOI: 10.1016/j.yhbeh.2013.12.006.

Kandel, E. R. and W. A. Spencer

1961 "ELECTROPHYSIOLOGY OF HIPPOCAMPAL NEURONS: II. AFTER-POTENTIALS AND REPETITIVE FIRING," *Journal of Neurophysiology*, 24, 3, pp. 243-259, ISSN: 0022-3077, DOI: 10.1152/jn.1961.24.3.243.

Kanwisher, Nancy, Josh McDermott, and Marvin M. Chun

1997 "The Fusiform Face Area: A Module in Human Extrastriate Cortex Specialized for Face Perception," *The Journal of Neuroscience*, 17, 11, pp. 4302-4311, ISSN: 0270-6474, DOI: 10.1523/jneurosci.17-11-04302.1997.

Kaur, Angeldeep" W., Tobias Ackels, Tsung-Han Kuo, Annika Cichy, Sandeepa Dey, Cristen Hays, Maria Kateri, Darren" W. Logan, Tobias" F. Marton, Marc Spehr, and Lisa Stowers

2014 "Murine Pheromone Proteins Constitute a Context-Dependent Combinatorial Code Governing Multiple Social Behaviors," *Cell*, 157, 3, pp. 676-688, ISSN: 0092-8674, DOI: 10.1016/j.cell.2014.02.025.

Kemppainen, Samuli, Esa Jolkkonen, and Asla Pitkänen

2002 "Projections from the posterior cortical nucleus of the amygdala to the hippocampal formation and parahippocampal region in rat," *Hippocampus*, 12, 6, pp. 735-755, ISSN: 1050-9631, DOI: 10.1002/hipo.10020.

Kerr, Kristin M., Kara L. Agster, Sharon C. Furtak, and Rebecca D. Burwell

2007 "Functional neuroanatomy of the parahippocampal region: The lateral and medial entorhinal areas," *Hippocampus*, 17, 9, pp. 697-708, ISSN: 1050-9631, DOI: 10.1002/hipo.20315.

Kevetter, Golda A. and Sarah S. Winans

1981 "Connections of the corticomedial amygdala in the golden hamster. II. Efferents of the olfactory amygdala," *Journal of Comparative Neurology*, 197, 1, pp. 99-111, ISSN: 0021-9967, DOI: 10.1002/cne.901970108.

Khona, Mikail and Ila R. Fiete

2022 "Attractor and integrator networks in the brain," *Nature Reviews Neuroscience*, 23, 12, pp. 744-766, ISSN: 1471-003X, DOI: 10.1038/s41583-022-00642-0.

Kimoto, Hiroko, Sachiko Haga, Koji Sato, and Kazushige Touhara

2005 "Sex-specific peptides from exocrine glands stimulate mouse vomeronasal sensory neurons," *Nature*, 437, 7060, pp. 898-901, ISSN: 0028-0836, DOI: 10.1038/nature04033.

Kinnavane, Lisa, Eman Amin, Cristian M. Olarte-Sánchez, and John P. Aggleton

2016 "Detecting and discriminating novel objects: The impact of perirhinal cortex disconnection on hippocampal activity patterns," *Hippocampus*, 26, 11, pp. 1393-1413, ISSN: 1050-9631, DOI: 10.1002/hipo.22615.

Kitamura, Takashi, Chen Sun, Jared Martin, Lacey J. Kitch, Mark J. Schnitzer, and Susumu Tonegawa

2015 "Entorhinal Cortical Ocean Cells Encode Specific Contexts and Drive Context-Specific Fear Memory," *Neuron*, 87, 6, pp. 1317-1331, ISSN: 0896-6273, DOI: 10.1016/j.neuron.2015.08.036.

Klink, R. and A. Alonso

1993 "Ionic mechanisms for the subthreshold oscillations and differential electroresponsiveness of medial entorhinal cortex layer II neurons," *Journal of Neurophysiology*, 70, 1, pp. 144-157, ISSN: 0022-3077, DOI: 10.1152/jn.1993.70.1.144.

Knierim, James J. and Joshua P. Neunuebel

2016 "Tracking the flow of hippocampal computation: Pattern separation, pattern completion, and attractor dynamics," *Neurobiology of Learning and Memory*, 129, pp. 38-49, ISSN: 1074-7427, DOI: 10.1016/j.nlm.2015.10.008.

Knierim, James J., Joshua P. Neunuebel, and Sachin S. Deshmukh

2014 "Functional correlates of the lateral and medial entorhinal cortex: objects, path integration and local-global reference frames," *Philosophical Transactions of the Royal Society B: Biological Sciences*, 369, 1635, p. 20130369, ISSN: 0962-8436, DOI: 10.1098/rstb.2013.0369.

Kohara, Keigo, Michele Pignatelli, Alexander J Rivest, Hae-Yoon Jung, Takashi Kitamura, Junghyup Suh, Dominic Frank, Koichiro Kajikawa, Nathan Mise, Yuichi Obata, Ian R Wickersham, and Susumu Tonegawa

2014 "Cell type-specific genetic and optogenetic tools reveal hippocampal CA2 circuits," *Nature Neuroscience*, 17, 2, pp. 269-279, ISSN: 1097-6256, DOI: 10.1038/nn.3614.

Kosel, Keith C., Gary W. Van Hoesen, and Douglas L. Rosene

1982 "Non-hippocampal cortical projections from the entorhinal cortex in the rat and rhesus monkey," *Brain Research*, 244, 2, pp. 201-213, ISSN: 0006-8993, DOI: 10.1016/0006-8993(82)90079-8.

Kropff, Emilio, James E. Carmichael, May-Britt Moser, and Edvard I. Moser

2015 "Speed cells in the medial entorhinal cortex," *Nature*, 523, 7561, pp. 419-424, ISSN: 0028-0836, DOI: 10.1038/nature14622.

Kwak, Jae, Claude C. Grigsby, George Preti, Mateen M. Rizki, Kunio Yamazaki, and Gary K. Beauchamp

2013 "Changes in volatile compounds of mouse urine as it ages: Their interactions with water and urinary proteins," *Physiology & Behavior*, 120, pp. 211-219, ISSN: 0031-9384, DOI: 10.1016/j.physbeh.2013.08.011.

Larriva-Sahd, Jorge

2008 "The accessory olfactory bulb in the adult rat: A cytological study of its cell types, neuropil, neuronal modules, and interactions with the main olfactory system," *Journal of Comparative Neurology*, 510, 3, pp. 309-350, ISSN: 0021-9967, DOI: 10.1002/cne.21790.

Laurent, Franí§ois, Jorge R. Brotons-Mas, Elena Cid, Diego Lopez-Pigozzi, Manuel Valero, Beatriz Gal, and Liset Menendez de la Prida

2015 "Proximodistal Structure of Theta Coordination in the Dorsal Hippocampus of Epileptic Rats," *The Journal of Neuroscience*, 35, 11, pp. 4760-4775, ISSN: 0270-6474, DOI: 10.1523/jneurosci.4297-14.2015.

Lee, Jason Y., Heechul Jun, Shogo Soma, Tomoaki Nakazono, Kaori Shiraiwa, Ananya Dasgupta, Tatsuki Nakagawa, Jiayun L. Xie, Jasmine Chavez, Rodrigo Romo, Sandra Yungblut, Meiko Hagihara, Koshi Murata, and Kei M. Igarashi

2021 "Dopamine facilitates associative memory encoding in the entorhinal cortex," *Nature*, 598, 7880, pp. 321-326, ISSN: 0028-0836, DOI: 10.1038/s41586-021-03948-8.

Leinders-Zufall, Trese, Andrew P. Lane, Adam C. Puche, Weidong Ma, Milos V. Novotny, Michael T. Shipley, and Frank Zufall

2000 "Ultrasensitive pheromone detection by mammalian vomeronasal neurons," *Nature*, 405, 6788, pp. 792-796, ISSN: 0028-0836, DOI: 10.1038/35015572.

Leitner, Frauke C, Sarah Melzer, Henry Lütcke, Roberta Pinna, Peter H Seeburg, Fritjof Helmchen, and Hannah Monyer

2016 "Spatially segregated feedforward and feedback neurons support differential odor processing in the lateral entorhinal cortex," *Nature Neuroscience*, 19, 7, pp. 935-944, ISSN: 1097-6256, DOI: 10.1038/nn.4303.

Leutgeb, Jill K., Stefan Leutgeb, May-Britt Moser, and Edvard I. Moser

2007 "Pattern Separation in the Dentate Gyrus and CA3 of the Hippocampus," *Science*, 315, 5814, pp. 961-966, ISSN: 0036-8075, DOI: 10.1126/science.1135801.

Leutgeb, Stefan, Jill K. Leutgeb, Alessandro Treves, May-Britt Moser, and Edvard I. Moser

2004 "Distinct Ensemble Codes in Hippocampal Areas CA3 and CA1," *Science*, 305, 5688, pp. 1295-1298, ISSN: 0036-8075, DOI: 10.1126/science.1100265.

Lever, Colin, Stephen Burton, Ali Jeewajee, John O'Keefe, and Neil Burgess

2009 "Boundary Vector Cells in the Subiculum of the Hippocampal Formation," *The Journal of Neuroscience*, 29, 31, pp. 9771-9777, ISSN: 0270-6474, DOI: 10.1523/jneurosci.1319-09.2009.

Lin, Weihong, Julie Arellano, Burton Slotnick, and Diego Restrepo

2004 "Odors Detected by Mice Deficient in Cyclic Nucleotide-Gated Channel Subunit A2 Stimulate the Main Olfactory System," *The Journal of Neuroscience*, 24, 14, pp. 3703-3710, ISSN: 0270-6474, DOI: 10.1523/jneurosci.0188-04.2004.

Lisman, John, György Buzsáki, Howard Eichenbaum, Lynn Nadel, Charan Ranganath, and A David Redish

2017 "Viewpoints: how the hippocampus contributes to memory, navigation and cognition," *Nature Neuroscience*, 20, 11, pp. 1434-1447, ISSN: 1097-6256, DOI: 10.1038/nn.4661.

Liu, Wei-Lin and Michael T. Shipley

1994 "Intrabulbar associational system in the rat olfactory bulb comprises cholecystokinin-containing tufted cells that synapse onto the dendrites of GABAergic granule cells," *Journal of Comparative Neurology*, 346, 4, pp. 541-558, ISSN: 0021-9967, DOI: 10.1002/cne.903460407.

Llorens-Martín, María, Jerónimo Jurado-Arjona, Jesí°s Avila, and Félix Hernández

2015 "Novel connection between newborn granule neurons and the hippocampal CA2 field," *Experimental Neurology*, 263, pp. 285-292, ISSN: 0014-4886, DOI: 10.1016/j.expneurol.2014.10.021.

Logan, Darren W., Tobias F. Marton, and Lisa Stowers

2008 "Species Specificity in Major Urinary Proteins by Parallel Evolution," *PLoS ONE*, 3, 9, e3280, DOI: 10.1371/journal.pone.0003280.

Lucas, Philippe, Kyrill Ukhanov, Trese Leinders-Zufall, and Frank Zufall

2003 "A Diacylglycerol-Gated Cation Channel in Vomeronasal Neuron Dendrites Is Impaired in TRPC2 Mutant Mice Mechanism of Pheromone Transduction," *Neuron*, 40, 3, pp. 551-561, ISSN: 0896-6273, DOI: 10.1016/s0896-6273(03)00675-5.

Luzynski, Kenneth C., Doris Nicolakis, Maria Adelaide Marconi, Sarah M. Zala, Jae Kwak, and Dustin J. Penn

2021 "Pheromones that correlate with reproductive success in competitive conditions," *Scientific Reports*, 11, 1, p. 21970, DOI: 10.1038/s41598-021-01507-9.

Macrides, Foteos and Stephen P. Schneider

1982 "Laminar organization of mitral and tufted cells in the main olfactory bulb of the adult hamster," *Journal of Comparative Neurology*, 208, 4, pp. 419-430, ISSN: 0021-9967, DOI: 10.1002/cne.902080410.

Majak, Katarzyna and Asla Pitkänen

2003 "Projections from the periamygdaloid cortex to the amygdaloid complex, the hippocampal formation, and the parahippocampal region: A PHA-L study in the rat," *Hippocampus*, 13, 8, pp. 922-942, ISSN: 1050-9631, DOI: 10.1002/hipo.10134.

Malnic, Bettina, Junzo Hirono, Takaaki Sato, and Linda B Buck

1999 "Combinatorial Receptor Codes for Odors," *Cell*, 96, 5, pp. 713-723, ISSN: 0092-8674, DOI: 10.1016/s0092-8674(00)80581-4.

Maras, P.M. and A. Petrulis

2008 "The posteromedial cortical amygdala regulates copulatory behavior, but not sexual odor preference, in the male Syrian hamster (Mesocricetus auratus)," *Neuroscience*, 156, 3, pp. 425-435, ISSN: 0306-4522, DOI: 10.1016/j.neuroscience.2008.08.004.

Martín-Sánchez, Ana, Lynn McLean, Robert J. Beynon, Jane L. Hurst, Guillermo Ayala, Enrique Lanuza, and Fernando Martínez-Garcia

2015 "From sexual attraction to maternal aggression: When pheromones change their behavioural significance," *Hormones and Behavior*, 68, pp. 65-76, ISSN: 0018-506X, DOI: 10.1016/j.yhbeh.2014.08.007.

Martinez-Marcos, Alino

2009 "On the organization of olfactory and vomeronasal cortices," *Progress in Neurobiology*, 87, 1, pp. 21-30, ISSN: 0301-0082, DOI: 10.1016/j.pneurobio.2008.09.010.

Masurkar, Arjun V., Kalyan V. Srinivas, David H. Brann, Richard Warren, Daniel C. Lowes, and Steven A. Siegelbaum

2017 "Medial and Lateral Entorhinal Cortex Differentially Excite Deep versus Superficial CA1 Pyramidal Neurons," *Cell Reports*, 18, 1, pp. 148-160, ISSN: 2211-1247, DOI: 10.1016/j.celrep.2016.12.012.

Mathis, Alexander, Pranav Mamidanna, Kevin M. Cury, Taiga Abe, Venkatesh N. Murthy, Mackenzie Weygandt Mathis, and Matthias Bethge

2018 "DeepLabCut: markerless pose estimation of user-defined body parts with deep learning," *Nature Neuroscience*, 21, 9, pp. 1281-1289, ISSN: 1097-6256, DOI: 10.1038/s41593-018-0209-y.

Matsunami, Hiroaki and Linda B Buck

1997 "A Multigene Family Encoding a Diverse Array of Putative Pheromone Receptors in Mammals," *Cell*, 90, 4, pp. 775-784, ISSN: 0092-8674, DOI: 10.1016/s0092-8674(00)80537-1.

McBride, Kathleen, Burton Slotnick, and Frank L. Margolis

2003 "Does Intranasal Application of Zinc Sulfate Produce Anosmia in the Mouse? An Olfactometric and Anatomical Study," *Chemical Senses*, 28, 8, pp. 659-670, ISSN: 0379-864X, DOI: 10.1093/chemse/bjg053.

McCarthy, Elizabeth A., Arman Maqsudlu, Matthew Bass, Sofia Georghiou, James A. Cherry, and Michael J. Baum

2017 "DREADD-induced silencing of the medial amygdala reduces the preference for male pheromones and the expression of lordosis in estrous female mice," *European Journal of Neuroscience*, 46, 4, pp. 2035-2046, ISSN: 0953-816X, DOI: 10.1111/ejn.13636.

McDonald, Alexander J., Sara J. Shammam-Lagnado, Changjun Shi, and Michael Davis

1999 "Cortical Afferents to the Extended Amygdala," *Annals of the New York Academy of Sciences*, 877, 1, pp. 309-338, ISSN: 0077-8923, DOI: 10.1111/j.1749-6632.1999.tb09275.x.

Meibach, Richard C. and Allan Siegel

1977 "Subicular projections to the posterior cingulate cortex in rats," *Experimental Neurology*, 57, 1, pp. 264-274, ISSN: 0014-4886, DOI: 10.1016/0014-4886(77)90062-0.

Meira, Torcato, Felix Leroy, Eric W. Buss, Azahara Oliva, Jung Park, and Steven A. Siegelbaum

2018 "A hippocampal circuit linking dorsal CA2 to ventral CA1 critical for social memory dynamics," *Nature Communications*, 9, 1, p. 4163, DOI: 10.1038/s41467-018-06501-w.

Mohedano-Moriano, Alicia, Palma Pro-Sistiaga, Isabel Úbeda-Bañón, Carlos Crespo, Ricardo Insausti, and Alino Martinez-Marcos

2007 "Segregated pathways to the vomeronasal amygdala: differential projections from the anterior and posterior divisions of the accessory olfactory bulb," *European Journal of Neuroscience*, 25, 7, pp. 2065-2080, ISSN: 0953-816X, DOI: 10.1111/j.1460-9568.2007.05472.x.

Mombaerts, Peter, Fan Wang, Catherine Dulac, Steve K Chao, Adriana Nemes, Monica Mendelsohn, James Edmondson, and Richard Axel

1996 "Visualizing an Olfactory Sensory Map," *Cell*, 87, 4, pp. 675-686, ISSN: 0092-8674, DOI: 10.1016/s0092-8674(00)81387-2.

Mori, Kensaku, Kiyoshi Kishi, and Hisayuki Ojima

1983 "Distribution of dendrites of mitral, displaced mitral, tufted, and granule cells in the rabbit olfactory bulb," *Journal of Comparative Neurology*, 219, 3, pp. 339-355, ISSN: 0021-9967, DOI: 10.1002/cne.902190308.

Moser, Edvard I, May-Britt Moser, and Bruce L McNaughton

2017 "Spatial representation in the hippocampal formation: a history," *Nature Neuroscience*, 20, 11, pp. 1448-1464, ISSN: 1097-6256, DOI: 10.1038/nn.4653.

Mucignat-Caretta, Carla

2010 "The rodent accessory olfactory system," *Journal of Comparative Physiology A*, 196, 10, pp. 767-777, ISSN: 0340-7594, DOI: 10.1007/s00359-010-0555-z.

Nagelhus, Anne, Sebastian O. Andersson, Soledad Gonzalo Cogno, Edvard I. Moser, and May-Britt Moser

2023 "Object-centered population coding in CA1 of the hippocampus," *Neuron*, 111, 13, 2091-2104.e14, ISSN: 0896-6273, DOI: 10.1016/j.neuron.2023.04.008.

Nestor, Adrian, David C. Plaut, and Marlene Behrmann

2011 "Unraveling the distributed neural code of facial identity through spatiotemporal pattern analysis," *Proceedings of the National Academy of Sciences*, 108, 24, pp. 9998-10003, ISSN: 0027-8424, DOI: 10.1073/pnas.1102433108.

Neunuebel, Joshua" P. and James" J. Knierim

2014 "CA3 Retrieves Coherent Representations from Degraded Input: Direct Evidence for CA3 Pattern Completion and Dentate Gyrus Pattern Separation," *Neuron*, 81, 2, pp. 416-427, ISSN: 0896-6273, DOI: 10.1016/j.neuron.2013.11.017.

Neves, Lívia, Bruno Lobíf£o-Soares, Ana Paula de Castro Araujo, Alan Michel Bezerra Furtunato, Izabela Paiva, Nicholy Souza, Anne Kelly Morais, George Nascimento, Elaine Gavioli, Adriano Bretanha Lopes Tort, Flávio Freitas Barbosa, and Hindiael Belchior

2022 "Theta and gamma oscillations in the rat hippocampus support the discrimination of object displacement in a recognition memory task," *Frontiers in Behavioral Neuroscience*, 16, p. 970083, ISSN: 1662-5153, DOI: 10.3389/fnbeh.2022.970083.

Nevison, C. M., S. Armstrong, R. J. Beynon, R. E. Humphries, and J. L. Hurst

2003 "The ownership signature in mouse scent marks is involatile," *Proceedings of the Royal Society of London. Series B: Biological Sciences*, 270, 1527, pp. 1957-1963, ISSN: 0962-8452, DOI: 10.1098/rspb.2003.2452.

Niedringhaus, Mark, Xin Chen, Katherine Conant, and Rhonda Dzakpasu

2013 "Synaptic Potentiation Facilitates Memory-like Attractor Dynamics in Cultured In Vitro Hippocampal Networks," *PLoS ONE*, 8, 3, e57144, DOI: 10.1371/journal.pone.0057144.

Nilssen, Eirik S., Bente Jacobsen, Gunhild Fjeld, Rajeevkumar R. Nair, Stefan Blankvoort, Clifford Kentros, and Menno P. Witter

2018 "Inhibitory Connectivity Dominates the Fan Cell Network in Layer II of Lateral Entorhinal Cortex," *The Journal of Neuroscience*, 38, 45, pp. 9712-9727, ISSN: 0270-6474, DOI: 10.1523/jneurosci.1290-18.2018.

Nodari, F, FF Hsu, X Fu, TF Holekamp, LF Kao, J Turk, and TE Holy

2008 "Sulfated Steroids as Natural Ligands of Mouse Pheromone-Sensing Neurons," *Journal of Neuroscience*, 28, 25, pp. 6407-6418, ISSN: 0270-6474, DOI: 10.1523/jneurosci.1425-08.2008.

Novotny, M, S Harvey, B Jemiolo, and J Alberts

1985 "Synthetic pheromones that promote inter-male aggression in mice." *Proceedings of the National Academy of Sciences*, 82, 7, pp. 2059-2061, ISSN: 0027-8424, DOI: 10.1073/pnas.82.7.2059.

Novotny, M., S. Harvey, and B. Jemiolo

1990 "Chemistry of male dominance in the house mouse,Mus domesticus," *Experientia*, 46, 1, pp. 109-113, ISSN: 0014-4754, DOI: 10.1007/bf01955433.

O'Keefe, J. and J. Dostrovsky

1971 "The hippocampus as a spatial map. Preliminary evidence from unit activity in the freely-moving rat," *Brain Research*, 34, 1, pp. 171-175, ISSN: 0006-8993, DOI: 10.1016/0006-8993(71)90358-1.

O'Keefe, John

1976 "Place units in the hippocampus of the freely moving rat," *Experimental Neurology*, 51, 1, pp. 78-109, ISSN: 0014-4886, DOI: 10.1016/0014-4886(76)90055-8.

O'Keefe, John and Lynn Nadel

1978 *The Hippocampus as a Cognitive Map*, Oxford: Clarendon Press, ISBN: 0-19-857206-9, http://hdl.handle.net/10150/620894.

Oddo, Salvatore, Antonella Caccamo, Jason D Shepherd, M.Paul Murphy, Todd E Golde, Rakez Kayed, Raju Metherate, Mark P Mattson, Yama Akbari, and Frank M LaFerla

2003 "Triple-Transgenic Model of Alzheimer's Disease with Plaques and Tangles Intracellular A-beta and Synaptic Dysfunction," *Neuron*, 39, 3, pp. 409-421, ISSN: 0896-6273, DOI: 10.1016/s0896-6273(03)00434-3.

Okamoto, Kazuki and Yuji Ikegaya

2019 "Recurrent connections between CA2 pyramidal cells," *Hippocampus*, 29, 4, pp. 305-312, ISSN: 1050-9631, DOI: 10.1002/hipo.23064.

Okuyama, Teruhiro, Takashi Kitamura, Dheeraj S. Roy, Shigeyoshi Itohara, and Susumu Tonegawa

2016 "Ventral CA1 neurons store social memory," *Science*, 353, 6307, pp. 1536-1541, ISSN: 0036-8075, DOI: 10.1126/science.aaf7003.

Olarte-Sánchez, Cristian M., Eman Amin, E. Clea Warburton, and John P. Aggleton

2015 "Perirhinal cortex lesions impair tests of object recognition memory but spare novelty detection," *European Journal of Neuroscience*, 42, 12, pp. 3117-3127, ISSN: 0953-816X, DOI: 10.1111/ejn.13106.

Oliva, Azahara, Antonio Fernández-Ruiz, György Buzsäki, and Antal Berényi
2016 "Role of Hippocampal CA2 Region in Triggering Sharp-Wave Ripples," *Neuron*, 91, 6, pp. 1342-1355, ISSN: 0896-6273, DOI: 10.1016/j.neuron.2016.08.008.

Oliva, Azahara, Antonio Fernández-Ruiz, and Lindsay A. Karaba
2023 "CA2 orchestrates hippocampal network dynamics," *Hippocampus*, 33, 3, pp. 241-251, ISSN: 1050-9631, DOI: 10.1002/hipo.23495.

Oliva, Azahara, Antonio Fernández-Ruiz, Felix Leroy, and Steven A. Siegelbaum
2020 "Hippocampal CA2 sharp-wave ripples reactivate and promote social memory," *Nature*, 587, 7833, pp. 264-269, ISSN: 0028-0836, DOI: 10.1038/s41586-020-2758-y.

Ormond, Jake and John O-Keefe
2022 "Hippocampal place cells have goal-oriented vector fields during navigation," *Nature*, 607, 7920, pp. 741-746, ISSN: 0028-0836, DOI: 10.1038/s41586-022-04913-9.

Osada, Kazumi, Takuya Tashiro, Kenji Mori, and Hiroshi Izumi
2008 "The Identification of Attractive Volatiles in Aged Male Mouse Urine," *Chemical Senses*, 33, 9, pp. 815-823, ISSN: 0379-864X, DOI: 10.1093/chemse/bjn045.

Osanai, Hisayuki, Indrajith R. Nair, and Takashi Kitamura
2023 "Dissecting cell-type-specific pathways in medial entorhinal cortical-hippocampal network for episodic memory," *Journal of Neurochemistry*, 166, 2, pp. 172-188, ISSN: 0022-3042, DOI: 10.1111/jnc.15850.

Ottersen, Ole P.
1982 "Connections of the amygdala of the rat. IV: Corticoamygdaloid and intraamygdaloid connections as studied with axonal transport of horseradish peroxidase," *Journal of Comparative Neurology*, 205, 1, pp. 30-48, ISSN: 0021-9967, DOI: 10.1002/cne.902050104.

Pardo-Bellver, Cecília, Sergio Martínez-Bellver, Fernando Martínez-García, Enrique Lanuza, and Vicent Teruel-Martí
2017 "Synchronized Activity in The Main and Accessory Olfactory Bulbs and Vomeronasal Amygdala Elicited by Chemical Signals in Freely Behaving Mice," *Scientific Reports*, 7, 1, p. 9924, DOI: 10.1038/s41598-017-10089-4.

Pardo-Bellver, Cecília, Bernardita Cádiz-Moretti, Amparo Novejarque, Fernando Martínez-García, and Enrique Lanuza
2012 "Differential efferent projections of the anterior, posteroventral, and posterodorsal subdivisions of the medial amygdala in mice," *Frontiers in Neuroanatomy*, 6, p. 33, DOI: 10.3389/fnana.2012.00033.

Pérez-Gómez, Anabel, Katherin Bleymehl, Benjamin Stein, Martina Pyrski, Lutz Birnbaumer, Steven D. Munger, Trese Leinders-Zufall, Frank Zufall, and Pablo Chamero
2015 "Innate Predator Odor Aversion Driven by Parallel Olfactory Subsystems that Converge in the Ventromedial Hypothalamus," *Current Biology*, 25, 10, pp. 1340-1346, ISSN: 0960-9822, DOI: 10.1016/j.cub.2015.03.026.

Persson, Bjorn M., Veronika Ambrozova, Stephen Duncan, Emma R. Wood, Akira R. O-Connor, and James A. Ainge
2022 "Lateral entorhinal cortex lesions impair odor-context associative memory in male rats," *Journal of Neuroscience Research*, 100, 4, pp. 1030-1046, ISSN: 0360-4012, DOI: 10.1002/jnr.25027.

Prida, Liset Menendez de la, Richard J. Staba, and Joshua A. Dian

2015 "Conundrums of High-Frequency Oscillations (80-800 Hz) in the Epileptic Brain," *Journal of Clinical Neurophysiology*, 32, 3, pp. 207-219, ISSN: 0736-0258, DOI: 10.1097/wnp.0000000000000150.

Quaglino, Elena, Maurizio Giustetto, Patrizia Panzanelli, Dario Cantino, Aldo Fasolo, and Marco Sassoè-Pognetto

1999 "Immunocytochemical localization of glutamate and gamma-aminobutyric acid in the accessory olfactory bulb of the rat," *Journal of Comparative Neurology*, 408, 1, pp. 61-72, ISSN: 0021-9967, DOI: 10.1002/(sici)1096-9861(19990524)408:1<61::aid-cne5>3.0.co;2-f.

Quiroga, R. Quian, L. Reddy, G. Kreiman, C. Koch, and I. Fried

2005 "Invariant visual representation by single neurons in the human brain," *Nature*, 435, 7045, pp. 1102-1107, ISSN: 0028-0836, DOI: 10.1038/nature03687.

Quiroga, Rodrigo Quian

2012 "Concept cells: the building blocks of declarative memory functions," *Nature Reviews Neuroscience*, 13, 8, pp. 587-597, ISSN: 1471-003X, DOI: 10.1038/nrn3251.

Raudies, Florian, James R. Hinman, and Michael E. Hasselmo

2016 "Modelling effects on grid cells of sensory input during self-motion," *The Journal of Physiology*, 594, 22, pp. 6513-6526, ISSN: 0022-3751, DOI: 10.1113/jp270649.

Ray, Saikat, Robert Naumann, Andrea Burgalossi, Qiusong Tang, Helene Schmidt, and Michael Brecht

2014 "Grid-Layout and Theta-Modulation of Layer 2 Pyramidal Neurons in Medial Entorhinal Cortex," *Science*, 343, 6173, pp. 891-896, ISSN: 0036-8075, DOI: 10.1126/science.1243028.

Rich, Tracey J and Jane L Hurst

1998 "Scent marks as reliable signals of the competitive ability of mates," *Animal Behaviour*, 56, 3, pp. 727-735, ISSN: 0003-3472, DOI: 10.1006/anbe.1998.0803.

Robert, Benjamin J.A., Maí¯té M. Moreau, Steve Dos Santos Carvalho, Gael Barthet, Claudia Racca, Mehdi Bhouri, Anne Quiedeville, Maurice Garret, Bénédicte Atchama, Alice Shaam Al Abed, Christelle Guette, Deborah J. Henderson, Aline Desmedt, Christophe Mulle, Aline Marighetto, Mireille Montcouquiol, and Nathalie Sans

2020 "Vangl2 in the Dentate Network Modulates Pattern Separation and Pattern Completion," *Cell Reports*, 31, 10, p. 107743, ISSN: 2211-1247, DOI: 10.1016/j.celrep.2020.107743.

Robert, Vincent, Ludivine Therreau, Vivien Chevaleyre, Eude Lepicard, Cécile Viollet, Julie Cognet, Arthur JY Huang, Roman Boehringer, Denis Polygalov, Thomas J McHugh, and Rebecca Ann Piskorowski

2021 "Local circuit allowing hypothalamic control of hippocampal area CA2 activity and consequences for CA1," *eLife*, 10, e63352, DOI: 10.7554/elife.63352.

Roberts, Sarah A, Deborah M Simpson, Stuart D Armstrong, Amanda J Davidson, Duncan H Robertson, Lynn McLean, Robert J Beynon, and Jane L Hurst

2010 "Darcin: a male pheromone that stimulates female memory and sexual attraction to an individual male's odour," *BMC Biology*, 8, 1, p. 75, DOI: 10.1186/1741-7007-8-75.

Roberts, Sarah A., Amanda J. Davidson, Lynn McLean, Robert J. Beynon, and Jane L. Hurst

2012 "Pheromonal Induction of Spatial Learning in Mice," *Science*, 338, 6113, pp. 1462-1465, ISSN: 0036-8075, DOI: 10.1126/science.1225638.

Robertson, Duncan H. L., Jane L. Hurst, Mark S. Bolgar, Simon J. Gaskell, and Robert J. Beynon

1997 "Molecular Heterogeneity of Urinary Proteins in Wild House Mouse Populations," *Rapid Communications in Mass Spectrometry*, 11, 7, pp. 786-790, ISSN: 0951-4198, DOI: 10.1002/(sici)1097-0231(19970422)11:7<786::aid-rcm876>3.0.co;2-8.

Robinson, N. Bryce, Katherine Krieger, Faiza M. Khan, William Huffman, Michelle Chang, Ajita Naik, Ruan Yongle, Irbaz Hameed, Karl Krieger, Leonard N. Girardi, and Mario Gaudino

2019 "The current state of animal models in research: A review," *International Journal of Surgery*, 72, pp. 9-13, ISSN: 1743-9191, DOI: 10.1016/j.ijsu.2019.10.015.

Rodriguez, Ivan, Paul Feinstein, and Peter Mombaerts

1999 "Variable Patterns of Axonal Projections of Sensory Neurons in the Mouse Vomeronasal System," *Cell*, 97, 2, pp. 199-208, ISSN: 0092-8674, DOI: 10.1016/s0092-8674(00)80730-8.

Rowland, David C., Aldis P. Weible, Ian R. Wickersham, Haiyan Wu, Mark Mayford, Menno P. Witter, and Clifford G. Kentros

2013 "Transgenically Targeted Rabies Virus Demonstrates a Major Monosynaptic Projection from Hippocampal Area CA2 to Medial Entorhinal Layer II Neurons," *The Journal of Neuroscience*, 33, 37, pp. 14889-14898, ISSN: 0270-6474, DOI: 10.1523/jneurosci.1046-13.2013.

Ryba, Nicholas J.P and Roberto Tirindelli

1997 "A New Multigene Family of Putative Pheromone Receptors," *Neuron*, 19, 2, pp. 371-379, ISSN: 0896-6273, DOI: 10.1016/s0896-6273(00)80946-0.

Santiago, Adriana C. and Sara J. Shammah-Lagnado

2004 "Efferent connections of the nucleus of the lateral olfactory tract in the rat," *Journal of Comparative Neurology*, 471, 3, pp. 314-332, ISSN: 0021-9967, DOI: 10.1002/cne.20028.

Sarel, Ayelet, Arseny Finkelstein, Liora Las, and Nachum Ulanovsky

2017 "Vectorial representation of spatial goals in the hippocampus of bats," *Science*, 355, 6321, pp. 176-180, ISSN: 0036-8075, DOI: 10.1126/science.aak9589.

Sargolini, Francesca, Marianne Fyhn, Torkel Hafting, Bruce L. McNaughton, Menno P. Witter, May-Britt Moser, and Edvard I. Moser

2006 "Conjunctive Representation of Position, Direction, and Velocity in Entorhinal Cortex," *Science*, 312, 5774, pp. 758-762, ISSN: 0036-8075, DOI: 10.1126/science.1125572.

Savelli, Francesco, D. Yoganarasimha, and James J. Knierim

2008 "Influence of boundary removal on the spatial representations of the medial entorhinal cortex," *Hippocampus*, 18, 12, pp. 1270-1282, ISSN: 1050-9631, DOI: 10.1002/hipo.20511.

Scalia, Frank and Sarah S. Winans

1975 "The differential projections of the olfactory bulb and accessory olfactory bulb in mammals," *Journal of Comparative Neurology*, 161, 1, pp. 31-55, ISSN: 0021-9967, DOI: 10.1002/cne.901610105.

Schaffer, Karl

1892 "Beitrag zur Histologie der Ammonshornformation," *Archiv für mikroskopische Anatomie*, 39, 1, pp. 611-632, ISSN: 0176-7364, DOI: 10.1007/bf02961541.

Schindelin, Johannes, Ignacio Arganda-Carreras, Erwin Frise, Verena Kaynig, Mark Longair, Tobias Pietzsch, Stephan Preibisch, Curtis Rueden, Stephan Saalfeld, Benjamin Schmid, Jean-Yves Tinevez, Daniel James White, Volker Hartenstein, Kevin Eliceiri, Pavel Tomancak, and Albert Cardona

2012 "Fiji: an open-source platform for biological-image analysis," *Nature Methods*, 9, 7, pp. 676-682, ISSN: 1548-7091, DOI: 10.1038/nmeth.2019.

Schneider, Steffen, Jin Hwa Lee, and Mackenzie Weygandt Mathis

2023 "Learnable latent embeddings for joint behavioural and neural analysis," *Nature*, 617, 7960, pp. 360-368, ISSN: 0028-0836, DOI: 10.1038/s41586-023-06031-6, eprint: 2204.00673.

Schneider, Stephen P. and Foteos Macrides

1978 "Laminar distributions of interneurons in the main olfactory bulb of the adult hamster," *Brain Research Bulletin*, 3, 1, pp. 73-82, ISSN: 0361-9230, DOI: 10.1016/0361-9230(78)90063-1.

Schwartzkroin, Philip A. and Knut Wester

1975 "Long-lasting facilitation of a synaptic potential following tetanization in thein vitro hippocampal slice," *Brain Research*, 89, 1, pp. 107-119, ISSN: 0006-8993, DOI: 10.1016/0006-8993(75)90138-9.

Schwerdtfeger, Walter K., Eberhard H. Buhl, and Peter Germroth

1990 "Disynaptic olfactory input to the hippocampus mediated by stellate cells in the entorhinal cortex," *Journal of Comparative Neurology*, 292, 2, pp. 163-177, ISSN: 0021-9967, DOI: 10.1002/cne.902920202.

Shannon, C. E.

1948 "A mathematical theory of communication," *The Bell System Technical Journal*, 27, 3, pp. 379-423, ISSN: 0005-8580, DOI: 10.1002/j.1538-7305.1948.tb01338.x.

Shih, Yu-Tzu, Jason Bondoc Alipio, and Amar Sahay

2023 "An inhibitory circuit-based enhancer of DYRK1A function reverses Dyrk1a-associated impairment in social recognition," *Neuron*, 111, 19, 3084-3101.e5, ISSN: 0896-6273, DOI: 10.1016/j.neuron.2023.09.009.

Skaggs, William E. and Bruce L. McNaughton

1996 "Replay of Neuronal Firing Sequences in Rat Hippocampus During Sleep Following Spatial Experience," *Science*, 271, 5257, pp. 1870-1873, ISSN: 0036-8075, DOI: 10.1126/science.271.5257.1870.

Solstad, Trygve, Charlotte N. Boccara, Emilio Kropff, May-Britt Moser, and Edvard I. Moser

2008 "Representation of Geometric Borders in the Entorhinal Cortex," *Science*, 322, 5909, pp. 1865-1868, ISSN: 0036-8075, DOI: 10.1126/science.1166466.

Sorrells, Shawn F., Mercedes F. Paredes, Arantxa Cebrian-Silla, Kadellyn Sandoval, Dashi Qi, Kevin W. Kelley, David James, Simone Mayer, Julia Chang, Kurtis I. Auguste, Edward F. Chang, Antonio J. Gutierrez, Arnold R. Kriegstein, Gary W. Mathern, Michael C. Oldham, Eric J. Huang, Jose Manuel Garcia-Verdugo, Zhengang Yang, and Arturo Alvarez-Buylla

2018 "Human hippocampal neurogenesis drops sharply in children to undetectable levels in adults," *Nature*, 555, 7696, pp. 377-381, ISSN: 0028-0836, DOI: 10.1038/nature25975.

Spalding, Kirsty L., Olaf Bergmann, Kanar Alkass, Samuel Bernard, Mehran Salehpour, Hagen B. Huttner, Emil Boström, Isabelle Westerlund, Céline Vial, Bruce A. Buchholz, Göran Possnert, Deborah C. Mash, Henrik Druid, and Jonas Frisén

2013 "Dynamics of Hippocampal Neurogenesis in Adult Humans," *Cell*, 153, 6, pp. 1219-1227, ISSN: 0092-8674, DOI: 10.1016/j.cell.2013.05.002.

Spencer, W. A. and E. R. Kandel

1961 "ELECTROPHYSIOLOGY OF HIPPOCAMPAL NEURONS: IV. FAST PREPOTENTIALS," *Journal of Neurophysiology*, 24, 3, pp. 272-285, ISSN: 0022-3077, DOI: 10.1152/jn.1961.24.3.272.

Stevenson, Erica L. and Heather K. Caldwell

2014 "Lesions to the CA2 region of the hippocampus impair social memory in mice," *European Journal of Neuroscience*, 40, 9, pp. 3294-3301, ISSN: 0953-816X, DOI: 10.1111/ejn.12689.

Steward, Oswald and Sheila A. Scoville

1976 "Cells of origin of entorhinal cortical afferents to the hippocampus and fascia dentata of the rat," *Journal of Comparative Neurology*, 169, 3, pp. 347-370, ISSN: 0021-9967, DOI: 10.1002/cne.901690306.

Storm-Mathisen, Jon

1977 "Glutamic acid and excitatory nerve endings: reduction of glutamic acid uptake after axotomy," *Brain Research*, 120, 2, pp. 379-386, ISSN: 0006-8993, DOI: 10.1016/0006-8993(77)90918-0.

Strange, Bryan A., Menno P. Witter, Ed S. Lein, and Edvard I. Moser

2014 "Functional organization of the hippocampal longitudinal axis," *Nature Reviews Neuroscience*, 15, 10, pp. 655-669, ISSN: 1471-003X, DOI: 10.1038/nrn3785.

Strauch, Christina and Denise Manahan-Vaughan

2020 "Orchestration of Hippocampal Information Encoding by the Piriform Cortex," *Cerebral Cortex*, 30, 1, pp. 135-147, ISSN: 1047-3211, DOI: 10.1093/cercor/bhz077.

Sugar, Jí¸rgen and May-Britt Moser

2019 "Episodic memory: Neuronal codes for what, where, and when," *Hippocampus*, 29, 12, pp. 1190-1205, ISSN: 1050-9631, DOI: 10.1002/hipo.23132.

Sun, Qian, Kalyan V Srinivas, Alaba Sotayo, and Steven A Siegelbaum

2014 "Dendritic Na+ spikes enable cortical input to drive action potential output from hippocampal CA2 pyramidal neurons," *eLife*, 3, e04551, ISSN: 2050-084X, DOI: 10.7554/elife.04551.

Swanson, L. W. and W. M. Cowan

1975 "Hippocampo-Hypothalamic Connections: Origin in Subicular Cortex, Not Ammon's Horn," *Science*, 189, 4199, pp. 303-304, ISSN: 0036-8075, DOI: 10.1126/science.49928.

Swanson, LW and C Kohler

1986 "Anatomical evidence for direct projections from the entorhinal area to the entire cortical mantle in the rat," *The Journal of Neuroscience*, 6, 10, pp. 3010-3023, ISSN: 0270-6474, DOI: 10.1523/jneurosci.06-10-03010.1986.

Takami, Shigeru and Pasquale P. C. Graziadei

1991 "Light microscopic golgi study of mitral/tufted cells in the accessory olfactory bulb of the adult rat," *Journal of Comparative Neurology*, 311, 1, pp. 65-83, ISSN: 0021-9967, DOI: 10.1002/cne.903110106.

Tamamaki, Nobuaki, Koutarou Abe, and Yoshiaki Nojyo

1988 "Three-dimensional analysis of the whole axonal arbors originating from single CA2 pyramidal neurons in the rat hippocampus with the aid of a computer graphic technique," *Brain Research*, 452, 1-2, pp. 255-272, ISSN: 0006-8993, DOI: 10.1016/0006-8993(88)90030-3.

Tang, Qiusong, Andrea Burgalossi, Christian" Laut Ebbesen, Saikat Ray, Robert Naumann, Helene Schmidt, Dominik Spicher, and Michael Brecht

2014 "Pyramidal and Stellate Cell Specificity of Grid and Border Representations in Layer 2 of Medial Entorhinal Cortex," *Neuron*, 84, 6, pp. 1191-1197, ISSN: 0896-6273, DOI: 10.1016/j.neuron.2014.11.009.

Tao, Kentaro, Myung Chung, Akiyuki Watarai, Ziyan Huang, Mu-Yun Wang, and Teruhiro Okuyama

2022 "Disrupted social memory ensembles in the ventral hippocampus underlie social amnesia in autism-associated Shank3 mutant mice," *Molecular Psychiatry*, 27, 4, pp. 2095-2105, ISSN: 1359-4184, DOI: 10.1038/s41380-021-01430-5.

Taube, JS, RU Muller, and JB Ranck

1990 "Head-direction cells recorded from the postsubiculum in freely moving rats. II. Effects of environmental manipulations," *The Journal of Neuroscience*, 10, 2, pp. 436-447, ISSN: 0270-6474, DOI: 10.1523/jneurosci.10-02-00436.1990.

Thos, M., K. C. Luzynski, V. M. Enk, E. Razzazi-Fazeli, J. Kwak, I. Ortner, and D. J. Penn

2019 "Regulation of volatile and non-volatile pheromone attractants depends upon male social status," *Scientific Reports*, 9, 1, p. 489, DOI: 10.1038/s41598-018-36887-y.

Traub, Roger D. and Miles A. Whittington

2022 "Processing of cell assemblies in the lateral entorhinal cortex," *Reviews in the Neurosciences*, 33, 8, pp. 829-847, ISSN: 0334-1763, DOI: 10.1515/revneuro-2022-0011.

Trinh, Kien and Daniel R. Storm

2004 "Detection of Odorants through the Main Olfactory Epithelium and Vomeronasal Organ of Mice," *Nutrition Reviews*, 62, suppl_3, S189-S192, ISSN: 0029-6643, DOI: 10.1111/j.1753-4887.2004.tb00098.x.

Tsao, Albert, Jorgen Sugar, Li Lu, Cheng Wang, James J. Knierim, May-Britt Moser, and Edvard I. Moser

2018 "Integrating time from experience in the lateral entorhinal cortex," *Nature*, 561, 7721, pp. 57-62, ISSN: 0028-0836, DOI: 10.1038/s41586-018-0459-6.

Tulving, Endel and Hans J. Markowitsch

1998 "Episodic and declarative memory: Role of the hippocampus," *Hippocampus*, 8, 3, pp. 198-204, ISSN: 1050-9631, DOI: 10.1002/(sici)1098-1063(1998)8:3<198::aid-hipo2>3.0.co;2-g.

Ubeda-Bañon, Isabel, Amparo Novejarque, Alicia Mohedano-Moriano, Palma Pro-Sistiaga, Carlos de la Rosa-Prieto, Ricardo Insausti, Fernando Martinez-Garcia, Enrique Lanuza, and Alino Martinez-Marcos

2007 "Projections from the posterolateral olfactory amygdala to the ventral striatum: neural basis for reinforcing properties of chemical stimuli," *BMC Neuroscience*, 8, 1, p. 103, DOI: 10.1186/1471-2202-8-103.

Unger, Elizabeth K., Kenneth J. Burke, Cindy F. Yang, Kevin J. Bender, Patrick M. Fuller, and Nirao M. Shah

2015 "Medial Amygdalar Aromatase Neurons Regulate Aggression in Both Sexes," *Cell Reports*, 10, 4, pp. 453-462, ISSN: 2211-1247, DOI: 10.1016/j.celrep.2014.12.040.

Valero, Manuel and Liset Menendez de la Prida

2018 "The hippocampus in depth: a sublayer-specific perspective of entorhinal-hippocampal function," *Current Opinion in Neurobiology*, 52, pp. 107-114, ISSN: 0959-4388, DOI: 10.1016/j.conb.2018.04.013.

Vandrey, Brianna, Jack Armstrong, Christina M Brown, Derek LF Garden, and Matthew F Nolan

2022 "Fan cells in lateral entorhinal cortex directly influence medial entorhinal cortex through synaptic connections in layer 1," *eLife*, 11, e83008, DOI: 10.7554/elife.83008.

Vandrey, Brianna, Derek L.F. Garden, Veronika Ambrozova, Christina McClure, Matthew F. Nolan, and James A. Ainge

2020 "Fan Cells in Layer 2 of the Lateral Entorhinal Cortex Are Critical for Episodic-like Memory," *Current Biology*, 30, 1, 169-175.e5, ISSN: 0960-9822, DOI: 10.1016/j.cub.2019.11.027.

Varga, Csaba, Soo Yeun Lee, and Ivan Soltesz

2010 "Target-selective GABAergic control of entorhinal cortex output," *Nature Neuroscience*, 13, 7, pp. 822-824, ISSN: 1097-6256, DOI: 10.1038/nn.2570.

Villafranca-Faus, María, Manuel Esteban Vila-Martín, Daniel Esteve, Esteban Merino, Anna Teruel-Sanchis, Ana Cervera-Ferri, Joana Martínez-Ricós, Ana Lloret, Enrique Lanuza, and Vicent Teruel-Martí

2021 "Integrating pheromonal and spatial information in the amygdalo-hippocampal network," *Nature Communications*, 12, 1, p. 5286, DOI: 10.1038/s41467-021-25442-5.

Vinader-Caerols, Concepción, Paloma Collado, Santiago Segovia, and Antonio Guillamón

1998 "Sex differences in the posteromedial cortical nucleus of the amygdala in the rat," *NeuroReport*, 9, 11, pp. 2653-2656, ISSN: 0959-4965, DOI: 10.1097/00001756-199808030-00042.

Waaga, Torgeir, Haggai Agmon, Valentin A. Normand, Anne Nagelhus, Richard J. Gardner, May-Britt Moser, Edvard I. Moser, and Yoram Burak

2022 "Grid-cell modules remain coordinated when neural activity is dissociated from external sensory cues," *Neuron*, 110, 11, 1843-1856.e6, ISSN: 0896-6273, DOI: 10.1016/j.neuron.2022.03.011.

Wada, Eiki, Ryuichi Shigemoto, Ayae Kinoshita, Hitoshi Ohishi, and Noboru Mizuno

1998 "Metabotropic glutamate receptor subtypes in axon terminals of projection fibers from the main and accessory olfactory bulbs: A light and electron microscopic immunohistochemical study in the rat," *Journal of Comparative Neurology*, 393, 4, pp. 493-504, ISSN: 0021-9967, DOI: 10.1002/(sici)1096-9861(19980420)393:4<493::aid-cne8>3.0.co;2-w.

Watarai, Akiyuki, Kentaro Tao, Mu-Yun Wang, and Teruhiro Okuyama

2021 "Distinct functions of ventral CA1 and dorsal CA2 in social memory," *Current Opinion in Neurobiology*, 68, pp. 29-35, ISSN: 0959-4388, DOI: 10.1016/j.conb.2020.12.008.

White, Edward L.
1972 "Synaptic organization in the olfactory glomerulus of the mouse," *Brain Research*, 37, 1, pp. 69-80, ISSN: 0006-8993, DOI: 10.1016/0006-8993(72)90346-0.

Whitebirch, Alexander C., John J. LaFrancois, Swati Jain, Paige Leary, Bina Santoro, Steven A. Siegelbaum, and Helen E. Scharfman
2022 "Enhanced excitability of the hippocampal CA2 region and its contribution to seizure activity in a mouse model of temporal lobe epilepsy," *Neuron*, 110, 19, 3121-3138.e8, ISSN: 0896-6273, DOI: 10.1016/j.neuron.2022.07.020.

Wilcox, Robin M. and Robert E. Johnston
1995 "Scent Counter-Marks: Specialized Mechanisms of Perception and Response to Individual Odors in Golden Hamsters (Mesocricetus auratus)," *Journal of Comparative Psychology*, 109, 4, pp. 349-356, ISSN: 0735-7036, DOI: 10.1037/0735-7036.109.4.349.

Wilson, David I.G., Rosamund F. Langston, Magdalene I. Schlesiger, Monica Wagner, Sakurako Watanabe, and James A. Ainge
2013 "Lateral entorhinal cortex is critical for novel object-context recognition," *Hippocampus*, 23, 5, pp. 352-366, ISSN: 1050-9631, DOI: 10.1002/hipo.22095.

Wilson, Matthew A. and Bruce L. McNaughton
1994 "Reactivation of Hippocampal Ensemble Memories During Sleep," *Science*, 265, 5172, pp. 676-679, ISSN: 0036-8075, DOI: 10.1126/science.8036517.

Winans, Sarah S.
1999 "The Medial Extended Amygdala in Male Reproductive Behavior A Node in the Mammalian Social Behavior Network," *Annals of the New York Academy of Sciences*, 877, 1, pp. 242-257, ISSN: 0077-8923, DOI: 10.1111/j.1749-6632.1999.tb09271.x.

Winans, Sarah S. and Frank Scalia
1970 "Amygdaloid Nucleus: New Afferent Input from the Vomeronasal Organ," *Science*, 170, 3955, pp. 330-332, ISSN: 0036-8075, DOI: 10.1126/science.170.3955.330.

Witter, Menno P., Thanh P. Doan, Bente Jacobsen, Eirik S. Nilssen, and Shinya Ohara
2017 "Architecture of the Entorhinal Cortex A Review of Entorhinal Anatomy in Rodents with Some Comparative Notes," *Frontiers in Systems Neuroscience*, 11, p. 46, ISSN: 1662-5137, DOI: 10.3389/fnsys.2017.00046.

Witter, Menno P., Arjan W. Griffioen, Barbara Jorritsma-Byham, and Jose L.M. Krijnen
1988 "Entorhinal projections to the hippocampal CA1 region in the rat: An underestimated pathway," *Neuroscience Letters*, 85, 2, pp. 193-198, ISSN: 0304-3940, DOI: 10.1016/0304-3940(88)90350-3.

Witter, Menno P., Pieterke A. Naber, Theo van Haeften, Willem C.M. Machielsen, Serge A.R.B. Rombouts, Frederik Barkhof, Philip Scheltens, and Fernando H. Lopes da Silva
2000 "Cortico-hippocampal communication by way of parallel parahippocampal-subicular pathways," *Hippocampus*, 10, 4, pp. 398-410, ISSN: 1050-9631, DOI: 10.1002/1098-1063(2000)10:4<398::aid-hipo6>3.0.co;2-k.

Wu, Si, Kosuke Hamaguchi, and Shun-ichi Amari
2008 "Dynamics and Computation of Continuous Attractors," *Neural Computation*, 20, 4, pp. 994-1025, ISSN: 0899-7667, DOI: 10.1162/neco.2008.10-06-378.

Wyass, J. Michael and Thomas Van Groen

1992 "Connections between the retrosplenial cortex and the hippocampal formation in the rat: A review," *Hippocampus*, 2, 1, pp. 1-11, ISSN: 1050-9631, DOI: 10.1002/hipo.450020102.

Xu, Xiangmin, Yanjun Sun, Todd C. Holmes, and Alberto J. López

2016 "Noncanonical connections between the subiculum and hippocampal CA1," *Journal of Comparative Neurology*, 524, 17, pp. 3666-3673, ISSN: 0021-9967, DOI: 10.1002/cne.24024.

Yonekura, Junichiro and Mineto Yokoi

2008 "Conditional genetic labeling of mitral cells of the mouse accessory olfactory bulb to visualize the organization of their apical dendritic tufts," *Molecular and Cellular Neuroscience*, 37, 4, pp. 708-718, ISSN: 1044-7431, DOI: 10.1016/j.mcn.2007.12.016.

Yu, Gene J., Jean-Marie C. Bouteiller, and Theodore W. Berger

2020 "Topographic Organization of Correlation Along the Longitudinal and Transverse Axes in Rat Hippocampal CA3 Due to Excitatory Afferents," *Frontiers in Computational Neuroscience*, 14, p. 588881, ISSN: 1662-5188, DOI: 10.3389/fncom.2020.588881.

Zapiec, Bolek and Peter Mombaerts

2020 "The Zonal Organization of Odorant Receptor Gene Choice in the Main Olfactory Epithelium of the Mouse," *Cell Reports*, 30, 12, 4220-4234.e5, ISSN: 2211-1247, DOI: 10.1016/j.celrep.2020.02.110.